Bacterial evasion strategies, urothelial biology and new treatments in urinary tract infection

Submitted by

Harry Horsley

BSc (Hons), MRes

Centre for Nephrology

Division of Medicine

University College London

A thesis submitted for the degree of Doctor of Philosophy

Declaration of Originality

I, Harry Horsley, declare that the work presented in this thesis was carried out entirely by myself, unless otherwise acknowledged.

Signature _____

Abstract

Urinary tract infections (UTI) are among the most prevalent infectious diseases worldwide, leading to significant morbidity and mortality and wreaking a substantial economic cost. Uropathogenic *Escherichia coli* (UPEC) has been shown to invade the urothelium in murine models of acute UTI, forming intracellular reservoirs that are thought to evade conventional antibiotic treatment and the immune response, allowing recurrence at a later date. However, the role of intracellular infection in chronic UTI causing more subtle lower urinary tract symptoms (LUTS), a particular problem in the growing elderly population, is not well understood. Moreover, the species of bacteria involved remains largely unknown, the model systems used to study them need improvement, and treatment options are not currently optimal. This thesis addresses these important research aims with a view towards improving the situation for LUTS patients who have an underlying UTI. In the first research section, we found strong evidence of intracellular *Enterococcus faecalis* harboured within urothelial cells shed via an innate immune response from the bladder of LUTS patients. Furthermore, these patient-isolated strains of *E. faecalis* showed robust invasive properties in a bladder cell line. However, *E. coli* only formed surface biofilms in these patients, suggesting that the murine UPEC model may not apply to patients with chronic LUTS. In the second section, we addressed the issue that the murine and human urinary bladder differ structurally and functionally, which may be hindering our understanding of UTI pathogenesis in humans. We therefore

designed and characterised a human three-dimensional (3D) bladder mimetic differentiated from primary urothelial progenitors, and showed that it closely resembles human tissue. Moreover, infection in this organoid model resulted in outcomes similar to those seen in LUTS patients. In the future we aim to use this 3D culture as a platform for modelling chronic infection and tissue regeneration in the presence of novel therapeutic agents. Finally, in the third section we tackled the issue that traditional oral antibiotic regimens for UTI fail in a high proportion of cases. This recurrence of disease post-treatment could be explained in part by the lack of cellular penetration of orally administered antibiotics, which are not able to accumulate to an effective concentration within intracellular bacterial niches. Meanwhile, oral antibiotics may also lead to antimicrobial resistance and systemic side effects. Using our human urothelial organoid, we tested the ability of novel liposome-coated ultrasound-activated lipid microbubbles to deliver drugs into the cortex of the apical cell layer. Ultrasound-activated intracellular delivery of gentamicin using microbubbles was over twice that achieved by liposomes alone. Moreover, little cell damage was detected and this therapeutic technology exhibited very encouraging antimicrobial activity, showing great promise as a more efficacious alternative to traditional oral antibiotic regimens. In conclusion, these collective results have implications for both the diagnosis and treatment of chronic UTI.

Impact statement

My work has and will continue to provide impact via dissemination locally, nationally and internationally through scholarly posters, papers, talks and peer-reviewed publications. Importantly, these conferences and journals have included both basic science venues as well as clinical ones. Moreover, the findings from my work will be of interest to a variety of disciplines, including cell biology, microbiology, tissue engineering, mechanical engineering, clinical science, drug delivery technology, and medicine.

My scientific papers will help advance the following academic and clinical fields:

- Chronic infection and bacterial reservoirs
- Host/pathogen interactions in UTI and other bacterial infections
- Human organoid development for basic and applied research
- Biology of the bladder epithelium including differentiation and innate immune responses
- The role of *Entrococcus faecalis* in UTI
- Increasing the awareness that other species aside from *E. coli* are worthy of academic study in the field of UTI
- Increasing the awareness that experiments done in mice might not be as physiologically relevant as previous appreciated, especially in UTI
- Challenging the universality of the UPEC mouse model of UTI for *E. coli* infections in humans

- Advancing the field of ultrasound-activated microbubbles for drug delivery and other novel treatments for UTI

From a commercial perspective, my work has led to two major branches of research that the group at large is taking forward. The 3D model now forms the basis for the host-pathogen interaction science being carried out by others in the lab, and is being used as a test-bed for multiple types of novel therapies in collaboration with industry. Several other academics have expressed interest in importing the organoid model technology into their own laboratories. Ultrasound-activated microbubbles are able to safely deliver high concentrations of drug into the bladder urothelium whilst avoiding antibiotic resistance and systemic side effects. These scientific advances could result in significant healthcare benefits in the near future. The microbubbles themselves are slated to enter preclinical development imminently with clinical trials envisaged within four years in collaboration with UCL Business as well as an industrial partner. Moreover, current treatments for chronic UTI are often unsuccessful and, therefore, costly. Our novel intravesical drug delivery system could potentially shorten recovery times and lead to significant economic savings.

This work has implications for the current NHS "one size fits all" guidelines for diagnosis and treatment of chronic UTI in cohorts of patient other than healthy young women with acute UTI. Together with other work from the same group, this knowledge will be used to attempt to alter clinical practice

and guidelines for the diagnosis and treatment of UTI in the UK. Other countries may choose to emulate this in time. This issue has already been raised in the House of Lords and seems set to escalate. Together with research undertaken by colleagues, this knowledge has inspired the formation of CUTIC, the Chronic Urinary Tract Infection Campaign (www.cutic.co.uk), which is politically and socially active.

Regarding public engagement, my work on the human organoid is being featured in *Research Matters*, a magazine published by the Multiple Sclerosis society, and several of the findings are regularly highlighted in talks given frequently to the public and other fora by Jennifer Rohn, my primary supervisor.

Acknowledgements

First and foremost, I would like to thank the Multiple Sclerosis Society for their generous support of this work.

I would like to extend my sincerest gratitude to my supervisors, Dr. Jennifer L. Rohn and Professor James Malone-Lee, for their time, advice, support and for believing in me over the years.

I would also like to thank every member of the Chronic UTI Group (past and present) and all the members at the Centre for Nephrology for their technical support and expertise. On a more personal note, I would like to thank Dr. Jill Norman for guiding me through some of the more difficult times.

Thank you to the co-authors of my papers "*Enterococcus faecalis* subverts and invades the host urothelium in patients with chronic urinary tract infection" (Appendix 1 and [1]) and "A urine-dependent human urothelial organoid offers a potential alternative to rodent models of infection" (Appendix 2 and [2]), the findings from which have been included in chapters 2 and 3 of this thesis.

I would also like to thank our collaborators at Oxford University; Professor Eleanor Stride, Dr. Dario Carugo and Dr. Joshua Owen for their technical expertise and support in regard to chapter 4.

Finally, I would like to thank my close friends and family for putting up with me during my studies.

Dedication

I would like to dedicate this work to my mum and dad, my wife Helen and our little boy Jet.

Table of Contents

List of figures

List of tables

List of appendices

List of abbreviations

API	Analytical profile index
AS	Aggregation substance
AUM	Asymmetric unit membrane
BC	Basal cell
BF	Bright field
BPE	Bovine pituitary extract
BPS	Bladder pain syndrome
BR	Background fluorescence
BSA	Bovine serum albumin
CAUTI	Catheter associated urinary tract infection
CBA	Columbia blood agar
CEHDF	Coaxial electrohydrodynamically formed
CFU	Colony forming units
CIM	CO_2 independent media
CK	Cytokeratin
CS	Chondroitin sulphate
CTC	Cyanoditolyl tetrazolium chloride
CTCF	Corrected total cellular fluorescence
DAPI	4'',6-diamidino-2-phenylindole
DMSO	Dimethyl sulfoxide
DSPC	1,2-distearoyl-sn-glycero-3-phosphocholine
DSPE	1,2-distearoyl-sn-glycero-3-phosphoethanolamine

EM	Electron microscopy
EPC	Epithelial cell
EUCAST	European Committee on Antimicrobial Susceptibility Testing
FBS	Foetal bovine serum
FV	Fusiform vesicle
GAG	Glycosaminoglycan
GCP	Good clinical practice
GENT	Gentamicin
HBEP	Human bladder epithelial progenitor
HBSS	Hank's balanced salt solution
HS	Heparan sulphate
IBC	Intracellular bacterial community
ID	Integrated density
IF	Immunofluorescence
INT	2-(4-iodophenyl)-3-(4-nitrophenyl)-5-phenyl-2H-tetrazolium (tetrazolium salt)
LB	Lysogeny broth
LDH	Lactate dehydrogenase
LUTS	Lower urinary tract symptoms
MHRA	The Medicines and Healthcare products Regulatory Agency
MIC	Minimum inhibitory concentration
MOI	Multiplicity of infection

MP	Microplicae
MS	Multiple sclerosis
MSU	Midstream urine
MV	Microvilli
NAD	Nicotinamide adenine dinucleotide
NBD	7-nitro-2-1,3-benzoxadiazol-4-yl
NGS	Normal goat serum
NHS	National Health Service
NICE	The National Institute for Health and Care Excellence
OAB	Overactive bladder
PBS	Phosphate buffered saline
PCF	Polycarbonate filter
PDMS	Polydimethylsiloxane
PEG	Polyethylene glycol
PHMB	Polyhexamethylene biguanide
PMSQ	Polymethylsilsesquioxane
PNA-FISH	Peptide nucleic acid fluorescent *in situ* hybridisation
QIR	Quiescent intracellular reservoir
RCF	Relative centrifugal force
RPMI	Roswell Park Memorial Institute medium
RT	Room temperature
SAT	System for acoustic transfection
SEM	Scanning electron microscopy
TEM	Transmission electron microscopy

TJ	Tight junction
TRITC	Tetramethylrhodamine
UC	Umbrella cell
UK	United Kingdom
UP	Uroplakin
UPEC	Uropathogenic *E. coli*
US	United States
UTI	Urinary tract infection
WAAAR	Declaration of the World Alliance Against Antibiotic Resistance
WBC	White blood cell
WGA	Wheat germ agglutinin
WHO	World Health Organisation

Chapter 1

Introduction

1. Introduction

1.1 Clinical Background

Urinary tract infection (UTI) is defined as an inflammatory response of the urinary epithelium to microbial infection of any anatomical constituent of the upper or lower urinary tract [3]. Technically, upper urinary tract infections (kidneys) are referred to as pyelonephritis and infections of the lower urinary tract (bladder, urethra) are termed cystitis and urethritis respectively [4]. In practice, however, the term UTI is used empirically to describe bacterial pathology of the bladder, rendering the terms UTI and cystitis almost interchangeable in most situations. Therefore, in this thesis, the term UTI will be used exclusively to describe infections of the bladder.

UTI is a significant cause of morbidity, ranking as one of the most prevalent infectious diseases worldwide [5, 6]. UTI is the most common reason for younger women to seek medical help [7]. Foxman et al. (2002) reported that by the age of 24, 30% of women will have developed an acute, self-limiting UTI and nearly 50% of all women will suffer from a bladder infection during their lifetime [6]. More problematic, however, is recurrence of the disease [8-11], which is known to have a significant detrimental effect on quality of life and to be particularly difficult to successfully treat [12, 13]. 10-15% of the cohort studied by Foxman et al. (2002) suffered from a recurrent or chronic form of the disease [6]. In another large-cohort study performed in Finland,

nearly half of the total women studied developed recurrent UTI [14]. Often attributed to anatomical differences, such as the length of the urethra and shorter distance between the urethra and the anus, females are fifty times more likely to suffer from bladder infections than men (Fig. 1) [15]. That being said, UTI is far from rare in males, with a third of men over the age of 80 years requiring antibiotic treatment from a general practitioner [16].

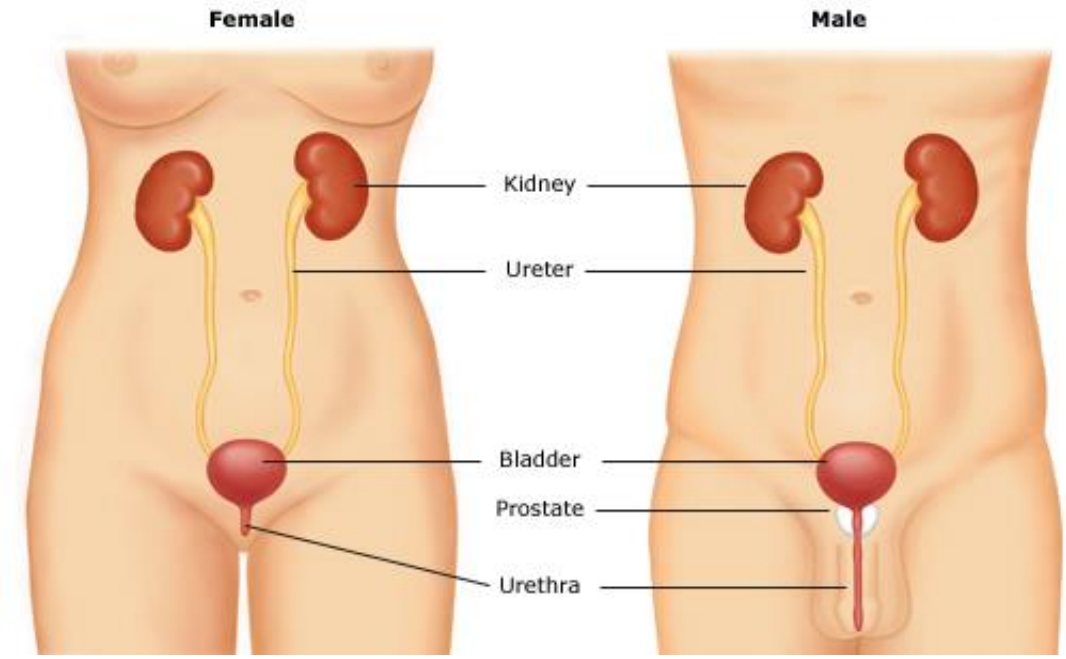

Figure 1. Simple anatomy of the human urinary tract

The urinary anatomy is made up of the upper (kidneys, ureters) and lower (urinary bladder, urethra) urinary tracts. As can be seen, the female urethra is significantly shorter than that of males. Image acquired from [17].

As with most diseases, the frequency of diagnosed UTI rises dramatically with age [6]. UTI is the most common bacterial infection in older people [18]

with the prevalence of bacteriuria rising from 0.1% in men and 5% in women within the young-to-middle aged bracket [19] to a worrying 10% and 20% respectively from the age of 65 onwards [18].

UTI is also problematic in more vulnerable subgroups: the risk of UTI dramatically increases in people with multiple sclerosis (MS) [20, 21], spinal injury [22], renal transplant patients [23] and anyone requiring urinary catheterization or other indwelling devices [24]. In fact, UTIs have accounted for 10.5 million ambulatory care visits in 2007 in the United States [25], with the direct and indirect costs being estimated at more than US$3.5 billion. This is likely to rise with the ageing global population and the emerging threat of antibiotic resistance. Finally, as mentioned above, amongst the elderly, UTIs are one of the most commonly diagnosed infections, accounting for over a third of all nursing home-associated infections [26]. More frequent UTI in these cohorts is not merely bothersome; UTI is known to exacerbate MS [27], lead to confusion and falls in the elderly [28], and increase the risk of organ rejection in renal transplant patients [29]. Furthermore, catheter-associated UTI (CAUTI) carries an increased risk of urosepsis [30], and bacteriuria in pregnant women is associated with preterm birth and other maternal morbidities [31].

The clinical signs and symptoms of UTI may include: dysuria (burning sensation on urination); increased nocturnal (nocturia) and day-time (pollakiuria) urinary frequency; reduced urine stream; straining to void; hesitancy (difficulty initiating micturition); intermittency (intermittent urine

flow); incomplete emptying; urgency (a sudden desire to micturate); general lower abdominal pain/ discomfort; various symptoms of urinary incontinence and odorous, cloudy or bloody urine [4, 32, 33]. Nevertheless, classically, acute UTI is not necessarily diagnostically challenging [34], as the rapid onset of urinary frequency, dysuria and urgency are clear indicators of the pathology [4]. A patient presenting with pyelonephritis will likely complain of some, if not all, of the symptoms outlined above with the addition of nausea, vomiting, costovertebral angle pain and fever [4, 35]. It would seem likely that pyelonephritis is a result of infection ascending the ureters from the urethra and bladder numerous studies, however, have been unable to ascertain a direct relationship [4, 35, 36].

Less clear cut are lower urinary tract symptoms (LUTS), a collective term describing a host of urological manifestations, including symptoms of urine storage and voiding, and pain attributed to the lower urinary tract [33]. LUTS have also been used interchangeably or in a partially overlapping fashion with the terms overactive bladder (OAB) and interstitial cystitis or bladder pain syndrome (BPS) but will be referred to as LUTS throughout this thesis [37-40]. While the role of infection in the generation of acute symptoms is well recognised, an infective aetiology in other LUTS is not typically assumed. In fact, most current guidance on the management of LUTS calls for the exclusion of UTI using routine urinalysis methods [41, 42]. In this context, the term LUTS had become synonymous with non-infectious disease. The clinical features of UTI and LUTS show considerable overlap,

however, and the prevalence of both disorders rises dramatically with age [18, 43-45].

Our research centre and others have found that the tests deployed to screen for UTI are largely inadequate, particularly in patients who do not present with classic acute infective symptoms [46-48]. Although LUTS can undoubtedly be caused by other factors (e.g. carcinoma, urethral stricture, prostatic disease, bladder stones [49, 50]), we now know that LUTS patients scoring as negative on routine tests for infection might in fact harbour a low-grade recurrent UTI [13, 40, 51-57]. Understanding more about the infective aetiology of LUTS is therefore crucial for informing guidelines on diagnosis and treatment.

1.2 Bladder Biology

To understand why urinary infections are often recalcitrant to treatment, the pathogens must be studied in their unique environment. The urinary bladder is lined by a transitional epithelium called the urothelium. This specialised tissue comprises 3-7 layers of cells: basal cells (above the basement membrane), intermediate cells (above basal cells) and morphologically distinct, highly specialised, often binucleated umbrella cells at the apical surface, which face inward into the bladder lumen (Fig. 2a,b) [58]. These enlarged, flattened urothelial umbrella cells or ‘facet cells’ partition urine and act as a powerful barrier to protect underlying tissue from harmful waste compounds (Fig. 2b,c,d) [59]. This barrier function is thought to be achieved

through the elaboration of a highly-durable apical asymmetric unit membrane (AUM) consisting of 0.5-1 µm plaques or ‘facets’ (Fig. 2c) which, in turn, are made up of 16.5 nm particles of four well-studied mannosylated glycoproteins named uroplakins (UP) (Fig. 2d) [59-61]. UP (namely UPIa, UPIb, UPII and UPIII) are a family of transmembrane proteins regarded as specific markers of terminal cytodifferentiation in the bladder [62].

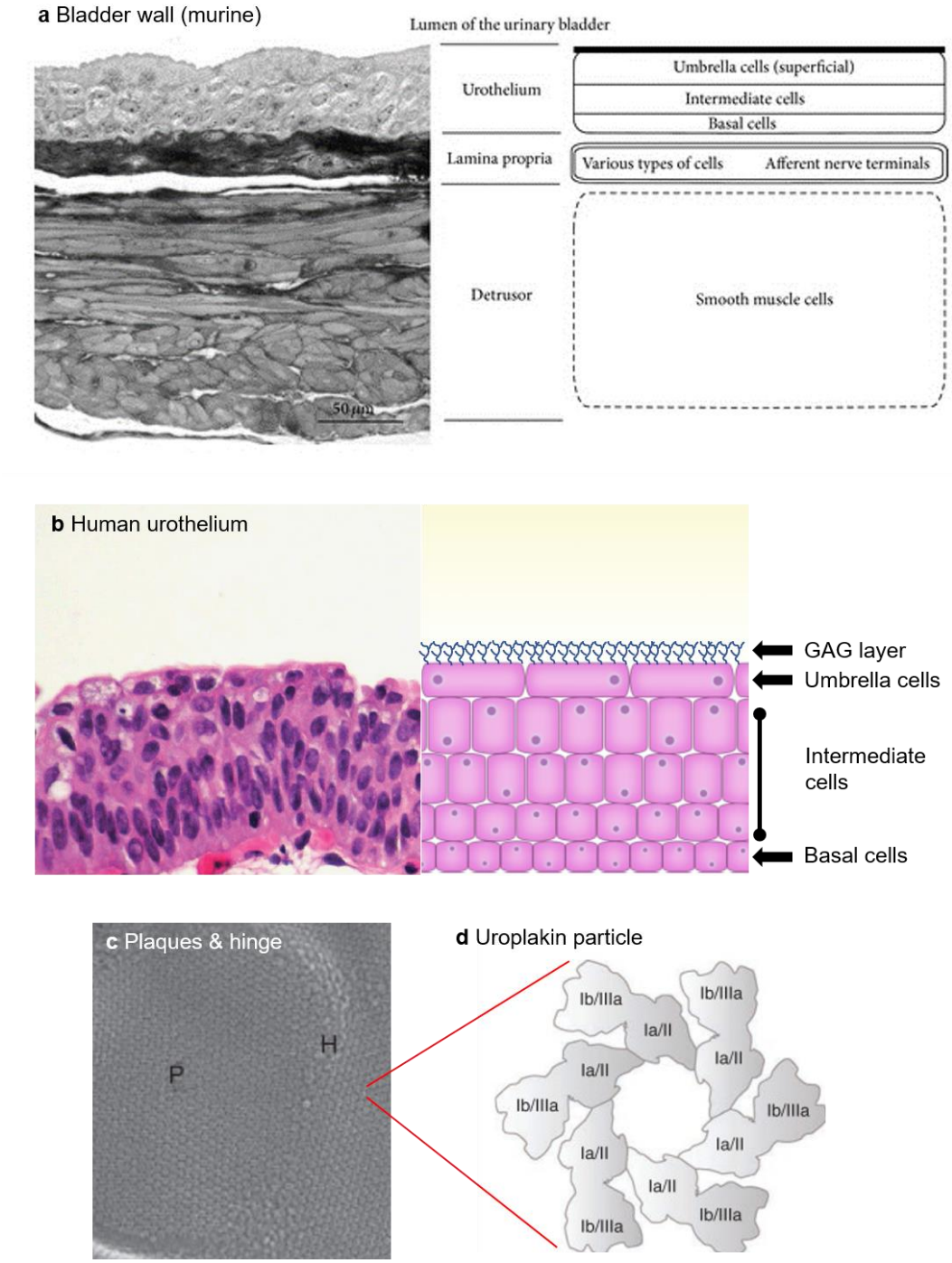

Figure 2. Functional anatomy of the bladder and urothelium

(a) H & E stained cross section of the murine bladder wall. The specialised urothelium points inward towards the lumen of the bladder. Note that the murine bladder urothelium is ~3 layers thick. Basal to the urothelium lies the lamina propria then the detrusor muscle layer responsible for contraction of the bladder. Image adapted from [63]. (b) Left, H & E stained section of

healthy human urothelium showing 5 – 7 layers of cells. Image adapted from [64]. The image to the right is a diagrammatic depiction of the human urothelium. Large, flat, highly-specialised umbrella cells coated with glycosaminoglycan (GAG) line the apical cell-urine interface. Deep to the umbrella cells are the smaller intermediate and basal cells. (c) Scanning electron micrograph of the surface of a murine umbrella cell. The asymmetric unit membrane (AUM) at the apical surface of the umbrella cells is made up of 0.5-1 μm plaques (p) interspersed by hinges (h). (d) These plaques are comprised of thousands of 16.5 nm particles formed from Uroplakins UPIa, UPIb, UPII and UPIII. Images shown in c and d were adapted from [61].

In addition to the uroplakin family, the urothelium also elaborates a mucopolysaccharide-rich layer of glycosaminoglycans (GAG) which are believed to protect the bladder from infection and urine-born irritants (Fig. 2b) [65]. Chondroitin sulphate, heparan sulphate, hyaluronic acid, dermatan sulphate and keratin sulphate are the most studied constituents of the bladder mucosal GAG barrier [66]. Chondroitin sulphate, in particular, is believed to play a key role in urothelial barrier function and exhibits luminal and basal expression in both human and porcine bladders [67]. In contrast, however, only heparan sulphate was detected in the luminal portion of calf bladders, elucidating possible differences between species [68].

A significant proportion of research on the urothelium has been conducted using mouse models [10, 61]. These findings have been widely translated into human oncology to locate the primary origin of metastatic tumours [69] and to understand the biology of UTI [10]. While invaluable in many cases and necessary for regulatory approval of drugs, some animal models of

human disease, the majority of which are murine, have received widespread criticism in recent years [70-74]. The limitations of murine models are particularly evident when modelling human infection and attempting to treat this induced pathology with novel antimicrobials [70]. In such studies, mice are frequently infected with far higher quantities of log-phase bacteria than would be evident in a slow-growing chronic human infection, and the pharmacokinetic profiles of a given drug are challenging to translate to humans [70, 75].

In the case of urinary infection studies, it is known that the human and mouse bladder urothelium differ in a number of structural ways. The markers expressed are similar, but in contrast to the murine situation, human bladder urothelium marker expression exhibits a relationship with the level of cellular differentiation [61, 76]. For example, the healthy human bladder has been shown to elaborate cytokeratin 20 at the luminal surface whereas cytokeratin 8 is expressed throughout the cells of the urothelium [58, 77]. The incorrect spatial expression of members of the cytokeratin family, namely cytokeratin 20 by terminally differentiated umbrella cells, has been linked to BPS and neurogenic bladder and is thought to predispose people with MS to chronic UTI [20, 58, 77]**.** Studies also suggest that murine and human bladders can differ in their innate immune response to uropathogens (for example in their expression and use of Toll-like receptors [78]). Moreover, rodent bladders differ from that of humans functionally. While larger mammals (>3Kg) share a scalable urinary capacity and consistent voiding duration, rodents urinate almost constantly, bringing into question whether their bladders are a true

storage organ [79]. The multiple disparities between the rodent and human bladders raise the possibility that relying so heavily on the former could be problematic for understanding UTI in the latter.

Given these species differences, there is therefore a need for alternative human-based models to augment the impressive body of elegant *in vivo* mouse experiments into UTI biology. Human bladder cancer cell lines grow readily and are tractable, but they are genetically abnormal and, therefore, bear little resemblance to primary urothelial cells in terms of structure and function [80]. In particular, although some retain the ability to form a stratified organoid, they do not form an organised and differentiated 3D architecture [81, 82], which is crucial not least for understanding host/pathogen interaction, as uropathogens are proposed to invade the urothelium via binding to factors only present in terminally differentiated umbrella cells [10]. On the other hand, recent years have seen advances in three-dimensional tissue engineering.

A number of promising 3D urothelial models have been described in the literature, the majority of which have been discussed in a comprehensive review by Baker *et al.* (2014) [65]. Briefly, existing bladder models are produced using one of three broad culture techniques: (1) organ culture of intact biopsies or explant culture; (2) culture of urothelial cells naturally shed into the urine or harvested from biopsies; and (3) organotypic culture whereby normal urothelial cells are stimulated to form 3D organoids on filter inserts [65]. Although arguably the most relevant model system, organ

culture of intact human tissue is time consuming, yields a finite amount of experimental material and requires fresh human tissue [65, 83]. Due to these limitations, a number of researchers have used rodent bladder biopsies; however, due to the aforementioned differences between species, these models may not be biologically germane [84]. More practical, therefore, is the cultivation of human urothelial cells isolated from host urine or biopsies which, when grown using a specialist protocol, have been shown to maintain the ability to stratify, differentiate and develop a robust barrier function *in vitro* [65, 85-88].

Although these models constitute impressive alternatives to animal models, to our knowledge, they last only a few hours up to a day in urine *in vitro* [65, 89], the natural apical substrate of this tissue. Therefore, the effect of urine exposure on urothelial differentiation and GAG expression remains unclear. Moreover, none of the human-derived urothelial biomimetics have been reported to correctly express cytokeratin 20 at the apical surface [77]. Therefore, the generation of a true urine-tolerant organotypic human urothelium that could be used as a platform studying for host/uropathogen interactions, treatment, and resolution in humans would be a very useful addition to the field.

1.3 Microbiology of UTI

By far the most prevalent bacterial species implicated in acute UTI is the common Gram-negative gut commensal *Escherichia coli*, which is responsible for as many as 90% of diagnosed cases of nosocomial and community-acquired bladder infection [90]. The mouse model of acute UTI caused by *E. coli* is widely used to help understand human UTI [10].Tissue tropism in murine uropathogenic *E. coli* (UPEC) infections is initiated by a complex interplay between the UPEC derived type 1 pili / fimbriae and UP proteins on the apical membrane of umbrella cells situated on the luminal surface of the bladder [91]. Type 1 pili are antigenic, heteropolymeric, hairlike proteinaceous organelles that line the extracellular surface of UPEC, and their selective adhesive properties are thought to be mediated by a minor component at the tip of the pili filament termed FimH or the “adhesin” [92]. Following bacterial attachment to the murine urothelium during experimental infections, UPEC invades and forms intracellular bacterial communities (IBCs) where they are able to evade immune surveillance and a number of systemic antibiotic treatments [10, 93-99]. The findings from these studies have resulted in a well-accepted model of the acute UTI UPEC life cycle (Fig. 3) [97]. Adhesion and invasion into the host cell cytoplasm are closely followed by three distinct stages of the intracellular bacterial community (IBC) lifecycle. During early IBC, loose collections of bacillus bacteria rapidly divide inside the cytoplasm proper. In middle IBC, daughter cells exhibiting a coccoid morphology pack tightly producing a biofilm-like “pod” [95]. At the late IBC stage, bacteria at the periphery of the intracellular biofilms regain a rod morphology and become highly motile, leading to bacterial efflux and re-infection of adjacent cells [97]. These later phases of IBC formation are

accompanied by a sub-population of filamentous UPEC some 70µm in length [10]. This morphological adaptation is believed to confer biological fitness and therefore persistence in the urinary bladder [97]. Although UP and integrins are thought to be involved in the process of invasion, a number of candidate receptors and mechanisms have also been implicated in the multifarious pathogenesis of UPEC colonisation [10].

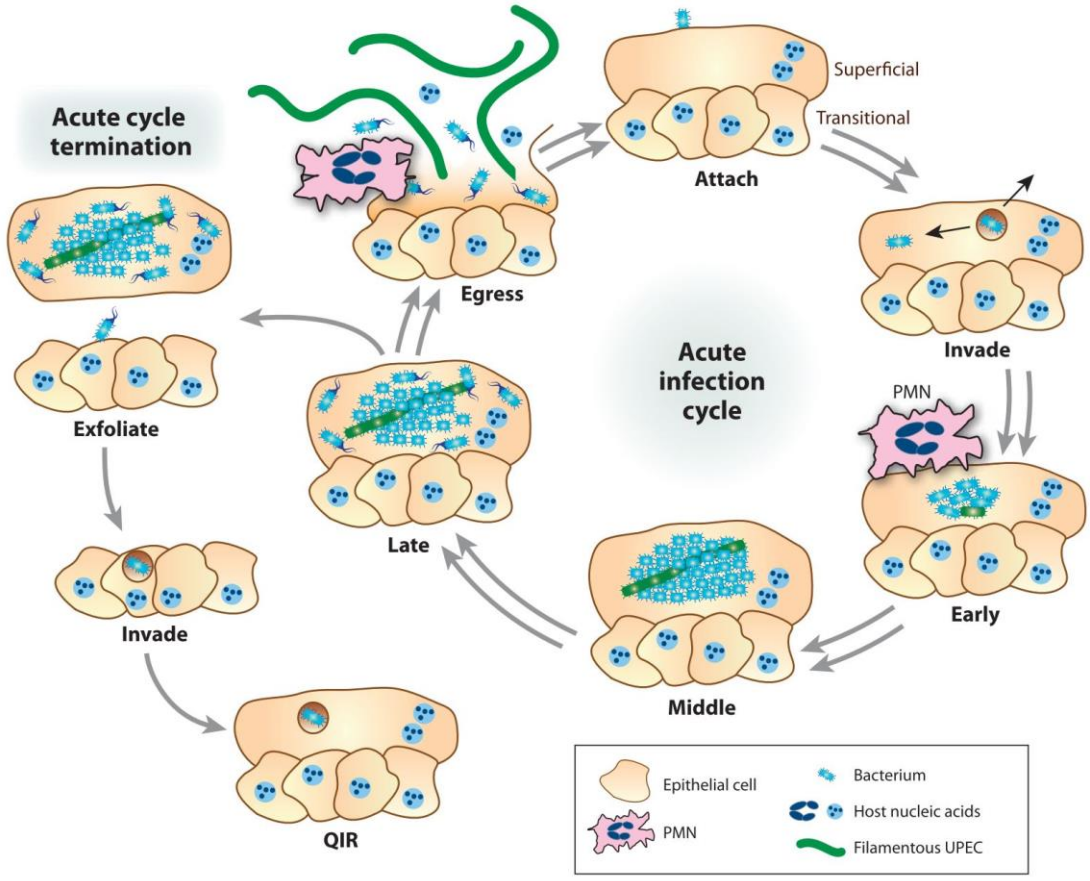

Figure 3. Intracellular lifestyle exhibited by uropathogenic *E. coli* (UPEC) in murine models of acute UTI

Planktonic-phase UPEC bind to uroplakins on the surface of the fully-differentiated umbrella cells. Post-tropism, the bacteria invade these superficial cells. Most bacteria spontaneously egress but a small proportion gain access to the cytoplasm proper. This invasive phenotype protects the

bacteria from host polymorphonuclear leukocyte cells (PMN). Invasion is followed by three distinct phases of the intracellular bacterial community (IBC) lifecycle. Early IBC describes the rapid division of loosely-packed intracellular bacillus UPEC. In the middle IBC phase, daughter UPEC cells take on a coccoid morphology and form a tightly-packed biofilm-like intracellular “pod”. During the late IBC stage, bacteria at the periphery of the “pod” take on a highly-motile filamentous phenotype before egressing and infecting adjacent cells. At the end of the acute infection phase, umbrella cells are rapidly shed as an innate immune response to bacterial insult. These gaps in the urothelium allow infection of intermediate and possibly basal urothelial cells, leading to quiescent intracellular reservoirs (QIR). QIR reactivate in response to cellular differentiation and, hence, the cycle repeats. QIR are, therefore, a possible explanation for the high rates of UTI recurrence in humans. Image acquired from [10].

Infected umbrella cells are shed from the epithelial lining into the urine. Such sloughing is known in both mice and humans to be a common response to infection [96, 100-103]. In mouse model experiments, this dramatic cell shedding response leaves a gap in the epithelial layer, exposing naive transitional cells (proximal to the submucosal coat (Fig. 3) to *de novo* UPEC invasion, a process which has been proposed, through an actin-gated pathway, to create quiescent intracellular reservoirs (QIR) responsible for latent recurrent and low-level chronic infection in mice [10, 94, 98, 103, 104]. Although QIR have not been observed in human patients, there is indirect evidence to suggest bacterial persistence in the human urothelium [10]. It could be argued, however, that these relapses are caused by reintroduction of pathogens from faecal flora arising from the anus or colonised vagina [4,

8, 105-107]. Nevertheless, the daily application of topical antibiotics to the female perineum does not prevent recurrent episodes, supporting the notion for a persistent low-level bacterial reservoir in the urinary tract [108]. Other IBC stages above, namely bacterial filamentation, have also been described in acute human UTI [96], although, in general, there is a paucity of human data.

Given the prevalence of UPEC as a causative agent in acute UTI, UPEC remains the most widely studied uropathogen. However, many other bacterial species can cause UTI (see Table 1) [109]. What's more, it is now recognized that urothelial invasion may not be restricted to *E. coli* alone, with *Staphylococcus saprophyticus* [110] and *Klebsiella pneumonia* [111] also exhibiting UPEC-like intracellular lifestyles in experimental murine acute UTI. Recently, we explored an infective aetiology in LUTS using a traditional gentamicin protection assay, in which shielded bacteria were enumerated after extracellular bacteria were killed off by antibiotics [13]. In this study, *Enterococcus faecalis*, *Streptococcus anginosus, E. coli,* and *Proteus mirabilis* were shown to be closely associated with the shed cells. Although this assay is a trusted and well-tested method for detecting intracellular bacteria [112, 113], the information gleaned from this technique is indirect. Furthermore, many antibiotic-susceptible bacteria readily form heavily antibiotic-resistant biofilms which could be responsible for false-positive outputs [114, 115]. Nonetheless, the gentamicin protection assay remains a standard tool in this field and has the advantage of allowing the researcher to

enumerate sequestered pathogens even if the nature of that sequestration is not entirely clear.

Table 1. Prevalence of uropathogens

Data acquired from Haque *et al.* (2015) [109].

Uropathogen	Prevalence (%)	Morphology	Gram status
E. coli	59.3	rod	negative
Staphylococcus saprophiticus	19.09	coccus	positive
Enterococcus spp.	11.5	coccus	positive
Klebsiella spp.	5.53	rod	negative
Pseudomonas spp.	2.01	rod	negative
Proteus spp.	1.51	rod	negative
Enterobacter spp.	1	rod	negative

In the past few years *Enterococcus spp.* have received a significant amount of attention. This opportunistic uropathogen is of particular concern in the clinical setting, where multi-drug resistant strains are frequently involved in hospital-acquired infection [116]. Moreover, the rapid acquisition of antibiotic resistance, biofilm formation [114, 115] and the innate ability to thrive and persist in the urinary tract make UTI caused by *Enterococcus spp*. particularly difficult to eradicate [117-121]. In the LUTS study described above, *E. faecalis* was the most cell-associated pathogen described, much more so than *E. coli*. In addition, *E. faecalis* is frequently isolated in acute UTI [18, 96] and non-dysuric LUTS patients [13]. Moreover, many patients

are frequently required to use urinary catheters, again, predisposing them to chronic infection with *E. faecalis* [20, 120, 122]. It is therefore not only of considerable interest to learn more about the host/pathogen interactions of less well studied uropathogens, but further scrutiny of *E. faecalis* in particular is warranted. It may well turn out that the “one size fits all” approach of UTI diagnosis and treatment typically modelled on *E. coli* that prevails in the clinic is not nuanced enough.

1.4 Treatment

The most common treatment for acute uncomplicated UTI is a three- to seven-day course of orally administered antibiotics [34]. In the UK, The National Institute for Health and Care Excellence (NICE) recommend the use of Nitrofurantoin, Trimethoprim, Amoxicillin, Ampicillin or Cephalosporins in the first instance [123]. If these agents are ineffective, encounter microbial resistance or are not well tolerated by the patient then the physician may prescribe co-amoxiclav, pivmecillinam, a quinolone or fosfomycin [123]. Unfortunately, as shown by a large-scale meta-analysis, these antimicrobial guidelines fail 37% of patients from a symptomatic perspective and 27% in regards to current microbiological standards [124]. Our research team collaborates with Professor Malone-Lee, who runs the Whittington Hospital LUTS outpatient clinic specialised in treating patients with recurrent UTI who have repeatedly failed to respond to standard treatment regimens. In this setting, full dose antimicrobial therapy is deployed for several weeks to months with favourable outcomes [57].

Nonetheless, the repeated use of systemic antibiotics to treat this frequently recalcitrant disease carries risks [8, 125]. Side effects consisting largely of nausea, vomiting, diarrhoea and candidiasis, due to perturbation of the body's commensal flora, are frequently reported [36, 57, 126, 127]. However, antimicrobial treatment can also adversely affect the central nervous, respiratory, musculoskeletal systems and promote harmful *Clostridium difficile* colonisation [57, 127, 128]. Moreover, many antibiotics can interact with concomitant medications, leading to less effective treatment selection and, when confounded by potential side effects, poor medication adherence [129]. Having said that, a recent paper describing the long-term antibiotic treatment of a large number of patients did not find an unduly high burden of adverse effects, suggesting that careful management and monitoring of long-term treatment can allay some of these concerns [57].

A more worrying ramification of traditional antimicrobial therapy is the rising emergence of antibiotic resistance in urogenital pathogens [130]. In 2014, the World Health Organization (WHO) released a fact sheet outlining the urgency for new treatments and responsible antibiotic stewardship [131]. Moreover, this document directly referenced the use of antimicrobials for UTI and urethritis as a particular concern [131]. This urgent global healthcare crisis also led to the 'Declaration of the World Alliance Against Antibiotic Resistance' or WAAAR, which aims to educate prescribers, scientists and officials on the use of antibiotics along with promoting novel drug development [132]. Given the frequency of cystitis in younger people caused

by *E. coli*, it is perhaps unsurprising that most studies on antibiotic resistance in UTI have concentrated on this bacteria [125, 133-138]. It should be noted, however, that resistance is also commonly encountered in other uropathogens such as *Enterococcus spp.,* particularly in older catheter users with a history of recurrent UTI, and *Klebsiella spp.* has higher resistance rates than *E. coli* [131, 139].

In summary, UTI frequently reoccur, *E. coli* may not always be responsible, particularly in older people with a refractory form of the disease, and traditional oral antimicrobial treatment fails a high number of patients. Additionally, the use of antibiotics is linked to a rise in resistance in urogenital pathogens along with causing a range of bothersome systemic side effects. The chronicity of this disease is thought to be attributable in part to the intracellular lifestyle displayed by the causal uropathogens [8] – although reintroduction from other niches in the body probably also play a role [140], as does host genetic background [141, 142]. Treatment of intracellular bacteria is further complicated by the relatively poor urothelial penetration exhibited by orally administered antibiotics which fail to reach these deep bacterial reservoirs [143, 144]. Due to these difficulties, a range of novel intravesically-administered therapies are being developed to avoid systemic side effects and antibiotic resistance; to ease LUTS associated with bladder pain syndrome (BPS) by attempting to ‘repair’ the GAG layer; or to introduce vaccines and FimH antagonists to bolster the hosts’ immune response to, or inhibit the binding of, *E. coli* [66, 144-147]. However, data for the use of GAG replenishment to treat recurrent UTI, although promising in animal models

[148], is limited to two small non-randomised trials and a single retrospective review study in humans [149-151]. Moreover, as discussed above, *E. coli* may not be the primary pathogen in chronic UTI, which limits the use of vaccines and blocking agents against this bacteria in a number of patients.

The simplest form of antibacterial intravesical therapy are antibiotic bladder instillations, whereby a high-concentration antibiotic solution is instilled into the bladder lumen via a catheter in an effort to eradicate chronic infections. Studies have reported some benefit in filling the urinary bladder with the broad-spectrum aminoglycoside gentamicin [152-155]. Nevertheless, a large-cohort study investigating the efficacy of gentamicin bladder instillations in recurrent UTI reported failure in 26% of cases [152]. Moreover, in the same study, 5% of cases failed due to antimicrobial resistance [152]. Indeed, *Enterococcus spp.* frequently acquire resistance to gentamicin [156] and aminoglycosides exhibit poor cell permeability which, considering the powerful barrier elicited by umbrella cells, could hinder the killing of intracellular uropathogens [157]. Even a cell-permeant antibiotic might struggle to achieve a therapeutic intracellular dose via free diffusion. Another study compared acetic acid, polymyxin-neomycin and normal saline bladder instillations; however, the authors did not find a clinical or microbiological improvement or, indeed, any difference amongst these treatments [158]. Please see Table 2 for a comprehensive list of reported and proposed intravesical treatments.

Table 2. Past, current and proposed intravesical treatments for UTI and LUTS

Drug	Activity	Indication	Reference
Gentamicin	Antibacterial	UTI	[152-155, 159]
Polymyxin B, neomycin	Antibacterial	UTI	[158]
Acetic acid	Antibacterial	UTI	[158]
Saline	Irrigation	UTI	[158]
Linezolid	Antibacterial	UTI	[160]
Amikacin sulfate	Antibacterial	UTI	[161]
Amphotericin B	Antifungal	Fungal UTI	[162]
Piperacillin, tazobactam	Antibacterial	UTI	[159]
Piperacillin	Antibacterial	UTI	[163]
Tobramycin	Antibacterial	UTI	[159]
Chlorhexidine	Antimicrobial	UTI	[164-166]
Chlorhexidine, silver nitrate	Antimicrobial	UTI	[167]
Trisdine (Chlorhexidine, ethylenediaminetetraacetic acid (EDTA))	Antimicrobial	UTI	[168]
Kanamycin, polymyxin B	Antibacterial	UTI	[168]
PMSQ microcapsules (encapsulated gentamicin)	Antibacterial	UTI	[169]
Quercetin micelles	Anti-inflammatory	UTI	[170]
Chlorin e6 photodynamic therapy	Antimicrobial	UTI	[171]
Liposomes	Various (drug delivery system)	UTI / BPS	[172-175]
Chondroitin sulphate (Gepan™, Uracyst™)	GAG repair	UTI / BPS	[176, 177]
Dimethyl sulfoxide	Anti-inflammatory,	BPS	[178]

(DMSO)	analgesic, muscle relaxant		
DMSO, hydrocortisone, bupivacaine, heparin sulphate	Anti-inflammatory, analgesic, muscle relaxant, GAG repair	BPS	[179]
Alkalised lidocaine	analgesic	BPS	[180]
Alkalised Lidocaine, Heparin	analgesic, GAG repair	BPS	[181]
Pentosan polysulfate sodium (PPS)	Anti-inflammatory, GAG repair	BPS	[182]
Sodium hyaluronate (hyaluronic acid, Cystistat™)	GAG repair	BPS	[183]
Sodium hyaluronate, chondroitin sulfate (Ialuril™)	GAG repair	BPS	[184]
Capsaicin	Neurotoxin	BPS	[185]
Resiniferatoxin	Neurotoxin	BPS	[186, 187]
Bacillus Calmette-Guerin (BCG)	Immunomodulatory	Bladder cancer / BPS	[188]

More apposite to this thesis is the emerging field of nanotechnology, which is thought to be revolutionising the field of intravesical drug delivery [144, 189]. Recently, we published pilot *in vitro* data on the use of coaxial electrohydrodynamically formed (CEHDF) polymethylsilsesquioxane (PMSQ) capsules containing gentamicin to treat chronic UTI [169]. In this study, we showed these biocompatible capsules were able to efficiently penetrate T24

human bladder cells and kill uropathogenic *E. faecalis* in a dose-responsive and slow-release manner [169]. Another study reported potent therapeutic efficacy through the intravesical treatment of UPEC-infected rats with self-assembled quercetin micelles [170]. Quercetin does not exhibit antimicrobial properties but is a powerful anti-inflammatory compound; therefore, it could be used as an adjunct to antimicrobial therapy or to ameliorate bothersome symptoms [170]. More recently, Liu *et al* (2015) published work on chlorin e6 (Ce6)-encapsulated charge-conversion polymeric nanoparticles stimulated using photodynamic therapy [171]. Encouragingly, this method appeared safe and effective against both gram-positive and gram-negative pathogens in a murine model of UTI [171]. Perhaps a more established approach is the use of lipidic nanoparticles, or 'liposomes', to deliver cell-impermeant or insoluble drugs into the intracellular compartment of mammalian cells [190]. Indeed, a number of studies have found this mode of delivery to be particularly useful in the bladder [143, 173, 174, 191-193]. To our knowledge, however, only one study concentrates on the use of intravesical liposome treatment for UTI-induced pathology with the remainder of work focusing on bladder cancer and symptomatic therapy [172]. Nonetheless, all of these reports highlight the use of liposomes as an efficacious drug-delivery system in the urothelium.

Microbubbles or 'bubbles' have been used for over twenty years as a biocompatible contrast agent in ultrasound-mediated diagnostic imaging [194]. Initially, these-lipid shelled and gas-filled microspheres (<8 μm diameter) were injected into the bloodstream to aid detection of heart

disease and arterial stenosis [195-197]. More recently, with the advent of more sophisticated imaging techniques, bubbles have been used to study vascular recruitment in tumours, to assess strokes and to detect urinary tract pathologies [194, 198-200]. More relevant to this study, however, is the use of bubbles to deliver high doses of therapeutic compounds to specific organs or sites in the body in a controlled-release fashion [194, 201-204]. Indeed, acoustic stimulation of bubbles has even shown promise in the delivery of therapeutic compounds through the blood-brain-barrier [205]. Moreover, ultrasound-activated bubbles 'decorated' with drug-encapsulating liposomes have been shown to be safe and an efficient intracellular drug delivery system for the treatment of cancer [206-209]. Nonetheless, this potentially advantageous drug delivery technology has yet to be developed for the treatment of UTI.

"Sonoporation" describes the ability for ultrasound to temporarily increase cell permeability and allow passage of cell-impermeant compounds into tissues and intracellular compartments [210]. In the late 1990's and early 2000's, the term 'sonoporation' was coined by researchers looking purely at the effect of ultrasound on biological systems [211-213] [214]. However, the addition of microbubbles, even simple sonicated albumin, dramatically increases cell permeability and viability at lower ultrasound intensities, likely due to a reduction in the cavitation threshold [215-217] [194, 210, 218]. In more contemporary studies, therefore, the term "sonoporation" usually assumes the simultaneous use of bubbles and ultrasound [194, 210, 219].

Cavitation describes the physical reaction of bubbles to an ultrasonic acoustic field. Due to their gas-filled structure, the bubbles expand and contract in response to the rarefaction and compression phases of an ultrasound pressure wave [220]. This phenomenon can manifest as stable or inertial cavitation, the former being a more gentle, stable oscillation and the latter leading to more violent biophysical outcomes [210]. Stable cavitation (Fig. 4) usually arises at lower ultrasound intensities, whereby the bubbles initially grow asymmetrically during each wave cycle until they reach their resonant size [194, 210, 221]. At this point the bubbles exhibit stable, low-amplitude and symmetrical oscillations [194, 210]. Stable cavitation is thought to drive sonoporation via two biophysical effects: 1) perpendicular 'push-pull' forces arising from expansion and contraction phases, which open pores in the nearby cell lipid bilayer (Fig. 4b) and; 2) microstreaming, which describes the transfer of lateral shear forces to the cell membrane via the formation of eddies in the surrounding fluid (Fig. 4c) [194, 210, 219]. Under higher intensities of ultrasound, bubbles demonstrate inertial cavitation (Fig. 5). In contrast to stable cavitation, during inertial cavitation the bubbles oscillate asymmetrically, rapidly swelling beyond their resonant size before collapsing violently (Fig 5) [194, 210]. Although potentially damaging, inertial cavitation can form cell pores via 1) the production of shockwaves at the bubble-cell interface (Fig. 5b) and; 2) a powerful cell-puncturing 'microjet' born from imploding bubbles (Fig. 5c) [194, 210, 219]. Given the robust barrier function of the urinary bladder, including its coverage by uroplakin plaques and the GAG layer, it is entirely possible that traditional forms of drug delivery, such as that bestowed by liposomes, would not provide

sufficient penetrative force to introduce drugs inside cells where they are needed to eradicate intracellular pathogens. Ultrasound-activated bubbles, therefore, are a promising area for developing novel intravesical treatments for UTI.

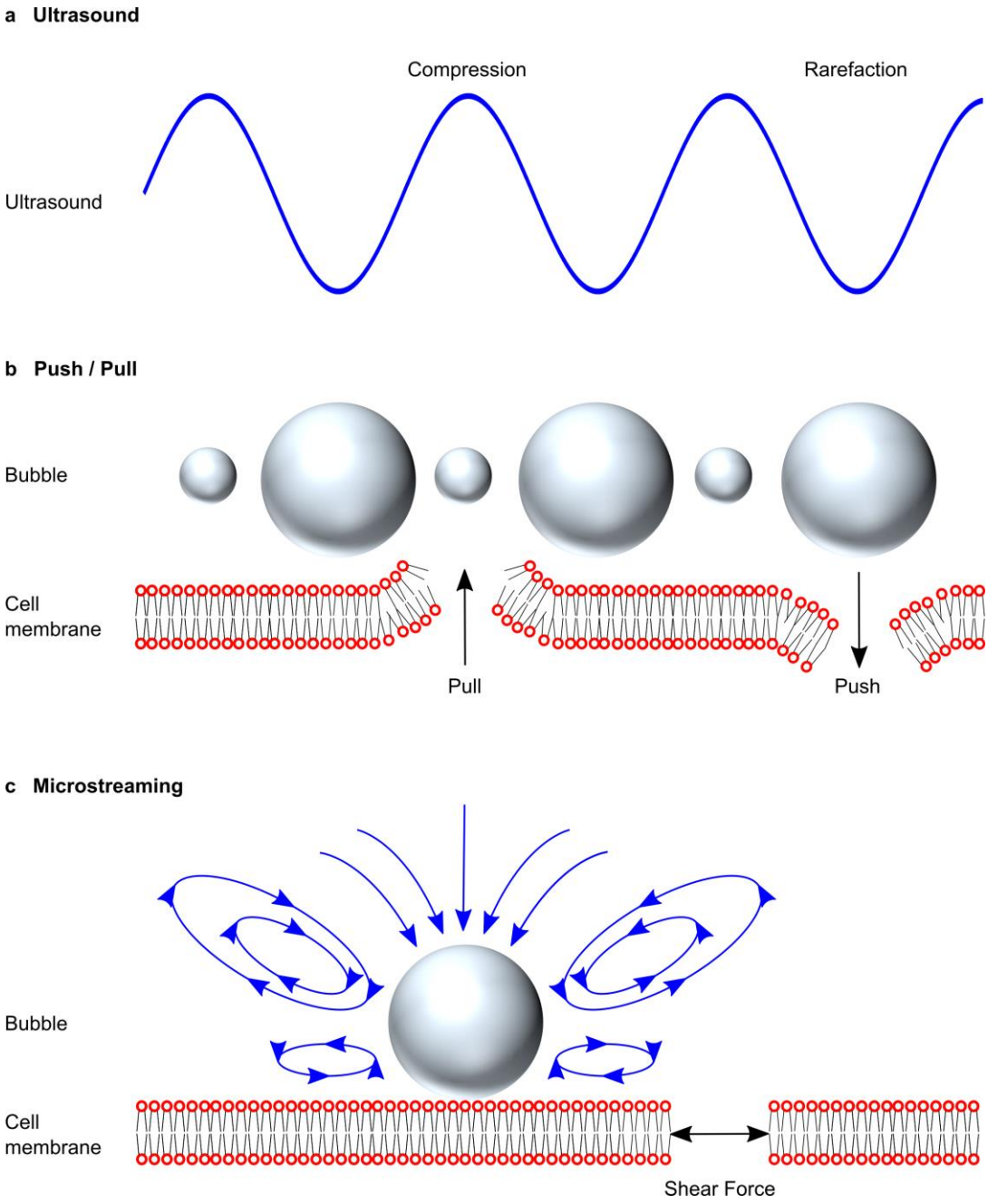

Figure 4. Sonoporation via stable cavitation of microbubbles

Microbubbles exposed to low-amplitude ultrasound radiation oscillate in a linear, symmetrical manner. When exposed to higher-amplitudes of acoustic energy, the bubbles oscillate asymmetrically and grow larger during each wave cycle until they reach their resonant size. At this point, the bubbles undergo stable cavitation, whereby they exhibit stable low-amplitude oscillations. (a) Sine wave representing the compression and rarefaction of an ultrasound pressure wave. (b) In close proximity to cells, microbubbles undergoing stable cavitation produce pores in the cell membranes through

the mechanical push / pull forces exerted during bubble expansion and compression phases. (c) The stable oscillations of microbubbles at the cell surface also produce eddies of fluid flux called microstreams. Microstreaming is thought to cause membrane pore formation through the transfer of notable shear forces to the cell surface.

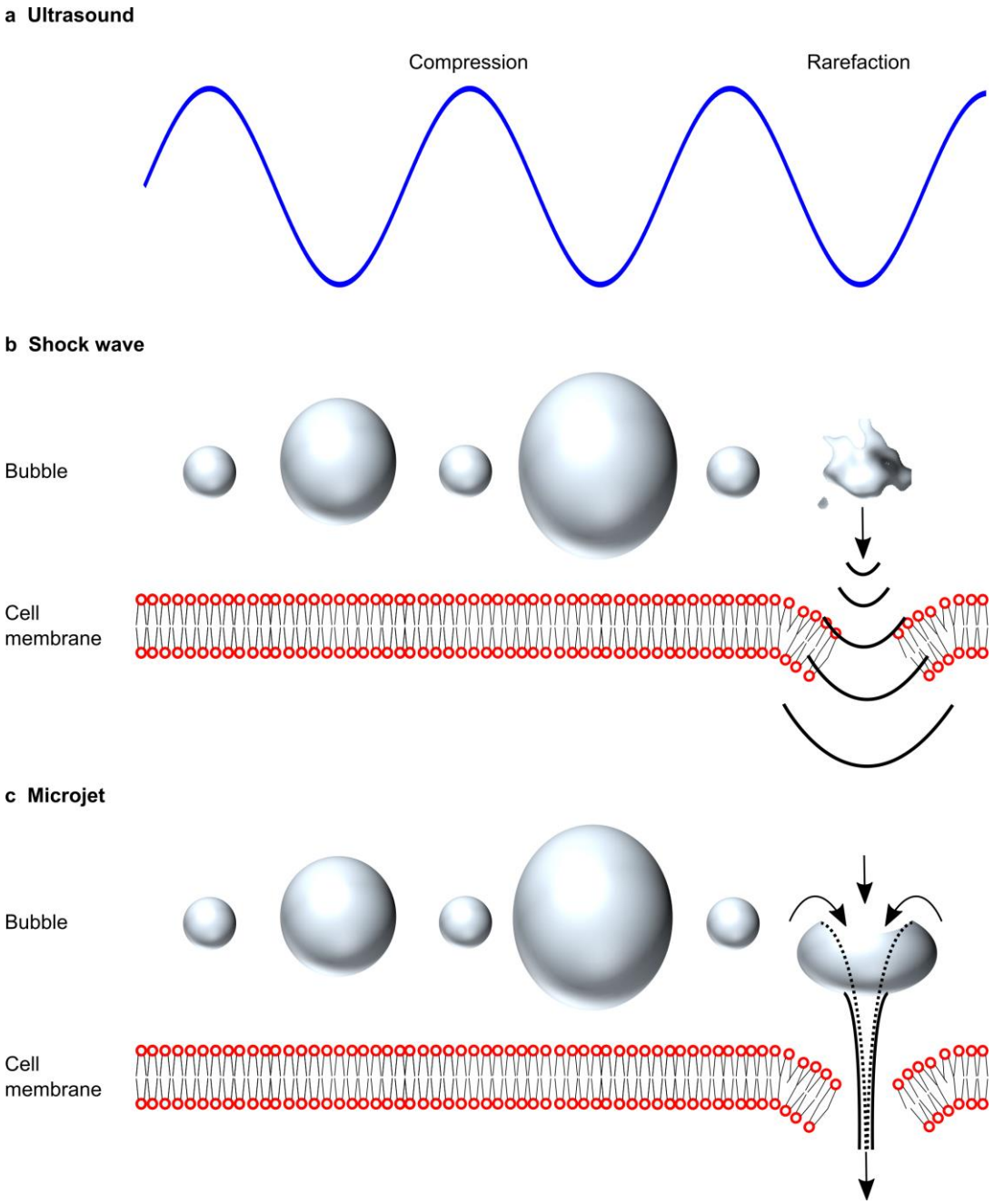

Figure 5. Sonoporation via inertial cavitation of microbubbles

When exposed to ultrasound intensities higher than that required for stable cavitation, microbubbles can exhibit inertial cavitation. During inertial cavitation, the microbubbles expand rapidly during the rarefaction phase but, unlike stable cavitation, they grow beyond their resonant size before collapsing violently. This phenomenon has been shown to drive sonoporation in two ways, namely the production of shock waves and microjets. (a) Sine wave representing the compression and rarefaction of an ultrasound pressure wave. (b) Schematic of microbubble inertial cavitation producing

membrane pores through implosion and the production of shock waves. (c) Violent asymmetric collapse of microbubble near cells can cause the bubble to fold in on itself. This folding leads to the propulsion of a powerful jet of fluid called a microjet through the nearby cell membrane.

1.4 Summary and project aims

In summary, mounting evidence would suggest low-level recurrent UTI to be responsible for a significant proportion LUTS. The prevalence of these diseases is very high, a fact which has resulted in a profound medical economic burden. Given the frequency of bladder infection, therapeutic failure rates and the drawbacks of traditional antimicrobial drugs, a better understanding of chronic UTI in humans along with more efficacious treatments are desperately needed. Our recent work along with other studies highlight differences between the largely UPEC-based acute UTI mouse model and the situation in human patients suffering from LUTS, demonstrating that the mouse model may not be physiologically relevant in all cases and that other uropathogens besides *E. coli* are relevant for study.

Despite the commonness of *E. faecalis* bladder infections and their relevance to catheterised patients, aside from our recent paper [13], there have been no reports of *E. faecalis* associated with patient-derived urothelial cells, nor any description of potential intracellular invasion more direct than the antibiotic protection assay. We therefore set out to explore the role of cell shedding and bacterial invasion in LUTS in more detail. Furthermore, we

now know that mouse urothelium is developmentally and functionally different to native human tissue. Given recent advances in 3D tissue culture [222], along with the questionable relevance, expense and ethical factors involved in animal research [70-72], we proposed to design a protocol to engineer organotypic human urothelium which could be used as a replicable test bed for infective disease formation, treatment and resolution in humans. We then proposed, in collaboration with Professor Eleanor Stride's team at The Institute of Biomedical Engineering, Oxford University, to test the plausibility of ultrasound-activated microbubble technology as a novel intravesical treatment for UTI.

1.5 Objectives

1. Investigate the role of cell shedding in LUTS patients and inspect these cells for signs of bacterial association, including by species other than *E. coli*

2. Explore the ability of patient-derived bacteria to invade and colonize cell culture model systems

3. Design a protocol to grow physiologically relevant human urothelium *in vitro* as assessed by morphology, ultrastructure and biomarker expression. Use this system as a test bed for disease formation, treatment and resolution

4. Asses the use of novel ultrasound-activated microbubbles as an intracellular drug delivery system for the treatment of UTI

1.6 Overall hypothesis

UTI is not one distinct disease but rather a biological continuum which may exhibit overlapping pathophysiological states requiring different treatment approaches

1.7 Specific hypotheses

1. *Enterococcus faecalis* invades cells of the urothelium

2. We can create a physiologically reminiscent 3D organoid from human stem cells

3. Ultrasound-activated microbubble therapy represents a safe and efficacious option for the treatment of UTI in an *in vitro* model

Chapter 2

Enterococcus faecalis Subverts and Invades the Host Urothelium in Patients with Chronic Urinary Tract Infection

2.1 Abstract

Bacterial urinary tract infections (UTI) are a major growing concern worldwide. Uropathogenic *Escherichia coli* has been shown to invade the urothelium during acute UTI in mice and humans, forming intracellular reservoirs that can evade antibiotics and the immune response, allowing recurrence at a later date. Other bacterial species, such as *Staphylococcus saprophyticus*, *Klebsiella pneumonia* and *Salmonella enterica* have also been shown to be invasive in acute UTI. However, the role of intracellular infection in chronic UTI causing more subtle lower urinary tract symptoms (LUTS) is poorly understood. A previous study of a large cohort of non-acute LUTS patients found that *Enterococcus faecalis* was frequently found in urine specimens. *E. faecalis* accounts for a significant proportion of chronic bladder infections worldwide, although the invasive lifestyle of this uropathogen has yet to be reported. Here, we wanted to explore this question in more detail. We harvested urothelial cells shed in response to inflammation and, using advanced imaging techniques, inspected them for signs of bacterial pathology and invasion. We found strong evidence of intracellular *E. faecalis* harboured within urothelial cells shed from the bladder of LUTS patients. Furthermore, using a culture model system, these patient-isolated strains of *E. faecalis* were able to invade a transitional carcinoma cell line. In contrast, we found no evidence of cellular invasion by *E. coli* in the patient cells or the culture model system. Our data show that *E.*

faecalis is highly competent to invade in this context; therefore, these results have implications for both the diagnosis and treatment of chronic LUTS.

2.2 Materials and methods

2.2.1 Ethics statement

Ethical committee approval for human urine sampling was obtained from The National Ethics Service (NRES, see Appendix 3). All study participants gave written consent to participate in the study and the process was documented as per Good Clinical Practice (GCP) and MHRA guidelines. The participants were assigned randomly generated study numbers which were used to anonymise all data and samples. Analysis was carried out by blinded researchers.

2.2.2 Patient sampling

Sampling was conducted at Professor James Malone-Lee's LUTS outpatient clinic, University College London, Division of Medicine. We sampled from 705 adults aged ≥18 years who were able to give consent and who were diagnosed with LUTS (see Figure 6 for a summary of the cohort's demographics and symptoms), excluding any patient with symptoms of acute UTI, with concurrent illnesses that in our opinion were likely to compromise the validity of the data, and pregnant women or those planning to conceive. When controls were required, we recruited with consent from staff that did not have any LUTS. All laboratory experiments used randomly selected sub-

sets of the main patient cohort. Details can be found in the respective results sections.

In all cases, subjects were provided with a sterile container and two hypoallergenic wipes. They were then given detailed (written and oral) instructions on meticulous MSU capture technique, namely (1) to wash their hands and thoroughly cleanse genital area with a hypoallergenic wipe to prevent contamination from the surrounding external genitalia; (2) to part labia or retract foreskin and urinate a small amount into the toilet before moving the container into the urine stream; and (3) to remove the container before urination was complete, thereafter to seal the container. The urine sample was divided into two aliquots. The first was submitted to immediate microscopy using a haemocytometer to enumerate leukocytes (WBC μl^{-1}) and shed epithelial cells (EPC μl^{-1}). The second aliquot, as per standard clinical guidelines, was sent for routine MSU culture at the Whittington Hospital NHS Trust, London, UK. The sampled urine was treated fresh, or after overnight storage at 4°C at the hospital laboratory. 1µl of urine was transferred by calibrated loop to chromogenic media, CPS3 (bioMerieux). The plate was incubated aerobically for 24 hrs at 37°C. Bacterial colonies were identified at the genus level by colour change. The result was reported as positive if greater than 10^5 (MSU) colony forming units (CFU) ml^{-1} of a single known urinary pathogen were observed.

2.2.3 Bacterial identification at the species level

To corroborate confocal data and identify bacteria prior to the invasion assays, the routine urine procedure above was repeated in-house with the addition of a dilution series and extensive phenotypic analyses to confirm bacterial identity at the species level.

For each sample, 50µl of undiluted urine and three serial dilutions (1:10, 1:100 and 1:1000) were added to the respective quartile of a chromogenic CPS3 agar plate (bioMérieux) before aerobic incubation for 24 hours at 37°C. Following incubation, the different coloured colonies present on the chromogenic agar were identified using the manufacturer's colour criteria. The colonies found in this study were identified as follows: *E. coli*; medium sized burgundy, pink or mauve colonies and *Enterococcus spp.*; small turquoise colonies.

To further confirm the identity as *E. coli*, the isolates were shown to be bacillus in morphology and negative under Gram staining, indole positive and identified as *E. coli* using API 20E (bioMérieux) biochemical test strips. Each of the *Enterococcus spp.* tested in this study were found to be *E. faecalis* owing to a coccoid morphology, positive Gram stain, negative catalase test, positive bile esculin test and by being identified as *E. faecalis* using API 20 Strep (bioMérieux) biochemical test strips.

2.2.4 Cell culture

A transformed cell line derived from a human bladder carcinoma (T24) [81] was kindly donated by Dr.Aled Clayton, Institute of Cancer and Genetics, School of Medicine, Cardiff University, United Kingdom. T24 cells were cultured at 37°C in a humidified incubator under 5% CO_2 in 9 cm dishes in RPMI 1640 medium (Gibco) supplemented with 10% foetal bovine serum (FBS, PAA) and antibiotics (50 µg/ml penicillin and 50 mg/ml streptomycin; Gibco). Cells were maintained, pre-experimentation, by splitting 1:20 at 80% confluency. All work was carried out within sterile class-II flow cabinets under strict aseptic conditions.

2.2.5 Immunofluorescence staining of patient samples

80µl of a urine specimen was added to a Shandon single funnel cuvette assembly containing a pre-labeled glass slide and a Shandon filter card (Fisher Scientific). This assembly was centrifuged in a Shandon Cytospin 2 cytocentrifuge at 800rpm (≈75g rcf) for 5 minutes resulting in a visible disc of urinary particulate deposited on the slide, which was circumscribed with a hydrophobic barrier pen (ImmEdge pen, Vector Laboratories). The cells were fixed in 4% formaldehyde (Thermo Scientific, Fisher Scientific) in phosphate buffered saline (PBS, Sigma-Aldrich) at RT for 15 minutes. The formaldehyde was aspirated and the preparation washed three times with PBS at 5 minute intervals. For uroplakin-III staining, cells were permeabilised

with 0.2% Triton-X100 (Sigma-Aldrich) in PBS for 5 minutes at RT followed by a single wash with PBS. The preparation was then blocked with 5% normal goat serum (Sigma-Aldrich) in PBS for 30 minutes prior to a 1 hour incubation with a 1:10 dilution of primary anti-uroplakin-III mouse monoclonal antibody (Progen Bioteknik) in 1% bovine serum albumin (BSA, Sigma-Aldrich). Following 3 further PBS washes, cells were incubated at RT for 40 minutes in a solution containing a 1:250 dilution of goat anti-mouse secondary antibody conjugated to Alexa Fluor-555 (Invitrogen), 1µg/µl of the DNA counterstain 4'',6-diamidino-2-phenylindole, (DAPI, Sigma-Aldrich) and 1% BSA in PBS.

For assessing bacterial infection, after fixation as above, wheat germ agglutinin (WGA) conjugated to Alexa Fluor-488 (Invitrogen) was used to label the cell membrane to aid cellular identification and demarcation, and to assess biofilm formation where applicable. Following 15 minutes of incubation at RT with 1µg/ml WGA in Hank's balanced salt solution minus phenol red (HBSS, Invitrogen), the labeling solution was removed and the cells washed twice at 5 minute intervals with HBSS. Fluorescent counterstaining of host and pathogen DNA was achieved through the addition of DAPI at 1µg/ml in PBS. After incubation for 15 minutes at RT, the DAPI solution was removed and the sediment washed twice in PBS. Following staining for uroplakin-III or infection, the preparations were immediately mounted with FluorSave reagent (Calbiochem) and a coverslip fixed in place with clear nail varnish. The percentage of UP3-positive cells was calculated by a blinded researcher using epi-fluorescent microscopy.

Counts were carried out in triplicate. Images were also taken using scanning confocal microscopy on a Leica SP5.

2.2.6 Invasion assay

5 frozen *Enterococcus faecalis* and 5 frozen *Escherichia coli* strains previously isolated and typed from human LUTS patients were grown on fresh chromogenic CPS3 agar plates. After aerobic incubation for 24 hours at 37°C, a colony from each of these 2 bacterial cultures was transferred to a 5ml sterile aliquot of LB, and incubated aerobically at 37°C for 24 hours. Two of the 5 *E. coli* isolates underwent stationary incubation and the remaining 3 shaking incubation at 300rpm to control for FimH expression in these strains, as stationary growth has been reported to promote expression of this virulence factor [223]. In our hands, the two different methods of culture produced similar functional FimH behaviour. *E. faecalis* isolates were all incubated in a shaking incubator at 300rpm. The level of growth was checked for each bacteria using a spectrophotometer and diluted as necessary with fresh LB to an A600 of approximately 0.5 [224]. Lab-Tek II 8 well chamber slides (Nunc, Thermo Scientific) were coated with 200µl of FBS and incubated for 2 hours at 37°C before aspiration. T24 cells were plated at $8x10^4$ cells per well in a total volume of 400 µL and incubated for 24 hours at 37°C under 5% CO_2 to allow cells to spread, then washed twice with PBS to remove routine antibiotics. Each of the bacterial LB cultures was diluted in CO_2-independent media (CIM, Gibco) supplemented with 10% FBS (with routine antibiotics omitted) and 200µl added to the cultured T24 cells giving a

multiplicity of infection (MOI) of approximately 10-15 bacteria per mammalian cell [224]. Cells were infected at 37°C for between 1 and 4 hours within a humidified aerobic incubator to optimise experimental parameters.

Post infection, cells were inspected for morphological changes and viability before the addition of a combination of membrane-impermeable antibiotics to kill extracellular bacteria and to limit further cellular damage [13, 112, 113, 224]. Briefly, infected CIM was carefully removed and a solution of gentamicin, linezolid and amoxycillin (Whittington Health NHS Trust Pharmacy, London) in 200µl fresh CIM was added at varying concentrations. Concentrations of gentamicin (200µg/ml), linezolid (25µg/ml) and amoxycillin (250µg/ml) were found to be most effective (adapted from [13]). The chamber slide was incubated, with antibiotics, aerobically for a further 24 hours at 37°C, after which the cells were fixed in 4% formaldehyde in PBS for 15 min at room temperature before washing three times in PBS at 5 minute intervals. The cell membranes were stained with 200µl WGA (1µg/ml) conjugated to Alexa Fluor-488 in HBSS minus phenol red for 15 min at RT. The labelling solution was removed and the cells washed twice at 5 minute intervals with HBSS. 0.2% Triton-X100 in PBS was then added and the cells allowed to incubate at room temperature for 5 min. Following removal of the Triton-X100, the permeabilised cells were washed once with PBS before staining with a 200µl solution of TRITC-conjugated phalloidin (0.6µg/ml) (Sigma-Aldrich), to label filamentous actin, and DAPI (1µg/ml) in PBS for 40 min at RT. The dual-labelling solution was gently aspirated and the cells

washed 3 times in PBS before removal of the upper-well section of the Lab-Tek II chamber slide and immediate mounting as above.

2.2.7 Imaging and Analysis

We performed epi-fluorescence microscopy on an Olympus CX-41 and Leica DM4000B upright microscope, and confocal laser scanning microscopy on a Leica SP5 microscope. Images were processed and analysed using Infinity Capture and Analyze V6.2.0, ImageJ 1.49o [225] and the Leica Application Suite, Advanced Fluorescence 3.1.0 build 8587 Software.

2.3 Results

2.3.1 Significant urothelial shedding in the LUTS bladder

In order to study the role of infection and inflammation in LUTS, and to determine whether shed epithelial cells could be used as a further means of studying intracellular infection in more detail, we recruited 705 patients presenting at first visit to the clinic, 606 females and 99 males with a mean age of 51 years (sd=17.5). Of the 705 urine samples, 522 (74%) were found to be negative on routine mid-stream urine (MSU) culture (using a culture positive threshold of $\geq 10^5$ cfu ml^{-1} of a single known uropathogen) and 183 (26%) were positive. It should be noted that this routine MSU culture threshold, while standard for the UK and some other countries, misses significant infection in our clinical experience. For main demographic data and symptomatology please see Figure 6.

A

Demographic	LUTS patients (N)
Cohort (total)	705
Gender Male	99
Gender female	606
Negative MSU (< 10^5 cfu ml^{-1})	522
Positive MSU (≥ 10^5 cfu ml^{-1})	183
Zero pyuria	215
Pyuria 1 to 9 WBC μl^{-1}	253
Pyuria ≥ 10 WBC μl^{-1}	202

	Mean	Std Deviation	95% CI		Median	Interquartile range	
			lower	upper		25%	75%
Age (years)	51.36	17.51	50.07	52.66	51	38.5	65
Duration of symptoms (years)	5.03	3.82	4.71	5.35	3	2	10
24hr urinary frequency	11.86	6.1	11.34	12.37	10	7	15
24hrs urinary incontinence	1.09	1.55	0.96	1.22	0.5	0	1.5
Number of urgency symptoms	2.93	2.80	2.73	3.14	3	0	5
Number of pain symptoms	1.50	2.49	1.31	1.68	0	0	2
Number of stress inc symptoms	0.74	1.43	0.64	0.85	0	0	1
Number of voiding symptoms	2.33	2.35	2.16	2.51	2	0	4
Number of LUTS (total)	7.56	5	7.14	7.98	7	4	11

B

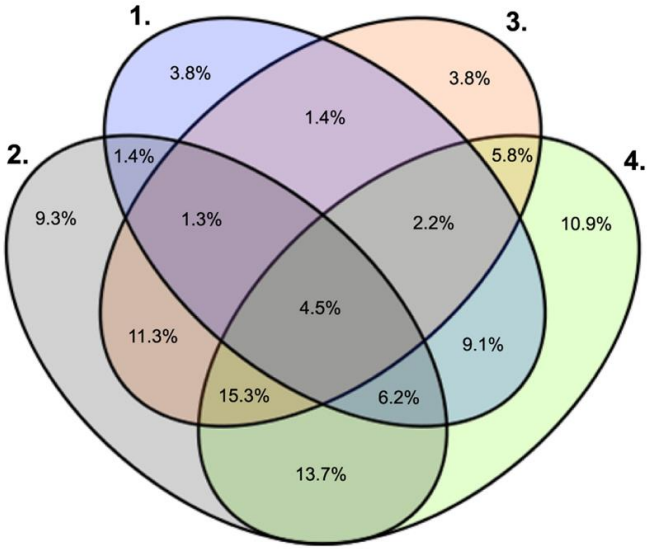

1.

≥ 1 Stress Incontinence
Exercise Incontinence
Lifting Incontinence
Laughing Incontinence
Passive Incontinence
Bending Incontinence
Standing Incontinence

2.

≥ 1 Voiding Symptoms
Hesitancy
Reduced Stream
Intermittent Stream
Straining to Void
Terminal Dribbling
Post Void Dribbling
Double Voiding

3.

≥ 1 Pain Symptoms
Suprapubic Pain
Filling Bladder Pain
Voiding Bladder Pain
Post Void Bladder Pain
Pain Fully Relieved by Voiding
Pain Partially Relieved by Voiding
Pain Unrelieved by Voiding
Loin Pain
Iliac Fossa Pain
Pain Radiation to Genitals
Pain Radiation to Legs
Dysuria
Urethral Pain

4.

≥ 1 OAB Symptoms
Urgency
Urgency Incontinence
Latchkey Urgency
Latchkey Incontinence
Waking Urgency
Waking Incontinence
Running Water Urgency
Running Water Incontinence
Cold Urgency
Anxiety Urgency
Premenstrual Aggravation

Figure 6. Demographics and symptoms

(A) Key demographic information. (B) A four-way Venn diagram illustrating the overlap of symptoms amongst the 705 patients studied. The ellipses circumscribe patients who had one or more symptoms in the particular subset. Each ellipse corresponds to a numbered list of specific symptoms.

The diagram is not scaled to the size of sets. Abbreviations; MSU (mid-stream urine culture); Pyuria (presence of white blood cells in the urine); WBC (white blood cell); inc (incontinence); LUTS (lower urinary tract symptoms); OAB (overactive bladder).

Pyuria (white blood cells [WBC] μl^{-1}), quantified immediately in fresh, unspun specimens of urine, is the best clinical indicator of UTI currently available. The patients were categorised into three groups according to pyuria expression: (1) for zero pyuria; (2) for pyuria 1 to 9 WBC μl^{-1}; and (3) for pyuria ≥10 WBC μl^{-1}. Pyuria ≥10 WBC μl^{-1} has long been advocated as a diagnostic threshold to discriminate between the presence or absence of lower urinary tract pathology. First described by Dukes in 1928 [226], this diagnostic threshold does not withstand contemporary scientific scrutiny [48], and there are no published data demonstrating that pyuria of 1 to 9 WBC μl^{-1} is non-pathological [227]. Indeed, 1-9 WBC μl^{-1} does predict underlying disease [227], so we thought it prudent to include this category.

In addition to WBC, mouse and human bladders shed urothelial cells into the urine as part of an innate immune response to bacterial insult in acute UTI [96, 100-103]. Therefore, we also counted epithelial cells (EPC μl^{-1}) in the urine of LUTS patients. First, we recognized the requirement for proof of cellular origin as a proportion of these cells could be contaminants originating from the genitalia and perineum. Uroplakin-III (UP3) is expressed solely on the asymmetric unit membrane of urothelial cells [76, 228]. Therefore, we targeted this glycoprotein using immunofluorescence to determine the

proportion of urinary epithelial cells that originated in the urinary tract (Fig. 7A,B). A subset of 44 randomly selected LUTS patients was included in this experiment. MSU samples from 22 patients with chronic LUTS (F=22; mean age=51; sd=19) were compared with vaginal swabs from 22 further chronic LUTS patients (F=22; mean age=50; sd=20). The median percentage of UP3-positive cells in the MSU samples was 75% (Q1=68, Q3=78.5) but only 25% (Q1=19, Q3=32) in the vaginal swabs (Fig. 7C). The results of a Mann-Whitney test show the proportion of UP3-positive cells found in the urine of chronic LUTS patients to be significantly higher than that in the vagina ($U=1$, $p < .001$). Therefore, we could be confident that our cell analyses were representative of underlying pathology of the bladder.

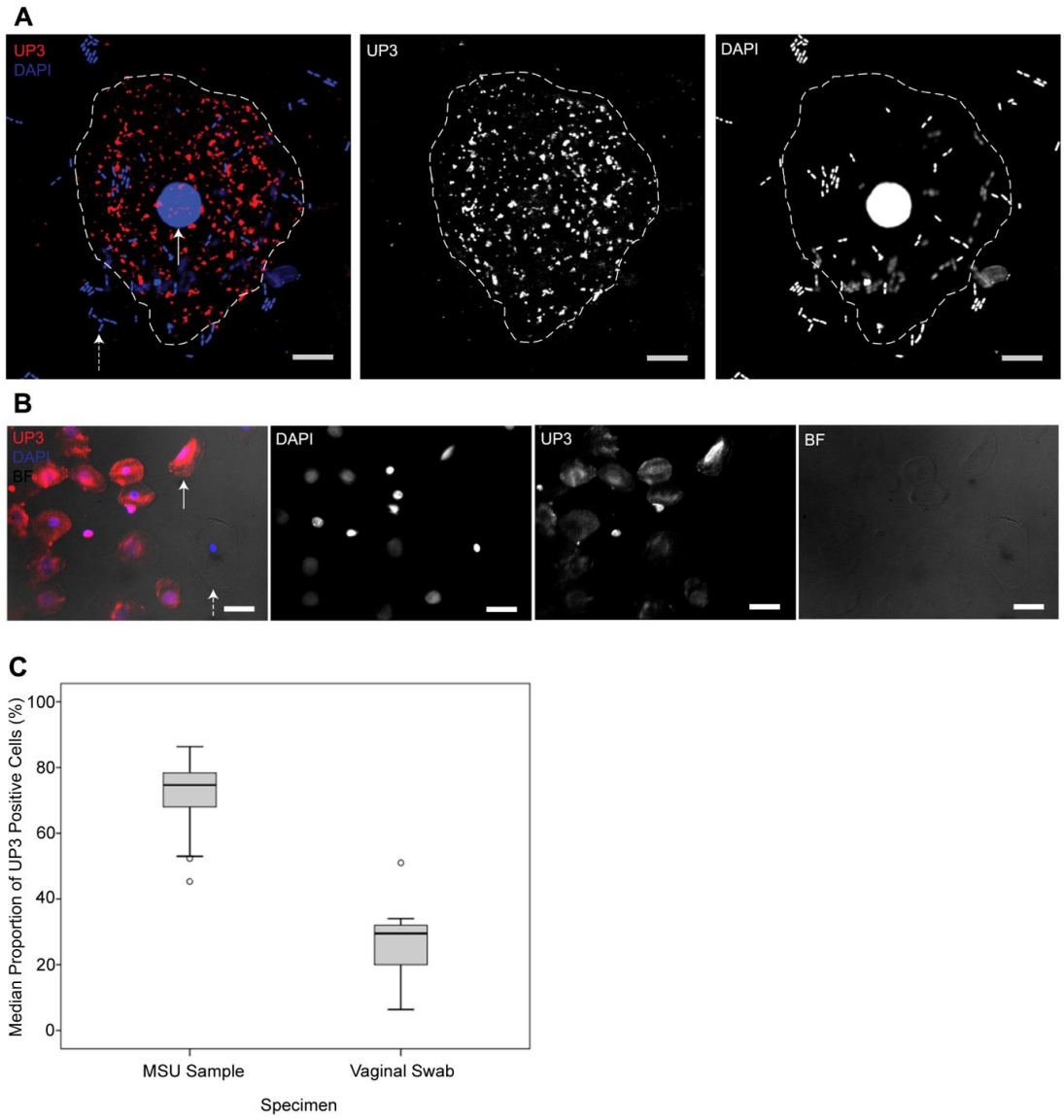

Figure 7. Uroplakin-3 (UP3) immunofluorescence

(A) Confocal image of a UP3-positive urothelial cell shed into the urine of a LUTS patient, a composite showing the expression of UP3 in red and DAPI-stained host (solid white arrow) and bacterial (broken white arrow) DNA in blue. Each channel is also shown in monochrome. The boundary of the cell is represented by a broken white line. White scale bar represents 10µm. (B) Epi-fluorescent image of UP3-positive urothelial cells (solid white arrow) and a single UP3-negative epithelial cell (broken white arrow) harvested from the urine of a patient with LUTS. The composite image shows UP3 in red, host DNA in blue and the brightfield (BF) channel in greyscale. Channels are also shown separately in monochrome. White scale bar is 50µm. (C) Graph

showing the median proportion of UP3-positive cells found in MSU samples (N=22) when compared with vaginal swabs (N=22). 75% (Q1=68, Q3=78.5) of the cells found in the MSU samples were UP3-positive in contrast to only 25% (Q1=19, Q3=32) in the vaginal swabs (U=1, p <.001).

We counted shed EPC in the 705 patient cohort (FIG 8A). The EPC counts were positively skewed and log transformation had a limited normalisation effect, changing the skewness from 13.4 to 0.63. We therefore compared the median $\log_{10}$ epithelial cell count ($\log_{10}$ EPC μl^{-1}) between categories, non-parametrically. Figure 8A shows clear between group differences between these categories (Kruskal-Wallis $X^2 = 75$, $p<.001$, $df=2$). Post hoc analysis using Mann-Whitney test comparisons with a Bonferroni correction confirmed that all three groups differed among one another ($p<.001$). A similar comparison between the 522 (74%) showing a negative MSU culture and the 183 (26%) that were positive showed no between group differences ($U=19x10^3$, $p=.5$). Therefore, the degree of EPC shedding corresponds to amount of pyuria, and by association, severity of infection.

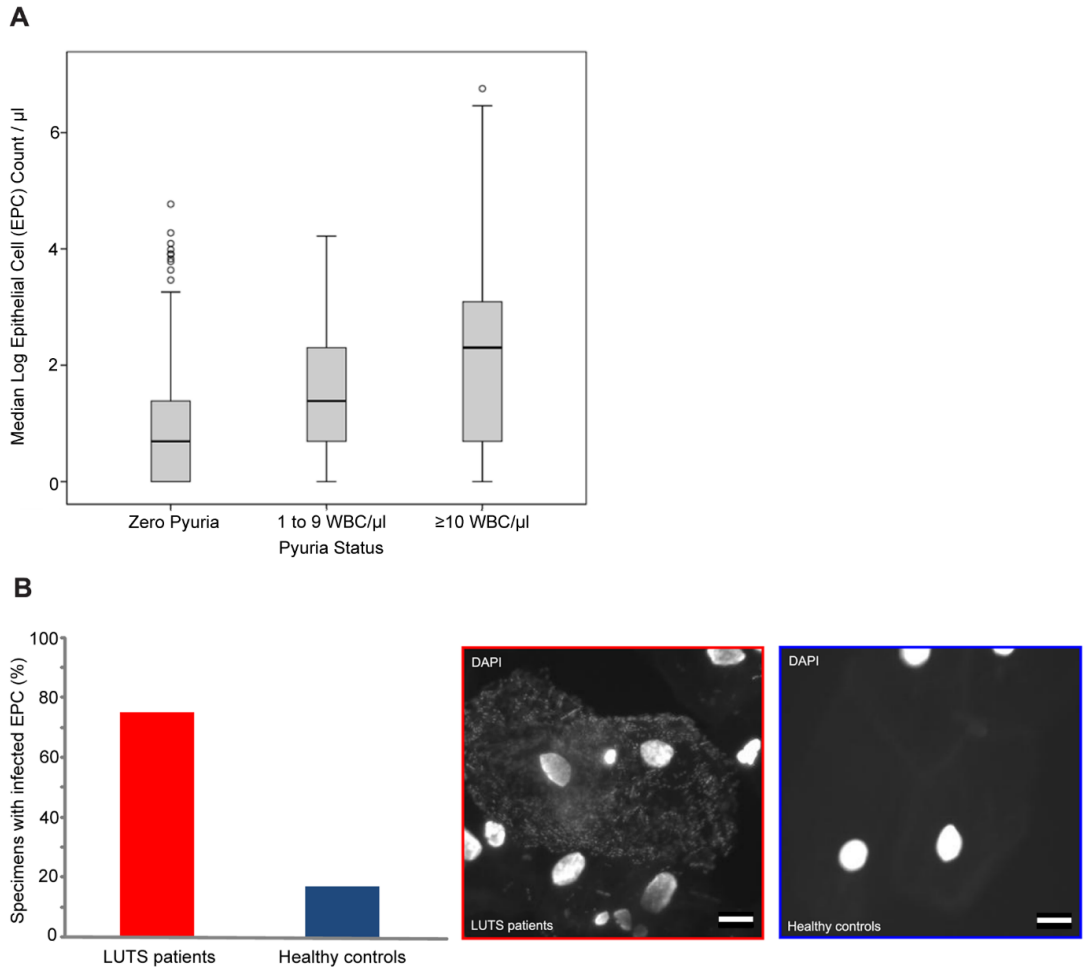

Figure 8. Urinary epithelial cell counts and bacterial pathology

(A) Relationship between the median log urinary epithelial count (EPC=epithelial cell) and the level of pyuria observed in the urine of LUTS patients (WBC=white blood cell). The median log epithelial cell counts at each state of pyuria proved to be significantly different. (B) Bar chart showing the percentage of specimens with bacteria-association urinary epithelial cells (EPC) in LUTS patients (75%) and healthy controls (17%). Representative images of infected urinary EPC from LUTS patients (red) and normal EPC for healthy controls (blue) shown for reference. White scale bar is 10µm.

In summary, this evidence supports the murine model of bacteria-induced urothelial inflammation and shedding in LUTS patients. Given that infection seemed to correlate with symptoms in this cohort, we set out to study the underlying microbiology in closer detail.

2.3.2 Implicating intracellular *E. faecalis* bacterial infection in the aetiopathology of LUTS

As with previous work exploring cellular invasion during acute UTI in humans [96], we inspected shed urothelial cells from LUTS patients with non-acute UTI for signs of bacterial association and intracellular pathology. Prior to imaging, the urine samples were cultured on chromogenic agar and any arising bacteria identified using a rigorous series of biochemical assays as outlined in the methods section.

For this experiment we studied a randomly selected subset of 48 specimens using epi-fluorescent microscopy to identify bacterial involvement. MSU samples were donated by 24 female LUTS patients (mean age=52; *sd*=10.7) and compared with an equal number of samples from female healthy normal controls (*N*=24; mean age=48; *sd*=9.9). Although these 24 LUTS patients were negative for routine MSU culture, growing $<10^5$ cfu ml^{-1} of a single known uropathogen, 10 exhibited growth of *E. coli* and/or *E. faecalis* with the addition of other species. One of these samples exhibited growth of only *E. coli* and *E. faecalis* with no other species present which gave us the

opportunity to compare how each bacterium behaved. This sample was selected for confocal microscopy to explore intracellular pathology.

Our previous work, which explored intracellular colonisation of the LUTS bladder, presented data from antibiotic protection assays alone [13]. This microbiological data is indirect and can be misleading, as detergents may liberate live membrane-bound bacteria. This technique is hindered further by the presence of extracellular biofilms which may be unaffected by even high concentrations of antibiotics. Therefore, to decisively inspect these cells for intracellular colonisation we conducted confocal laser-scanning microscopy in conjunction with a bank of extensive 3D digital analyses.

On epi-fluorescent analysis, 75% (N=18) of the LUTS patient samples showed evidence of infected urothelial cells in comparison to only 17% (N=4) in the control group (Fig. 8B). Data from the confocal analysis of a representative sample suggested that *E. faecalis* and *E. coli* employ distinct pathological strategies in these patients, with only *E. faecalis* exhibiting cellular invasion. Figure 9 shows two representative cells shed from the bladder of a LUTS patient with a mixed sub-threshold infection with *E. faecalis* and *E. coli.* Cells that were associated with adherent extracellular bacilli (*E. coli*) did not contain intracellular bacterial communities (Fig. 9D). However, in cells exhibiting adherent, extracellular coccoid *E. faecalis* (Fig. 9A, broken white arrow), we found compelling evidence of intracellular pathology (Fig. 9A, white arrow, B,C). Although uropathogenic *E. coli* have the unusual ability to transform from a rod to coccoid morphology within the

intracellular niche within the centre of a tightly packed IBC [95, 96], we saw isolated intracellular coccoid forms, too dispersed to be coccoid *E. coli,* suggesting that the organism was indeed *E. faecalis*.

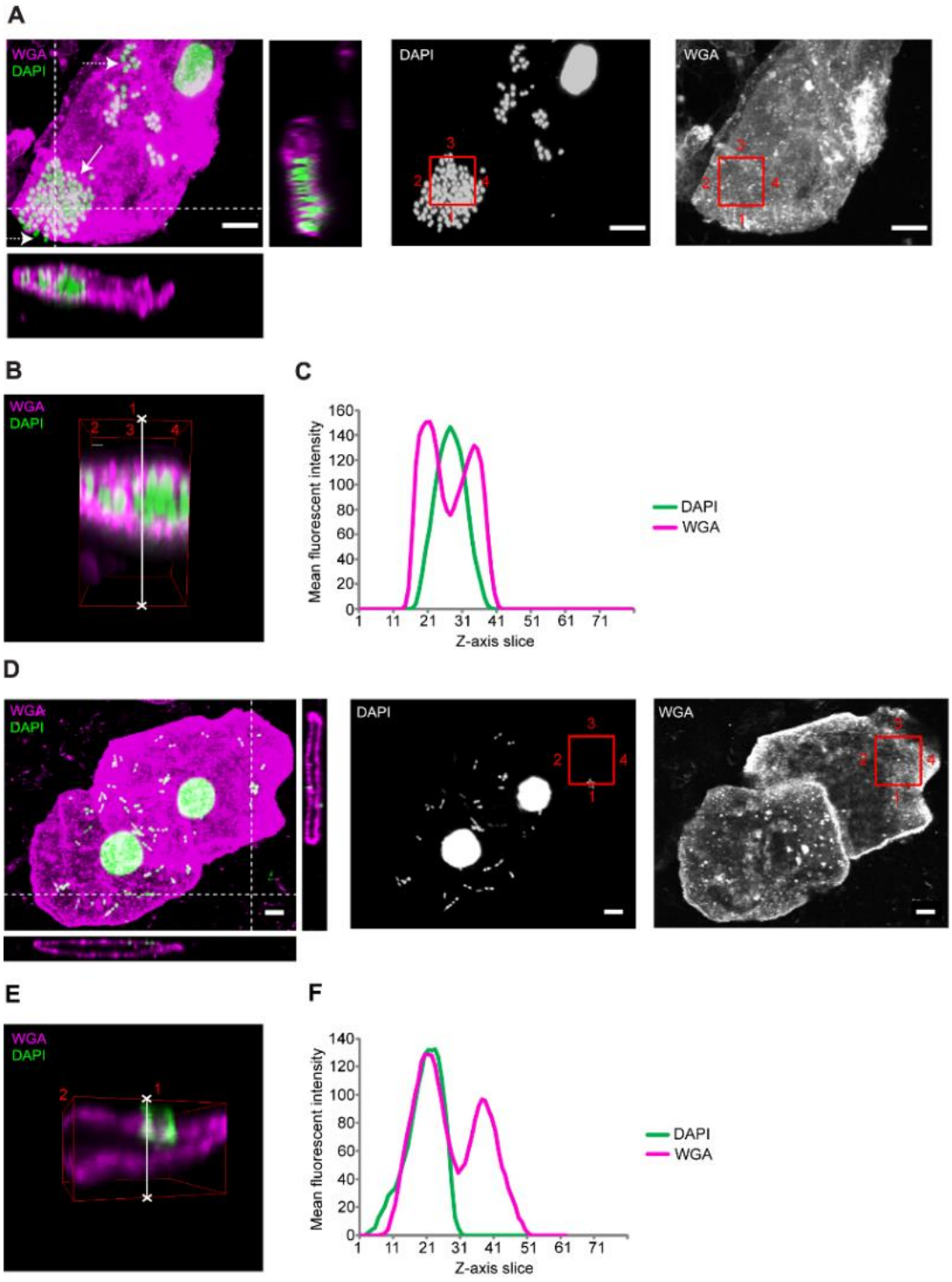

Figure 9. Bacterial invasion in shed urothelial cells

By supporting the confocal data with culture results and bacterial identity we were able recognize bacteria by morphology during confocal analysis. (A) Maximum projection confocal image of a cell shed from the bladder of a LUTS patient with a mixed sub-threshold infection with *E. faecalis* and *E. coli*. The left image is a composite showing the wheat germ agglutinin

(WGA)-stained plasma membrane in magenta and DAPI stained host and bacterial DNA in green. Solid white arrow highlights a cluster of intracellular coccoid bacteria, broken white arrow highlights extracellular coccoid bacteria. Bacteria were identified as *E. faecalis* owing to morphology. Orthogonal views are through entire Z-stack at a position corresponding to white broken lines on the left image, showing intracellular colonisation. The centre and right image show the respective DAPI and WGA channels in monochrome. White scale bar is 5µm. (B) A 3-dimensional volume through the entire Z-stack at a position corresponding to the red squares in image A (numbered for orientation); bacteria are clearly residing within the cell. (C) A region of bacterial colonisation was selected (highlighted by the white line in 3D construct B) and used to produce a Z-axis profile plot, which presents the average pixel intensity of a given channel moving through the 80-slice Z-stack. This graphical representation shows further evidence of cellular invasion, with the peak mean pixel intensity of the DAPI channel (*E. faecalis*, green) corresponding with a striking reduction in the WGA (plasma membrane, magenta) channel at slice 29 (~centre of the cell). (D) Maximum projection confocal image of a cell shed from the same patient as above with a mixed sub-threshold infection with *E. faecalis* and *E. coli*. Images were analysed and presented as above. Bacteria were identified as *E. coli* owing to bacillus morphology. Orthogonal views show the *E. coli* to be strongly associated with the plasma membrane but entirely extracellular. White scale bar is 5µm. (E) 3-dimensional volume corresponding to the red squares in image D (numbered for orientation); again, the *E. coli* were shown to be ubiquitously extracellular. (F) A region of bacterial colonisation was selected (highlighted by the white line in 3D construct E) to produce a Z-axis profile plot. This graphical representation shows further evidence of external cellular colonisation alone. The peak mean pixel intensity of the DAPI channel corresponded with that of the WGA stained apical plasma membrane channel at slice 21.

2.3.3 LUTS patient-isolated *E. coli* does not invade cells in a cell culture model system

So far, we have shown that the presence of LUTS is associated with shedding of the urothelium, which is likely activated by the presence of bacteria. The confocal data from analysis of shed patient cells suggested that *E. faecalis* employed an invasive lifestyle whereas *E. coli* was ubiquitously extracellular.

Given the difficulty of identifying in advance patient cells that harboured *E.coli* and/or *E. faecalis* in the absence of other species, we decided to use defined infections in cell culture to explore this issue further. We designed a cell culture system to model the infection process using five strains of *E. coli* isolated from routine MSU-culture negative LUTS patients. We infected a T24 transitional bladder cell line before, as with the shed urothelial cells, fluorescently staining and imaging using high-resolution confocal microscopy. The invasive properties of these strains were analysed using a series of 3D digital analyses.

All of the five *E. coli*-infected T24 cells exhibited marked bacterial adhesion and colonisation (See Fig. 10A,D for a representative example). Orthogonal views of Z-stack 3D constructs, however, showed the colonies of each strain of bacteria to be entirely extracellular (Fig. 10B). Further analysis using Z-axis profile plots supported these findings, with the peak mean pixel intensity

of the DAPI labelled bacteria (blue) found to be some distance away (in the Z-axis) from that of the phalloidin labelled F-actin (red) (Fig. 10C).

Remarkably, it appeared that these LUTS-isolated strains of *E. coli* formed tightly packed extracellular biofilms on the surface of the T24 cells (Fig. 10D). Positive staining with wheat germ agglutinin (WGA) in a Gram-negative organism like *E. coli* signifies the secretion of an exopolymeric matrix, inherent in biofilm formation (Fig. 10A, white arrows) [229] [230].

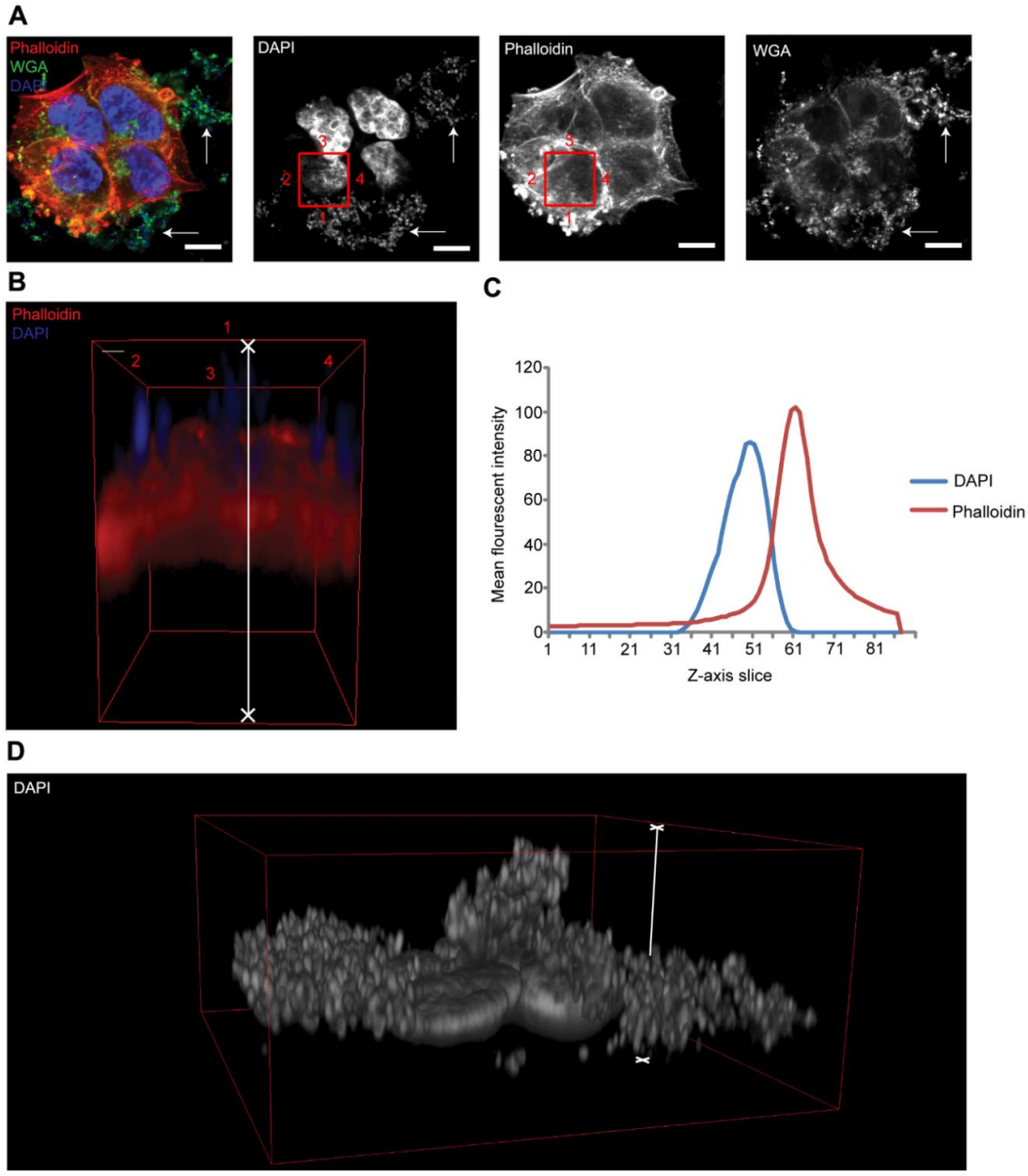

Figure 10. 3D confocal analysis of cultured cells infected with LUTS-isolated *E. coli*

(A) Confocal image of a group of T24 cells infected for 2.5hrs with *E. coli* isolated from LUTS patients at an MOI of approximately 10-15 bacteria per mammalian cell. The left image is a composite showing the phalloidin-stained F-actin in red, wheat germ agglutinin (WGA) stained plasma membrane in green and DAPI stained host and bacterial DNA in blue. The left centre, right centre and far right images show the respective DAPI, phalloidin and WGA channels in monochrome. Solid white arrows highlight WGA-positive staining of an exopolymeric matrix secreted by *E. coli* during

biofilm formation. White scale bar is 10µm. (B) A 3-dimensional volume through entire Z-stack at a position corresponding to the red squares in image A (numbered for orientation); the *E. coli* is clearly bound to the extracellular space. (C) A Z-axis profile plot was produced as in Figure 3. The DAPI channel is approximately 16 slices (in the Z-axis) from that of the phalloidin channel, confirming purely extracellular colonisation. (D) 3D construct of the cells shown in A with the DAPI channel shown alone. This image shows the extent of bacterial infection. Very deep and tightly packed *E. coli* biofilms can be seen covering the apical membrane of the T24 cells. The region of interest analysed in B and C is indicated with a white line.

2.3.4 LUTS patient-isolated *E. faecalis* invades cells in a cell culture model system

Confocal analysis of shed LUTS patient urothelial cells demonstrated cellular invasion by *E. faecalis*. To test further whether *E. faecalis* is competent to invade urothelial cells, as our earlier findings would suggest, we challenged the same T24 bladder cell culture model system as described above with five strains of *E. faecalis* isolated from routine MSU-culture negative LUTS patients. Again, the infected cells were imaged using confocal microscopy and explored extensively with 3D digital analyses.

Unlike *E. coli*, *E. faecalis* adhered to the T24 cells in looser, more diffuse clusters (See Fig. 11 for a representative example). More organised colonies were evident, although they manifested close to the T24 nuclei and within the horizontal boundaries of the cells, which suggested cellular invasion (Fig.

11A). Z-stack 3D constructs of these bacterial colonies clearly showed all five of the LUTS patient isolated *E. faecalis* to be sandwiched within the intracellular space of the T24 cells (Fig. 11B,D). These findings were mirrored in the Z-axis profile plots, which showed a marked decrease in mean pixel intensity of phalloidin-labelled F-actin (red) and a striking increase in the mean pixel intensity of the DAPI labelled *E. faecalis* at mid-cell slices (Fig. 11C).

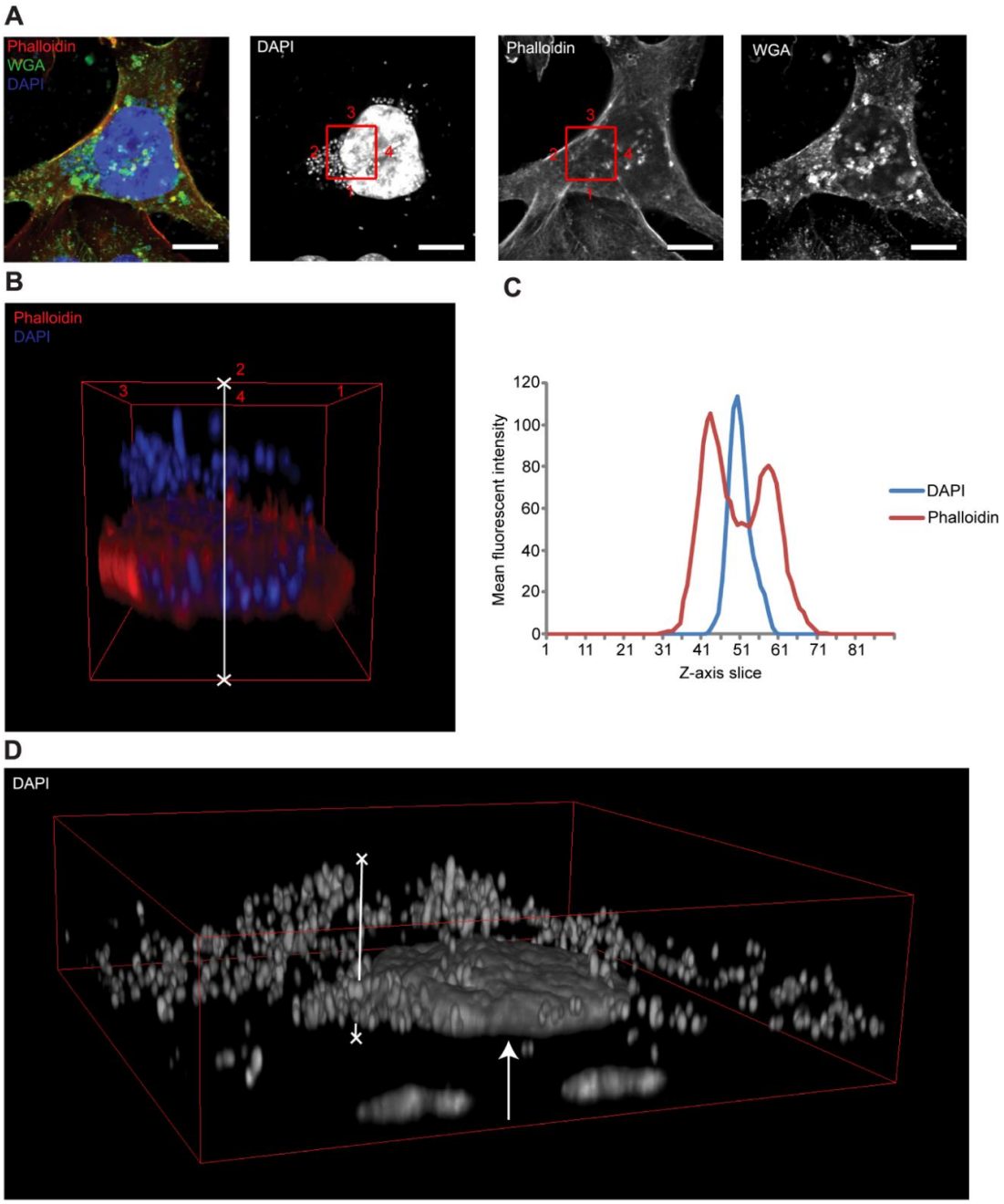

Figure 11. 3D confocal analysis of cultured cells infected with LUTS-isolated *E. faecalis*

(A) Confocal image of a group of T24 cells infected for 2.5hrs with *E. faecalis* isolated from LUTS patients at an MOI of approximately 10-15 bacteria per mammalian cell. The left image is a composite showing the phalloidin stained F-actin in red, wheat germ agglutinin (WGA)-stained plasma membrane in green and DAPI stained host and bacterial DNA in blue. The left centre, right centre and far right images show the respective DAPI, phalloidin and WGA channels in monochrome. White scale bar is 10µm. (B) A 3-dimensional

volume through entire Z-stack at a position corresponding to the red squares in image A (numbered for orientation). This construct shows clear and extensive invasion and colonisation of the T24 cell by *E. faecalis*. (C) A Z-axis profile plot was produced as in Figure 3 and 4. The peak mean pixel intensity of the DAPI channel corresponds with a striking reduction of the phalloidin channel at slice 51 (~centre of the cell), confirming intracellular infection. (D) 3D construct of the entire cell as in Figure 5. This image shows the tightly packed intracellular biofilm like cluster of *E. faecalis* in close proximity to the T24 nucleus (white arrow).

Significant bacterial pathology associated with the urothelium is clearly evident in the LUTS population and the results of these 3D analyses support the hypothesis of intracellular colonisation by *E. faecalis* in human urothelium and, indeed, LUTS patients. In contrast to the case of acute infection, it would appear that *E. coli* may not be ubiquitously invasive in the context of chronic low-grade UTI. It is important to note, however, that the lack of invasion may not necessarily preclude pathogenicity; the ability to form extracellular biofilms, as *E. coli* did in this study, could prove equally challenging to treat.

Chapter 3

A urine-dependent human urothelial organoid offers a potential alternative to rodent models of infection

3.1 Abstract

Murine models describe a defined host/pathogen interaction for urinary tract infection, but human cell studies are scant. Although recent human urothelial organoid models are promising, none demonstrate long-term tolerance to urine, the natural substrate of the tissue and of the uropathogens that live there. We developed a novel human organoid from progenitor cells which demonstrates key structural hallmarks and biomarkers of the urothelium. After three weeks of transwell culture with 100% urine at the apical interface, the organoid stratified into multiple layers. The apical surface differentiated into enlarged and flattened umbrella-like cells bearing characteristic tight junctions, structures resembling asymmetric unit membrane plaques, and a glycosaminoglycan layer. The apical cells also expressed cytokeratin-20, a spatial feature of the mammalian urothelium. Urine itself was necessary for full development, and undifferentiated cells were urine-tolerant despite the lack of membrane plaques and a glycosaminoglycan layer. Infection with *Enterococcus faecalis* revealed the expected invasive outcome, including urothelial sloughing and the formation of intracellular colonies similar to those previously observed in patient cells. This new biomimetic model could help illuminate invasive behaviours of uropathogens, and serve as a reproducible test bed for disease formation, treatment and resolution in patients.

3.2 Materials and methods

3.2.1 Human Primary progenitor cell expansion and handling in 2D

Commercially available human bladder epithelial progenitor cells (HBEP, Cell N Tec) [231] and their spontaneously immortalised, non-transformed counterparts (HBLAK, Cell N Tec) were supplied in frozen aliquots containing ~$5x10^5$ cells at passage 2 and ~$0.5x10^5$ at passage 25 respectively. Cells were isolated from bladder trigone biopsies from male patients undergoing surgery for benign prostatic hyperplasia. HBEP cells are guaranteed to grow for a further 15 population doublings before senescing whereas HBLAK cells, although spontaneously immortalised, should not be differentiated into 3D cultures once past a passage number of 40-50. Both cell types were cultured identically, with the exception of slight differences in incubation time, due to the slightly increased rate of cell division exhibited by HBLAK cells.

Thawed cells were seeded (~300 cell clumps / cm^2) into pre-warmed and equilibrated low-calcium, high-bovine pituitary extract, primary epithelial medium (CnT-Prime, Cell N Tec) in 9cm polystyrene dishes and incubated at 37°C in a humidified incubator under 5% CO_2. Culture medium was replaced after overnight incubation to remove residual dimethyl sulfoxide (DMSO). Antibiotics were not added to culture medium at any point due to adverse effects on cytodifferentiation, metabolism and morphology [232]. Furthermore, trypsin is known to damage primary cells; therefore, Accutase solution (Innovative Cell Technologies) was used to detach cells at all stages

of experimentation [233]. Cells were allowed to expand to ~70% confluency before freezing batches of cells at a density of ~1x10^6 cells/ml in defined freezing medium (CnT-CRYO-50, Cell N Tec) in preparation for later experiments. Cells were not allowed to become fully confluent during cell expansion in an effort to maintain a proliferative phenotype.

3.2.2 Differentiation of 3D human urothelium *in vitro*

In preparation for organotypic culture, previously frozen progenitor cells were thawed and expanded on 9cm culture dishes as above. Once 70-80% confluent, the cells were washed briefly with calcium- and magnesium-free phosphate buffered saline (PBS, Sigma-Aldrich) and incubated at 37°C in ~3ml of pre-warmed Accutase solution for 2-5min. The dishes were lightly tapped and detached cells re-suspended in 7ml of warm CnT-Prime. Post centrifugation at 200 x g for 5min, the supernatant was removed and the pellet re-suspended in fresh CnT-Prime. This cell suspension was counted whilst allowing the cells to equilibrate for 3min at room temperature. 2x10^5 cells in 400µl of CnT-Prime (internal medium) were added to 6 12mm 0.4µm pore polycarbonate filter (PCF) inserts (Millipore) standing in 6cm culture dishes containing ~3ml of fresh pre-warmed CnT-Prime medium (external medium, level with insert filters). A further 8ml of CnT-Prime medium was added to the 6cm dish (external to the filter inserts) ensuring identical internal and external fluid levels. The 3D culture inserts were incubated for 3-5 days until 100% confluent. Confluency was determined through the fluorescent staining of 1 insert and visualisation under epi-fluorescence microscopy (see

section below). Once deemed confluent, internal and external medium was removed and replaced with low-BPE, calcium-rich (1.2mM) differentiation barrier medium (CnT-Prime-3D, Cell N Tec) to promote differentiation. Subsequent to overnight incubation, the internal medium (apical surface of cell culture) was removed and replaced with filter-sterilised human urine from healthy volunteers to aid terminal differentiation into umbrella cells. The external CnT-Prime-3D medium and the internal human urine were replaced every 3 days and the culture incubated for 14-24 days at 37°C in 5% CO_2.

To explore the effect of urine on differentiation in 2D the HBLAK cells were seeded on 8-well permanox Lab-Tek slides (Sigma-Aldrich) and grown to confluency. The cells were then exposed to CnT-Prime-3D medium alone or 25%/50% sterile human urine diluted in CnT-Prime-3D for 72 hours at 37°C in 5% CO_2. To analyse the effect of urine on HBLAK organoid formation, cells were grown to confluency on filter inserts as above. The basal compartment was treated with CnT-Prime-3D throughout, however, the apical compartment was filled with either CnT-Prime-3D alone, 50% sterile human urine diluted in CnT-Prime-3D or 100% urine. The specified medium or urine was changed every 3 days and the culture incubated for 14 days at 37°C in 5% CO_2.

3.2.3 Characterisation of the 3D urothelium

Prior to fluorescent staining and immunofluorescence (IF), filter inserts were carefully transferred to 8-well plates (Nunc) and submerged in 4% methanol-

free formaldehyde (Thermo Scientific, Fisher Scientific) in PBS overnight at 4°C. After fixation, the filter inserts were kept at 4°C in 1% formaldehyde in sealed containers in preparation for processing.

To determine confluency and analyse morphology, the pre-fixed tissue was permeabilised in 0.2% Triton-X100 (Sigma-Aldrich) in PBS for 15 minutes at RT followed by a single wash with PBS. The cells were stained with TRITC or Alexa Fluor-633-conjugated phalloidin (0.6µg/ml)(Sigma-Aldrich), to label filamentous actin, and the DNA stain 4'',6-diamidino-2-phenylindole, (DAPI, 1µg/µl; Sigma-Aldrich) in PBS for 1 hour at RT. The dual-labelling solution was gently aspirated and the cells washed 5 times in PBS.

For indirect IF, the tissue was permeabilised as above, washed with PBS then blocked with 10% normal goat serum (NGS, Thermo Fisher) in PBS for 1 hour. Tissue was incubated overnight at 4°C with a combination of the following primary antibodies in PBS containing 1% NGS: 1:10 dilution of mouse anti-uroplakin-III (UP3) monoclonal antibody (clone AU1, 651108, Progen Bioteknik); 1:50 dilution of mouse anti-Cytokeratin 8 (CK8) monoclonal antibody (clone H1, MA1-06317, Thermo Fisher); 1:100 dilution of rabbit anti-Cytokeratin 20 (CK20) polyclonal antibody (PA5-22125, Merck Millipore); 1:200 dilution of rat anti-muscarinic acetylcholine receptor m2 (M2) monoclonal antibody (clone M2-2-B3, Merck Millipore); 1:200 dilution of rabbit anti-muscarinic acetylcholine receptor m3 (M3) polyclonal antibody (ab126168, Abcam); 1:100 dilution of mouse anti-chondroitin sulphate monoclonal antibody (clone CS-56, ab11570, Abcam) or 1:100 dilution of rat

anti-heparan sulphate proteoglycan (large) monoclonal antibody (clone A7L6, ab2501, Abcam). Post incubation with primary antibodies, the tissue was washed 5 times with PBS containing 1% NGS then incubated at RT for 1 hour with a 1:250 dilution of the following secondary antibodies (depending on the species of primary antibody used): goat anti-mouse, goat anti-rabbit or goat anti-rat conjugated to either Alexa Fluor-555, Alexa Fluor-488 or Alexa Fluor-633 (Invitrogen). Labelled cells were washed 5 times with PBS to remove unbound secondary antibody before staining with phalloidin and DAPI as above. In some experiments, prior to permeabilization, cell plasma membranes were labelled with 1µg/ml wheat germ agglutinin (WGA) conjugated to Alexa Fluor-488/633 (Invitrogen) in Hank's balanced salt solution (HBSS, Invitrogen) for 20min at RT. Controls were performed by using primary and secondary antibodies in isolation.

In preparation for imaging, filters were carefully removed from inserts using a scalpel, mounted with FluorSave reagent (Calbiochem), and a coverslip fixed in place with clear nail varnish. Lab-Tek slide wells and gaskets were carefully removed prior to the addition of FluorSave and a coverslip as above.

3.2.4 Electron microscopy

Electron microscopy was conducted by technicians at the Division of Medicine, University College London electron microscopy unit at the Royal Free Campus, Hampstead, London.

For transmission electron microscopy (TEM), samples were fixed in Karnovsky's fixative (2.5% glutaraldehyde / 2% paraformaldehyde) and then washed in 1M PBS 3x10 min, followed by a post-fixation in 1% Osmium tetroxide for 1 hour at room temperature. Tissue was rinsed with distilled water 3x10 min. Samples were dehydrated in an ethanol series (30, 50, 70, 90 and 100%) then treated with resin-ethanol (1:1) overnight. Subsequently, samples were embedded in 100 % LEMIX resin and incubated at 65ºC for 24 hours. Ultra-thin sections of the resin block were cut and post stained with 2% Uranyl acetate and Lead citrate.

For scanning electron microscopy (SEM), the samples were fixed and dehydrated as above. Samples were then incubated in Tetramethylsilane for 10 min and air dried before mounting on stubs and sputter coated with gold.

3.2.5 Experimental infection of the human urothelial organoid and the gentamicin protection assay

A single strain of *Enterococcus faecalis (E. faecalis)* originally derived from a patient with chronic UTI[1] was grown aerobically in a shaking incubator at 37°C for 24 hours. Once a batch of 6 HBLAK 3D urothelial cultures had reached 14 days of growth, $1.6x10^7$ colony-forming units of bacteria (MOI of 25) were added to the filter-sterile human urine at the apical liquid-liquid interface of each culture. The experimentally infected cultures were incubated for 2 hours at 37°C under 5% CO_2. The 3D culture filter inserts

were washed with PBS before fixation and staining as above. For the gentamicin protection assay, after the infection was completed, the cultures were washed 3 times in PBS before the addition of 3D barrier medium containing 2000µg/ml of gentamicin (Sigma-Aldrich) to the apical and basal compartments of the culture filter. The organoids with antibiotics were incubated for a further 2 hours at 37°C under 5% CO_2 to kill any extracellular bacteria. Post incubation the supernatant was serially diluted in PBS (undiluted, 1:100, 1:1000, 1:10000) and 25µl of each dilution spread on a quartile of a Columbia blood agar plate (CBA, Oxoid) before being incubated for 24 hours aerobically at 37°C to enumerate live bacteria. The organoids were washed a further 3 times in PBS before being lysed with 1% Triton-X100 in PBS for 10 minutes at RT. The lysate was added to CBA plates and incubated as above to detect intracellular bacteria. All experiments were completed in triplicate.

3.2.6 Analysis of shed epithelial cells

Patient urine specimens were included to explore the pattern of uroplakin staining present on shed urothelial cells. Samples were collected with informed consent and analyzed in accordance with the National Research Ethics Service (NRES, see Appendix 3).

Experimentally infected organoid supernatants, or patient urine specimens, were collected, cytocentrifuged on to glass slides and fixed and stained prior to imaging [1]. Briefly, 80µl of supernatant or patient urine was

cytocentrifuged using a Shandon Cytospin 2 cytocentrifuge at 800rpm (≈75g rcf) for 5 minutes. The cellular deposit was circumscribed with a ImmEdge pen (Vector Laboratories) before fixing, staining and mounting as above.

3.2.7 Imaging and Analysis

We performed epi-fluorescence microscopy on an Olympus CX-41 upright microscope, and confocal laser scanning microscopy on Leica SP5 and SP2 microscopes. Images were processed and analysed using Infinity Capture and Analyze V6.2.0, ImageJ 1.50h[225] and the Leica Application Suite, Advanced Fluorescence 3.1.0 build 8587 Software.

TEM was conducted using a Jeol 1200-Ex digital image capture system with a side mount 2Kv AMT camera. SEM was performed using a Jeol JSM-5300 fitted with a Semafore digital image capture system.

The proportion of the HBLAK organoids exhibiting evidence of differentiation was calculated by analyzing low-power SEM micrographs (N=3) using ImageJ automatic thresholding and measure tools[225]. The number of bacteria per cell was calculated using nearest neighbour 3D connectivity analysis with the ImageJ Object counter3D plugin[225, 234]. The DAPI channel of 3D laser scanning confocal constructs were analysed using Differential Voxel Filters allowing the enumeration of mammalian nuclei and bacteria.

3.2.7 Statistical analyses

Data were analysed using IBM SPSS Statistics version 24. Non-parametric Friedman tests of differences among repeated measures were performed due to non-normal distributions. 3 experimental replicates were performed for statistical testing.

3.3 Results

3.3.1 HBLAK and HBEP cells can form three-dimensional urothelial organoids

HBEP cells were derived from normal human bladder biopsies by CellNTec and provided commercially in cryovials. We also grew HBLAK cells, which are spontaneously immortalised but not transformed version of HBEP available from the same company. These latter cells retain the ability to differentiate but have increased longevity without senescing. On thawing, both cell types were seeded on plastic in fully defined, serum-free, BPE containing CNT-Prime media, which favours the proliferative phenotype. Both HBEP and HBLAK shared a ‘spindle-like’ morphology, a hallmark of multipotent epithelial progenitors. When 70% confluent, the cells were transferred to Millicell transwells (Millipore) with CNT-Prime media in the apical and basal chambers and grown to confluency. At this point, the media was shifted to high-calcium, differentiation media (CNT-Prime-3D) in both chambers. After overnight incubation, we replaced filter-sterilized human urine in the apical chamber and left the cultures to develop for 14 (HBLAK) to 25 (HBEP) days depending on the experiment, with periodic media and urine changes. At endpoint, the organoid-coated filters were retrieved, fixed, and stained for various biomarkers and inspected microscopically.

3D confocal analyses showed that both cultures were viable despite the prolonged presence of urine. The HBEP tissue contained multiple layers

(approximately 3) with tightly-packed spheroid basal cells, intermediate cells and enlarged and flattened umbrella-like cells at the apical surface (Fig. 12a,b). The HBLAK tissue was morphologically similar, but in contrast, likely due to increased rate of growth, these produced approximately 5-7 cell layers with multiple layers of intermediate cells (Fig. 12c,d). Optical slices at the basal region of the HBEP and HBLAK organoids respectively showed the typically small, tightly-packed and spheroid morphology of urothelial basal cells (Fig. 12e,g). Basal cells in the HBLAK organoid (~ø10µm) appeared to be slightly smaller than those in the HBEP culture (~ø20µm) (Fig. 12e,g). Similarly, single optical slices at the apical regions of the HBEP and HBLAK organoids showed the formation of a large, flat and often hexagonal cellular morphology typical of well-differentiated umbrella cells (Fig. 12f and 12i for HBEP, Fig. 12h and 12j for HBLAK). As shown in Figure 12j, lower-magnification views of HBLAK show a more heterogeneous differentiation pattern, with cells elaborating distinct multi-layered zones of organoid formation with large umbrella-like cells at their surface, flanked by regions of very much smaller undifferentiated basal cell-like monolayers and occasional areas of hypertrophy.

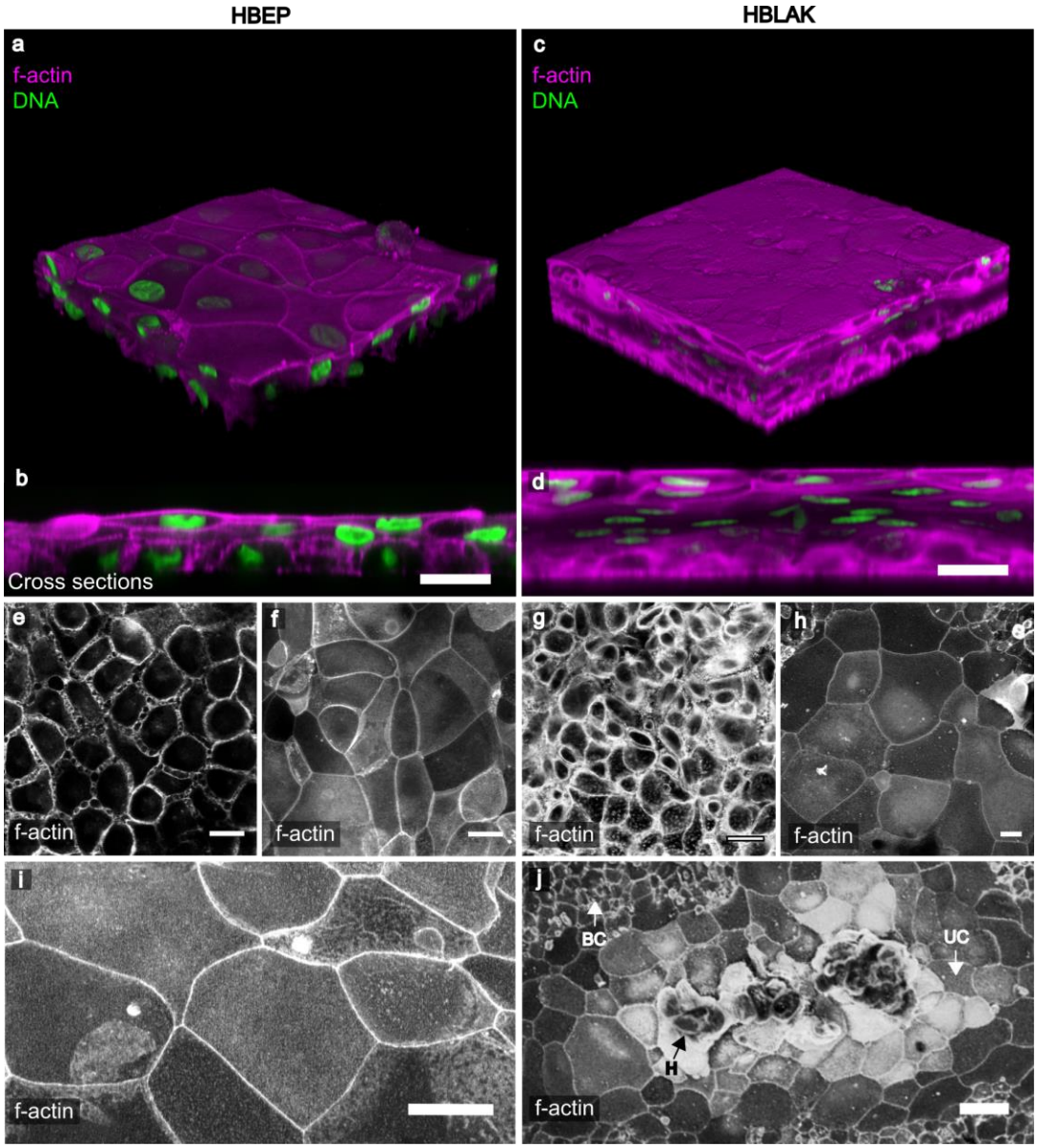

Figure 12. HBLAK cells retain the ability to differentiate into 3D urothelial organoids

Colour images are composites showing the phalloidin-stained F-actin in magenta and DAPI-stained DNA in green. Lower images show phalloidin-stained F-actin in monochrome. (a) 3D confocal model constructed from a 200 slice Z-stack of HBEP organoid. Umbrella-like cells are large and flat. (b) Orthogonal view of the Z-stack shows the tissue to be ~3 layers in depth and the basal cells to be spheroid in morphology. (c) 3D confocal model constructed from a ~300 slice Z-stack of HBLAK organoid. The HBLAK tissue is significantly better developed than the HBEP tissue in terms of thickness and number of cell layers. (d) Orthogonal reslice of the HBLAK

tissue shows ~5-7 cell layers with flattened apical cells and more spheroid cells beneath. (e) Single optical slice at lowest region of the HBEP organoid showing small tightly packed basal cells. (f) Single optical slice at apical region of HBEP organoid showing well-differentiated, characteristically large umbrella-like cells. (g, h) Single optical slices of basal and umbrella-like cells respectively in HBLAK bladder bio-mimetic. Scale bars represent 20µm. (i) A further single optical slice showing large umbrella-like cells at the surface of the HBEP organoid. Scale bar represents 20µm. (j) Maximum projection confocal image of a region of HBLAK organoid formation. Large, flat umbrella-like cells (UC) lined the apical surface of the organoid surrounded by monolayers of small undifferentiated basal-like cells (BC). Areas of hyperplasia (H) were noted at the 'peak' of a small proportion of investigated regions of differentiation. Scale bar represents 40µm.

In summary, both models are morphologically similar to native human bladder tissue and formed well-differentiated umbrella cells at their apical surface. Moreover, both models were exposed to sterile human urine for several weeks (14-25 days) without exhibiting any signs of toxicity.

3.3.2 HBLAK and HBEP organoids exhibit key biomarkers of the human urothelium

We characterised the HBEP and HBLAK human urothelial organoids further by targeting urinary tract-specific antigen expression using indirect IF in conjunction with high-resolution laser scanning confocal microscopy. The resulting organoids had the correct spatial expression of several key biomarkers. Studies exploring cytokeratin (CK) expression in normal human bladders have shown a relationship between the level of cytodifferentiation

and sub-type CK expression[58]. Both HBEP- and HBLAK organoids exhibited correct spatial expression of CK8 and CK20; specifically, CK8 was expressed throughout the strata of the *in vitro* tissues whereas CK20 was expressed preferentially by the umbrella-like cells at the apical surface (Fig. 13 a,b,c,d). In contrast to the rodent bladder, muscarinic receptors are expressed throughout the human urothelium[235, 236]. This finding was echoed in our model with evidence of muscarinic receptors M2 and M3 expressed in all cell layers of both organoids (Fig. 13e and g). Uroplakin-III (UP3), an indispensable part of the asymmetric unit membrane[228], was present at the apical surface of the HBEP (Fig. 13f) and HBLAK (Fig. 13h) organoids, in a speckled pattern (HBEP, Fig. 13i; HBLAK, Fig. 13k) similar to that seen in urothelial cells shed in the urine of a chronic UTI patient (Fig. 13j,l). Multinucleation of the umbrella-like cells was a relatively rare occurrence (e.g. examples can be seen in Fig 13g, i and k).

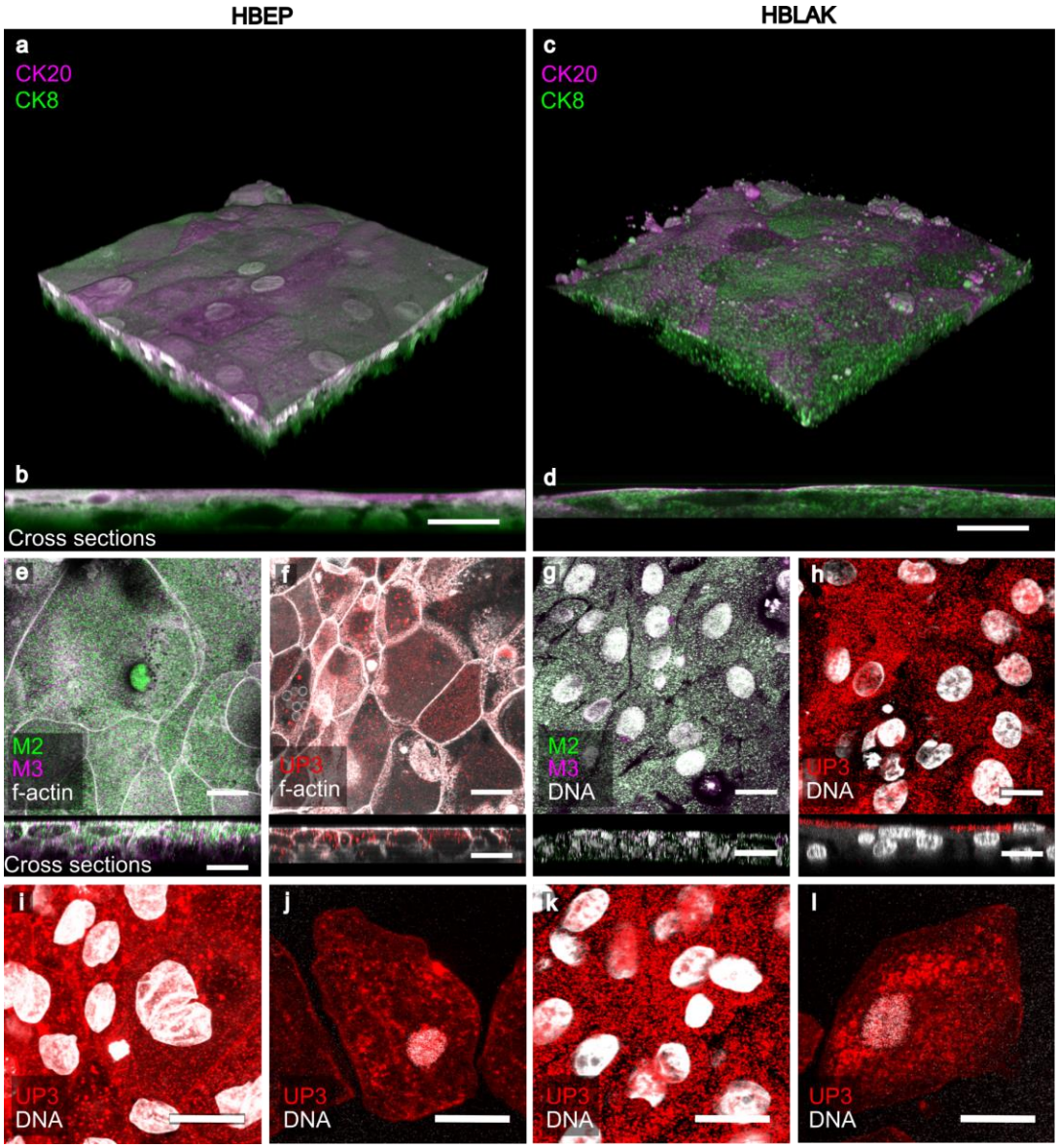

Figure 13. Characterisation of HBEP (left) and HBLAK (right) urothelial organoids using IF

(a) 3D confocal model and (b) orthogonal reslice from a 100 slice Z-stack of HBEP organoid. The HBEP organoid exhibited the correct spatial expression of Cytokeratin-20 (CK20, umbrella cells, magenta) and Cytokeratin-8 (CK8, throughout urothelium, green). (c) 3D confocal model and (d) orthogonal reslice from a 120 slice Z-stack of HBLAK organoid. As with the primary HBEP mimetic, the HBLAK organoid also expressed CK20 (magenta) at the apical surface and CK8 (green) throughout the tissue. (e-h) Single optical slices at apical region of HBEP (e,f) and HBLAK (g,h) organoids with corresponding orthogonal cross sections shown directly beneath. (e,g)

Expression of muscarinic receptor 2 (M2, green) and muscarinic receptor 3 (M3, magenta). Both receptors were found throughout the tissue in both models. Phalloidin-stained F-actin is presented in grey. (f,h) Expression of Uroplakin-III (UP3, red) preferentially at apical region of both models. Phalloidin-stained F-actin is presented in grey. (i) High-power single optical slice of UP3 (red) expression in HBEP model. (j) Pattern of UP3 (red) expression found in an exfoliated urothelial cell harvested from a chronic UTI patient. (k) High-power single optical slice of UP3 (red) expression in HBLAK model. (l) Further example of the pattern of UP3 (red) expression found in patient-isolated urothelial cells. DAPI-stained DNA is presented in grey. Scale bars represent 20µm.

3.3.3 HBLAK organoids possess correct topographical and ultrastructural features

Given these promising results, we went forward with the more tractable and thicker HBLAK urothelial mimetic model, using scanning electron microscopy (SEM) and transmission electron microscopy (TEM) to analyse its ultrastructure, organisation and overall topography. Low-power SEM echoed what was seen in Figure 12j, namely that the HBLAK cells elaborated distinct multi-layered zones of organoid formation with umbrella-like cells at their surface (approximately two-thirds of the tissue, 64.8% +/- 10.4) along with zones of undifferentiated basal cell-like monolayers (Fig. 14a) and areas of disorganised hyperplasia (Fig. 14b). The surface of each differentiated zone exhibited very large (up to ~80µm), often hexagonal umbrella-like cells (Fig. 14c,d,e). A comparison with the undifferentiated basal cells (Fig. 14e vs. f) showed that the umbrella-like cells were up to approximately 50 times larger

in terms of surface area than their undifferentiated counterparts. SEM micrographs also showed evidence of tight junction formation (Fig. 14c) [237] and structures resembling, in size and spacing, characteristic microplicae or ‘hinges’ at the apical surface of each umbrella-like cell (Fig. 14g) [237, 238]. Orthogonal sections of fully differentiated organoid zones were analysed using TEM. As with the laser scanning confocal imaging, TEM elucidated distinct layers of basal, intermediate and umbrella cells (Fig. 14h). Structures consistent in size and spacing with rigid plaques could be seen residing between the ‘hinges’ at the apical surface of the umbrella cells (Fig. 14i,j) [237, 238]. Structures were also seen that may correspond to the specialised fusiform vesicles (Fig. 14j) necessary for trafficking uroplakins [239]. In contrast, TEM analysis of the small, undifferentiated cells making up the monolayers flanking the organoid zones did not exhibit the putative hinges, plaques or fusiform vesicles (Fig. 14k,l). Taken together, these observations suggest that the fully differentiated regions of the organoids possess some key features expected of a human urothelium.

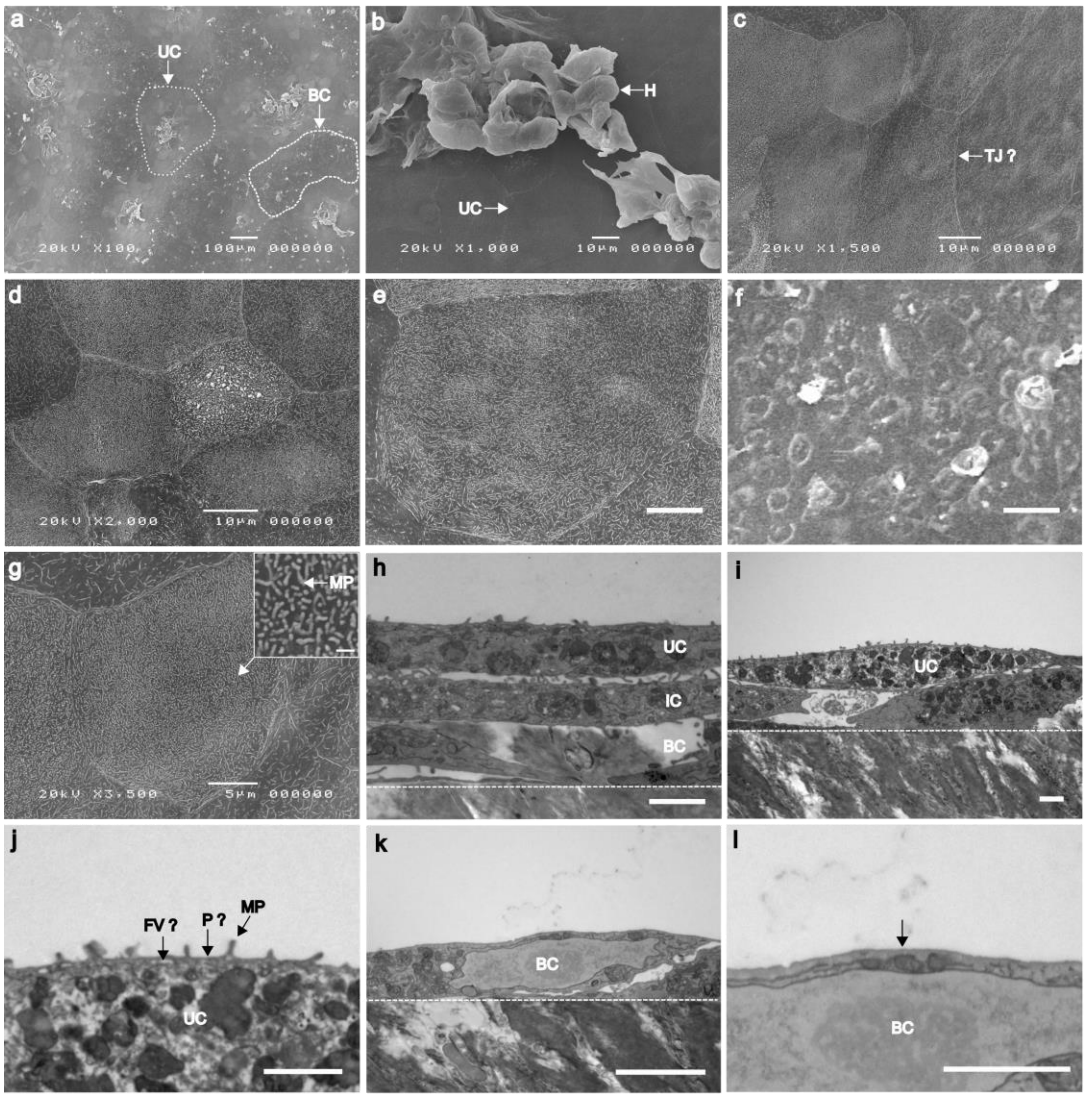

Figure 14. Analysis of HBLAK organoid topography and ultrastructure using scanning electron microscopy (SEM) and transmission electron microscopy (TEM)

(a) SEM micrograph showing 'islands' of organoid formation. Umbrella-like cells (UC) can be seen at the apical surface of each 'island' interspersed by areas of undifferentiated monolayers of basal-like cells (BC). (b) SEM at the apical surface of organoid. Large (~50-60µm), flat umbrella-like cells (UC) are present at the upper-most surface of each 'island'. Areas of hyperplasia (H), however, were frequently observed. (c) SEM of umbrella-like cells showing structures resembling tight junctions (TJ?). (d-e) SEM of further regions of large, characteristically tessellated umbrella-like cells. Scale bars represents 10µm. (f) SEM of region of small undifferentiated basal-like cells. Scale bar represents 10µm. (g) SEM of a single umbrella cell. Microplicae

(MP) or 'hinges' can be seen covering the surface of the umbrella-like cells. Inset scale bar represents 500nM. (h) TEM of 3-4 layered organoid. Basal cells (BC) can be seen above the polycarbonate culture filter (white broken line). Large, distended intermediate cells (IC) and umbrella-like cells (UC) are superior to the basal cells. Scale bar represents 2µm. (i) TEM of 2-3 layered organoid. White broken line represents the upper surface of the polycarbonate culture filter. Scale bar represents 2µm. (j) Enlarged version of TEM image i. Plaque-like structures (P?) are situated between each hinge (microplicae, MP). White structures were evident that might be fusiform vesicles (FV?), responsible for trafficking uroplakin to the umbrella cell plaques. Scale bar represents 1µm. (k) TEM of a monolayer of undifferentiated basal cells (BC, as highlighted in image a) found between the organoid 'islands'. These non-differentiated cells measure ~8µm across, making them approximately 10-50 times smaller than the umbrella-like cells in the same system. White broken line represents the upper surface of the polycarbonate culture filter. Scale bar represents 2µm. (l) TEM of the apical surface of the basal cell (BC) shown in image i. Structures resembling microplicae, plaques and fusiform vesicles were not seen (white arrow). Scale bar represents 1µm.

3.3.4 Urine strongly influences HBLAK differentiation, organoid development and GAG formation

As shown above, the HBLAK organoid expresses key urothelial markers and is morphologically reminiscent of a urothelium. Of key importance, however, is the tolerance exhibited by these cultures to urine. In this group of experiments, we investigated whether urine is merely tolerated or indeed necessary for differentiation in 2D, organoid formation and the elaboration of

a GAG layer. To achieve this, we exposed the cells, in 2D and 3D, to various dilutions of sterile human urine before examining microscopically.

To decouple the influence of urine from any effects that might be exerted by developing intermediate cells below, we grew HBLAK cells as 2D monolayers on chamber slides and exposed them to medium containing urine. As shown in Figure 15, HBLAK cells exhibited a marked dose response to urine after 72 hours. Cells grown in high calcium medium alone took on a small, tightly packed basal cell-like appearance with visually well-formed intercellular junctions as assessed by actin staining (Fig. 15a) and the elaboration of actin-containing microvilli (Fig. 15a inset, red arrow). With the addition of 25% human urine, however, a small proportion of the cells began to exhibit an enlarged morphology, but intercellular junctions were partially disrupted (Fig. 15b). After 72 hours in 50% sterile human urine, extensive colonies of HBLAK cells took on a large, flat umbrella cell-like morphology (Fig. 15c) devoid of microvilli (Fig 15c inset, red arrow). However, intercellular junctions seemed almost entirely compromised, possibly because increased urine came at the expense of calcium concentration.

Strikingly, we found human urine to be necessary for organoid formation and the elaboration of a GAG layer in HBLAK cells. Cells cultured for 14 days on filter inserts with high calcium medium in the basal and apical compartments

were comprised of only one layer, showing no stratified organoid formation, little heparan sulphate, and no detectable expression of chondroitin sulphate (Fig. 15d). Moreover, these cells appeared to exhibit a degree of anaplasia, with a more ‘spindle-like’ multipotent progenitor cell-like morphology (data not shown). In contrast, HBLAK cells cultured in 50% or 100% human urine at the apical surface produced zones of organoid formation between 3 and 6 cell layers thick (Fig. 15e,f) as previously seen in the experiments presented in Figure 12, and both stimulated the expression of a heparan and chondroitin sulphate-rich GAG layer at the urine-umbrella cell interface (Fig. 15e,f). Taken together with the data in Figure 14, these experiments suggest that urine is an indispensable effector of urothelial differentiation in this model. Nevertheless, despite a lack of GAG layer and of the structures that appear to be asymmetric unit membrane plaques, undifferentiated cells remain viable for long periods in urine, which suggests that these “barriers” are not required for urine tolerance.

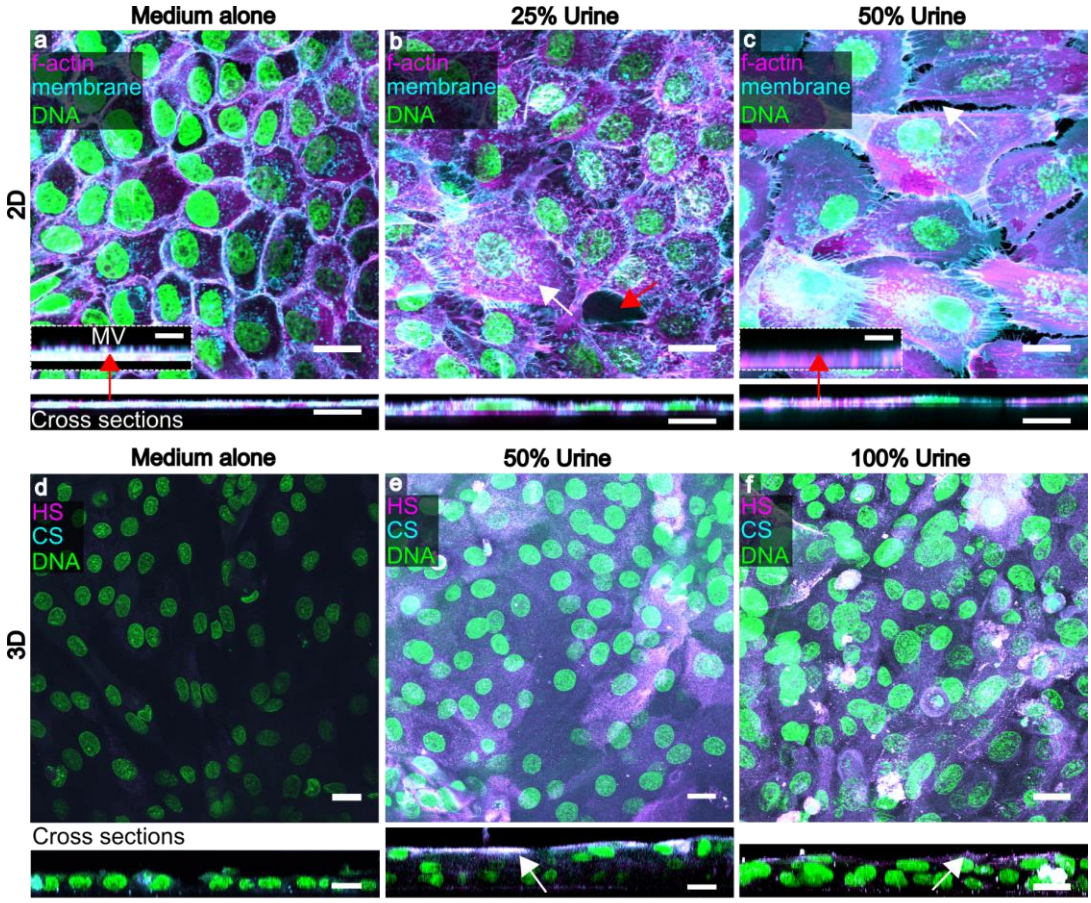

Figure 15. Human urine affects HBLAK differentiation, 3D organoid formation and GAG expression

Upper images are maximum projections and corresponding orthogonal cross sections (below) from 12 slice Z-stacks of HBLAK cells cultured in 2D on glass. Cells were grown to confluency and incubated for 72hrs in varying proportions of human urine in culture medium. WGA-stained plasma membrane is presented in cyan, phalloidin-treated F-actin in magenta and DAPI-labelled DNA in green. (a) Monolayer grown in 3D barrier medium alone. Basal cell morphology was maintained and intercellular junctions appeared to be intact. Inset displays high magnification cross section showing actin-rich microvilli (MV) at apical surface. Inset scale bars represents 5µm. (b) HBLAK monolayer cultured in 25% human urine. A subset of cells began to differentiate (white arrow) exhibiting a large, flat umbrella cell-like morhology. Cell junction integrity was disrupted (red arrow). (c) HBLAK monolayer cultured in 50% human urine. Large colonies of cells exhibited an umbrella cell-like morphology. Cell junctions, however, were

almost entirely compromised (white arrow). Inset shows the lack of microvilli on the surface of the umbrella-like cells. Inset scale bars represents 5µm. Lower images are maximum projections (and cross sections below) from 20-slice Z-stacks of HBLAK cells grown on 3D culture filter inserts. Cultures were exposed to 3D barrier medium in the basal compartment and varying proportions of human urine at their apical surface for 14 days. The glycosaminoglycan (GAG) constituents heparan sulphate (HS) and chondroitin sulphate (CS) were labelled and are shown here in magenta and cyan respectively. DAPI-stained DNA is shown in green. (d) Cells cultured in 3D barrier medium only in the basal and apical compartments. No stratified organoid formation was observed. Little GAG expression was seen. (e) Cells cultured with 50% urine at the apical surface. Urothelium-like organoids were formed. Heperan sulphate and chondroitin sulphate were strongly expressed by umbrella-like cells (white arrow). White represents colocalization. (f) Cells cultured with 100% urine at the apical surface. Again, well organised bladder organoids were formed and a GAG (heparan sulphate and chondroitin sulphate) mucin layer was elaborated at the cell-urine interface (white arrow). Scale bars represent 20µm.

3.3.5 The HBLAK organoid is a promising model for studying *Enterococcus* infection

Our laboratory studies the uropathogen *Enterococcus faecalis*. This bacterium is commonly implicated in chronic UTI in the elderly and is frequently associated with multi-drug resistance, hospital-acquired infection, and catheter-associated biofilm formation; we previously demonstrated that it exhibits intracellular invasion in patient cells [1, 13, 114, 117-122]. To determine whether the organoid is a good model for studying host-pathogen interactions with this bacteria, we infected the HBLAK organoid with patient-

isolated *E. faecalis* [1]. When we inspected the cultures two hours after infection, we found that *E. faecalis* exhibited robust tropism in this model, with the resulting adherent colonies relatively loosely packed (Fig. 16a). As with human patients suffering from acute and chronic UTI, the apical cell layer was shed in response to bacterial insult [1], leaving an uneven surface of basal and intermediate cells (Fig. 16a). Inspection of supernatants post-infection revealed extensive shed umbrella-like cells (Fig 16b) reminiscent of those seen in the urine of infected patients (Fig. 16c and chapter 2 [1]). Significantly, in the tissue that remained, we saw frequent examples of large intracellular bacterial colonies (Fig. 16d, arrows) within the superficial layer of cells, showing a similar loosely-packed morphology to those we previously observed in shed urinary umbrella cells from patients in chapter 2 [1]. Image analysis showed that 7.3% of cells harboured intracellular colonies with a mean of 37.8 (+/- SD of 11.5) bacteria per cell. A gentamicin protection assay was performed as requested during the peer review process to enumerate sequestered bacteria. The results of this assay (Fig. 16e) supported confocal inspection, with viable intracellular bacteria liberated after extracellular sterilization and host cell lysis. Specifically, treatment with 2000 µg/ml of gentamicin resulted in zero detected growth within the organoid supernatant. Detergent treatment liberated intracellular bacteria resulting in the detection of a median of $4.8x10^3$ cfu/ml in the lysate (approx. 55% bacterial recovery) (Fig. 16e). A non-parametric Friedman test of differences among repeated measures was conducted on the median cfu/ml data from the untreated (control, N=3) and gentamicin treated (N=3) organoids. A statistically significant difference was found among the gentamicin treated

organoids ($\chi^2(2)=6$, p=.04) whereas no difference was found among the untreated control data ($\chi^2(2)=3.8$, p=.15) (Fig. 16e). Taken together, these findings suggest that the model recapitulates some key aspects the host/pathogen interaction of *E. faecalis* with its human host.

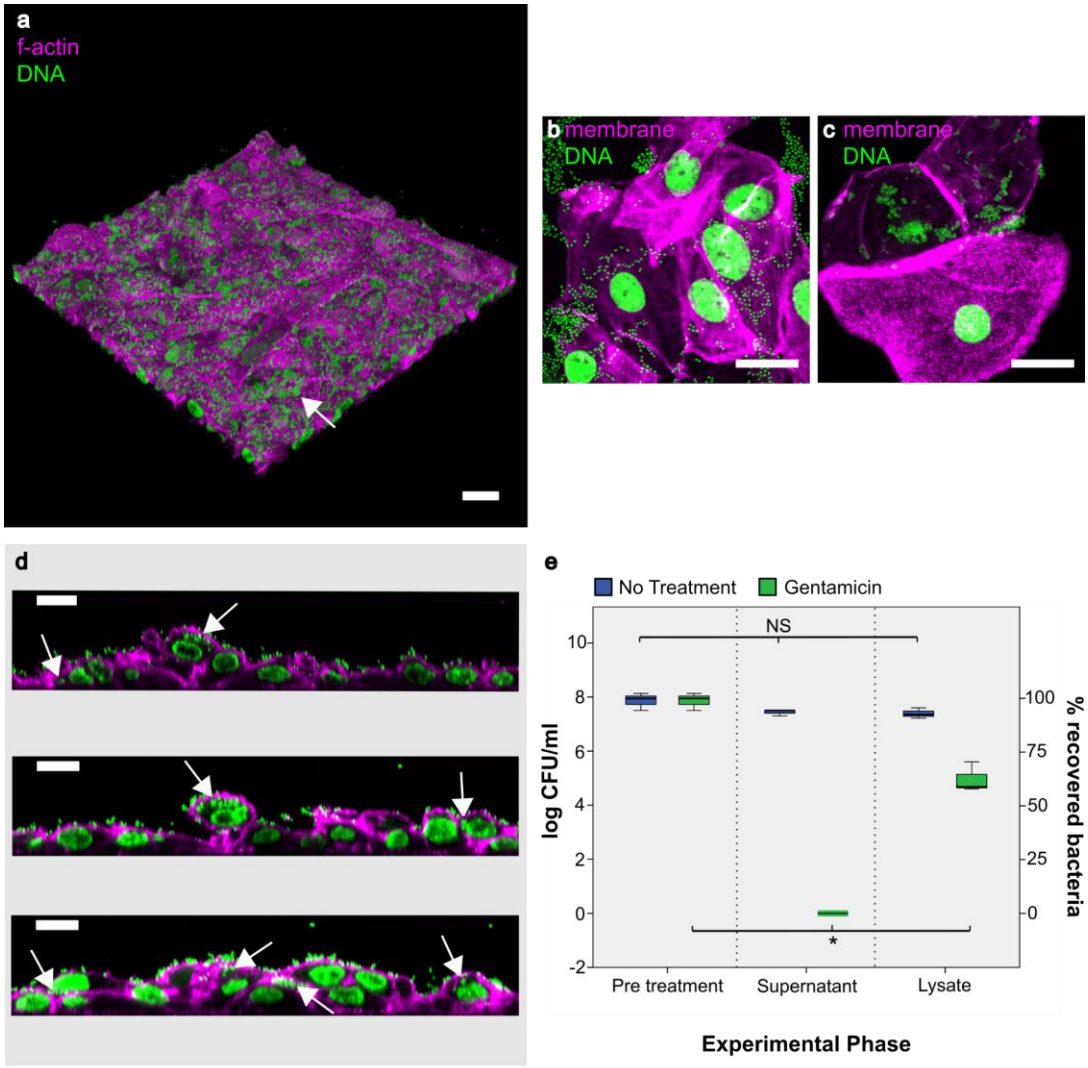

Figure 16. Analysis of HBLAK-derived urothelial organoids infected with uropathogenic *E. faecalis*

Composites showing (a) 3D confocal model constructed from a 100 slice Z-stack of HBLAK organoid post infection with *E. faecalis* (MOI of 25). phalloidin-stained F-actin in magenta and DAPI-stained DNA (host and pathogen) in green. The characteristically smooth and flat umbrella-like cell layer was lost in response to infection. Loose colonies of *E. faecalis* could be seen adhering to the now unprotected basal and intermediate cells (white arrow). (b) Surface cells shed from organoid in response to infection with *E. faecalis.* WGA-labelled membrane shown in magenta and DAPI-stained DNA (host and pathogen) in green. (c) Patient-isolated urothelial cells shed into the urine in response to infection. (d) Orthogonal cross sections prepared from image a. White arrows show evidence of intracellular *E. faecalis* within

the basal and intermediate cells of the HBLAK organoid. 7.3% of cells exhibited intracellular colonisation with a mean of 37.8 (+/- SD of 11.5) bacteria per cell. Phalloidin-stained F-actin in magenta and DAPI-stained DNA (host and pathogen) in green. Scale bars represent 20µm. (d) Box and whisker plot showing the results of gentamicin protection assays undertaken on HBLAK organoids infected with uropathogenic *E. faecalis*. Results are represented as log10 median CFU/ml with a % bacterial recovery derived axis. Treatment with 2000µg/ml of gentamicin resulted in zero detected growth within the organoid supernatant. Detergent treatment liberated intracellular bacteria resulting in the detection of $4.8x10^3$ cfu/ml in the lysate (approx. 55% bacterial recovery). N=3 per treatment. NS = No statistically significant difference (P>.05), *P≤.05.

In summary, this model, to our knowledge, represents the first long-term urine-tolerant human bladder organoid produced *in vitro*. This tissue is reminiscent of normal human bladder urothelium and expresses a number of key markers in the correct spatial compartments in response to exposure to urine. Therefore, in support of my specific hypothesis, we created a physiologically convincing 3D organoid from human stem cells. As with patients, this organoid rapidly sheds the apical cell layer in response to bacterial insult. Moreover, *E. faecalis* displayed invasive phenotypes, supporting our previous findings in shed patient cells in chapter 2 [1].

Chapter 4

Ultrasound-activated microbubbles as a novel drug delivery system for the treatment of UTI

4.1 Abstract

The development of modalities for high-efficiency intracellular drug delivery is a priority for a number of disease areas and could find broad utility as alternatives to traditional treatments. One such area is UTI, which is one of the most common infectious diseases globally and which imposes an immense economic and healthcare burden. Common uropathogenic bacteria have been shown to invade the urothelial wall during acute UTI, forming latent intracellular reservoirs that can evade antimicrobials and the immune response, allowing recurrence at a later date. This behaviour explains the high recurrence rates after oral antibiotic treatments, which are not able to penetrate the bladder wall and accumulate to an effective concentration. Meanwhile, oral antibiotics may also lead to antimicrobial resistance and cause systemic side effects. Using a human urothelial organoid model developed in chapter 3, we tested the ability of novel ultrasound-activated lipid microspheres to deliver drugs into the cortex of the apical cell layer. The lipid microspheres were decorated with liposomes containing gentamicin (which is unable to penetrate the plasma membrane on its own) and a fluorescent marker. The microsphere solution was added to buffer at the apical surface of the bladder model before being exposed to a specific frequency and amplitude of ultrasound. Drug delivery was calculated using corrected total cellular fluorescence enumerated from intracellular slices from confocal laser scanning micrographs. Ultrasound activated intracellular delivery of gentamicin using microbubbles was over twice than that achieved by liposomes alone. Moreover, little cell damage was detected and this

therapeutic technology exhibited very encouraging antimicrobial activity. In conclusion, ultrasound-activated microspheres were able to safely deliver high concentrations of drugs into urothelial cells. Therefore, they show great promise as a more efficacious alternative to traditional oral antibiotic regimes, and serve as proof of principle for intracellular drug delivery in other niches where such penetration would aid in treatment.

4.2 Materials and methods

4.2.1 Liposome Production

Conducted by Dr. Joshua Owen and Dr. Dario Carugo at Oxford University

1,2-distearoyl-sn-glycero-3-phosphocholine (DSPC), cholesterol, 1,2-distearoyl-sn-glycero-3-phosphoethanolamine-N-[methoxy(polyethylene glycol)-2000] (ammonium salt) (DSPE-PEG(2000)), 1,2-distearoyl-sn-glycero-3-phosphoethanolamine-N-[methoxy(polyethylene glycol)-2000] – biotin (DSPE-PEG(2000)-biotin), 1,2-distearoyl-sn-glycero-3-phosphoethanolamine-N-(7-nitro-2-1,3-benzoxadiazol-4-yl) (ammonium salt) (DSPE-NBD) (Avanti Polar Lipids, Alabaster, Alabama, USA) dissolved in chloroform were combined in molar ratio of (55.5:39:2.5:2.5:0.5) at a total of 33 mg. The chloroform was removed and gentamicin solution (40 mg/ml) (Sigma-Aldrich) was added followed by heating to 60°C for one hour under constant rotation to dissolve the lipid film. The liposomes were then extruded 11 times through a 400nm membrane followed by extrusion 11 times through a 200nm membrane at 55°C. The liposome size was then measured via dynamic light scattering [240] (Zetasizer Nano ZS, Malvern Instruments) and transferred to Phosphate Buffered Saline (PBS) (Sigma-Aldrich) via a G75 column (Sephadex G-75, Sigma-Aldrich) giving a lipid concentration of 40 mg/ml. The quantity of gentamicin encapsulated in the liposomes was calculated by the Oxford University engineering team (Dr. Joshua Owen, Dr.

Dario Carugo) using a previously described fluorometric o-phthaldialdehyde assay [241]

4.2.2 Microbubble (bubble) production

Conducted by Dr. Joshua Owen and Dr. Dario Carugo at Oxford University

DSPC, DSPE-PEG(2000), DSPE-PEG(2000)-biotin, 1,2-dipalmitoyl-sn-glycero-3-phosphoethanolamine-N-(lissamine rhodamine B sulfonyl) (ammonium salt) (Rod-PE) dissolved in chloroform were added to a glass vial in a ratio of 79.5:10:10:0.5 molar percent (7 mg total), This was allowed to dry overnight to produce a lipid film. PBS (2 ml) was then added and the temperature was raised above the lipid transition temperature (55 °C) under constant stirring for approximately 1 hour. The solution was then probe sonicated for 90 seconds to disperse the lipids using an ultrasonic cell disruptor (XL 2000, probe diameter 3 mm, Misonix Inc.) (setting 4, 1 minute). The headspace of the vial was then filled with Sulfur Hexafluoride (SF6) and the gas-liquid interface sonicated again (setting 19, 15 seconds) producing a white solution. This was then centrifuged (300 RCF, 10 minutes) to concentrate the microbubbles [242].

4.2.3 Binding of Liposomes to bubbles

Excess avidin (sigma Aldrich) at a concentration of 50 mg/ml was added to the microbubbles for 10 minutes followed by washing via centrifugation (300

RCF, 10 minutes). The biotin liposomes (100 µl) were then added to the microbubbles (500 µl). Liposome coated bubble solution was added to an improved Neubauer hemocytometer counting chamber and the number of bubbles per µl calculated using brightfield microscopy.

4.2.4 Ultrasound Instrumentation and organoid treatment

Ultrasonic exposures were carried out using the SAT (system for acoustic transfection) chamber. This system was based on a prior design [243] with engineering modifications to allow a decrease in the exposure area for 3D bladder organoids.

Cells and treatment agents (e.g. microbubbles, liposomes) were contained in a “sonolid” assembly, consisting of a cell culture dish (µ-Dish 35 mm, Ibidi) friction fit to a lid molded from PDMS (polydimethylsiloxane, Sylgard 184, Dow Corning). Details of the construction and assembly are the same as in Carugo *et al.* except that for the present work, a 3D culture insert was fixed between the cell culture dish and the sonolid. The sonolid was sealed onto the dish ensuring no air pockets within the cell culture insert.

The sonolid was held in the SAT by a circular bracket in the pre-focal region of a 40mm radius, 120 mm radius of curvature, 1.1 MHz center frequency ultrasound transducer (Sonic Concepts, Inc. Bothell), such that the incident pressure field was focused on the cell filter insert. The transducer drive signal path consisted of a waveform generator (33220A, Agilent

Technologies), low-pass filter (BLP-1.9+, Mini-Circuits) and power amplifier (A300, E&I Ltd.).

4.2.5 Ultrasound exposure conditions

Filter inserts, culture dishes and sonolids were assembled, placed in the ultrasound chamber and exposed to 1.1 MHz, 120 mV, 5,500 cycles at 20 ms pulse duration of ultrasound for 20 seconds. These ultrasound conditions were kept constant throughout the experimental series.

4.2.6 Compound-mediated lactate dehydrogenase (LDH) cytotoxicity assay

Cell damage caused by free gentamicin and various doses of ultrasound-activated microbubbles was measured using a commercially available colorimetric LDH assay kit (Thermo Scientific). The assay procedure was carried out as previously described and as directed by the manufacturer [244-246]. HBLAK-derived bladder organoids were grown for 14 days as above (sections 3.1.1 – 3.1.2 and [2]). The bladder organoids (N=3 per each treatment) were then exposed to 1000µl of controls (culture medium, urine, PBS alone exposed to ultrasound) or 1000µl of PBS containing: 200µg/ml gentamicin; 10-100µl of bubble solution with ultrasound; 100µl of 10X lysis buffer (maximum LDH control) or culture medium containing 10% ultra-pure water (spontaneous LDH release). Organoids receiving ultrasound exposure were treated as above for 20 seconds (sections 4.1.4 – 4.1.5). All organoids

were subsequently incubated for 45 minutes at 37ºC in 5% CO_2. Post incubation, 50µl of medium from the apical liquid-liquid interface of each treated organoid was transferred to 3 wells of a flat bottomed 96-well plate (Corning). 50µl of reaction buffer (lactate, NAD^+, tetrazolium salt (INT)) was then added to each well and gently mixed before protecting from light and incubating the plate at room temperature for 30 minutes. After this 30 minute period, the reaction was halted by adding 50µl of stop solution (0.16M sulfuric acid) to each well. To measure the quantity of LDH, the 96-well plate was read using a colorimetric spectrophotometer (Biochrom EZ Read 400) at an absorbance of 492nm (LDH) and 650nm (background). Microsoft Excel was used to subtract the instruments background reading from the LDH reading before calculating cytotoxicity in % using the following formula:

$$\%\boldsymbol{Cytotoxicity} = \frac{\boldsymbol{Treatment\ associated\ LDH\ release - Spontaneous\ LDH\ release}}{\boldsymbol{Maximum\ LDH\ activity - Spontaneous\ LDH\ release}} \times \mathbf{100}$$

4.2.7 Intracellular drug delivery

Human urothelial organoids (N=3 per each treatment) were grown for two weeks as in chapter 3 (see sections 3.1.1 – 3.1.2) before being exposed to 1000µl of PBS containing: 0.2mg/ml NBD (fluorophore); 2µl NBD-labelled liposomes containing gentamicin; or 10µl bubbles coated with 2µl NBD-labelled liposomes with or without gentamicin. Organoids were then exposed (see section 4.1.4) or not exposed to ultrasound for 20 seconds. After

washing 3 times in PBS the tissue was fixed in 4% formaldehyde in PBS overnight at 4°C. The fixed tissue was then permeabilised in 0.2% Triton-X100 in PBS for 15 minutes at RT followed by a single wash with PBS. Cells were stained with Alexa Fluor-633-conjugated phalloidin (0.6µg/ml), to label filamentous actin, and the DNA stain 4'',6-diamidino-2-phenylindole, (DAPI, 1µg/µl) in PBS for 1 hour at RT. The dual-labelling solution was gently aspirated and the cells washed 5 times in PBS. Filters were carefully removed from the culture inserts with a scalpel before being mounted on a microscope slide in FluorSave reagent and a coverslip affixed with clear nail varnish. High-definition confocal Z-stacks were taken at random areas of the organoids. The intracellular compartment of 20 umbrella cells per organoid (N=20 per Z-stack) were inspected for the presence of NBD (Ex. 488nm, Em. 536nm) using the ImageJ particle measurement tool [225]. To accurately compare the level of intracellular drug delivered by different treatments, fluorescence was expressed as corrected total cell fluorescence (CTCF) which accounts for integrated cell density (ID), surface area (SA) and background fluorescence readings (BR) [247, 248]. CTCF was calculated using the following formula in Microscoft Excel:

$$\boldsymbol{CTCF = ID\ of\ selected\ cell - (SA\ of\ selected\ cell \times BR)}$$

CTCF values were averaged for each treatment prior to statistical analysis.

4.2.8 Microbial killing and microbial clearance assays

Human urothelial organoids were grown (N=3 per each treatment) for 14 days as per sections 3.1.1 – 3.1.2 before being experimentally infected with patient-isolated *E. faecalis* as per section 3.1.5. The infected organoids were then left untreated (control) or treated with either 20-200µl/ml of free gentamicin or 10-25µl/ml bubbles coated with gentamicin-containing liposomes. Free gentamicin-treated organoids were incubated for 2 hours whereas the bubble treated organoids were stimulated with ultrasound for 20 seconds only (see section 4.1.4). To thoroughly study treatment efficacy, two independent experimental procedures were undertaken post infection and treatment (see a and b below).

a) Organoids were processed using a microbial killing assay which relied on a traditional agar plate technique to enumerate live bacteria. the organoids were lysed with 1% Triton-X100 in PBS for 10 minutes at RT. The lysate was then serially diluted in PBS (neat, 1:100, 1:1000, 1:10000) and 25µl of each lysate dilution spread on a quartile of a Columbia blood agar (CBA, Oxoid) plate. Inoculated agar plates were incubated aerobically at 37ºC for 24 hours, after which the colonies were counted to enumerate the colony forming units per millilitre (CFU/ml).

b) Organoids were inspected using a state-of-the-art imaging analyses to measure bacterial load. After washing 3 times in PBS the tissue was fixed in

4% formaldehyde in PBS overnight at 4°C. Cells were stained with DAPI at a concentration of 1µg/µl in PBS for 1 hour at RT to label human and bacterial DNA. The DAPI solution was gently aspirated and the cells washed 3 times in PBS. Filters were removed from the culture inserts with a scalpel before being mounted on a microscope slide in FluorSave reagent and a coverslip affixed with clear nail varnish. High resolution Z-stacks were gathered at random regions of the organoids using confocal laser scanning microscopy. These 3D constructs were then analysed using nearest neighbour 3D connectivity analysis with ImageJ Object counter3D [225, 234].

4.2.9 Antimicrobial susceptibility testing

The minimum inhibitory concetration (MIC) of gentamicin activity against uropathogenic *E. faecalis* was calculated using the Etest method [249]. This work was performed by the Royal Free hospital, Hampstead microbiology department in accordance with the European Committee on Antimicrobial Susceptibility Testing (EUCAST) guidelines [250].

4.2.10 Imaging

Brightfield and epi-fluorescence microscopy was conducted on an Olympus CX-41 upright microscope, and confocal laser scanning microscopy on Leica SP5 and SP2 microscopes. Images were processed and analysed using Infinity Capture and Analyze V6.2.0, ImageJ 1.50j [225] and the Leica Application Suite, Advanced Fluorescence 3.1.0 build 8587 Software.

4.2.11 Statistical analyses

Data were analysed using IBM SPSS Statistics version 24. Non-parametric tests were performed throughout this chapter due to non-normal distribution of data. Kruskal-Wallis tests were performed in the first instance before performing pairwise post hoc Mann Whitney U tests to determine differences between groups. Bonferroni corrections were applied to all P values generated during post hoc testing. 3 experimental replicates were performed for statistical testing.

4.3 Results

4.3.1 Bubble Characterisation

SF6-filled bubbles consisting of biocompatible lipid shells (DSPC, DSPE-PEG, DSPE-PEG-biotin) and fluorescently labeled gentamicin-containing liposomes (DSPC, DSPE-PEG, DSPE-PEG-biotin, DSPE-NBD, gentamicin) were produced in collaboration with The Institute of Biomedical Engineering, Oxford University (see Figure 17a for a schematic representation). Drug encapsulation was successful, with a concentration of 320 µg/ml gentamicin detected in the liposome solution using a fluorometric o-phthaldialdehyde assay. Liposomes were bound to the bubbles at a ratio of 1:6, giving a final gentamicin concentration of 53 µg/ml in the liposome-coated bubble solution.

Visual inspection of uncoated bubbles (no liposomes) using brightfield microscopy showed the bubbles to be spherical in appearance and homogeneous in size (~5 µm) at a given focal plane (Fig. 17b). Epi-fluorescent microscopy of bubbles decorated with liposomes containing gentamicin and fluorescently labelled with NBD demonstrated the expected staining at the bubble circumference (Fig. 17c). As with the uncoated bubbles, the coated bubbles appeared spherical and homogeneous in size, however, the liposome-coated bubbles were slightly larger with a diameter of approximately 7 µm.

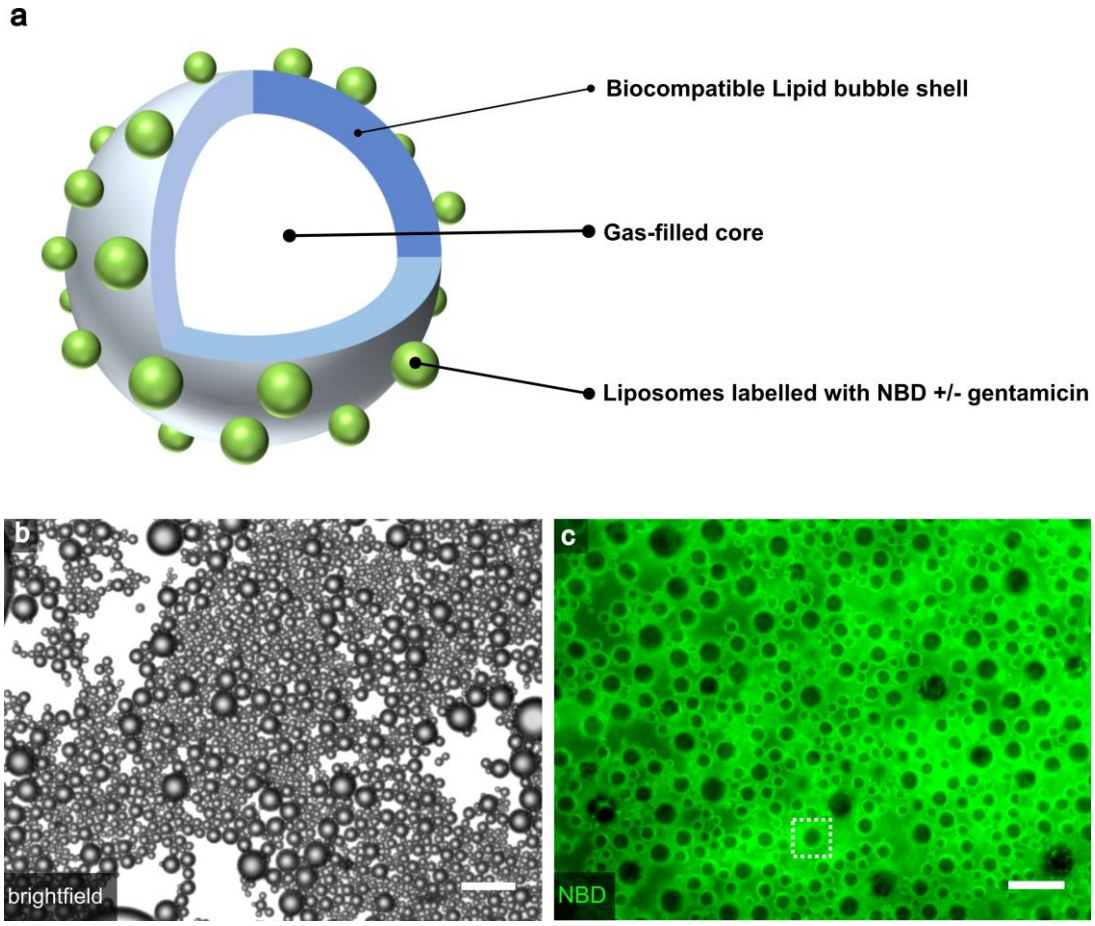

Figure 17. Microscopic inspection and structural schematic of bubbles

(a) Schematic of a single liposome-decorated bubble (white box in c). Bubble shells were constructed from biocompatible lipids surrounding a gaseous sulphur hexafluoride (SF6) core. The central bubble is coated with liposomes containing fluorescent dye (NBD, nitrobenzoxadiazole) with or without gentamicin. (b) Monochrome image of uncoated bubbles taken using brightfield microscopy. Each bubble is approximately 5µm in diameter. Scale bar represents 40 µm. (c) Epi-fluorescence image of bubbles decorated with liposomes containing gentamicin and labelled with NBD (green). Each coated bubble is approximately 7µm in diameter. Scale bar represents 20µm.

4.3.2 The cytotoxicity of low-dose ultrasound-activated bubble therapy is comparable to that of conventional antimicrobial treatment in a human urothelial organoid model.

In the first set of experiments we challenged HBLAK-derived human urothelial organoids (chapter 3 and [2]) with controls, a therapeutic dose of gentamicin and a range of bubble concentrations stimulated with ultrasound. The quantity of released LDH was then detected using a colorimetric LDH assay to explore and compare the levels of cytotoxicity induced by these differing treatments and dosages.

Firstly, to standardise bubble treatment dosages, the freshly prepared bubble solution was added to a haemocytometer to count the number of intact bubbles per µl (Fig. 18a). This procedure was repeated prior to all subsequent experimentation to ensure repeatability.

As expected, the addition of culture medium to the human urothelial organoid resulted in zero cytotoxicity (n=3) (Fig. 18b). Moreover, supporting the urine-dependent nature of the urothelial organoid [2], human urine also resulted in zero cell damage (n=3) (Fig. 18b). Additionally, toxicity caused by ultrasound exposure alone was negligible (n=3) (Med=0.23%, Q1=0, Q3=0.42) (Fig. 18b). Exposure of urothelial organoids to 200 µg/ml gentamicin solution (comparable to human urinary concentrations post intramuscular gentamicin treatment for UTI [251]) had a median cytotoxic effect of 11.61% (Q1=10.65, Q3=13.51) (n=3) (Fig. 18b).

Cytotoxicity induced by ultrasound-activated bubbles, coated with blank or gentamicin-containing liposomes, increased in a dose responsive manner (Fig. 18b). However, bubbles decorated with gentamicin-containing liposomes appeared to be more toxic than those decorated with blank liposomes, particularly at higher doses. For example, treatment with 10 µl of bubble solution, containing blank or gentamicin liposomes, caused a median of 13.51% (Q1=13.39, Q3=14.12) (n=3) and 13.65% (Q1=13.56, Q3=13.90) (n=3) cell disruption respectively. In contrast, 100 µl of blank bubble solution induced a median of 26.57% (Q1=26.34, Q3=27.47) (n=3) cell death whereas 100 µl of their gentamicin-containing counterparts caused 36.35% (Q1=35.98, Q3=37.69) (n=3) (Fig. 18b).

In summary, low-dose ultrasound-activated bubble therapy exhibits a comparable level of cytotoxicity to that of conventional gentamicin treatment in a human urothelial model. Higher doses (50 and 100 µl) of the bubble preparation, at least in this model system, resulted in dramatically increased levels of cell death. Therefore, we decided to exclude the higher doses in subsequent experiments.

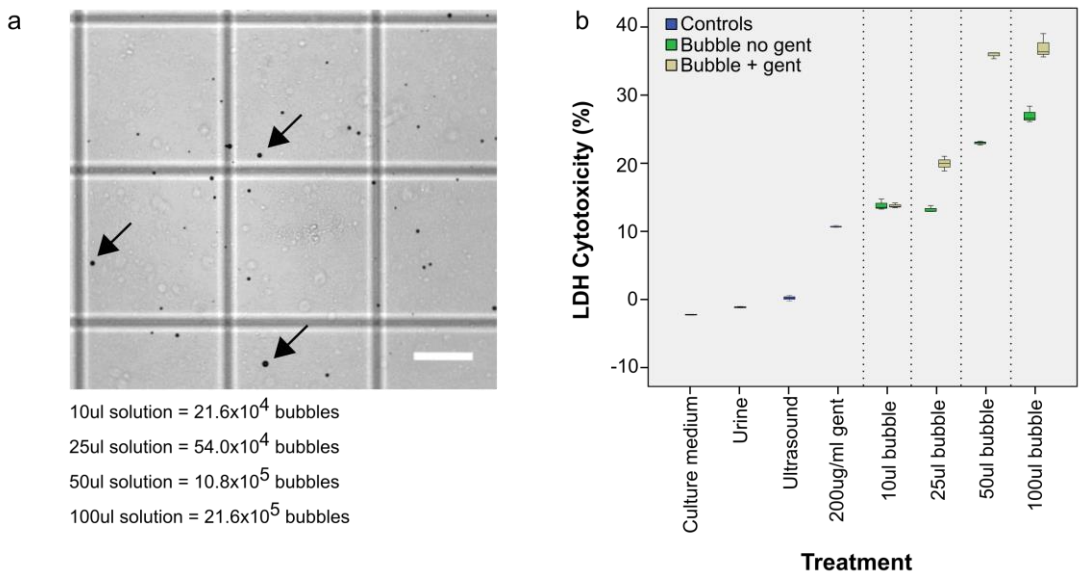

Figure 18. The cytotoxicity of low-dose ultrasound-activated bubble therapy is comparable to that of conventional antimicrobial treatment in a human urothelial organoid model

Human urothelial organoids were exposed to ultrasound alone, control substances, free gentamicin or a range of bubble doses activated with ultrasound. Bubbles were coated with blank liposomes or liposomes containing gentamicin. Cytotoxicity was calculated by measuring LDH release using a colorimetric assay. All experiments were repeated in triplicate. Box and whisker plots represent median, interquartile range and maximum and minimum LDH values. (a) Monochrome brightfield image of Neubauer hemocytometer counting chamber loaded with bubble solution. The number of bubbles (black arrows) were enumerated per µl to calculate the total number of bubbles added during subsequent experimentation. Scale bar represents 100µm. (b) Box and whisker plot showing the degree of cytotoxicity induced by control substances and increasing quantities of ultrasound-activated bubbles with or without gentamicin (see colour coded key). Control substances and ultrasound alone caused no cell damage whereas cytotoxicity due to free gentamicin and ultrasound-activated bubbles increased in a dose-dependent manner. N=3 per treatment. Abbreviations; gent (gentamicin), LDH (lactate dehydrogenase).

4.3.3 Ultrasound-activated bubbles exhibit significantly higher intracellular drug delivery than do liposomes alone.

In the next set of experiments we explored the ability of liposomes and liposome decorated bubbles to deliver a fluorescent compound into the intracellular compartment of human urothelial cells in the presence of ultrasound. Human urothelial organoids (chapter 3 and [2]) were exposed to nitrobenzoxadiazole alone (NBD, fluorophore), 2µl NBD-labelled liposomes containing gentamicin; or 10µl bubbles coated with 2µl NBD-labelled liposomes with or without gentamicin. Half of the organoids were exposed to ultrasound for 20 seconds and the remainder left untreated. Post treatment, the organoids were stained and imaged using confocal microscopy to determine and compare the level of intracellular NBD using corrected total cellular fluorescence (CTCF) (Fig 19a).

Treatment with NBD solution alone (n=3) resulted in a median intracellular CTCF value of 425.66 (Q1=377.26, Q3=1024.84) (Fig 19a). Liposomes without ultrasound stimulation (n=3) readily delivered NBD into the umbrella cells of the organoid (Med=3533.57, Q1=2847.72, Q3=4352.12), however, acoustic stimulation (n=3) appeared to have little influence (Med=4100.16, Q1=3815.55, Q3=4149.05) (Fig 19b).

Intracellular NBD delivery via the blank-liposome coated bubbles without ultrasound (n=3) was similar to liposomes alone (Med=4553.93, Q1=4402.26, Q3=5446.87). That said, when stimulated with ultrasound

(n=3), the intracellular NBD CTCF value increased by a factor of two (Med=9544.68, Q1=7049.89, Q3=10418.96) (Fig 19b). Bubbles decorated with gentamicin containing liposomes, in the absence of ultrasound (n=3), appeared to deliver a relatively low concentration of NBD (Med=427.34, Q1=404.32, Q3=2334.6) (Fig 19b). However, as with the bubbles coated with blank liposomes, the intracellular CTCF increased dramatically under acoustic stimulation (n=3) (Med=7132.13, Q1=6775.41, Q3=9224.22) (Fig 19b). The result of a Kruskal-Wallis test showed there to be a statistically significant difference between the intracellular NBD CTCF values delivered by these various treatment modalities $\chi^2(6)=16.364$, p=.012 (Fig 19b).

Taken together, ultrasound-activated liposome-coated bubbles can efficiently deliver high concentrations of compounds into the intracellular compartment of human urothelial cells. Moreover, they were able to deliver far higher concentrations than liposomes alone, and the addition of gentamicin appeared to have little influence.

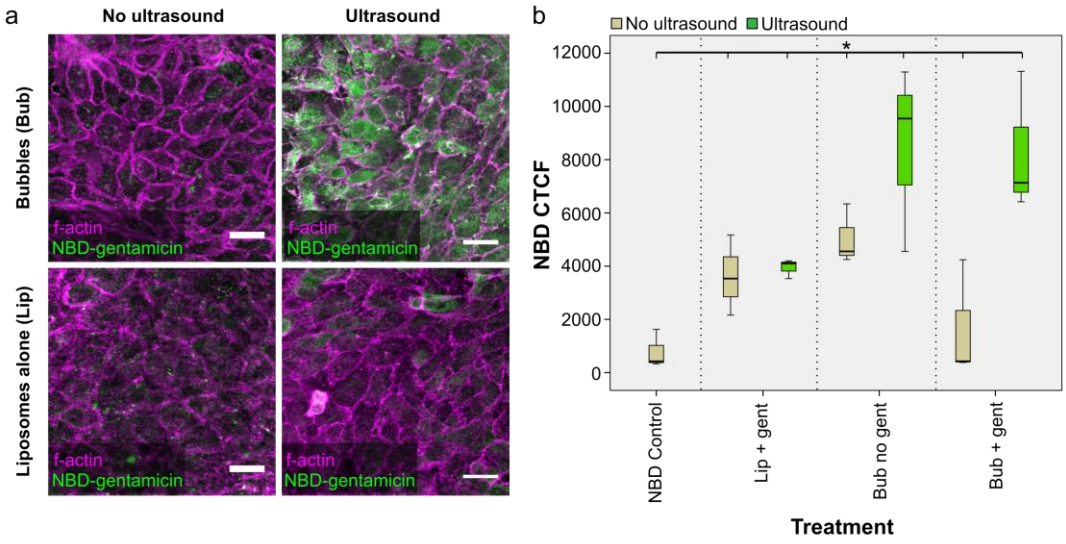

Figure 19. Ultrasound-activated bubbles exhibit significantly higher intracellular drug delivery than do liposomes alone

Human urothelial organoids were exposed to NBD (fluorophore) in solution, NBD-labelled liposomes containing gentamicin, or bubbles coated with NBD-labelled liposomes with or without gentamicin. After exposure to ultrasound or no exposure to ultrasound, treated organoids were fixed. high definition laser scanning confocal z-stacks of each organoid were analysed to measure intracellular delivery using corrected total cellular fluorescence (CTCF). All experiments were repeated in triplicate. Box and whisker plots represent median, interquartile range and maximum and minimum CTCF values. (a) Representative intracellular confocal slices within the umbrella cell layer of human organoid after liposome or bubble treatment with or without ultrasound. Phalloidin labelled f-actin is shown in magenta and intracellular NBD is shown in green. Scale bars represent 40µm. (b) Box and whisker plot comparing intracellular drug delivery of each treatment with or without the addition of gentamicin and acoustic stimulation (see colour coded key). N=3 per treatment. Abbreviations; Bub (bubbles), Lip (liposomes), gent (gentamicin), NBD (nitrobenzoxadiazole). *P≤.05.

4.3.4 Ultrasound-activated bubble therapy is as effective as high-dose gentamicin treatment at killing uropathogenic *E. faecalis* in a human model of UTI.

As discussed in the previous chapters, *E. faecalis* is responsible for a significant proportion of chronic UTI cases [1], a fact which is likely due to this pathogens' ability to invade the cells of the urothelium [1, 2]. In the next set of experiments, we infected human urothelial organoids with a patient-isolated strain of *E. faecalis* before treating the mimetics with gentamicin for 2 hours or ultrasound-activated bubble (coated with gentamicin containing liposomes) therapy for 20 seconds. Post treatment, the 3D cultures were lysed with detergent and the lysate plated on microbiological agar to measure the quantity of live bacteria.

The lysate harvested from untreated organoids (n=6) grew a median of $3x10^7$ CFU/ml ($Q1=2x10^7$, $Q3=3.2x10^7$) (Fig 20a). The number of live *E. faecalis* after treatment for 2 hours with 20 µg/ml of free gentamicin (n=3) was lower than in the untreated mimetics, if not substantially ($Med=2.28x10^7$, $Q1=1.97x10^7$, $Q3=2.34x10^7$) (Fig 20a). Unsurprisingly, considering an Etest indicated a MIC of 7 µg/ml of gentamicin in this bacterial strain (Fig 20b), the addition of 200 µg/ml (n=3) was far more potent ($Med=1.96x10^6$, $Q1=1.43x10^6$, $Q3=3.18x10^6$) (Fig 20a). A less expected result, given the far lower gentamicin concentrations (0.53 µg/ml and 1.32 µg/ml respectively) was the antimicrobial properties exerted by the 10 µl ($Med=8x10^6$, $Q1=4.7x10^6$, $Q3=8.2x10^6$) and 25 µl ($Med=8x10^6$, $Q1=4.8x10^6$, $Q3=9x10^6$)

doses of acoustically stimulated bubbles (Fig 20a). The result of a Kruskal-Wallis test showed there to be a statistically significant difference between the number of *E. faecalis* killed by these treatments $\chi^2(4)=12.074$, $p=.007$ (Fig 20a).

To summarise, acoustically stimulated bubble therapy shows promising antimicrobial activity against uropathogenic *E. faecalis* embedded in a human urothelial organoid. Furthermore, this bactericidal action was achieved within 20 seconds by sub-clinical concentrations of encapsulated gentamicin.

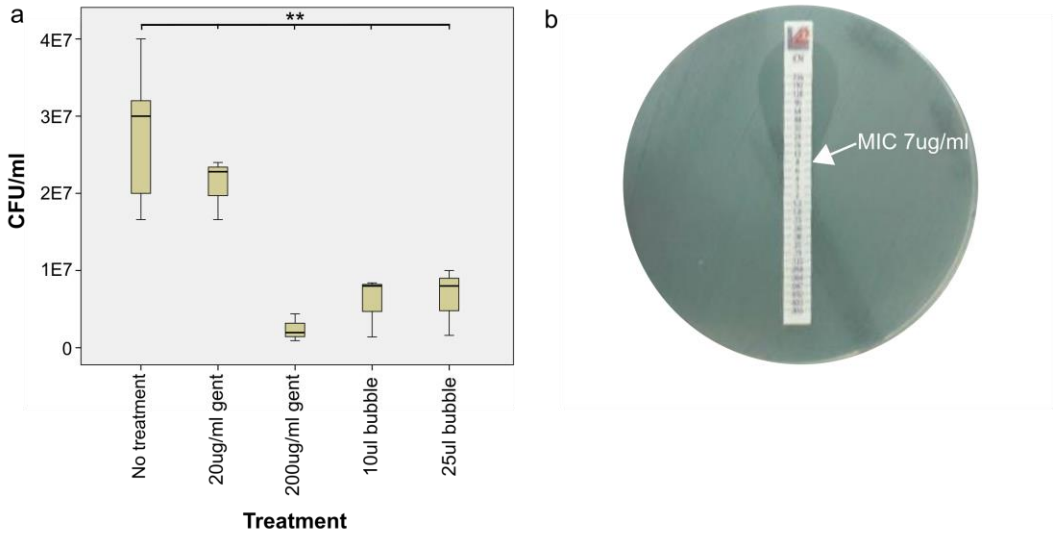

Figure 20. Ultrasound-activated bubble therapy is as effective as high-dose gentamicin treatment at killing uropathogenic *E. faecalis* in a human model of UTI

Human urothelial organoids were infected with patient-isolated *E. faecalis* before being treated with either free gentamicin or bubbles coated with gentamicin-containing liposomes. Free gentamicin-treated organoids were incubated for 2 hours whereas the bubble treated organoids were stimulated with ultrasound for 20 seconds only. Post treatment the organoids were lysed with detergent and the lysate added to agar plates to enumerate the bacterial colony forming units per millilitre (CFU/ml). All experiments were repeated in triplicate. Box and whisker plots represent median, interquartile range and maximum and minimum CFU/ml values. (a) Box and whisker plot presenting the number of live bacteria detected after no treatment (N=3), free gentamicin treatment (N=3 at each dose) and ultrasound-activated bubble therapy (N=3 at each dose). (b) Photograph of antimicrobial susceptibility Etest conducted in this study. The image shows that this strain of *E. faecalis* required a minimum inhibitory concentrations (MIC) of 7µg/ml of gentamicin (white arrow). Abbreviations; gent (gentamicin). **P≤.01.

4.3.5 Ultrasound-activated bubble therapy is more effective than conventional antibiotic treatment at reducing the bacterial load in a human model of UTI.

In addition to the microbiological methods deployed in the last section (4.3.4), we also analysed infected organoids using an imaging technique to ascertain the level of bacterial burden pre- and post-treatment. To achieve this, a further set of human urothelial organoids were grown, infected and treated as above but, in contrast to the last experiments, the mimetics were then fixed and stained in preparation for confocal microscopy. High resolution Z-stacks were acquired (Fig. 21a) at random fields before analysing these 3D constructs using a 3D nearest neighbour connectivity technique to enumerate the number of *E. faecalis* per human cell.

The untreated organoids (n=3) contained a median of 34.17 (Q1=28.85, Q3=38.7) bacteria per urothelial cell (Fig. 21b). Interestingly, 2 hours of exposure to either 20 µl/ml (n=3) or 200 µl/ml (n=3) of free gentamicin appeared to have little effect on bacterial burden (Med=43.07, Q1=39.29, Q3=45.49 and Med=36.15, Q1=33.56, Q3=41.28 respectively) (Fig. 21b). In contrast, however, the 10 µl dose (n=3) of ultrasound-activated bubble treatment dramatically lowered the bacterial load in this system (Med=12.61, Q1=11.14, Q3=19.53) (Fig. 21b). Furthermore, bacterial burden in the infected urothelial organoids treated with the higher bubble dose (25 µl) (n=3) appeared lower still (Med=9.11, Q1=8.08, Q3=9.72) (Fig. 21b). The result of a Kruskal-Wallis test showed there to be a statistically significant

difference between the number of *E. faecalis* per urothelial cell after each of these treatments $\chi^2(4)=10.6$, p=.031 (Fig. 21b).

To better compare these findings, data acquired from each gentamicin and bubble dose were pooled together into treatment types (Fig. 21c). The result of a Mann-Whitney U test showed there to be no statistically significant difference in bacterial load after no treatment (n=3, Med=34.17, Q1=28.85, Q3=38.7) and treatment with free gentamicin (n=6, Med=39.61, Q1=35.52, Q3=46.41) (U=5, p=.381) (Fig. 21c). However, further Mann-Whitney tests showed there to be a statistically significant difference in bacterial burden between bubble treatment (n=6, Med=10, Q1=9.11, Q3=12.61), no treatment (U=1, p=.039) and gentamicin treatment (U=0, p=.002) (Fig. 21c).

Taken together, ultrasound-stimulated bubble therapy would appear to be more effective than therapeutic doses of gentamicin at removing *E. faecalis* from a human urothelial organoid.

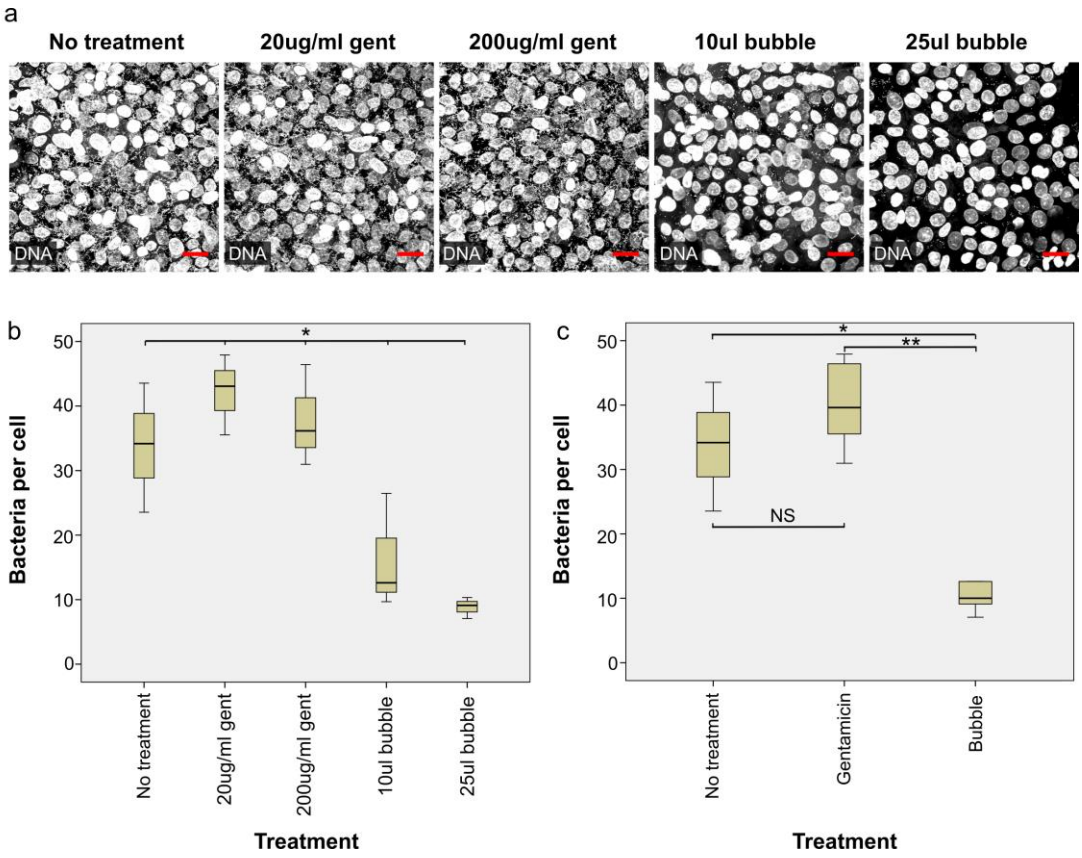

Figure 21. Ultrasound-activated bubble therapy is more effective than conventional antibiotic treatment at reducing the bacterial load in a human model of UTI

Human urothelial organoids were infected with patient-isolated *E. faecalis* before being treated with either free gentamicin or bubbles coated with gentamicin-containing liposomes. Free gentamicin-treated organoids were incubated for 2 hours whereas the bubble-treated organoids were stimulated with ultrasound for 20 seconds only. Post treatment the organoids were fixed, stained and imaged using confocal laser scanning microscopy to produce high-definition 3D constructs. These constructs were then investigated using nearest neighbour 3D connectivity analysis [234] with voxel size filters to enumerate the number of bacteria per urothelial cell. All experiments were repeated in triplicate. Box and whisker plots represent median, interquartile range and maximum and minimum number of bacteria per human cell. (a) Representative maximum projection confocal images of infected human urothelial organoids post treatment. Host (urothelial nuclei, larger circular structures) and bacterial (*E. faecalis*, small circular specks) DNA were labelled with DAPI. (b) Box and whisker plot comparing the

median number of bacteria adhered to each urothelial cell after no treatment (N=3), free gentamicin (N=3 for each dose) and ultrasound-activated bubble treatment (N=3 for each dose). (c) Box and whisker plot comparing no treatment data (N=3) with pooled free gentamicin (N=6) and bubble treatment (N=6) data. Abbreviations; gent (gentamicin). NS = No statistically significant difference (P>.05), *P≤.05, **P≤.01, ***P≤.001.

In summary, this pilot data shows, in support of my hypothesis, that acoustically-stimulated bubble treatment is safe, fast and effective in regards to both killing and removal of uropathogenic *E. faecalis* in a human-derived bladder mimetic. Furthermore, this mode of treatment shows great promise in its ability to concentrate drug in the intracellular space of these highly-specialised cells.

Chapter 5

Discussion, future aims and conclusion

5. Discussion, future aims and conclusion

Over the past decade, a model of the pathophysiology of UTI has solidified into accepted fact. Stemming from the initial elegant description of intracellular UPEC in mouse models of acute UTI [95], a number of studies have generally supported these initial findings. The data in mouse models is indeed robust [10, 93-99]. It is worth noting, however, that the evidence for the presence of intracellular bacteria in human patients suffering acute UTI is lacking [96] [252] [253] [53]. Therefore, more data on the pervasiveness of intracellular bacteria in acute human UTI would be welcome.

In the case of non-acute, low-grade UTI responsible for chronic LUTS, even less is known about the bacterial lifecycle within the bladder. Our previous study showed that *E. coli* is not the sole or even foremost pathogen in these patients, and that a spectrum of species may be capable of causing such troublesome symptoms [13]. In that report we showed close association of four bacterial species – *E. faecalis, Streptococcus angiosus, E. coli and Proteus spp.* with epithelial cells shed from patients, suggestive of intracellular colonization, and further demonstrated that these bacterial isolates seemed competent to invade a bladder cell line, as assessed by an antibiotic protection assay. We were aware, however, that this assay, although widely trusted and used, could give misleading results if all extracellular bacteria were not killed by the antibiotics – for example if they were protected by biofilm formation or by very close association within niches in the external cell membrane.

In chapter 2 we improved on these methods. We saw compelling evidence of intracellular bacteria in patient-isolated urothelial cells using fluorescence confocal microscopy. Furthermore, these data strongly suggested *E. faecalis* was an invasive pathogen whereas *E. coli* appeared to be associated with the surface membrane of the cell. Although UPEC at the centre of IBCs can exhibit a coccoid morphology, these biofilm-like pods in experimental mouse models are very tightly packed and UPEC residing at the circumference of this pod, along with extracellular adherent bacteria, maintain a more rod-shaped (or filamentous) morphology [10, 95, 97]. In contrast, in this study, the colonies of Enterococcus observed were far more loosely organised and both extracellular and intracellular bacteria were equally coccoid in morphology. We concluded therefore, with corresponding culture results and phenotypic bacterial typing, that the invasive pathogen was indeed *E. faecalis*. Nevertheless, in future work, species-specific labelling using molecular methods such as peptide nucleic acid fluorescent *in situ* hybridisation (PNA-FISH) could be employed for definitive identification [254]. It will also be vital to survey more patients to see how widespread this phenomenon is.

When isolates of *E. coli* or *E. faecalis* were used to infect a human bladder cell line, which could be fixed post-infection and examined via confocal microscopy, we detected unequivocal intracellular colonization by five out of five isolates of *E. faecalis*. Surprisingly, although all five *E. coli* isolates demonstrated extensive extracellular adherence and biofilm-like formation,

none were able to invade the cells. It is known that the bacterial virulence factor FimH is required for *E. coli* to invade bladder cells [223], so it is possible that our LUTS-derived isolates were deficient in some way for expression or sequence of this domain. However, this is unlikely, as we confirmed using a standard blood agglutination assay that our LUTS-derived *E. coli* expressed functional FimH (data not shown). Also, FimH is required for extracellular adhesion [91, 255, 256] and pathogenic biofilm formation [257], which all five strains were able to achieve in our tissue culture experiments. This suggests that *E. coli* isolated from these patients are indeed pathogenic but may lack the necessary putative downstream post-adhesion factors required for invasion. Further exploration of the FimH sequence in these strains and of other virulence factors could shed light on this interesting difference.

Biofilm formation in UTI was not within the scope of this thesis; nonetheless, as discussed previously, the absence of an invasive lifestyle does not necessarily preclude disease [258]. Indeed, clearing extracellular biofilms in the bladder could prove equally challenging for the host's immune system and traditional treatments [259]. We are currently gathering data on uropathogenic biofilm formation on a variety of substrates. By exposing these biofilms to traditional antibiotics and novel therapeutics and incubating with the fluorescent redox dye cyanoditolyl tetrazolium chloride (CTC), which can distinguish metabolically active bacteria from dead/persister cells, we have designed a robust assay for analysing antimicrobial efficacy. Furthermore, we acquired software named Comstat 2 which allows us to glean numerical

data from physical attributes such as biomass, density and the proportion of metabolically active bacteria [260]. We hope to publish on this topic during my postdoctoral position.

Taken together, the results from chapter 2 [1] suggest that, in contrast to the case of acute UTI, *Enterococci* may be a key invasive pathogen in LUTS. The mechanism by which *E. faecalis* invades urothelial cells is unknown. However, it is likely that, as with *E. coli* invasion, a necessary first step would be adhesion, in which case various previously described adhesion proteins are likely to be involved [261]. Afterwards, it is possible that, like *E. coli*, *E. faecalis* may take advantage of the unique fusiform / discoid vesicle trafficking system used by urothelial cells during compensatory endocytosis, and become passively engulfed [10, 262]. Alternatively, it is known that *E. faecalis* are able to invade intestinal epithelial cells via the production of aggregation substance (AS) and therefore it is possible that a similar mechanism is involved in urothelial invasion [263]. It is important to note, with emerging discovery of the urinary microbiome, that polymicrobial infections are highly plausible and that several opportunistic bacterial species may be involved in the pathogenesis of UTI [264-266]. Additional studies, therefore, with more isolates will be needed to see how widespread *E. faecalis* is in LUTS patients, the invasive mechanisms involved and whether other species can also invade. Meanwhile, these data constitute, to our knowledge, the first report of definitive intracellular invasion of urothelial cells by *E. faecalis*.

One of the problems of pinpointing an infective aetiology for LUTS lies in the poor sensitivity of routine urine testing, whose weakness has been amply demonstrated [46-48, 267]. Infection associated with lower counts of bacteria, which may nevertheless be significant in the case of LUTS patients [13, 40, 51, 53, 54, 57, 267, 268], tend not to be detected by urinary dipstick for nitrite (produced only by Gram-negative bacteria [269]) or leukocyte esterase, nor by routine MSU cultures with high thresholds for what is considered “positive” (e.g. in the UK and many other countries, this breakpoint is $\geq 10^5$ cfu ml^{-1}). Therefore, there is much interest in markers that might help diagnose such lower-grade urinary infections. Pyuria is one such validated marker. In addition, during acute UPEC-mediated UTI, inflammatory responses are known to cause urothelial cell shedding in both mice and humans [96, 100-103]. This jettisoning is thought to be a defense mechanism to reduce bacterial burden in the urothelium. While some have dismissed urothelial cells in urine as contamination from the urogenital area during sample collection, our data show that the majority of these cells stain positive for uroplakin-3 and can therefore be considered to originate from the urothelium. In our study, epithelial shedding showed a strong relationship with pyuria: the higher the white blood cell count in the urine, the more epithelial cells were shed. Interestingly, even low pyuria counts (1 to 9 WBC μl^{-1}) were associated with shedding, supporting the hypothesis that examining such cells in fresh urine, along with pyuria, might help diagnose infection undetected by dipstick or routine MSU culture.

The development and use of *in vitro* human tissue mimetics is thought to be accelerating the drug discovery process [270] and improving our understanding of human tissue morphogenesis. Due to improved physiological relevance, such models could even reduce the use of animal models in the coming years [271]. In chapter 3, we present a urine-tolerant, three-dimensional urothelial organoid derived from human progenitors that is easy to grow from commercially-sourced, quality-controlled materials, that displays key hallmarks of the human urothelium, and which may serve as an alternative to the murine model. If desired, it should also be possible to create similar urine-tolerant organoids from fresh human biopsies using the protocols and defined medium we describe.

An even more physiological response could well be achieved in future studies by embedding the organoid into a perfusion-based bioreactor allowing the flow of apical urine. Indeed, the introduction of relevant shear forces and metabolite flux have been shown to effect host cell development and pathogen binding and virulence [89] [272-275]. A company named Provitro™ in Germany has helped us design a perfusion chamber circuit to grow and infect engineered human urothelium under a controlled, automated environment, which they subsequently manufactured for us. Using programmable state-of-the-art peristaltic pumps, gas permeable media bags, digital hot plates and a perfusion chamber designed to hold 3D culture inserts, we will be able to mimic voiding of the bladder (Fig. 22). This system should not only improve the phenotypic characteristics of the cultured tissue but will also allow us to very accurately infect and treat the organotypic

model in order to explore the generation and resolution of chronic infection. A further future aim is to introduce servo-controlled devices to impart stretch forces within the mimetic during modelled fill and empty cycles [276]. Umbrella cells dramatically alter their membrane surface area via compensatory endocytosis during bladder fill/empty cycles by trafficking uroplakin plaques in and out of the cytoplasm [59, 262]. This dynamic process is believed to be involved in intracellular pathogenesis [59, 262]. By mimicking detrusor activity with stretch forces, we hope to be able to stimulate compensatory endocytosis and study its involvement in the pathogenesis of UTI in a highly-controlled environment.

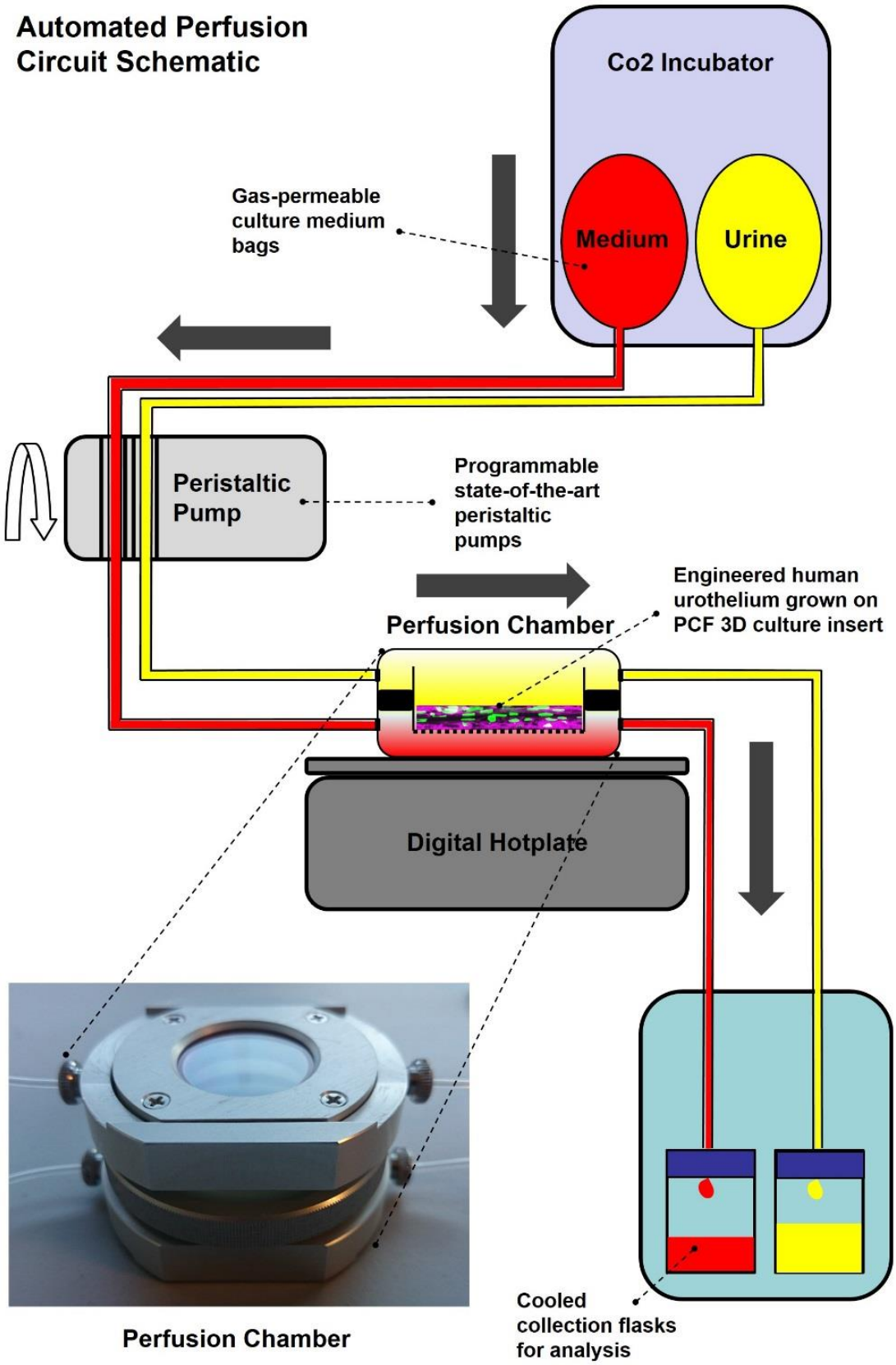

Figure 22. Automated perfusion circuit schematic

As our organoid model was generated in a similar manner to others that have been reported [65], it is not clear why it has superior urine tolerance. Additional work in our laboratory has not revealed any differences in outcome depending on the source of the human urine. The primary cells, and their HBLAK derivatives, were obtained from standard healthy adult human biopsy of the trigone region, and we do not anticipate this being materially different from trigone biopsies taken from other young healthy donors; indeed, we achieved good results with similar cells sourced from a different company. Therefore, the most likely factor is the specialized medium, which is free of serum and other growth factor supplements that could impair differentiation. We are currently using an empirical approach to determine which aspects of the growth media and urine are important for differentiation. Indeed, our findings so far show that low osmolarity in the apical medium appears to drive differentiation in these cells.

Morphologically, the HBEP and HBLAK cells produced tissue with encouraging similarities to human urothelium [10, 58, 59, 65]. HBEP cells produced tissue ~3 cell layers thick whereas HBEP cell-derived tissue elaborated ~5-7 layers. In contrast to mice, higher mammals such as humans have multiple intermediate cell layers, a feature which may favor the use of HBLAK cells [61]. However, rate of cell division could have played a role in this outcome, as could cell senescence in the HBEP population [277]. Both culture types developed an apical layer of enlarged, flattened cells that appeared umbrella-cell-like [61] in morphology. Multiple nuclei were not very common in these cells, as would be expected from the mouse urothelium.

We could find no consensus in the literature about the expected percentage of multinucleation in the human urothelium, with studies being scant, and it is also not clear whether the multinucleated state plays any functional role. Further work is needed to understand how tissue thickness and multinucleation is regulated in both cell types.

Phenotypic analysis of both the HBEP and HBLAK urothelial organoid tissue elucidated the presence of some important urothelial markers. Uroplakins are a group of highly conserved glycoproteins which are unique to mammalian urothelium [228]. Uroplakin-III (UP3) was expressed on the apical surface throughout the differentiated tissue and its expression was morphologically similar to that of patient-shed urothelial cells. Laguna *et al.* (2006)[58] found that the normal human urothelium expresses a range of cytokeratins in relation to the level of cytodifferentiation. Our 3D culture mimicked these findings with cytokeratin-8 (CK8) found throughout the tissue and cytokeratin-20 (CK20) being a preferential phenotype of well-developed umbrella cells [58]. To our knowledge, this is the first human bladder organoid demonstrating the correct spatial expression of CK20 [77].

Patients with overactive bladder symptoms are frequently treated with antimuscarinics which target muscarinic receptors in the detrusor and urothelium [235]. Crucially, rodent bladder urothelial cells do not express muscarinic receptors [236]. In the case of the HBEP and HBLAK tissue grown in this study, muscarinic receptors M2 and M3 were detected throughout the urothelial cell layers, further supporting its physiological

relevance and potential use in the development of novel therapeutic agents for the bladder symptoms of MS and other neurogenic disorders.

More detailed analysis revealed several interesting aspects to our HBLAK organoid model. First, EM showed that the tissue was not homogenously differentiated; instead, the surface consisted of three discrete zones: ‘valleys’ of undifferentiated monolayer; ‘plateaus’ of fully differentiated 3D tissue; and ‘mountains’ of hyperplasia. Second, inspection of GAG layer markers revealed that the presence of urine correlates with its elaboration, in parallel with differentiation and organoid formation. Third, focusing on the differentiated plateaus, which comprised about two-thirds of the total area, our EM imaging shows expected key features, including morphologically distinct layers, and the enlarged flat nature of the distended umbrella-like cells. We also noted structures consistent in shape, size and spacing with the characteristic hinges and plaques associated with the AUM, and with the fusiform vesicles responsible for trafficking during bladder filling and emptying phases. These structures were entirely absent from the zone of undifferentiated cells, showing a possible correlation with differentiation status. However, higher resolution EM imaging and immunostaining is needed to confirm their identity.

Intriguingly, when we tested the barrier function of the organoid by several methods, including transepithelial resistance and fluorescent dextran permeability (see Appendix 4. for fluorescent dextran assay data), we found a lack of what is traditionally thought of as urothelial “barrier function”. We

presume that this result was caused by the sporadic presence of undifferentiated cells across the tissue, which in essence short-circuit the apicobasal electrical potential difference. This result, taken together with the fact that the non-differentiated zone devoid of AUM-like structures and GAG can grow for several weeks in the presence of urine, strongly suggests that AUM and GAG are not required for urine tolerance, and that something intrinsic in the cells themselves confer resistance to its toxic effects. It also suggests that apical urine is necessary for full differentiation. Whilst it may be the case that urine is not sufficient for differentiation, given the presence of the undifferentiated 'valleys', it may also be the case that a subset of HBLAK cells are subtly different. Further exploration into the nature of urine tolerance and the effect of urine and other media components on differentiation and hyperplasia are warranted. Genomic analysis of cells from various regions, compared with starting cells, would also be interesting. In the meantime, researchers performing image-based studies should be able to focus on areas of the organoid corresponding to their desired level of differentiation.

Our model shows great promise for studying the host/pathogen interactions of UTI in a human-cell system. The majority of host/pathogen interaction studies in UTI focus on the most common uropathogen *E. coli*, but very little is known about other uropathogens such as *Enterococcus faecalis*, which is more common in certain cohorts, such as the elderly, the hospitalized and those using urinary catheters. In chapter 2 we reported the discovery of intracellular colonies of *E. faecalis* harbored within the urothelial cells of chronic UTI patients [1]. These results also showed sloughing of umbrella

cells from the epithelial lining into the urine, which is known in both mice and humans to be a common response to infection [96, 100-103]. These findings were echoed in our urothelial organoid in chapter 3, where *E. faecalis* formed significant intracellular colonies within the intermediate and basal cells of the urothelial mimetic after its umbrella-cell layer had been jettisoned. These results further support the notion that *E. faecalis* exhibits an intracellular phenotype.

In many murine studies, uropathogenic *E. coli* has been shown to invade urothelial cells as part of a well-described intracellular lifestyle [10]. As a result, it is now widely accepted that UPEC exhibits an intracellular phase in UTI patients. However, since the initial report of intracellular “pods” in the mouse model in 2003 [95], to our knowledge only four papers [96] [252] [253] [53] have reported IBC in the shed cells of human UTI patients, only two of which (representing studies of one and 49 children respectively) deployed orthogonal analysis at the Z resolution necessary to minimise point spread function and pinpoint the bacteria to an intracellular compartment [278] [252, 253] . Another report has shown that UPEC isolated from women with acute cystitis were competent to form IBC in mice [99], but this evidence is not direct proof of their presence in the original patients. Hence, more studies on the universality of intracellular UPEC in human UTI would be welcomed.

As discussed earlier, UTI frequently reoccur and current oral antibiotic regimens fail in a higher percentage of cases [10, 124], Moreover, the use of antibiotics can cause a number of bothersome systemic side effects and is

linked to a worrying increase in worldwide antibiotic resistance [57, 130, 131]. In an effort to avoid these problems, some clinics advocate the use of antibiotic bladder irrigations; however, these appear to share a similar failure rate to that of oral administration [152]. More recently the use of novel nanotechology-driven drug delivery systems have been gaining attention in this research arena [144]. Indeed, the use of liposome coated microbubbles stimulated with ultrasound are showing promise in a number of disciplines [206-208]. Until now, however, this technology had not been translated for drug delivery in the bladder. We decided, in collaboration with Oxford University, to explore the potential for ultrasound-activated microbubble drug-delivery as an alternative intravesical treatment for UTI. Using our characterised human urothelial organoid as an *in vitro* test-bed, microbubble therapy safely delivered drug into the intracellular space of highly-specialised umbrella cells. Furthermore, this delivery system was effective at both killing and clearing uropathogenic *E. faecalis* in a human model of UTI.

In chapter 4, a commercially available cytotoxicity assay showed low-dose ultrasound-activated bubble therapy to be no more harmful than 200 µg/ml of gentamicin solution (a level approved for in *vivo* use, see below). The higher bubble doses induced far higher levels of cellular damage, a fact which could limit the tolerability and safety of these doses in humans. It must be noted, however, that the treatment of recurrent UTI with intravesical instillations of gentamicin regularly involves doses ranging from ~500 µg/ml to 2.6 mg/ml and these concentrations cause little to no adverse effects [152, 153, 155]. It is possible, therefore, that even the detection of over 40% cytotoxicity in a

human organoid may well be perfectly safe in a human patient. Further studies would be required to inform and assuage safety concerns; however, the lower bubble doses (10 – 25 µl) found to be effective in this study caused little damage. It is also plausible that sonoporation may have induced detectable levels of LDH 'leakage' without killing the host cell, resulting in false positive cytotoxicity readings [279]. It would be interesting, therefore, to conduct a viability assay to help verify the cytotoxicity data [280].

The ultrasound-activated bubbles were able to deliver nearly twice the concentration of drug into the organoid umbrella cells than liposomes alone. Considering the efficiency of liposomal drug delivery for the treatment of other pathologies, this is a very promising result [281]. Moreover, ultrasound had a highly significant effect on drug delivery by the bubbles, demonstrating activation and hence presumably cavitation in response to the acoustic field. Nonetheless, our CTCF assay measured the delivery of a fluorescent dye rather than the antibiotic itself. In future work, it would seem prudent to develop an assay to determine intracellular concentrations of the active drug. Indeed, antibodies raised against gentamicin (and other antibiotics) and tetrazolium chloride assays have been developed to detect this aminoglycoside in the milk of dairy herd cattle [282, 283] and could prove useful. Another future consideration would be identifying the specific intracellular compartments that receive 'payload' during ultrasound-mediated microbubble delivery. A myriad of endocytic pathways have been implicated in the trafficking of therapeutic nanoparticles [284]. Due to the mechanical activity of sonoporation, however, it would seem likely that delivery is

achieved via direct membrane penetration (translocation) into the cytosol proper [284]. Later, once we fully understand how *E. faecalis* and other uropathogens gain access to the intracellular space, ligands could be added to the microbubble / liposome shells to provide targeted delivery [285].

In addition to the encouraging safety profile and intracellular delivery data, ultrasound-activated bubble therapy was also effective at killing and clearing *E. faecalis* from a human urothelial organoid. A 20-second exposure to this novel therapy was as potent as 2 hours of 200 µg/ml gentamicin at killing *E. faecalis*. Moreover, ultrasound-activated bubble therapy resulted in a ~75% reduction in bacterial burden when compared to free gentamicin treatment. Patients suffering from LUTS may find it difficult to tolerate long exposure times during administration of intravesical drugs. A recent study reported only half of participants suffering from recurrent UTI were able to tolerate a 30 minute installation of Cystistat™ [286]. Therefore, shorter treatment times may confer an advantage in the clinical setting. Interestingly, the concentration of gentamicin encapsulated in the liposomes coating the microbubbles was far lower that the reported MIC value for this uropathogen. This raises the question of whether this antimicrobial effect would have been achieved without the addition of gentamicin. It would be of interest, therefore, to repeat these experiments with microbubbles coated with blank liposomes. It is possible, however, that this notable bactericidal activity is a result of this delivery system concentrating drug in the intracellular space of infected cells. In this case, gentamicin levels could be in excess of the aforementioned MIC

value within the bacterial niche. Again, this would need to be confirmed by measuring the levels of gentamicin delivered into the cells.

The detection of intracellular bacteria via confocal microscopy is arduous and the use of a modified gentamicin protection assay during the experimentation in reported in chapter 4 was not possible due to logistical difficulties. Nonetheless, investigating the ability of microbubbles to eradicate intracellular bacterial communities in this model would be a crucial step in the development of this and other treatments. We have recently installed a motorised ultra-fast live-imaging microscope system with programmable 3D analysis software in an effort to fully automate this process [287].

Chapter 4 of this thesis represents proof-of-concept pilot data and therefore a small number of repeats were performed. Non-parametric statistical tests were selected owing to non-normal distribution of data. Due to small sample sizes it was not possible to satisfy the 4th assumption of Kruskall-Wallis and Mann-Whitney U tests, which requires all distributions have a similar shape, with certainty [288]. It is possible, if unlikely, therefore, that the unavoidable violation of this assumption may have influenced our findings. Nonetheless, the box and whisker plots show clear differences and the statistical testing merely confirmed this. However, future work would benefit from increased numbers of replicates. This work will be taken forward with a view towards preclinical validation and ultimately, patient trials. Furthermore, this work is being finalised in a manuscript to be submitted within the next few months.

In conclusion, our collective data suggest that some LUTS may be generated by low-grade intracellular infection of the bladder by *E. faecalis.* These results therefore may have far-reaching implications for the diagnosis, treatment and understanding of the aetiology of infective bladder disease. Moreover, current advances in tissue engineering enabled us to grow physiologically relevant organotypic human models of the bladder. Engineered human bladder models could be used as a reproducible test bed for chronic infective disease formation, treatment and resolution in humans. Indeed, our 3D model is currently being used in pre-clinical trials to test the efficacy of an industry-funded novel therapeutic [289]. Additionally, we recently published, in collaboration with The Royal Veterinary College, on the antimicrobial mechanisms exhibited by the biocompatible polymer PHMB (polyhexamethylene biguanide) [290]. We have since received funding to use our organoid to test the ability for PHMB to clear UTI. We aim to achieve this during my postdoctoral position. Finally, new treatments are desperately needed and the use of ultrasound-activated microbubbles could prove to be highly efficacious whilst avoiding the common drawbacks of systemic treatment in an already vulnerable population.

The human urothelium is more complex both structually and functionally than that of a mouse. In keeping with my overall hypothesis, UTI in patients with LUTS appears to differ from that seen in the UPEC mouse model as well as traditionally understood acute E. coli-associated UTI in humans, but there is still much to be learned. It is my hope that the human model system developed in this thesis, along with the prototype microbubble delivery

system, will go some ways towards making life better for UTI patients in the future.

References

1. Horsley, H., et al., *Enterococcus faecalis subverts and invades the host urothelium in patients with chronic urinary tract infection.* PLoS One, 2013. 8(12): p. e83637.
2. Horsley, H., et al., *A urine-dependent human urothelial organoid offers a potential alternative to rodent models of infection.* Scientific Reports, 2018. 8(1): p. 1238.
3. *Urinary tract infection*. 2018 08/03/2018; Available from: http://www.online-medical-dictionary.org/.
4. Nicolle, L.E., *Uncomplicated Urinary Tract Infection in Adults Including Uncomplicated Pyelonephritis.* Urologic Clinics of North America, 2008. 35(1): p. 1-12.
5. Foxman, B., et al., *Urinary tract infection: self-reported incidence and associated costs.* Ann Epidemiol, 2000. 10(8): p. 509-15.
6. Foxman, B., *Epidemiology of urinary tract infections: incidence, morbidity, and economic costs.* Am J Med, 2002. 113 Suppl 1A: p. 5S-13S.
7. Baerheim, A. and S. Hunskar, *[Current management of uncomplicated acute cystitis in general practice].* Tidsskr Nor Laegeforen, 1997. 117(9): p. 1304-7.
8. Hooton, T.M., *Recurrent urinary tract infection in women.* Int J Antimicrob Agents, 2001. 17(4): p. 259-68.
9. Pouwels, K.B., S.T. Visser, and E. Hak, *Effect of pravastatin and fosinopril on recurrent urinary tract infections.* J Antimicrob Chemother, 2013. 68(3): p. 708-14.
10. Hunstad, D.A. and S.S. Justice, *Intracellular lifestyles and immune evasion strategies of uropathogenic Escherichia coli.* Annu Rev Microbiol, 2010. 64: p. 203-21.
11. Foxman, B., *Recurring urinary tract infection: incidence and risk factors.* Am J Public Health, 1990. 80(3): p. 331-3.

12. **Renard, J., et al., *Recurrent Lower Urinary Tract Infections Have a Detrimental Effect on Patient Quality of Life: a Prospective, Observational Study.* Infect Dis Ther, 2015. 4(1): p.125-135.**
13. **Khasriya, R., et al., *The spectrum of bacterial colonisation associated with urothelial cells from patients with chronic lower urinary tract symptoms.* J Clin Microbiol, 2013. 51(7): p. 2054-62.**
14. **Ikaheimo, R., et al., *Recurrence of urinary tract infection in a primary care setting: analysis of a 1-year follow-up of 179 women.* Clin Infect Dis, 1996. 22(1): p. 91-9.**
15. **Margariti, P.A., A.L. Astorri, and C. Mastromarino, *[Urinary tract infections: risk factors and therapeutic trends].* Recenti Prog Med, 1997. 88(2): p. 65-8.**
16. **Koeijers, J.J., et al., *Urinary tract infection in male general practice patients: uropathogens and antibiotic susceptibility.* Urology, 2010. 76(2): p. 336-40.**
17. ***Urinary tract anatomy*. 05/03/2018; Available from: www.uroklinik.com.tr.**
18. **Lutters, M. and N.B. Vogt-Ferrier, *Antibiotic duration for treating uncomplicated, symptomatic lower urinary tract infections in elderly women.* Cochrane Database Syst Rev, 2008(3): p. CD001535.**
19. **Kaye, D., *Urinary tract infections in the elderly.* Bull N Y Acad Med, 1980. 56(2): p. 209-20.**
20. **Mahadeva, A., R. Tanasescu, and B. Gran, *Urinary tract infections in multiple sclerosis: under-diagnosed and under-treated? A clinical audit at a large University Hospital.* Am J Clin Exp Immunol, 2014. 3(1): p. 57-67.**
21. **Buljevac, D., *Prospective study on the relationship between infections and multiple sclerosis exacerbations.* Brain, 2002. 125(Pt 5): p. 952.**
22. **Pannek, J., *Treatment of urinary tract infection in persons with spinal cord injury: guidelines, evidence, and clinical practice: A***

questionnaire-based survey and review of the literature. **The Journal of Spinal Cord Medicine, 2011. 34(1): p. 11-15.**

23. **Giessing, M., *Urinary tract infection in renal transplantation.* Arab Journal of Urology, 2012. 10(2): p. 162-168.**
24. **Hooton, T.M., et al., *Diagnosis, Prevention, and Treatment of Catheter-Associated Urinary Tract Infection in Adults: 2009 International Clinical Practice Guidelines from the Infectious Diseases Society of America.* Clinical Infectious Diseases, 2010. 50(5): p. 625-663.**
25. **Schappert, S.M. and E.A. Rechtsteiner, *Ambulatory medical care utilization estimates for 2007.* Vital Health Stat 13, 2011(169): p. 1-38.**
26. **Cotter, M., et al., *Healthcare-associated infection in Irish long-term care facilities: results from the First National Prevalence Study.* Journal of Hospital Infection, 2012. 80(3): p. 212-216.**
27. **Correale, J., M. Fiol, and W. Gilmore, *The risk of relapses in multiple sclerosis during systemic infections.* Neurology, 2006. 67(4): p. 652-9.**
28. **Soliman, Y., R. Meyer, and N. Baum, *Falls in the Elderly Secondary to Urinary Symptoms.* Reviews in Urology, 2016. 18(1): p. 28-32.**
29. **Lorenz, E.C. and F.G. Cosio, *The impact of urinary tract infections in renal transplant recipients.* Kidney Int, 2010. 78(8): p. 719-21.**
30. **Peach, B.C., et al., *Risk Factors for Urosepsis in Older Adults: A Systematic Review.* Gerontology and geriatric medicine, 2016. 2: p. 2333721416638980.**
31. **Schieve, L.A., et al., *Urinary tract infection during pregnancy: its association with maternal morbidity and perinatal outcome.* American Journal of Public Health, 1994. 84(3): p. 405-410.**
32. **Tan, P.C., A.S. King, and S.Z. Omar, *Screening for urinary tract infection in women with hyperemesis gravidarum.* J Obstet Gynaecol Res, 2012. 38(1): p. 145-53.**

33. **Abrams, P., et al., *The standardisation of terminology in lower urinary tract function: report from the standardisation sub-committee of the International Continence Society.* Urology, 2003. 61(1): p. 37-49.**
34. **Colgan, R. and M. Williams, *Diagnosis and treatment of acute uncomplicated cystitis.* Am Fam Physician, 2011. 84(7): p. 771-6.**
35. **Stamm, W.E., et al., *Natural history of recurrent urinary tract infections in women.* Rev Infect Dis, 1991. 13(1): p. 77-84.**
36. **Zalmanovici Trestioreanu, A., et al., *Antimicrobial agents for treating uncomplicated urinary tract infection in women.* Cochrane Database Syst Rev, 2010(10): p. CD007182.**
37. **Gacci, M., et al., *Tolterodine extended release in the treatment of male OAB/storage LUTS: a systematic review.* BMC Urol, 2014. 14: p. 84.**
38. **Parsons, C.L., *Interstitial Cystitis and Lower Urinary Tract Symptoms in Males and Females—The Combined Role of Potassium and Epithelial Dysfunction.* Reviews in Urology, 2002. 4(Suppl 1): p. S49-S55.**
39. **Li, G.Z., et al., *Risk factors for interstitial cystitis/painful bladder syndrome in patients with lower urinary tract symptoms: a Chinese multi-center study.* Chin Med J (Engl), 2010. 123(20): p. 2842-6.**
40. **Scott, V.C.S., et al., *Intracellular Bacterial Communities: A Potential Etiology for Chronic Lower Urinary Tract Symptoms.* Urology, 2015. 86(3): p. 425-431.**
41. **N.I.C.E. *Urinary incontinence in women*. 06/03/2015; Available from: https://www.nice.org.uk/guidance/qs77.**
42. **Gormley, E.A., et al., *Diagnosis and treatment of overactive bladder (non-neurogenic) in adults: AUA/SUFU guideline.* J Urol, 2012. 188(6 Suppl): p. 2455-63.**
43. **Coyne, K.S., et al., *The prevalence of lower urinary tract symptoms (LUTS) in the USA, the UK and Sweden: results from***

the Epidemiology of LUTS (EpiLUTS) study. **BJU Int, 2009. 104(3): p. 352-60.**

44. Irwin, D.E., et al., *Population-based survey of urinary incontinence, overactive bladder, and other lower urinary tract symptoms in five countries: results of the EPIC study.* Eur Urol, 2006. 50(6): p. 1306-14; discussion 1314-5.

45. Perry, S., et al., *An epidemiological study to establish the prevalence of urinary symptoms and felt need in the community: the Leicestershire MRC Incontinence Study. Leicestershire MRC Incontinence Study Team.* J Public Health Med, 2000. 22(3): p. 427-34.

46. Stamm, W.E., et al., *Diagnosis of coliform infection in acutely dysuric women.* N Engl J Med, 1982. 307(8): p. 463-8.

47. Khasriya, R., et al., *The Inadequacy of Urinary Dipstick and Microscopy as Surrogate Markers of Urinary Tract Infection in Urological Outpatients With Lower Urinary Tract Symptoms Without Acute Frequency and Dysuria.* Journal of Urology, 2010. 183(5): p. 1843-1847.

48. Kupelian, A.S., et al., *Discrediting microscopic pyuria and leucocyte esterase as diagnostic surrogates for infection in patients with lower urinary tract symptoms: results from a clinical and laboratory evaluation.* Bju International, 2013. 112(2): p. 231-238.

49. Chapple, C.R., et al., *Lower urinary tract symptoms revisited: a broader clinical perspective.* Eur Urol, 2008. 54(3): p. 563-9.

50. Nakipoglu, G.F., et al., *Urinary dysfunction in multiple sclerosis.* J Clin Neurosci, 2009. 16(10): p. 1321-4.

51. Pearce, M.M., et al., *The female urinary microbiome: a comparison of women with and without urgency urinary incontinence.* MBio, 2014. 5(4): p. e01283-14.

52. Sorrentino, F., et al., *Associations between individual lower urinary tract symptoms and bacteriuria in random urine samples in women.* Neurourol Urodyn, 2015. 34(5): p. 429-33.

53. **Cheng, Y., et al., *Detection of intracellular bacteria in exfoliated urothelial cells from women with urge incontinence.* Pathog Dis, 2016. 74(7).**
54. **Moore, K.H. and A.P. Malykhina, *What is the role of covert infection in detrusor overactivity, and other LUTD? ICI-RS 2013.* Neurourol Urodyn, 2014. 33(5): p. 606-10.**
55. **Walsh, C.A. and K.H. Moore, *Overactive bladder in women: does low-count bacteriuria matter? A review.* Neurourol Urodyn, 2011. 30(1): p. 32-7.**
56. **Kelley, S.P., et al., *Urinary ATP and visualization of intracellular bacteria: a superior diagnostic marker for recurrent UTI in renal transplant recipients?* Springerplus, 2014. 3: p. 200.**
57. **Swamy, S., et al., *Recalcitrant chronic bladder pain and recurrent cystitis but negative urinalysis – What should we do? .* International Urogynecology Journal; Accepted manuscript, 2018.**
58. **Rosette, J.d.l., et al., *Keratin Expression Profiling of Transitional Epithelium in the Painful Bladder Syndrome/Interstitial Cystitis.* American Journal of Clinical Pathology, 2006. 125(1): p. 105-110.**
59. **Khandelwal, P., S.N. Abraham, and G. Apodaca, *Cell biology and physiology of the uroepithelium.* American Journal of Physiology-Renal Physiology, 2009. 297(6): p. F1477-F1501.**
60. **Chen, Y.R., et al., *Rab27b is associated with fusiform vesicles and may be involved in targeting uroplakins to urothelial apical membranes.* Proceedings of the National Academy of Sciences of the United States of America, 2003. 100(24): p. 14012-14017.**
61. **Wu, X.R., et al., *Uroplakins in urothelial biology, function, and disease.* Kidney Int, 2009. 75(11): p. 1153-65.**
62. **Olsburgh, J., et al., *Uroplakin gene expression in normal human tissues and locally advanced bladder cancer.* J Pathol, 2003. 199(1): p. 41-9.**
63. **Winder, M., et al., *Signalling molecules in the urothelium.* Biomed Res Int, 2014. 2014: p. 297295.**

64. **Foster, C.S. and G.J. Netto, *The urinary bladder, urachal remnants, urethra, renal pelves, and ureters*, in *Silverberg's Principles and Practice of Surgical Pathology and Cytopathology*, E.B. Stelow, et al., Editors., Cambridge University Press: Cambridge. p. 2322-2412.**
65. **Baker, S.C., S. Shabir, and J. Southgate, *Biomimetic urothelial tissue models for the in vitro evaluation of barrier physiology and bladder drug efficacy.* Mol Pharm, 2014. 11(7): p. 1964-70.**
66. **Cervigni, M., *Interstitial cystitis/bladder pain syndrome and glycosaminoglycans replacement therapy.* Transl Androl Urol, 2015. 4(6): p. 638-42.**
67. **Janssen, D.A.W., et al., *The Distribution and Function of Chondroitin Sulfate and Other Sulfated Glycosaminoglycans in the Human Bladder and Their Contribution to the Protective Bladder Barrier.* The Journal of Urology, 2013. 189(1): p. 336-342.**
68. **Rübben, H., et al., *Quantitative analysis of glycosaminoglycans in urothelium and bladder wall of calf.* Urology, 1983. 22(6): p. 655-657.**
69. **Tian, W., et al., *Utility of uroplakin II expression as a marker of urothelial carcinoma.* Hum Pathol, 2015. 46(1): p. 58-64.**
70. **Craig, W., *Relevance of animal models for clinical treatment.* European Journal of Clinical Microbiology and Infectious Diseases, 1993. 12(1): p. S55-S57.**
71. **van der Worp, H.B., et al., *Can Animal Models of Disease Reliably Inform Human Studies?* PLoS Med, 2010. 7(3): p. e1000245.**
72. **Perel, P., et al., *Comparison of treatment effects between animal experiments and clinical trials: systematic review.* Bmj, 2007. 334(7586): p. 197.**
73. **Bhogal, N. and R. Combes, *The relevance of genetically altered mouse models of human disease.* Altern Lab Anim, 2006. 34(4): p. 429-54.**

74. **Lin, J.H., *Applications and limitations of genetically modified mouse models in drug discovery and development.* Curr Drug Metab, 2008. 9(5): p. 419-38.**
75. **Mordenti, J., *Forecasting cephalosporin and monobactam antibiotic half-lives in humans from data collected in laboratory animals.* Antimicrobial Agents and Chemotherapy, 1985. 27(6): p. 887-891.**
76. **Wu, X.R., et al., *Large scale purification and immunolocalization of bovine uroplakins I, II, and III. Molecular markers of urothelial differentiation.* J Biol Chem, 1990. 265(31): p. 19170-9.**
77. **Vaidyanathan, S., et al., *A study of cytokeratin 20 immunostaining in the urothelium of neuropathic bladder of patients with spinal cord injury.* BMC Urol, 2002. 2: p. 7.**
78. **Smith, N.J., et al., *Toll-Like Receptor Responses of Normal Human Urothelial Cells to Bacterial Flagellin and Lipopolysaccharide.* The Journal of Urology, 2011. 186(3): p. 1084-1092.**
79. **Yang, P.J., et al., *Duration of urination does not change with body size.* Proceedings of the National Academy of Sciences, 2014. 111(33): p. 11932-11937.**
80. **Kaur, G. and J.M. Dufour, *Cell lines: Valuable tools or useless artifacts.* Spermatogenesis, 2012. 2(1): p. 1-5.**
81. **Bubenik, J., et al., *Established cell line of urinary bladder carcinoma (T24) containing tumour-specific antigen.* Int J Cancer, 1973. 11(3): p. 765-73.**
82. **Georgopoulos, N.T., et al., *Immortalisation of normal human urothelial cells compromises differentiation capacity.* Eur Urol, 2011. 60(1): p. 141-9.**
83. **Knowles, M.A., et al., *Long-term organ culture of normal human bladder.* Cancer Res, 1983. 43(1): p. 374-85.**
84. **Kreft, M.E., et al., *Urothelial injuries and the early wound healing response: tight junctions and urothelial cytodifferentiation.* Histochem Cell Biol, 2005. 123(4-5): p. 529-39.**

85. **Feil, G., et al., *Immunoreactivity of p63 in Monolayered and In Vitro Stratified Human Urothelial Cell Cultures Compared with Native Urothelial Tissue.* European Urology, 2008. 53(5): p. 1066-1073.**
86. **Nagele, U., et al., *In vitro investigations of tissue-engineered multilayered urothelium established from bladder washings.* Eur Urol, 2008. 54(6): p. 1414-22.**
87. **Sugasi, S., et al., *In vitro engineering of human stratified urothelium: analysis of its morphology and function.* J Urol, 2000. 164(3 Pt 2): p. 951-7.**
88. **Cross, W.R., et al., *A biomimetic tissue from cultured normal human urothelial cells: analysis of physiological function.* American Journal of Physiology - Renal Physiology, 2005. 289(2): p. F459-F468.**
89. **Andersen, T.E., et al., *Escherichia coli uropathogenesis in vitro: invasion, cellular escape, and secondary infection analyzed in a human bladder cell infection model.* Infect Immun, 2012. 80(5): p. 1858-67.**
90. **BetsyáFoxman, *Epidemiology of urinary tract infections: Incidence, morbidity, and economic costs.* Disease-a-Month, 2003. 49(2): p. 53-70.**
91. **Wright, K.J. and S.J. Hultgren, *Sticky fibers and uropathogenesis: bacterial adhesins in the urinary tract.* Future Microbiol, 2006. 1(1): p. 75-87.**
92. **Orndorff, P.E., et al., *Immunoglobulin-mediated agglutination of and biofilm formation by Escherichia coli K-12 require the type 1 pilus fiber.* Infect Immun, 2004. 72(4): p. 1929-38.**
93. **Anderson, G.G., S.M. Martin, and S.J. Hultgren, *Host subversion by formation of intracellular bacterial communities in the urinary tract.* Microbes Infect, 2004. 6(12): p. 1094-101.**
94. **Anderson, G.G., et al., *Intracellular bacterial communities of uropathogenic Escherichia coli in urinary tract pathogenesis.* Trends Microbiol, 2004. 12(9): p. 424-30.**

95. Anderson, G.G., et al., *Intracellular bacterial biofilm-like pods in urinary tract infections.* Science, 2003. 301(5629): p. 105-7.
96. Rosen, D.A., et al., *Detection of intracellular bacterial communities in human urinary tract infection.* PLoS Med, 2007. 4(12): p. e329.
97. Justice, S.S., et al., *Differentiation and developmental pathways of uropathogenic Escherichia coli in urinary tract pathogenesis.* Proc Natl Acad Sci U S A, 2004. 101(5): p. 1333-8.
98. Blango, M.G. and M.A. Mulvey, *Persistence of uropathogenic Escherichia coli in the face of multiple antibiotics.* Antimicrob Agents Chemother, 2010. 54(5): p. 1855-63.
99. Garofalo, C.K., et al., *Escherichia coli from urine of female patients with urinary tract infections is competent for intracellular bacterial community formation.* Infection and Immunity, 2007. 75(1): p. 52-60.
100. Dalal, E., *Moderate stress protects female mice against bacterial-infection of the bladder by eliciting uroepithelial shedding.* Infection and Immunity, 1994. 62(12): p. 5505-5510.
101. Smith, Y.C., et al., *Hemolysin of uropathogenic Escherichia coli evokes extensive shedding of the uroepithelium and hemorrhage in bladder tissue within the first 24 hours after intraurethral inoculation of mice.* Infection and Immunity, 2008. 76(7): p. 2978-2990.
102. Thumbikat, P., et al., *Bacteria-induced uroplakin signaling mediates bladder response to infection.* PLoS Pathog, 2009. 5(5): p. e1000415.
103. Hannan, T.J., et al., *Early severe inflammatory responses to uropathogenic E. coli predispose to chronic and recurrent urinary tract infection.* PLoS Pathog, 2010. 6(8): p. e1001042.
104. Mysorekar, I.U. and S.J. Hultgren, *Mechanisms of uropathogenic Escherichia coli persistence and eradication from the urinary tract.* Proc Natl Acad Sci U S A, 2006. 103(38): p. 14170-5.

105. **Russo, T.A., et al., *Chromosomal restriction fragment length polymorphism analysis of Escherichia coli strains causing recurrent urinary tract infections in young women.* J Infect Dis, 1995. 172(2): p. 440-5.**
106. **Brauner, A., S.H. Jacobson, and I. Kuhn, *Urinary Escherichia coli causing recurrent infections--a prospective follow-up of biochemical phenotypes.* Clin Nephrol, 1992. 38(6): p. 318-23.**
107. **Gupta, K., et al., *Inverse association of H2O2-producing lactobacilli and vaginal Escherichia coli colonization in women with recurrent urinary tract infections.* J Infect Dis, 1998. 178(2): p. 446-50.**
108. **Cass, A.S. and G.W. Ireland, *Antibacterial perineal washing for prevention of recurrent urinary tract infections.* Urology, 1985. 25(5): p. 492-4.**
109. **Haque, R., M.L. Akter, and M.A. Salam, *Prevalence and susceptibility of uropathogens: a recent report from a teaching hospital in Bangladesh.* BMC Research Notes, 2015. 8: p. 416.**
110. **Szabados, F., et al., *Staphylococcus saprophyticus ATCC 15305 is internalized into human urinary bladder carcinoma cell line 5637.* Fems Microbiology Letters, 2008. 285(2): p. 163-169.**
111. **Rosen, D.A., et al., *Utilization of an intracellular bacterial community pathway in Klebsiella pneumoniae urinary tract infection and the effects of FimK on type 1 pilus expression.* Infect Immun, 2008. 76(7): p. 3337-45.**
112. **Mandell, G.L., *Interaction of intraleukocytic bacteria and antibiotics.* J Clin Invest, 1973. 52(7): p. 1673-9.**
113. **Edwards, A.M. and R.C. Massey, *Invasion of human cells by a bacterial pathogen.* J Vis Exp, 2011(49).**
114. **Mohamed, J.A. and D.B. Huang, *Biofilm formation by enterococci.* J Med Microbiol, 2007. 56(Pt 12): p. 1581-8.**
115. **Chai, W.L., et al., *Susceptibility of Enterococcus faecalis biofilm to antibiotics and calcium hydroxide.* J Oral Sci, 2007. 49(2): p. 161-6.**

116. da Silva, N.S., et al., *Identification of temporal clusters and risk factors of bacteremia by nosocomial vancomycin-resistant enterococci.* Am J Infect Control, 2014. 42(4): p. 389-92.
117. Felmingham, D., et al., *Enterococcus species in urinary tract infection.* Clin Infect Dis, 1992. 15(2): p. 295-301.
118. Hanin, A., et al., *Screening of in vivo activated genes in Enterococcus faecalis during insect and mouse infections and growth in urine.* PLoS One, 2010. 5(7): p. e11879.
119. Nichol, K.A., et al., *Molecular epidemiology of urinary tract isolates of vancomycin-resistant Enterococcus faecium from North America.* Int J Antimicrob Agents, 2006. 27(5): p. 392-6.
120. Guiton, P.S., et al., *Enterococcus faecalis overcomes foreign body-mediated inflammation to establish urinary tract infections.* Infect Immun, 2013. 81(1): p. 329-39.
121. Swaminathan, S. and G.J. Alangaden, *Treatment of resistant enterococcal urinary tract infections.* Curr Infect Dis Rep, 2010. 12(6): p. 455-64.
122. Poulsen, L.L., et al., *Enterococcus and Streptococcus spp. associated with chronic and self-medicated urinary tract infections in Vietnam.* BMC Infect Dis, 2012. 12(1): p. 320.
123. NICE. *Urinary-tract infections*. 2018 08/02/2018; Available from: https://bnf.nice.org.uk/treatment-summary/urinary-tract-infections.html.
124. Milo, G., et al., *Duration of antibacterial treatment for uncomplicated urinary tract infection in women.* Cochrane Database Syst Rev, 2005(2): p. Cd004682.
125. O'Brien, V.P., et al., *Drug and Vaccine Development for the Treatment and Prevention of Urinary Tract Infections.* Microbiology spectrum, 2016. 4(1): p. 10.1128/microbiolspec.UTI-0013-2012.
126. Greenberg, R.N., et al., *Randomized study of single-dose, three-day, and seven-day treatment of cystitis in women.* J Infect Dis, 1986. 153(2): p. 277-82.

127. **Penn, R.G. and J.P. Griffin, *Adverse reactions to nitrofurantoin in the United Kingdom, Sweden, and Holland.* British Medical Journal (Clinical research ed.), 1982. 284(6327): p. 1440-1442.**
128. **Lteif, L., *The Daniel K. Inouye College of Pharmacy Scripts: Updates on Clostridium difficile Infection: Advances in Laboratory Testing to Aid Diagnosis and Treatment.* Hawai'i Journal of Medicine & Public Health, 2017. 76(2): p. 59-64.**
129. **Leekha, S., C.L. Terrell, and R.S. Edson, *General Principles of Antimicrobial Therapy.* Mayo Clinic Proceedings, 2011. 86(2): p. 156-167.**
130. **Wagenlehner, F.M., et al., *[Antibiotic resistance and their significance in urogenital infections: new aspects].* Urologe A, 2014. 53(10): p. 1452-7.**
131. **(WHO), W.H.O., *Antimicrobial resistance. Fact sheet 194.* 2014.**
132. **Carlet, J., *Antibiotic resistance: Protecting antibiotics - the declaration of the world alliance against antibiotic resistance.* Indian J Crit Care Med, 2014. 18(10): p. 643-5.**
133. **Jadoon, R.J., M. Jalal-ud-Din, and S.A. Khan, *E. coli Resistance to Ciprofloxacin and Common Associated Factors.* J Coll Physicians Surg Pak, 2015. 25(11): p. 824-7.**
134. **Niranjan, V. and A. Malini, *Antimicrobial resistance pattern in Escherichia coli causing urinary tract infection among inpatients.* Indian J Med Res, 2014. 139(6): p. 945-8.**
135. **Wang, Y., et al., *Drug resistance and virulence of uropathogenic Escherichia coli from Shanghai, China.* J Antibiot (Tokyo), 2014. 67(12): p. 799-805.**
136. **Al-Mayahie, S. and J.J. Al Kuriashy, *Distribution of ESBLs among Escherichia coli isolates from outpatients with recurrent UTIs and their antimicrobial resistance.* J Infect Dev Ctries, 2016. 10(6): p. 575-83.**
137. **El Bouamri, M.C., et al., *[Current antibiotic resistance profile of uropathogenic Escherichia coli strains and therapeutic consequences].* Prog Urol, 2014. 24(16): p. 1058-62.**

138. **Adib, N., et al., *Antibiotic resistance profile and virulence genes of uropathogenic Escherichia coli isolates in relation to phylogeny.* Trop Biomed, 2014. 31(1): p. 17-25.**
139. **Medina-Polo, J., et al., *Community-associated urinary infections requiring hospitalization: risk factors, microbiological characteristics and patterns of antibiotic resistance.* Actas Urol Esp, 2015. 39(2): p. 104-11.**
140. **Altoparlak, U., A. Kadanali, and S. Kadanali, *[Correlation of urinary tract infections with the vaginal colonization in postmenopausal women].* Mikrobiyol Bul, 2004. 38(4): p. 377-83.**
141. **Godaly, G., I. Ambite, and C. Svanborg, *Innate immunity and genetic determinants of urinary tract infection susceptibility.* Curr Opin Infect Dis, 2015. 28(1): p. 88-96.**
142. **Scholes, D., et al., *Risk factors for recurrent urinary tract infection in young women.* J Infect Dis, 2000. 182(4): p. 1177-82.**
143. **GuhaSarkar, S., P. More, and R. Banerjee, *Urothelium-adherent, ion-triggered liposome-in-gel system as a platform for intravesical drug delivery.* J Control Release, 2017. 245: p. 147-156.**
144. **Zacchè, M.M. and I. Giarenis, *Therapies in early development for the treatment of urinary tract inflammation.* Expert Opinion on Investigational Drugs, 2016. 25(5): p. 531-540.**
145. **Poolman, J.T. and M. Wacker, *Extraintestinal Pathogenic Escherichia coli, a Common Human Pathogen: Challenges for Vaccine Development and Progress in the Field.* J Infect Dis, 2016. 213(1): p. 6-13.**
146. **Gulpinar, O., et al., *Clinical comparision of intravesical hyaluronic acid and hyaluronic acid-chondroitin sulphate therapy for patients with bladder pain syndrome/interstitital cystitis.* Can Urol Assoc J, 2014. 8(9-10): p. E610-4.**
147. **Mydock-McGrane, L.K., T.J. Hannan, and J.W. Janetka, *Rational design strategies for FimH antagonists: new drugs on the***

horizon for urinary tract infection and Crohn's disease. **Expert Opin Drug Discov, 2017. 12(7): p. 711-731.**

148. **Lee, D.G., et al., *Preventive effects of hyaluronic acid on Escherichia coli-induced urinary tract infection in rat.* Urology, 2010. 75(4): p. 949-54.**
149. **Constantinides, C., et al., *Prevention of recurrent bacterial cystitis by intravesical administration of hyaluronic acid: a pilot study.* BJU Int, 2004. 93(9): p. 1262-6.**
150. **Lipovac, M., et al., *Prevention of recurrent bacterial urinary tract infections by intravesical instillation of hyaluronic acid.* Int J Gynaecol Obstet, 2007. 96(3): p. 192-5.**
151. **Gugliotta, G., et al., *Is intravesical instillation of hyaluronic acid and chondroitin sulfate useful in preventing recurrent bacterial cystitis? A multicenter case control analysis.* Taiwan J Obstet Gynecol, 2015. 54(5): p. 537-40.**
152. **Defoor, W., et al., *Safety of gentamicin bladder irrigations in complex urological cases.* J Urol, 2006. 175(5): p. 1861-4.**
153. **van Nieuwkoop, C., et al., *Intravesical gentamicin for recurrent urinary tract infection in patients with intermittent bladder catheterisation.* Int J Antimicrob Agents, 2010. 36(6): p. 485-90.**
154. **Naderi, K., G. Urwin, and R. Casey, *Intravesical gentamicin treatment of recurrent Escherichia coli urinary tract infections in a patient with multiple antibiotic allergies.* Journal of Clinical Urology, 2014. 7(5): p. 364-366.**
155. **Cox, L., et al., *Gentamicin bladder instillations decrease symptomatic urinary tract infections in neurogenic bladder patients on intermittent catheterization.* Can Urol Assoc J, 2017. 11(9): p. E350-e354.**
156. **Dadfarma, N., et al., *High level of gentamicin resistance (HLGR) among enterococcus strains isolated from clinical specimens.* Journal of Infection and Public Health, 2013. 6(3): p. 202-8.**

157. **Elsinghorst, E.A., *Measurement of invasion by gentamicin resistance*, in *Methods in Enzymology*. 1994, Academic Press. p. 405-420.**
158. **Waites, K.B., et al., *Evaluation of 3 Methods of Bladder Irrigation to Treat Bacteriuria in Persons With Neurogenic Bladder.* The Journal of Spinal Cord Medicine, 2006. 29(3): p. 217-226.**
159. **Harmon, C. and A. Hassoun, *Antibiotic Bladder Irrigation in Preventing and Reducing Chronic Urinary Catheter-Related Urinary Tract Infections (UTI)*. Vol. 4. 2017. S347-S347.**
160. **Hill, D.M., G.C. Wood, and W.L. Hickerson, *Linezolid bladder irrigation as adjunctive treatment for a vancomycin-resistant Enterococcus faecium catheter-associated urinary tract infection.* Ann Pharmacother, 2015. 49(2): p. 250-3.**
161. **Zacharias, S., et al., *A comparative study to assess the effect of amikacin sulfate bladder wash on catheter-associated urinary tract infection in neurosurgical patients.* Indian J Crit Care Med, 2009. 13(1): p. 17-20.**
162. **Tuon, F.F., V.S. Amato, and S.R. Penteado Filho, *Bladder irrigation with amphotericin B and fungal urinary tract infection--systematic review with meta-analysis.* Int J Infect Dis, 2009. 13(6): p. 701-6.**
163. **Curtis, L. and B. Biundo, *Irrigation with piperacillin for the treatment of bladder infection: a case study.* Int J Pharm Compd, 2001. 5(3): p. 195.**
164. **Paterson, M.L., W. Barr, and S. Macdonald, *Urinary infection after colporrhaphy: its incidence, causation and prevention.* J Obstet Gynaecol Br Emp, 1960. 67: p. 394-401.**
165. **McFadyen, I.R. and S.C. Simmons, *Prevention of urinary infection following major vaginal surgery.* J Obstet Gynaecol Br Commonw, 1968. 75(8): p. 871-5.**
166. **Gillespie, W.A., et al., *Prevention of catheter infection of urine in female patients.* Br Med J, 1962. 2(5296): p. 13-6.**

167. Bruun, J.N. and A. Digranes, *Bladder irrigation in patients with indwelling catheters.* Scand J Infect Dis, 1978. 10(1): p. 71-4.

168. Pearman, J.W., M. Bailey, and W.E. Harper, *Comparison of the efficacy of "Trisdine" and kanamycin-colistin bladder instillations in reducing bacteriuria during intermittent catheterisation of patients with acute spinal cord trauma.* Br J Urol, 1988. 62(2): p. 140-4.

169. Labbaf, S., et al., *An encapsulated drug delivery system for recalcitrant urinary tract infection.* J R Soc Interface, 2013. 10(89): p. 20130747.

170. Wang, B.L., et al., *Treating acute cystitis with biodegradable micelle-encapsulated quercetin.* Int J Nanomedicine, 2012. 7: p. 2239-47.

171. Liu, S., et al., *Surface charge-conversion polymeric nanoparticles for photodynamic treatment of urinary tract bacterial infections.* Nanotechnology, 2015. 26(49): p. 495602.

172. Zhao, J., et al., *Effects of intravesical liposome-mediated human beta-defensin-2 gene transfection in a mouse urinary tract infection model.* Microbiol Immunol, 2011. 55(4): p. 217-23.

173. Tyagi, P., et al., *Bladder Instillation of Liposomes for Bladder Coating and Drug Delivery Platform.* LUTS: Lower Urinary Tract Symptoms, 2009. 1: p. S90-S93.

174. Tyagi, P., et al., *Intravesical liposome therapy for interstitial cystitis.* Int J Urol, 2017. 24(4): p. 262-271.

175. Chuang, Y.C., et al., *Intravesical liposome versus oral pentosan polysulfate for interstitial cystitis/painful bladder syndrome.* J Urol, 2009. 182(4): p. 1393-400.

176. Nordling, J. and A. van Ophoven, *Intravesical glycosaminoglycan replenishment with chondroitin sulphate in chronic forms of cystitis. A multi-national, multi-centre, prospective observational clinical trial.* Arzneimittelforschung, 2008. 58(7): p. 328-35.

177. Nickel, J.C., et al., *A real-life multicentre clinical practice study to evaluate the efficacy and safety of intravesical chondroitin*

sulphate for the treatment of interstitial cystitis. **BJU Int, 2009. 103(1): p. 56-60.**

178. **Perez-Marrero, R., L.E. Emerson, and J.T. Feltis, *A controlled study of dimethyl sulfoxide in interstitial cystitis.* J Urol, 1988. 140(1): p. 36-9.**
179. **Cvach, K. and A. Rosamilia, *Review of intravesical therapies for bladder pain syndrome/interstitial cystitis.* Translational Andrology and Urology, 2015. 4(6): p. 629-637.**
180. **Nickel, J.C., et al., *Intravesical alkalinized lidocaine (PSD597) offers sustained relief from symptoms of interstitial cystitis and painful bladder syndrome.* BJU Int, 2009. 103(7): p. 910-8.**
181. **Parsons, C.L., *Successful downregulation of bladder sensory nerves with combination of heparin and alkalinized lidocaine in patients with interstitial cystitis.* Urology, 2005. 65(1): p. 45-8.**
182. **Davis, E.L., et al., *Safety and efficacy of the use of intravesical and oral pentosan polysulfate sodium for interstitial cystitis: a randomized double-blind clinical trial.* J Urol, 2008. 179(1): p. 177-85.**
183. **Riedl, C.R., et al., *Hyaluronan treatment of interstitial cystitis/painful bladder syndrome.* Int Urogynecol J Pelvic Floor Dysfunct, 2008. 19(5): p. 717-21.**
184. **Cervigni, M., et al., *A combined intravesical therapy with hyaluronic acid and chondroitin for refractory painful bladder syndrome/interstitial cystitis.* Int Urogynecol J Pelvic Floor Dysfunct, 2008. 19(7): p. 943-7.**
185. **Fagerli, J., et al., *Intravesical capsaicin for the treatment of interstitial cystitis: a pilot study.* Can J Urol, 1999. 6(2): p. 737-744.**
186. **Apostolidis, A., G.E. Gonzales, and C.J. Fowler, *Effect of intravesical Resiniferatoxin (RTX) on lower urinary tract symptoms, urodynamic parameters, and quality of life of patients with urodynamic increased bladder sensation.* Eur Urol, 2006. 50(6): p. 1299-305.**

187. **Payne, C.K., et al., *Intravesical resiniferatoxin for the treatment of interstitial cystitis: a randomized, double-blind, placebo controlled trial.* J Urol, 2005. 173(5): p. 1590-4.**
188. **Mayer, R., et al., *A randomized controlled trial of intravesical bacillus calmette-guerin for treatment refractory interstitial cystitis.* J Urol, 2005. 173(4): p. 1186-91.**
189. **Yan, L., et al., *Advanced materials and nanotechnology for drug delivery.* Adv Mater, 2014. 26(31): p. 5533-40.**
190. **Allen, T.M. and P.R. Cullis, *Liposomal drug delivery systems: from concept to clinical applications.* Adv Drug Deliv Rev, 2013. 65(1): p. 36-48.**
191. **Rajaganapathy, B.R., et al., *Bladder Uptake of Liposomes after Intravesical Administration Occurs by Endocytosis.* PLoS ONE, 2015. 10(3): p. e0122766.**
192. **Hung, S.-Y., et al., *Role of liposome in treatment of overactive bladder and interstitial cystitis.* Urological Science, 2015. 26(1): p. 3-6.**
193. **Lee, Y., et al., *Targeting and Internalization of Liposomes by Bladder Tumor Cells Using a Fibronectin Attachment Protein-Derived Peptide–Lipopolymer Conjugate.* Bioconjugate Chemistry, 2017. 28(5): p. 1481-1490.**
194. **Stride, E., *Physical principles of microbubbles for ultrasound imaging and therapy.* Front Neurol Neurosci, 2015. 36: p. 11-22.**
195. **Porter, T.R., F. Xie, and A. Kricsfeld, *The mechanism and clinical implication of improved left ventricular videointensity following intravenous injection of multi-fold dilutions of albumin with dextrose.* Int J Card Imaging, 1995. 11(2): p. 117-25.**
196. **Al-Mansour, H.A., et al., *Usefulness of harmonic imaging for left ventricular opacification and endocardial border delineation by optison.* Am J Cardiol, 2000. 85(6): p. 795-9, a10.**
197. **Lindner, J.R., K. Wei, and S. Kaul, *Imaging of Myocardial Perfusion with SonoVue TM in Patients with a Prior Myocardial Infarction.* Echocardiography, 1999. 16(7, Pt 2): p. 753-760.**

198. **McDonald, D.M. and P.L. Choyke, *Imaging of angiogenesis: from microscope to clinic.* Nat Med, 2003. 9(6): p. 713-25.**
199. **Meairs, S., *Contrast-enhanced ultrasound perfusion imaging in acute stroke patients.* Eur Neurol, 2008. 59 Suppl 1: p. 17-26.**
200. **Darge, K., et al., *Diagnosis of vesicoureteric reflux with low-dose contrast-enhanced harmonic ultrasound imaging.* Pediatr Radiol, 2005. 35(1): p. 73-8.**
201. **Bull, J.L., *The application of microbubbles for targeted drug delivery.* Expert Opin Drug Deliv, 2007. 4(5): p. 475-93.**
202. **Unger, E., et al., *Cardiovascular drug delivery with ultrasound and microbubbles.* Adv Drug Deliv Rev, 2014. 72: p. 110-26.**
203. **Liu, H.L., et al., *Combining microbubbles and ultrasound for drug delivery to brain tumors: current progress and overview.* Theranostics, 2014. 4(4): p. 432-44.**
204. **Kilroy, J.P., et al., *Localized in vivo model drug delivery with intravascular ultrasound and microbubbles.* Ultrasound Med Biol, 2014. 40(10): p. 2458-67.**
205. **Meairs, S., *Facilitation of Drug Transport across the Blood-Brain Barrier with Ultrasound and Microbubbles.* Pharmaceutics, 2015. 7(3): p. 275-93.**
206. **Escoffre, J.M., et al., *Doxorubicin liposome-loaded microbubbles for contrast imaging and ultrasound-triggered drug delivery.* IEEE Trans Ultrason Ferroelectr Freq Control, 2013. 60(1): p. 78-87.**
207. **Geers, B., et al., *Self-assembled liposome-loaded microbubbles: The missing link for safe and efficient ultrasound triggered drug-delivery.* J Control Release, 2011. 152(2): p. 249-56.**
208. **Geers, B., et al., *Crucial factors and emerging concepts in ultrasound-triggered drug delivery.* J Control Release, 2012. 164(3): p. 248-55.**
209. **Wallace, N. and S.P. Wrenn, *Ultrasound triggered drug delivery with liposomal nested microbubbles.* Ultrasonics, 2015. 63: p. 31-8.**

210. Lentacker, I., et al., *Understanding ultrasound induced sonoporation: Definitions and underlying mechanisms.* Advanced Drug Delivery Reviews, 2014. 72: p. 49-64.

211. Brayman, A.A., et al., *Transient poration and cell surface receptor removal from human lymphocytes in vitro by 1 MHz ultrasound.* Ultrasound in Medicine & Biology, 1999. 25(6): p. 999-1008.

212. Amabile, P.G., et al., *High-efficiency endovascular gene delivery via therapeutic ultrasound.* Journal of the American College of Cardiology, 2001. 37(7): p. 1975-1980.

213. Frenkel, V., *Ultrasound mediated delivery of drugs and genes to solid tumors.* Advanced Drug Delivery Reviews, 2008. 60(10): p. 1193-1208.

214. Guzmán, H.R., et al., *Ultrasound-mediated disruption of cell membranes. II. Heterogeneous effects on cells.* The Journal of the Acoustical Society of America, 2001. 110(1): p. 597-606.

215. Bao, S., B.D. Thrall, and D.L. Miller, *Transfection of a reporter plasmid into cultured cells by sonoporation in vitro.* Ultrasound Med Biol, 1997. 23(6): p. 953-9.

216. Frenkel, P.A., et al., *DNA-loaded albumin microbubbles enhance ultrasound-mediated transfection in vitro.* Ultrasound Med Biol, 2002. 28(6): p. 817-22.

217. Karshafian, R., et al., *Microbubble mediated sonoporation of cells in suspension: clonogenic viability and influence of molecular size on uptake.* Ultrasonics, 2010. 50(7): p. 691-7.

218. Vandenbroucke, R.E., et al., *Ultrasound assisted siRNA delivery using PEG-siPlex loaded microbubbles.* J Control Release, 2008. 126(3): p. 265-73.

219. Delalande, A., et al., *Sonoporation: mechanistic insights and ongoing challenges for gene transfer.* Gene, 2013. 525(2): p. 191-9.

220. McEwan, C., et al., *Oxygen carrying microbubbles for enhanced sonodynamic therapy of hypoxic tumours.* J Control Release, 2015. 203: p. 51-6.

221. Ferrara, K., R. Pollard, and M. Borden, *Ultrasound microbubble contrast agents: fundamentals and application to gene and drug delivery.* Annu Rev Biomed Eng, 2007. 9: p. 415-47.

222. Haycock, J.W., *3D cell culture: a review of current approaches and techniques.* Methods Mol Biol, 2011. 695: p. 1-15.

223. Rosen, D.A., et al., *Molecular variations in Klebsiella pneumoniae and Escherichia coli FimH affect function and pathogenesis in the urinary tract.* Infect Immun, 2008. 76(7): p. 3346-56.

224. Eto, D.S., J.L. Sundsbak, and M.A. Mulvey, *Actin-gated intracellular growth and resurgence of uropathogenic Escherichia coli.* Cell Microbiol, 2006. 8(4): p. 704-17.

225. Schneider, C.A., W.S. Rasband, and K.W. Eliceiri, *NIH Image to ImageJ: 25 years of image analysis.* Nat Meth, 2012. 9(7): p. 671-675.

226. Dukes, C., *Some Observations on Pyuria.* Proc R Soc Med, 1928. 21(7): p. 1179-1183.

227. Gill, K., et al., *The Problem of Pyuria 1-9 wbc ul-1; Are We Missing Significant Disease*, in *Int Urogynecol J*. 2011, Springer-Verlag. p. 1769-2008.

228. Wu, X.R., et al., *Mammalian uroplakins. A group of highly conserved urothelial differentiation-related membrane proteins.* J Biol Chem, 1994. 269(18): p. 13716-24.

229. Sizemore, R.K., J.J. Caldwell, and A.S. Kendrick, *Alternate Gram Staining Technique Using a Fluorescent Lectin.* Applied and Environmental Microbiology, 1990. 56(7): p. 2245-2247.

230. Romero, R., et al., *Detection of a microbial biofilm in intraamniotic infection.* Am J Obstet Gynecol, 2008. 198(1): p. 135 e1-5.

231. Hertting, O., et al., *Vitamin D induction of the human antimicrobial Peptide cathelicidin in the urinary bladder.* PLoS One, 2010. 5(12): p. e15580.

232. **Kuhlmann, I., *The prophylactic use of antibiotics in cell culture.* Cytotechnology, 1995. 19(2): p. 95-105.**
233. **Bajpai, R., et al., *Efficient propagation of single cells Accutase-dissociated human embryonic stem cells.* Mol Reprod Dev, 2008. 75(5): p. 818-27.**
234. **Bolte, S. and F.P. CordeliÈRes, *A guided tour into subcellular colocalization analysis in light microscopy.* Journal of Microscopy, 2006. 224(3): p. 213-232.**
235. **Andersson, K.E., *Current and future drugs for treatment of MS-associated bladder dysfunction.* Annals of Physical and Rehabilitation Medicine, 2014. 57(5): p. 321-328.**
236. **Saito, M., I. Nakamura, and I. Miyagawa, *[Autoradiographic localization of muscarinic receptors in diabetic rat bladder].* Nihon Hinyokika Gakkai Zasshi, 1997. 88(10): p. 858-67.**
237. **Lavelle, J.P., et al., *Disruption of guinea pig urinary bladder permeability barrier in noninfectious cystitis.* American Journal of Physiology - Renal Physiology, 1998. 274(1): p. F205-F214.**
238. **Liebhold, M., et al., *[Light- and electron-microscopic studies of the structure of normal bladder epithelium in female swine].* Anat Histol Embryol, 1995. 24(1): p. 47-52.**
239. **Derganc, J., B. Božič, and R. Romih, *Shapes of Discoid Intracellular Compartments with Small Relative Volumes.* PLoS ONE, 2011. 6(11): p. e26824.**
240. **Matsuzaki, K., et al., *Optical characterization of liposomes by right angle light scattering and turbidity measurement.* Biochimica et Biophysica Acta (BBA) - Biomembranes, 2000. 1467(1): p. 219-226.**
241. **Gubernator, J., Z. Drulis-Kawa, and A. Kozubek, *A simply and sensitive fluorometric method for determination of gentamicin in liposomal suspensions.* Int J Pharm, 2006. 327(1-2): p. 104-9.**
242. **Feshitan, J.A., et al., *Microbubble size isolation by differential centrifugation.* Journal of Colloid and Interface Science, 2009. 329(2): p. 316-324.**

243. Carugo, D., et al., *Biologically and Acoustically Compatible Chamber for Studying Ultrasound-Mediated Delivery of Therapeutic Compounds.* Ultrasound in Medicine and Biology, 2015. 41(7): p. 1927-37.
244. Nachlas, M.M., et al., *The determination of lactic dehydrogenase with a tetrazolium salt.* Analytical Biochemistry, 1960. 1(4): p. 317-326.
245. Korzeniewski, C. and D.M. Callewaert, *An enzyme-release assay for natural cytotoxicity.* J Immunol Methods, 1983. 64(3): p. 313-20.
246. Decker, T. and M.-L. Lohmann-Matthes, *A quick and simple method for the quantitation of lactate dehydrogenase release in measurements of cellular cytotoxicity and tumor necrosis factor (TNF) activity.* Journal of Immunological Methods, 1988. 115(1): p. 61-69.
247. Burgess, A., et al., *Loss of human Greatwall results in G2 arrest and multiple mitotic defects due to deregulation of the cyclin B-Cdc2/PP2A balance.* Proc Natl Acad Sci U S A, 2010. 107(28): p. 12564-9.
248. McCloy, R.A., et al., *Partial inhibition of Cdk1 in G 2 phase overrides the SAC and decouples mitotic events.* Cell Cycle, 2014. 13(9): p. 1400-12.
249. Nachnani, S., et al., *E-test: a new technique for antimicrobial susceptibility testing for periodontal microorganisms.* J Periodontol, 1992. 63(7): p. 576-83.
250. *EUCAST: AST of bacteria*. 21/07/2017; Available from: http://www.eucast.org/ast_of_bacteria/.
251. Labovitz, E., M.E. Levison, and D. Kaye, *Single-Dose Daily Gentamicin Therapy in Urinary Tract Infection.* Antimicrobial Agents and Chemotherapy, 1974. 6(4): p. 465-470.
252. Robino, L., et al., *Detection of intracellular bacterial communities in a child with Escherichia coli recurrent urinary tract infections.* Pathog Dis, 2013. 68(3): p. 78-81.

253. Robino, L., et al., *Intracellular bacteria in the pathogenesis of Escherichia coli urinary tract infection in children.* Clin Infect Dis, 2014. 59(11): p. e158-64.
254. Stender, H., *PNA FISH: an intelligent stain for rapid diagnosis of infectious diseases.* Expert Rev Mol Diagn, 2003. 3(5): p. 649-55.
255. Snyder, J.A., et al., *Role of phase variation of type 1 fimbriae in a uropathogenic Escherichia coli cystitis isolate during urinary tract infection.* Infect Immun, 2006. 74(2): p. 1387-93.
256. Wright, K.J., P.C. Seed, and S.J. Hultgren, *Development of intracellular bacterial communities of uropathogenic Escherichia coli depends on type 1 pili.* Cell Microbiol, 2007. 9(9): p. 2230-41.
257. Schembri, M.A. and P. Klemm, *Biofilm formation in a hydrodynamic environment by novel fimh variants and ramifications for virulence.* Infect Immun, 2001. 69(3): p. 1322-8.
258. Costerton, J.W., P.S. Stewart, and E.P. Greenberg, *Bacterial biofilms: a common cause of persistent infections.* Science, 1999. 284(5418): p. 1318-22.
259. Soto, S.M., *Importance of Biofilms in Urinary Tract Infections: New Therapeutic Approaches.* Advances in Biology, 2014. vol. 2014, Article ID 543974, 13 pages, 2014. https://doi.org/10.1155/2014/543974.
260. Chavez de Paz, L.E., *Image analysis software based on color segmentation for characterization of viability and physiological activity of biofilms.* Appl Environ Microbiol, 2009. 75(6): p. 1734-9.
261. Sava, I.G., E. Heikens, and J. Huebner, *Pathogenesis and immunity in enterococcal infections.* Clin Microbiol Infect, 2010. 16(6): p. 533-40.
262. Khandelwal, P., W.G. Ruiz, and G. Apodaca, *Compensatory endocytosis in bladder umbrella cells occurs through an integrin-regulated and RhoA- and dynamin-dependent pathway.* Embo Journal, 2010. 29(12): p. 1961-1975.
263. Sartingen, S., et al., *Aggregation substance increases adherence and internalization, but not translocation, of Enterococcus*

faecalis through different intestinal epithelial cells in vitro. **Infect.Immun., 2000. 68(10): p. 6044-6047.**

264. Brubaker, L. and A.J. Wolfe, *The new world of the urinary microbiome in women.* Am J Obstet Gynecol, 2015.

265. Brubaker, L. and A.J. Wolfe, *The Female Urinary Microbiota/Microbiome: Clinical and Research Implications.* Rambam Maimonides Medical Journal, 2017. 8(2): p. e0015.

266. Wolfe, A.J., et al., *Evidence of uncultivated bacteria in the adult female bladder.* J Clin Microbiol, 2012. 50(4): p. 1376-83.

267. Price, T.K., et al., *The Clinical Urine Culture: Enhanced Techniques Improve Detection of Clinically Relevant Microorganisms.* J Clin Microbiol, 2016. 54(5): p. 1216-22.

268. Moore, E.E., et al., *Urinary incontinence and urinary tract infection: temporal relationships in postmenopausal women.* Obstet Gynecol, 2008. 111(2 Pt 1): p. 317-23.

269. Holloway, J., N. Joshi, and T. O'Bryan, *Positive urine nitrite test: an accurate predictor of absence of pure enterococcal bacteriuria.* South Med J, 2000. 93(7): p. 681-2.

270. Bhadriraju, K. and C.S. Chen, *Engineering cellular microenvironments to improve cell-based drug testing.* Drug Discov Today, 2002. 7(11): p. 612-20.

271. Knight, E. and S. Przyborski, *Advances in 3D cell culture technologies enabling tissue-like structures to be created in vitro.* J Anat, 2014.

272. Brindley, D., et al., *Bioprocess Forces and Their Impact on Cell Behavior: Implications for Bone Regeneration Therapy.* Journal of Tissue Engineering, 2011. 2011: p. 620247.

273. Pekor, C., et al., *Induction of Hepatic and Endothelial Differentiation by Perfusion in a Three-Dimensional Cell Culture Model of Human Fetal Liver.* Tissue Eng Part C Methods, 2015.

274. Soyer, M. and G. Duménil, *Introducing Shear Stress in the Study of Bacterial Adhesion.* Journal of Visualized Experiments : JoVE, 2011(55): p. 3241.

275. **Rosenzweig, J.A., et al., *Low-Shear Force Associated with Modeled Microgravity and Spaceflight Does Not Similarly Impact the Virulence of Notable Bacterial Pathogens.* Applied microbiology and biotechnology, 2014. 98(21): p. 8797-8807.**
276. **Chin, M.S., et al., *In vivo acceleration of skin growth using a servo-controlled stretching device.* Tissue Eng Part C Methods, 2010. 16(3): p. 397-405.**
277. **Maqsood, M.I., et al., *Immortality of cell lines: challenges and advantages of establishment.* Cell Biol Int, 2013. 37(10): p. 1038-45.**
278. **Sa, Y., et al., *WE-C-217BCD-05: A Novel Interpolation Method for the 3D Reconstruction of Cell Structures.* Med Phys, 2012. 39(6Part27): p. 3950.**
279. **K. Hansen, L., et al., *The effect of low intensity shockwave treatment (Li-SWT) on human myoblasts and mouse skeletal muscle*. Vol. 18. 2017.**
280. **Adan, A., Y. Kiraz, and Y. Baran, *Cell Proliferation and Cytotoxicity Assays.* Curr Pharm Biotechnol, 2016. 17(14): p. 1213-1221.**
281. **Madni, A., et al., *Liposomal drug delivery: a versatile platform for challenging clinical applications.* J Pharm Pharm Sci, 2014. 17(3): p. 401-26.**
282. **Place, J.D., et al., *Production and characterization of monoclonal antibody to gentamicin.* Hybridoma, 1984. 3(2): p. 187-93.**
283. **Tan, X., et al., *Persistence of gentamicin residues in milk after the intramammary treatment of lactating cows for mastitis.* Journal of Zhejiang University. Science. B, 2009. 10(4): p. 280-284.**
284. **Garnacho, C., *Intracellular Drug Delivery: Mechanisms for Cell Entry.* Curr Pharm Des, 2016. 22(9): p. 1210-26.**
285. **Vhora, I., et al., *Receptor-targeted drug delivery: current perspective and challenges.* Ther Deliv, 2014. 5(9): p. 1007-24.**
286. **Raymond, I., et al., *The clinical effectiveness of intravesical sodium hyaluronate (cystistat(R)) in patients with interstitial***

cystitis/painful bladder syndrome and recurrent urinary tract infections. **Curr Urol, 2012. 6(2): p. 93-8.**

287. Ganti, S., et al., *Three-dimensional (3D) analysis of white etching bands (WEBs) in AISI M50 bearing steel using automated serial sectioning.* Materials Characterization, 2018. 138: p. 11-18.

288. Lantz, B., *The impact of sample non-normality on ANOVA and alternative methods.* Br J Math Stat Psychol, 2013. 66(2): p. 224-44.

289. Atocap. 27/02/2018; Available from: www.atocap.com.

290. Chindera, C., et al., *The antimicrobial polymer PHMB enters cells and selectively condenses bacterial chromosomes.* Sci. Rep., 2016. 6: 23121.

Appendix 1

OPEN ACCESS Freely available online

PLOS ONE

Enterococcus faecalis Subverts and Invades the Host Urothelium in Patients with Chronic Urinary Tract Infection

Harry Horsley[1], James Malone-Lee[1], David Holland[1], Madeleine Tuz[1], Andrew Hibbert[2], Michael Kelsey[3], Anthony Kupelian[1], Jennifer L. Rohn[1*]

1 Centre for Clinical Science and Technology, Research Department of Clinical Physiology, Division of Medicine, University College London, London, United Kingdom, **2** Imaging Suite, Royal Veterinary College, London, United Kingdom, **3** Department of Microbiology, The Whittington Hospital NHS Trust, London, United Kingdom

Abstract

Bacterial urinary tract infections (UTI) are a major growing concern worldwide. Uropathogenic *Escherichia coli* has been shown to invade the urothelium during acute UTI in mice and humans, forming intracellular reservoirs that can evade antibiotics and the immune response, allowing recurrence at a later date. Other bacterial species, such as *Staphylococcus saprophyticus*, *Klebsiella pneumonia* and *Salmonella enterica* have also been shown to be invasive in acute UTI. However, the role of intracellular infection in chronic UTI causing more subtle lower urinary tract symptoms (LUTS), a particular problem in the elderly population, is poorly understood. Moreover, the species of bacteria involved remains largely unknown. A previous study of a large cohort of non-acute LUTS patients found that *Enterococcus faecalis* was frequently found in urine specimens. *E. faecalis* accounts for a significant proportion of chronic bladder infections worldwide, although the invasive lifestyle of this uropathogen has yet to be reported. Here, we wanted to explore this question in more detail. We harvested urothelial cells shed in response to inflammation and, using advanced imaging techniques, inspected them for signs of bacterial pathology and invasion. We found strong evidence of intracellular *E. faecalis* harboured within urothelial cells shed from the bladder of LUTS patients. Furthermore, using a culture model system, these patient-isolated strains of *E. faecalis* were able to invade a transitional carcinoma cell line. In contrast, we found no evidence of cellular invasion by *E. coli* in the patient cells or the culture model system. Our data show that *E. faecalis* is highly competent to invade in this context; therefore, these results have implications for both the diagnosis and treatment of chronic LUTS.

Citation: Horsley H, Malone-Lee J, Holland D, Tuz M, Hibbert A, et al. (2013) *Enterococcus faecalis* Subverts and Invades the Host Urothelium in Patients with Chronic Urinary Tract Infection. PLoS ONE 8(12): e83637. doi:10.1371/journal.pone.0083637

Editor: Willem van Schaik, University Medical Center Utrecht, Netherlands

Received August 13, 2013; **Accepted** November 5, 2013; **Published** December 10, 2013

Funding: This work was partially funded by Research into Ageing (grant number: 315; http://www.ageuk.org.uk). The funders had no role in study design, data collection and analysis, decision to publish, or preparation of the manuscript. No additional external funding was received for this study.

Competing interests: The authors have declared that no competing interests exist.

* E-mail: j.rohn@ucl.ac.uk

Introduction

Urinary tract infection (UTI) is a significant cause of morbidity, ranking as one of the most prevalent infectious diseases worldwide [1,2]. By the age of 24, nearly one third of women will have sought medical attention for an acute, self-limiting UTI and between 15-25% of this group will suffer from a recurrent or chronic form of this disease [2–5]. Acute UTI is not diagnostically challenging [6], as the rapid onset of urinary frequency and dysuria are clear indicators of the pathology.

Less clear cut are lower urinary tract symptoms (LUTS), a collective term describing a host of urological manifestations, including symptoms of urine storage and voiding, and pain attributed to the lower urinary tract [7]. While the role of infection in the generation of acute symptoms is well recognised, an infective aetiology in other LUTS is not typically assumed. In fact, most current guidance on the management of LUTS calls for the exclusion of UTI using routine urinalysis methods [8,9]. In this context, the term LUTS had become synonymous with non-infectious disease. The clinical features of UTI and LUTS show considerable overlap, however, and the prevalence of both disorders rises dramatically with age [10–13].

Our research centre and others have found that the tests deployed to screen for UTI are largely inadequate, particularly in patients who do not present with classic acute infective symptoms [14–16]. Although LUTS can undoubtedly be caused by other factors (e.g. carcinoma, urethral stricture, prostatic

disease, bladder stones or affective disorders such as those common in multiple sclerosis [17,18]), we now know that patients scoring as negative on routine tests for infection might in fact harbour a low-grade bacterial pathology [19].

By far the most prevalent bacterial species implicated in acute UTI is *E. coli*, which is responsible for as many as to 90% of diagnosed cases of nosocomial and community-acquired bladder infection [20]. Murine models of acute UTI have shown that uropathogenic *E. coli* (UPEC) invades and forms intracellular bacterial communities (IBCs) in the bladder where it is able to evade immune surveillance and a number of systemic antibiotic treatments [5,21–27]. The findings from these studies have resulted in a well-accepted model of the acute UTI UPEC life cycle [25]. Adhesion and invasion into the host cell cytoplasm are closely followed by three distinct stages of the intracellular bacterial community (IBC) lifecycle. During early IBC, loose collections of bacillus bacteria rapidly divide inside the cytoplasm proper. In middle IBC, daughter cells exhibiting a coccoid morphology pack tightly producing a biofilm-like pod [23]. At the late IBC stage, bacteria at the periphery of the intracellular biofilms regain a rod morphology and become highly motile, leading to bacterial efflux and re-infection of adjacent cells [25].

Infected umbrella cells will be shed from the epithelial lining into the urine. Such sloughing is known in both mice and humans to be a common response to infection [24,28–31]. This dramatic cell shedding response leaves a gap in the epithelial layer, exposing naive transitional cells (proximal to the submucosal coat) to *de novo* UPEC invasion, a process which has been proposed to create quiescent intracellular reservoirs (QIR) responsible for latent recurrent and low-level chronic infection in mice [5,22,26,31,32]. Although QIR have not been directly observed in human patients, there is much evidence to suggest their existence [5,22,26,31,33–35]. Other IBC stages above, namely bacterial filamentation, have also been described in acute human UTI [24], although murine models remain more thoroughly studied.

Given the prevalence of UPEC as a causative agent in UTI, UPEC remains the most widely studied uropathogen. It is now recognized, however, that urothelial invasion may not be restricted to *E. coli* alone, with *Staphylococcus saprophyticus* [36] and *Klebsiella pneumonia* [37] also exhibiting UPEC-like intracellular lifestyles in experimental murine acute UTI. Recently, we explored an infective aetiology in LUTS using a traditional gentamicin protection assay, in which shielded bacteria were enumerated after extracellular bacteria were killed off by antibiotics [19]. In this study, *Enterococcus faecalis*, *Streptococcus anginosus*, *E. coli*, and *Proteus mirabilis* were shown to be closely associated with the shed cells. Although this assay is a trusted and well-tested method for detecting intracellular bacteria [38,39], the information gleaned from this technique is indirect. Furthermore, antibiotic-susceptible *E. faecalis* readily forms heavily antibiotic-resistant biofilms which could be responsible for false-positive outputs [40,41].

In the LUTS study described above, *E. faecalis* was the most cell-associated pathogen described, much more so than *E. coli*. In addition, *E. faecalis* is frequently isolated in acute UTI [10,24] and non-dysuric LUTS patients [19], and is commonly implicated in catheter-associated and chronic urinary tract infection [42,43]. In the past few years *Enterococcus spp.* have received a significant amount of attention. This opportunistic uropathogen is of particular concern in the clinical setting, where multi-drug resistant strains are frequently involved in hospital-acquired infection. Moreover, the rapid acquisition of antibiotic resistance, biofilm formation [40,41] and the innate ability to thrive and persist in the urinary tract make UTIs caused by *Enterococcus* spp. particularly difficult to eradicate [42,44–47]. Despite its commonness in bladder infections, aside from our recent paper [19], there have been no reports of *E. faecalis* associated with patient urothelial cells, nor any description of its potential intracellular invasion more direct than the antibiotic protection assay. We therefore set out to explore the role of cell shedding and bacterial invasion in LUTS in more detail.

Results

Significant urothelial shedding in the LUTS bladder

In order to study the role of infection and inflammation in LUTS, and to determine whether shed epithelial cells could be used as a further means of studying intracellular infection in more detail, we recruited 705 patients presenting at first visit to the clinic, 606 females and 99 males with a mean age of 51 years (sd=17.5). Of the 705 urine samples, 522 (74%) were found to be negative on routine mid-stream urine (MSU) culture (using a culture positive threshold of $\geq 10^5$ cfu ml^{-1} of a single known uropathogen) and 183 (26%) were positive. It should be noted that this routine MSU culture threshold, while standard for the UK and some other countries, misses significant infection in our clinical experience. For main demographic data and symptomatology please see Figure **S1**.

Pyuria (white blood cells [WBC] μl^{-1}), quantified immediately in fresh, unspun specimens of urine, is the best clinical indicator of UTI currently available. The patients were categorised into three groups according to pyuria expression: (1) for zero pyuria; (2) for pyuria 1 to 9 WBC μl^{-1}; and (3) for pyuria ≥10 WBC μl^{-1}. Pyuria ≥10 WBC μl^{-1} has long been advocated as a diagnostic threshold to discriminate between the presence or absence of lower urinary tract pathology. First described by Dukes in 1928 [48], this diagnostic threshold does not withstand contemporary scientific scrutiny [16], and there are no published data demonstrating that pyuria of 1 to 9 WBC μl^{-1} is non-pathological [49]. Indeed, 1-9 WBC μl^{-1} does predict underlying disease [49], so we thought it prudent to include this category.

In addition to WBC, mouse and human bladders shed urothelial cells into the urine as part of an innate immune response to bacterial insult in acute UTI [24,28–31]. Therefore, we also counted epithelial cells (EPC μl^{-1}) in the urine of LUTS patients. First, we recognized the requirement for proof of cellular origin as a proportion of these cells could be contaminants originating from the genitalia and perineum. Uroplakin-III (UP3) is expressed solely on the asymmetric unit membrane of urothelial cells [50,51]. Therefore, we targeted this glycoprotein using immunofluorescence to determine the

proportion of urinary epithelial cells that originated in the urinary tract (Figure **1A, B**). A subset of 44 randomly selected LUTS patients was included in this experiment. MSU samples from 22 patients with chronic LUTS (F=22; mean age=51; sd=19) were compared with vaginal swabs from 22 further chronic LUTS patients (F=22; mean age=50; sd=20). The median percentage of UP3-positive cells in the MSU samples was 75% (Q1=68, Q3=78.5) but only 25% (Q1=19, Q3=32) in the vaginal swabs (Figure **1C**). The results of a Mann-Whitney test show the proportion of UP3-positive cells found in the urine of chronic LUTS patients to be significantly higher than that in the vagina (U=1, p <.001). Therefore we could be confident that our cell analyses were representative of underlying pathology of the bladder.

We counted shed EPC in the 705 patient cohort (Figure **2A**). The EPC counts were positively skewed and log transformation had a limited normalisation effect, changing the skewness from 13.4 to 0.63. We therefore compared the median $\log_{10}$ epithelial cell count ($\log_{10}$ EPC μl^{-1}) between categories, non-parametrically. Figure **2A** shows clear between group differences between these categories (Kruskal-Wallis $X^2 = 75$, p<.001, df=2). Post hoc analysis using Mann-Whitney test comparisons with a Bonferroni correction confirmed that all three groups differed among one another (p<.001). A similar comparison between the 522 (74%) showing a negative MSU culture and the 183 (26%) that were positive showed no between group differences ($U=19x10^3$, P=.5). Therefore, the degree of EPC shedding corresponds to amount of pyuria, and by association, severity of infection.

In summary, this evidence supports the murine model of bacteria-induced urothelial inflammation and shedding in LUTS patients. Given that infection seemed to correlate with symptoms in this cohort, we set out to study the underlying microbiology in closer detail.

Implicating intracellular *E. faecalis* bacterial infection in the aetiopathology of LUTS

As with previous work exploring cellular invasion during acute UTI in humans [24], we inspected shed urothelial cells from LUTS patients with non-acute UTI for signs of bacterial association and intracellular pathology. Prior to imaging, the urine samples were cultured on chromogenic agar and any arising bacteria identified using a rigorous series of biochemical assays as outlined in the methods section.

For this experiment we studied a randomly selected subset of 48 specimens using epi-fluorescent microscopy to identify bacterial involvement. MSU samples were donated by 24 female LUTS patients (mean age=52; *sd*=10.7) and compared with an equal number of samples from female healthy normal controls (*N*=24; mean age=48; *sd*=9.9). Although these 24 LUTS patients were negative for routine MSU culture, growing $<10^5$ cfu ml^{-1} of a single known uropathogen, 10 exhibited growth of *E. coli* and/or *E. faecalis* with the addition of other species. One of these samples exhibited growth of only *E. coli* and *E. faecalis* with no other species present which gave us the opportunity to compare how each bacterium behaved. This sample was selected for confocal microscopy to explore intracellular pathology.

Our previous work, which explored intracellular colonisation of the LUTS bladder, presented data from antibiotic protection assays alone [19]. This microbiological data is indirect and can be misleading, as detergents may liberate live membrane-bound bacteria. This technique is hindered further by the presence of extracellular biofilms which may be unaffected by even high concentrations of antibiotics. Therefore, to decisively inspect these cells for intracellular colonisation we conducted confocal laser-scanning microscopy in conjunction with a bank of extensive 3D digital analyses.

On epi-fluorescent analysis, 75% (N=18) of the LUTS patient samples showed evidence of infected urothelial cells in comparison to only 17% (N=4) in the control group (Figure **2B**). Data from the confocal analysis of a representative sample suggested that *E. faecalis* and *E. coli* employ distinct pathological strategies in these patients, with only *E. faecalis* exhibiting cellular invasion. Figure **3** shows two representative cells shed from the bladder of a LUTS patient with a mixed sub-threshold infection with *E. faecalis* and *E. coli*. Cells that were associated with adherent extracellular bacilli (*E. coli*) did not contain intracellular bacterial communities (Figure **3D**). However, in cells exhibiting adherent, extracellular coccoid *E. faecalis* (Figure **3A**, broken white arrow), we found compelling evidence of intracellular pathology (Figure **3A**, white arrow, B, C). Although uropathogenic *E. coli* have the unusual ability to transform from a rod to coccoid morphology within the intracellular niche within the centre of a tightly packed IBC [23,24], we saw isolated intracellular coccoid forms, too dispersed to be coccoid *E. coli*, suggesting that the organism was indeed *E. faecalis*.

LUTS patient-isolated *E. coli* does not invade cells in a cell culture model system

So far, we have shown that the presence of LUTS is associated with shedding of the urothelium, which is likely activated by the presence of bacteria. The confocal data from analysis of shed patient cells suggested that *E. faecalis* employed an invasive lifestyle whereas *E. coli* was ubiquitously extracellular.

Given the difficulty of identifying in advance patient cells that harboured *E. coli* and/or *E. faecalis* in the absence of other species, we decided to use defined infections in cell culture to explore this issue further. We designed a cell culture system to model the infection process using five strains of *E. coli* isolated from routine MSU-culture negative LUTS patients. We infected a T24 transitional bladder cell line before, as with the shed urothelial cells, fluorescently staining and imaging using high-resolution confocal microscopy. The invasive properties of these strains were analysed using a series of 3D digital analyses.

All of the five *E. coli*-infected T24 cells exhibited marked bacterial adhesion and colonisation (See Figure **4A, D** for a representative example). Orthogonal views of Z-stack 3D constructs, however, showed the colonies of each strain of bacteria to be entirely extracellular (Figure **4B**). Further analysis using Z-axis profile plots supported these findings, with the peak mean pixel intensity of the DAPI labelled bacteria

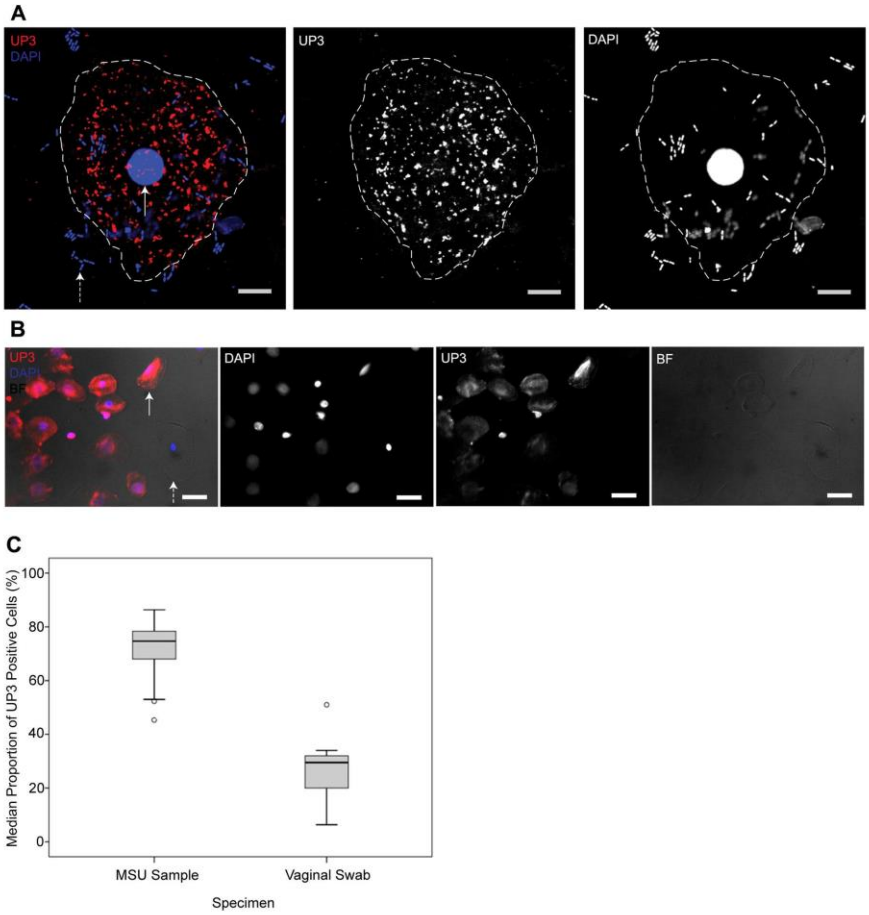

Figure 1. Uroplakin-3 (UP3) immunofluorescence. (A) Confocal image of a UP3-positive urothelial cell shed into the urine of a LUTS patient, a composite showing the expression of UP3 in red and DAPI-stained host (solid white arrow) and bacterial (broken white arrow) DNA in blue. Each channel is also shown in monochrome. The boundary of the cell is represented by a broken white line. White scale bar is 10μm. (B) Epi-fluorescent image of UP3-positive urothelial cells (solid white arrow) and a single UP3-negative epithelial cell (broken white arrow) harvested from the urine of a patient with LUTS. The composite image shows UP3 in red, host DNA in blue and the brightfield (BF) channel in greyscale. Channels are also shown separately in monochrome. White scale bar is 50μm. (C) Graph showing the median proportion of UP3-positive cells found in MSU samples (N=22) when compared with vaginal swabs (N=22). 75% (Q1=68, Q3=78.5) of the cells found in the MSU samples were UP3-positive in contrast to only 25% (Q1=19, Q3=32) in the vaginal swabs (U=1, $p < .001$).

doi: 10.1371/journal.pone.0083637.g001

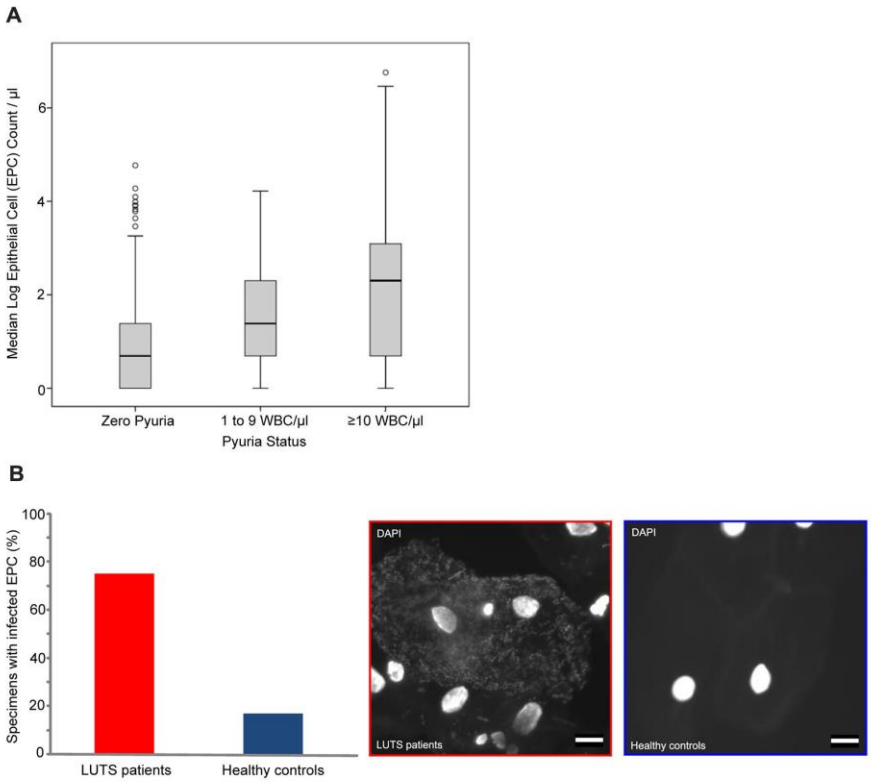

Figure 2. Urinary epithelial cell counts and bacterial pathology. (A) Relationship between the median log urinary epithelial count (EPC=epithelial cell) and the level of pyuria observed in the urine of LUTS patients (WBC=white blood cell). The mean log epithelial cell counts at each state of pyuria proved to be significantly different. (B) Bar chart showing the percentage of specimens with bacteria-association urinary epithelial cells (EPC) in LUTS patients (75%) and healthy controls (17%). Representative images of infected urinary EPC from LUTS patients (red) and normal EPC for healthy controls (blue) shown for reference. White scale bar is 10µm.

doi: 10.1371/journal.pone.0083637.g002

(blue) found to be some distance away (in the Z-axis) from that of the phalloidin labelled F-actin (red) (Figure **4C**).

Remarkably, it appeared that these LUTS-isolated strains of *E. coli* formed tightly packed extracellular biofilms on the surface of the T24 cells (Figure **4D**). Positive staining with wheat germ agglutinin (WGA) in a gram-negative organism like *E. coli* signifies the secretion of an exopolymeric matrix, inherent in biofilm formation [52] [53] (Figure **4A**, white arrows).

LUTS patient-isolated *E. faecalis* invades cells in a cell culture model system

Confocal analysis of shed LUTS patient urothelial cells demonstrated cellular invasion by *E. faecalis*. To test further whether *E. faecalis* is competent to invade urothelial cells, as our earlier findings would suggest, we challenged the same T24 bladder cell culture model system as described above with five strains of *E. faecalis* isolated from routine MSU-culture negative LUTS patients. Again, the infected cells were imaged

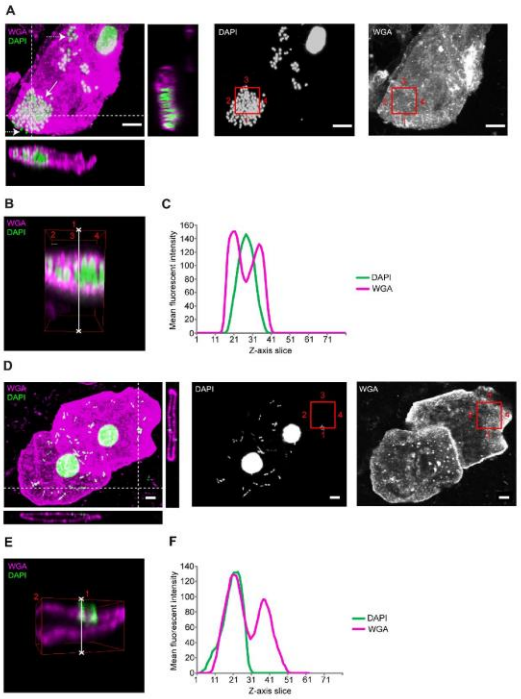

Figure 3. Bacterial invasion in shed urothelial cells. Prior to imaging, the urine sample was cultured on chromogenic agar and bacterial identities confirmed using a bank of biochemical assays as outlined in the methods section. By supporting the confocal data with culture results and bacterial identity we were able recognize bacteria by morphology during confocal analysis. (A) Maximum projection confocal image of a cell shed from the bladder of a LUTS patient with a mixed sub-threshold infection with *E. faecalis* and *E. coli*. The left image is a composite showing the wheat germ agglutinin (WGA)-stained plasma membrane in magenta and DAPI stained host and bacterial DNA in green. Solid white arrow highlights a cluster of intracellular coccoid bacteria, broken white arrow highlights extracellular coccoid bacteria. Bacteria were identified as *E. faecalis* owing to morphology. Orthogonal views are through entire Z-stack at a position corresponding to white broken lines on the left image, showing intracellular colonisation. The centre and right image show the respective DAPI and WGA channels in monochrome. White scale bar is 5μm. (B) A 3-dimensional volume through the entire Z-stack at a position corresponding to the red squares in image A (numbered for orientation); bacteria are clearly residing within the cell. (C) A region of bacterial colonisation was selected (highlighted by the white line in 3D construct B) and used to produce a Z-axis profile plot, which presents the average pixel intensity of a given channel moving through the 80-slice Z-stack. This graphical representation shows further evidence of cellular invasion, with the peak mean pixel intensity of the DAPI channel (*E. faecalis*, green) corresponding with a striking reduction in the WGA (plasma membrane, magenta) channel at slice 29 (centre of the cell). (D) Maximum projection confocal image of a cell shed from the same patient as above with a mixed sub-threshold infection with *E. faecalis* and *E. coli*. Images were analysed and presented as above. Bacteria were identified as *E. coli* owing to bacillus morphology. Orthogonal views show the *E. coli* to be strongly associated with the plasma membrane but entirely extracellular. White scale bar is 5μm. (E) 3-dimensional volume corresponding to the red squares in image D (numbered for orientation); again, the *E. coli* were shown to be ubiquitously extracellular. (F) A region of bacterial colonisation was selected (highlighted by the white line in 3D construct E) to produce a Z-axis profile plot. This graphical representation shows further evidence of external cellular colonisation alone. The peak mean pixel intensity of the DAPI channel corresponded with that of the WGA stained apical plasma membrane channel at slice 21.

doi: 10.1371/journal.pone.0083637.g003

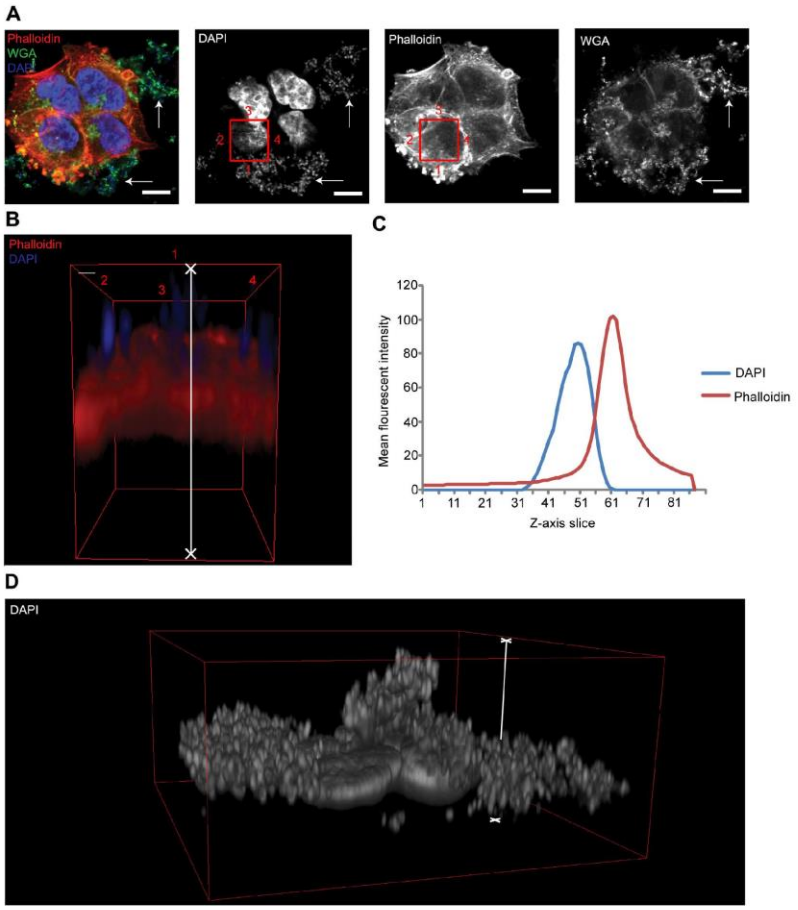

Figure 4. 3D confocal analysis of cultured cells infected with LUTS-isolated *E. coli*. (A) Confocal image of a group of T24 cells infected for 2.5hrs with *E. coli* isolated from LUTS patients at an MOI of approximately 10-15 bacteria per mammalian cell. The left image is a composite showing the phalloidin-stained F-actin in red, wheat germ agglutinin (WGA) stained plasma membrane in green and DAPI stained host and bacterial DNA in blue. The left centre, right centre and far right images show the respective DAPI, phalloidin and WGA channels in monochrome. Solid white arrows highlight WGA-positive staining of an exopolymeric matrix secreted by *E. coli* during biofilm formation. White scale bar is 10μm. (B) A 3-dimensional volume through entire Z-stack at a position corresponding to the red squares in image A (numbered for orientation); the *E. coli* is clearly bound to the extracellular space. (C) A Z-axis profile plot was produced as in Figure 3. The DAPI channel is approximately 16 slices (in the Z-axis) from that of the phalloidin channel, confirming purely extracellular colonisation. (D) 3D construct of the cells shown in A with the DAPI channel shown alone. This image shows the extent of bacterial infection. Very deep and tightly packed *E. coli* biofilms can be seen covering the apical membrane of the T24 cells. The region of interest analysed in B and C is indicated with a white line.

doi: 10.1371/journal.pone.0083637.g004

using confocal microscopy and explored extensively with 3D digital analyses.

Unlike *E. coli*, *E. faecalis* adhered to the T24 cells in looser, more diffuse clusters (See Figure **5** for a representative example). More organised colonies were evident, although they manifested close to the T24 nuclei and within the horizontal boundaries of the cells, which suggested cellular invasion (Figure **5A**). Z-stack 3D constructs of these bacterial colonies clearly showed all five of the LUTS patient isolated *E. faecalis* to be sandwiched within the intracellular space of the T24 cells (Figure **5B, D**). These findings were mirrored in the Z-axis profile plots, which showed a marked decrease in mean pixel intensity of phalloidin-labelled F-actin (red) and a striking increase in the mean pixel intensity of the DAPI labelled *E. faecalis* at mid-cell slices (Figure **5C**).

Significant bacterial pathology associated with the urothelium is clearly evident in the LUTS population and the results of these 3D analyses support the hypothesis of intracellular colonisation by *E. faecalis* in LUTS patients. In contrast to the case of acute infection, it would appear that *E. coli* may not be ubiquitously invasive in the context of chronic low-grade UTI. It is important to note, however, that the lack of invasion may not necessarily preclude pathogenicity; the ability to form extracellular biofilms, as *E. coli* did in this study, could prove equally challenging to treat.

Discussion

Over the past decade, a model of the pathophysiology of UTI has solidified into accepted fact. Stemming from the initial elegant description of intracellular UPEC in mouse models of acute UTI [23], a number of studies have generally supported these initial findings. The data in mouse models is indeed robust [5,21–27]. It is worth noting, however, that the evidence for the presence of intracellular bacteria in human patients suffering acute UTI is confined to only one report of 80 women [24]. Another report has shown that UPEC isolated from women with acute cystitis were competent to form IBC in mice [27], but this evidence is not direct proof of their presence in the original patients. Hence, more data on the pervasiveness of intracellular bacteria in acute human UTI would be welcome.

In the case of non-acute, low-grade UTI responsible for chronic lower urinary tract symptoms, such as those exhibited by the patients in our clinic, even less is known about the bacterial lifecycle within the bladder. Our previous study showed that *E. coli* is not the sole or even foremost pathogen in these patients, and that a spectrum of species may be capable of causing such troublesome symptoms [19]. In that report we showed close association of four bacterial species – *E. faecalis, Streptococcus angiosus, E. coli and Proteus spp.* with epithelial cells shed from patients, suggestive of intracellular colonization, and further demonstrated that these bacterial isolates seemed competent to invade a bladder cell line, as assessed by an antibiotic protection assay. We were aware, however, that this assay, although widely trusted and used, could give misleading results if all extracellular bacteria were not killed by the antibiotics, for example if they were protected by biofilm formation or by very close association within niches in the external cell membrane.

Our current efforts improve on these methods. We saw compelling evidence of intracellular bacteria in patient-isolated urothelial cells using fluorescence confocal microscopy. Furthermore, these data strongly suggested *E. faecalis* was the invasive pathogen whereas *E. coli* appeared to be associated with the surface membrane. Although UPEC at the centre of IBCs can exhibit a coccoid morphology, these biofilm-like pods in experimental mouse models are very tightly packed and UPEC residing at the circumference of this pod, along with extracellular adherent bacteria, maintain a more rod-shaped (or filamentous) morphology [5,23,25]. In contrast, in this study, the colonies observed were far more loosely organised and both extracellular and intracellular bacteria were equally coccoid in morphology. We concluded therefore, with corresponding culture results and phenotypic bacterial typing, that the invasive pathogen was indeed *E. faecalis*. Nevertheless, in future work, species-specific labelling using molecular methods such as PNA-FISH could be employed for definitive identification [54]. It will also be important to survey more patients to see how widespread this phenomenon is.

When isolates of *E. coli* or *E. faecalis* were used to infect a human bladder cell line, which could be fixed post-infection and examined via confocal microscopy, we detected unequivocal intracellular colonization by five out of five isolates of *E. faecalis*. Surprisingly, although all five *E. coli* isolates demonstrated extensive extracellular adherence and biofilm formation, none were able to invade the cells. It is known that the bacterial virulence factor FimH is required for *E. coli* to invade bladder cells [55], so it is possible that our LUTS-derived isolates were deficient in some way for expression or sequence of this domain. However, this is unlikely, as we confirmed using a standard blood agglutination assay that our LUTS-derived *E. coli* expressed functional FimH (data not shown). Also, FimH is required for extracellular adhesion [56–58] and pathogenic biofilm formation [59], which all five strains were able to achieve in our tissue culture experiments. This suggests that *E. coli* isolated from these patients are indeed pathogenic but may lack the necessary downstream post-adhesion factors required for invasion. Further exploration of the FimH sequence in these strains and of other virulence factors could shed light on this interesting difference.

Taken together, these results suggest that, in contrast to the case of acute UTI, *Enterococci* may be a key invasive pathogen in LUTS. The mechanism by which *E. faecalis* invades urothelial cells is unknown. However, it is likely that, as with *E. coli* invasion, a necessary first step would be adhesion, in which case various previously described adhesion proteins are likely to be involved [60]. Afterwards, it is possible that, like *E. coli*, *E. faecalis* may take advantage of the unique fusiform vesicle trafficking system used by urothelial cells to rapidly change the tissue surface area, and become passively engulfed [5]. Alternatively, it is known that *E. faecalis* are able to invade intestinal epithelial cells via the production of aggregation substance (AS) and therefore it is possible that a similar mechanism is involved in urothelial invasion [61]. Additional studies with more isolates will be needed to see how

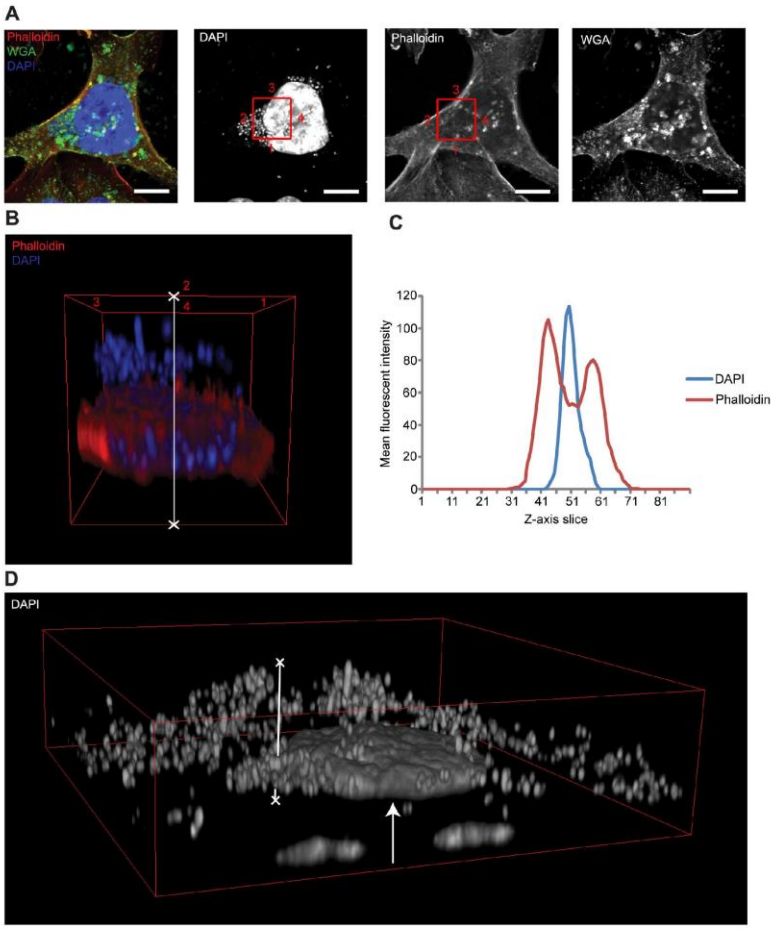

Figure 5. 3D confocal analysis of cultured cells infected with LUTS-isolated *E. faecalis*. (A) Confocal image of a group of T24 cells infected for 2.5hrs with *E. faecalis* isolated from LUTS patients at an MOI of approximately 10-15 bacteria per mammalian cell. The left image is a composite showing the phalloidin stained F-actin in red, wheat germ agglutinin (WGA)-stained plasma membrane in green and DAPI stained host and bacterial DNA in blue. The left centre, right centre and far right images show the respective DAPI, phalloidin and WGA channels in monochrome. White scale bar is 10μm. (B) A 3-dimensional volume through entire Z-stack at a position corresponding to the red squares in image A (numbered for orientation). This construct shows clear and extensive invasion and colonisation of the T24 cell by *E. faecalis*. (C) A Z-axis profile plot was produced as in Figures 3 and 4. The peak mean pixel intensity of the DAPI channel corresponds with a striking reduction of the phalloidin channel at slice 51-(centre of the cell), confirming intracellular infection. (D) 3D construct of the entire cell as in Figure 5. This image shows the tightly packed intracellular biofilm like cluster of *E. faecalis* in close proximity to the T24 nucleus (white arrow).

doi: 10.1371/journal.pone.0083637.g005

widespread *E. faecalis* is in LUTS patients, the invasive mechanisms involved and whether other species can also invade. Meanwhile, these data constitute, to our knowledge, the first report of definitive intracellular invasion of urothelial cells by *E. faecalis*.

One of the problems of pinpointing an infective aetiology for LUTS lies in the poor sensitivity of routine urine testing, whose weakness has been amply demonstrated [14–16]. Infection associated with lower counts of bacteria, which may nevertheless be significant in the case of LUTS patients [19], tend not to be detected by urinary dipstick for nitrite or leukocyte esterase, nor by routine MSU cultures with high thresholds for what is considered "positive" (e.g. in the UK and many other countries, this breakpoint is $\geq 10^5$ cfu ml^{-1}). Therefore, there is much interest in markers that might help diagnose such lower-grade urinary infections. Pyuria is one such validated marker. In addition, during acute UPEC-mediated UTI, inflammatory responses are known to cause urothelial cell shedding in both mice and humans [24,28–31]. This jettisoning is thought to be a defense mechanism to reduce bacterial burden in the urothelium. While some have dismissed urothelial cells in urine as contamination from the urogenital area during sample collection, our data show that the vast majority of these cells stain positive for uroplakin-3 and can therefore be considered to originate from the urothelium. In our study, epithelial shedding showed a strong relationship with pyuria: the higher the white blood cell count in the urine, the more epithelial cells were shed. Interestingly, even low pyuria counts (1 to 9 WBC μl^{-1}) were associated with shedding, supporting the hypothesis that examining such cells in fresh urine, along with pyuria, might help diagnose infection undetected by dipstick or routine MSU culture.

In mouse models, urothelial shedding has been proposed to facilitate the deeper invasion of the bladder by allowing access of bacteria to exposed transitional layers. Quiescent intracellular reservoirs (QIR) can result, leading to a chronic and/or recurrent infection situation [5,22,26,31,32]. Data from human recurrent UTI demonstrate that 68% of bacteriological recurrence is caused by identical bacterial strains to that of the index infection [33]. Although it could be argued that these relapses are caused by reintroduction of pathogen from faecal flora [3], same-strain infections can occur up to 3 years later [35] and the application of daily topical antibiotics to the perineum does not prevent recurrent episodes [34]. Although QIR have not been directly seen in human patients, these data are at least suggestive that QIR might play a role in intransigent LUTS. Further studies are needed to confirm this hypothesis.

In summary, our data suggest that some LUTS may be generated by low-grade intracellular infection of the bladder by *E. faecalis*. These results therefore may have far-reaching implications for our diagnosis, treatment and understanding of the aetiology of LUTS

Materials and Methods

Ethics statement

Ethical committee approval for human urine sampling was obtained from East Central London REC1 (Research Ethical Committee). All study participants gave written consent to participate in the study and the process was documented as per Good Clinical Practice (GCP) and MHRA guidelines. The participants were assigned randomly generated study numbers which were used to anonymise all data and samples. Analysis was carried out by blinded researchers.

Patient sampling

Sampling was conducted at Professor James Malone-Lee's LUTS outpatient clinic, University College London, Division of Medicine. We sampled from 705 adults aged ≥18 years who were able to give consent and who were diagnosed with LUTS (see Figure **S1** for a summary of the cohort's demographics and symptoms), excluding any patient with symptoms of acute UTI, with concurrent illnesses that in our opinion were likely to compromise the validity of the data, and pregnant women or those planning to conceive. When controls were required, we recruited with consent from staff that did not have any LUTS. All laboratory experiments used randomly selected sub-sets of the main patient cohort. Details can be found in the respective results sections.

In all cases, subjects were provided with a sterile container and two hypoallergenic wipes. They were then given detailed (written and oral) instructions on meticulous MSU capture technique, namely (1) to wash their hands and thoroughly cleanse genital area with a hypoallergenic wipe to prevent contamination from the surrounding external genitalia; (2) to part labia or retract foreskin and urinate a small amount into the toilet before moving the container into the urine stream; and (3) to remove the container before urination was complete, thereafter to seal the container. The urine sample was divided into two aliquots. The first was submitted to immediate microscopy using a haemocytometer to enumerate leukocytes (WBC μl^{-1}) and shed epithelial cells (EPC μl^{-1}). The second aliquot, as per standard clinical guidelines, was sent for routine MSU culture at the Whittington Hospital NHS Trust, London, UK. The sampled urine was treated fresh, or after overnight storage at 4°C at the hospital laboratory. 1µl of urine was transferred by calibrated loop to chromogenic media, CPS3 (bioMerieux). The plate was incubated aerobically for 24 hrs at 37°C. Bacterial colonies were identified at the genus level by colour change. The result was reported as positive if greater than 10^5 (MSU) colony forming units (cfu) ml^{-1} of a single known urinary pathogen were observed.

Bacterial identification at the species level

To corroborate confocal data and identify bacteria prior to the invasion assays, the routine urine procedure above was repeated in-house with the addition of a dilution series and extensive phenotypic analyses to confirm bacterial identity at the species level.

For each sample, 50µl of undiluted urine and three serial dilutions (1:10, 1:100 and 1:1000) were added to the respective quartile of a chromogenic CPS3 agar plate (bioMérieux) before aerobic incubation for 24 hours at 37°C. Following incubation, the different coloured colonies present on the chromogenic agar were identified using the manufacturer's colour criteria. The colonies found in this study were identified as follows: *E. coli*; medium sized burgundy, pink or mauve colonies and *Enterococcus spp.*; small turquoise colonies.

To further confirm the identity as *E. coli*, the isolates were shown to be bacillus in morphology and negative under Gram staining, indole positive and identified as *E. coli* using API 20E (bioMérieux) biochemical test strips. Each of the *Enterococcus spp.* tested in this study were found to be *E. faecalis* owing to a coccoid morphology, positive Gram stain, negative catalase test, positive bile esculin test and by being identified as *E. faecalis* using API 20 Strep (bioMérieux) biochemical test strips.

Cell culture

A transformed cell line derived from a human bladder carcinoma (T24) [62] was kindly donated by Dr. Aled Clayton, Institute of Cancer and Genetics, School of Medicine, Cardiff University, United Kingdom. T24 cells were cultured at 37°C in a humidified incubator under 5% CO_2 in 9 cm dishes in RPMI 1640 medium (Gibco) supplemented with 10% fetal bovine serum (FBS, PAA) and antibiotics (50 µg/ml penicillin and 50 mg/ml streptomycin; Gibco). Cells were maintained, pre-experimentation, by splitting 1:20 at 80% confluency. All work was carried out within sterile class-II flow cabinets under strict aseptic conditions.

Immunofluorescence staining of patient samples

80µl of a urine specimen was added to a Shandon single funnel cuvette assembly containing a pre-labeled glass slide and a Shandon filter card (Fisher Scientific). This assembly was centrifuged in a Shandon Cytospin 2 cytocentrifuge at 800rpm (≈75g rcf) for 5 minutes resulting in a visible disc of urinary particulate deposited on the slide, which was circumscribed with a hydrophobic barrier pen (ImmEdge pen, Vector Laboratories). The cells were fixed in 4% formaldehyde (Thermo Scientific, Fisher Scientific) in phosphate buffered saline (PBS, Sigma-Aldrich) at RT for 15 minutes. The formaldehyde was aspirated and the preparation washed three times with PBS at 5 minute intervals. For uroplakin-III staining, cells were permeabilised with 0.2% Triton-X100 (Sigma-Aldrich) in PBS for 5 minutes at RT followed by a single wash with PBS. The preparation was then blocked with 5% normal goat serum (Sigma-Aldrich) in PBS for 30 minutes prior to a 1 hour incubation with a 1:10 dilution of primary anti-uroplakin-III mouse monoclonal antibody (Progen Bioteknik) in 1% bovine serum albumin (BSA, Sigma-Aldrich). Following 3 further PBS washes, cells were incubated at RT for 40 minutes in a solution containing a 1:250 dilution of goat anti-mouse secondary antibody conjugated to Alexa Fluor-555 (Invitrogen), 1µg/µl of the DNA counterstain 4'',6-diamidino-2-phenylindole, (DAPI, Sigma-Aldrich) and 1% BSA in PBS.

For assessing bacterial infection, after fixation as above, wheat germ agglutinin (WGA) conjugated to Alexa Fluor-488 (Invitrogen) was used to label the cell membrane to aid cellular identification and demarcation, and to assess biofilm formation where applicable. Following 15 minutes of incubation at RT with 1µg/ml WGA in Hank's balanced salt solution minus phenol red (HBSS, Invitrogen), the labeling solution was removed and the cells washed twice at 5 minute intervals with HBSS. Fluorescent counterstaining of host and pathogen DNA was achieved through the addition of DAPI at 1µg/ml in PBS. After incubation for 15 minutes at RT, the DAPI solution was removed and the sediment washed twice in PBS. Following staining for uroplakin-III or infection, the preparations were immediately mounted with FluorSave reagent (Calbiochem) and a coverslip fixed in place with clear nail varnish. The percentage of UP3-positive cells was calculated by a blinded researcher using epi-fluorescent microscopy. Counts were carried out in triplicate. Images were also taken using scanning confocal microscopy on a Leica SP5.

Invasion assay

5 frozen *Enterococcus faecalis* and 5 frozen *Escherichia coli* strains previously isolated and typed from human LUTS patients were grown on fresh chromogenic CPS3 agar plates. After aerobic incubation for 24 hours at 37°C, a colony from each of these 2 bacterial cultures was transferred to a 5ml sterile aliquot of LB, and incubated aerobically at 37°C for 24 hours. Two of the 5 *E. coli* isolates underwent stationary incubation and the remaining 3 shaking incubation at 300rpm to control for FimH expression in these strains, as stationary growth has been reported to promote expression of this virulence factor [55]. In our hands, the two different methods of culture produced similar functional FimH behaviour. *E. faecalis* isolates were all incubated in a shaking incubator at 300rpm. The level of growth was checked for each bacteria using a spectrophotometer and diluted as necessary with fresh LB to an A600 of approximately 0.5 [63]. Lab-Tek II 8 well chamber slides (Nunc, Thermo Scientific) were coated with 200µl of FBS and incubated for 2 hours at 37°C before aspiration. T24 cells were plated at $8x10^4$ cells per well in a total volume of 400 µL and incubated for 24 hours at 37°C under 5% CO_2 to allow cells to spread, then washed twice with PBS to remove routine antibiotics. Each of the bacterial LB cultures was diluted in CO_2-independent media (CIM, Gibco) supplemented with 10% FBS (with routine antibiotics omitted) and 200µl added to the cultured T24 cells giving a multiplicity of infection (MOI) of approximately 10-15 bacteria per mammalian cell [63]. Cells were infected at 37°C for between 1 and 4 hours within a humidified aerobic incubator to optimise experimental parameters.

Post infection, cells were inspected for morphological changes and viability before the addition of a combination of membrane-impermeable antibiotics to kill extracellular bacteria and to limit further cellular damage [19,38,39,63]. Briefly, infected CIM was carefully removed and a solution of gentamicin, linezolid and amoxycillin (Whittington Health NHS Trust Pharmacy, London) in 200µl fresh CIM was added at varying concentrations. Concentrations of gentamicin (200µg/

ml), linezolid (25µg/ml) and amoxycillin (250µg/ml) were found to be most effective (adapted from [19]). The chamber slide was incubated, with antibiotics, aerobically for a further 24 hours at 37°C, after which the cells were fixed in 4% formaldehyde in PBS for 15 min at room temperature before washing three times in PBS at 5 minute intervals. The cell membranes were stained with 200µl WGA (1µg/ml) conjugated to Alexa Fluor-488 in HBSS minus phenol red for 15 min at RT. The labelling solution was removed and the cells washed twice at 5 minute intervals with HBSS. 0.2% Triton-X100 in PBS was then added and the cells allowed to incubate at room temperature for 5 min. Following removal of the Triton-X100, the permeabilised cells were washed once with PBS before staining with a 200µl solution of TRITC-conjugated phalloidin (0.6µg/ml)(Sigma-Aldrich), to label filamentous actin, and DAPI (1µg/ml) in PBS for 40 min at RT. The dual-labelling solution was gently aspirated and the cells washed 3 times in PBS before removal of the upper-well section of the Lab-Tek II chamber slide and immediate mounting as above.

Imaging and analysis

We performed epi-fluorescent microscopy on a Olympus CX-41 and Leica DM4000B upright microscope, and confocal laser scanning microscopy on a Leica SP5 microscope. Images were processed and analysed using Infinity Capture and Analyze V6.2.0, ImageJ 1.46r and the Leica Application Suite, Advanced Fluorescence 3.1.0 build 8587 Software.

References

1. Foxman B (2000) Urinary tract infection: self-reported incidence and associated costs. Ann Epidemiol 10: 509–515. doi:10.1016/S1047-2797(00)00072-7. PubMed: 11118930.
2. Foxman B (2002) Epidemiology of urinary tract infections: incidence, morbidity, and economic costs. Am J Med 113(Suppl 1A): 5S. doi: 10.1016/S0002-9343(02)01054-9. PubMed: 1211386612601337.
3. Hooton TM (2001) Recurrent urinary tract infection in women. Int J Antimicrob Agents 17: 259-268. doi:10.1016/S0924-8579(00)00350-2. PubMed: 11295405.
4. Pouwels KB, Visser ST, Hak E (2013) Effect of pravastatin and fosinopril on recurrent urinary tract infections. J Antimicrob Chemother 68: 708-714. doi:10.1093/jac/dks419. PubMed: 23111852.
5. Hunstad DA (2010) Intracellular lifestyles and immune evasion strategies of uropathogenic Escherichia coli. Annu Rev Microbiol 64: 203–221. doi:10.1146/annurev.micro.112408.134258. PubMed: 20825346.
6. Colgan R (2011) Diagnosis and treatment of acute uncomplicated cystitis. Am Fam Physician 84: 771–776. PubMed: 22010614.
7. Abrams P (2003) The standardisation of terminology in lower urinary tract function: report from the standardisation sub-committee of the International Continence Society. Urology 61: 37–49. doi:10.1016/S0090-4295(02)02243-4. PubMed: 12559262.
8. National Institute for Health and Clinical Excellence (2006) Urinary incontinence: the management of urinary incontinence in women. Available: http://www.nice.org.uk/nicemedia/live/10996/30281/30281.pdf. Accessed 10 June 2013
9. Gormley EA, Lightner DJ, Burgio KL, Chai TC, Clemens JQ, et al. (2012) Diagnosis and treatment of overactive bladder (non-neurogenic) in adults: AUA/SUFU guideline. J Urol 188: 2455-2463. Available online at: S0022-5347(12)04959-2 [pii] doi:10.1016/j.juro.2012.09.079.
10. Lutters M, Vogt-Ferrier NB (2008) Antibiotic duration for treating uncomplicated, symptomatic lower urinary tract infections in elderly women. Cochrane Database of Systematic Reviews. doi: 10.1002/14651858.CD001535.pub2. PubMed: 1864607412137628.
11. Coyne KS, Sexton CC, Thompson CL, Milsom I, Irwin D et al. (2009) The prevalence of lower urinary tract symptoms (LUTS) in the USA, the UK and Sweden: results from the Epidemiology of LUTS (EpiLUTS) study. BJU Int 104: 352-360. doi:10.1111/j.1464-410X.2009.08427.x. PubMed: 19281467.
12. Irwin DE, Milsom I, Hunskaar S, Reilly K, Kopp Z et al. (2006) Population-Based Survey of Urinary Incontinence, Overactive Bladder, and Other Lower Urinary Tract Symptoms in Five Countries : Results of the EPIC Study. European Urology: 1306-1315.
13. Perry S, Shaw C, Assassa P, Dallosso H, Williams K et al. (2000) An epidemiological study to establish the prevalence of urinary symptoms and felt need in the community: the Leicestershire MRC incontinence study. Journal of Public Health 22: 427-434. doi:10.1093/pubmed/22.3.427.
14. Stamm WE (1982) Diagnosis of coliform infection in acutely dysuric women. N Engl J Med 307: 463-468. doi:10.1056/NEJM198208193070802. PubMed: 7099208.
15. Khasriya R, Khan S, Lunawat R, Bishara S, Bignall J et al. (2010) The Inadequacy of Urinary Dipstick and Microscopy as Surrogate Markers of Urinary Tract Infection in Urological Outpatients With Lower Urinary Tract Symptoms Without Acute Frequency and Dysuria. J Urol 183: 1843-1847. doi:10.1016/j.juro.2010.01.008. PubMed: 20303096.
16. Kupelian AS, Horsley H, Khasriya R, Amussah RT, Badiani R et al. (2013) Discrediting microscopic pyuria and leucocyte esterase as diagnostic surrogates for infection in patients with lower urinary tract symptoms: results from a clinical and laboratory evaluation. BJU Int 112: 231-238. doi:10.1111/j.1464-410X.2012.11694.x. PubMed: 23305196.
17. Chapple CR, Wein AJ, Abrams P, Dmochowski RR, Giuliano F et al. (2008) Lower Urinary Tract Symptoms Revisited: A Broader Clinical Perspective. European Urology 54: 563-569. doi:10.1016/j.eururo.2008.03.109.
18. Nakipoglu GF, Kaya AZ, Orhan G, Tezen O, Tunc H et al. (2009) Urinary dysfunction in multiple sclerosis. J Clin Neurosci 16: 1321-1324. doi:10.1016/j.jocn.2008.12.012. PubMed: 19560927.
19. Khasriya R, Sathiananthamoorthy S, Ismail S, Kelsey M, Wilson M, et al. (2013) The spectrum of bacterial colonisation associated with urothelial cells from patients with chronic lower urinary tract symptoms. J Clin Microbiol. doi:10.1128/JCM.03314-12.

Supporting Information

Figure S1. Demographics and symptoms. (A) Key demographic information. (B) A four-way Venn diagram illustrating the overlap of symptoms amongst the 705 patients studied. The ellipses circumscribe patients who had one or more symptoms in the particular subset. Each ellipse corresponds to a numbered list of specific symptoms. The diagram is not scaled to the size of sets. Abbreviations; MSU (mid-stream urine culture); Pyuria (presence of white blood cells in the urine); WBC (white blood cell); inc (incontinence); LUTS (lower urinary tract symptoms); OAB (overactive bladder).
(TIF)

Acknowledgements

We thank all the colleagues in our group and Dr. Liam Good for helpful discussion and clinical input. We would also like to thank Dr. Aled Clayton for kindly donating the T24 cell line.

Author Contributions

Conceived and designed the experiments: HH JML JLR. Performed the experiments: HH JML JLR DH MT AK AH. Analyzed the data: HH JML JLR AH MK. Contributed reagents/materials/analysis tools: HH JML JLR AH MK. Wrote the manuscript: HH JML JLR AK.

20. Foxman B (2003) Epidemiology of urinary tract infections: Incidence, morbidity, and economic costs. Disease-a-Month 49: 53-70. doi: 10.1067/mda.2003.7. PubMed: 12601337.
21. Anderson GG, Martin SM, Hultgren SJ (2004) Host subversion by formation of intracellular bacterial communities in the urinary tract. Microbes Infect 6: 1094-1101. PubMed: 15380779.
22. Anderson GG (2004) Intracellular bacterial communities of uropathogenic Escherichia coli in urinary tract pathogenesis. Trends Microbiol 12: 424-430. doi:10.1016/j.tim.2004.07.005. PubMed: 15337164.
23. Anderson GG, Palermo JJ, Schilling JD, Roth R, Heuser J et al. (2003) Intracellular Bacterial Biofilm-Like Pods in Urinary Tract Infections. Science 301: 105-107. doi:10.1126/science.1084550. PubMed: 12843396.
24. Rosen DA, Hooton TM, Stamm WE, Humphrey PA, Hultgren SJ (2007) Detection of Intracellular Bacterial Communities in Human Urinary Tract. Infection - PLOS Med 4: e329. doi:10.1371/journal.pmed.0040329.
25. Justice SS (2004) Differentiation and developmental pathways of uropathogenic Escherichia coli in urinary tract pathogenesis. Proc Natl Acad Sci U S A 101: 1333-1338. doi:10.1073/pnas.0308125100. PubMed: 14739341.
26. Blango MG, Mulvey MA (2010) Persistence of Uropathogenic Escherichia coli in the Face of Multiple Antibiotics. Antimicrobial Agents and Chemotherapy 54: 1855-1863. doi:10.1128/AAC.00014-10.
27. Garofalo CK, Hooton TM, Martin SM, Stamm WE, Palermo JJ et al. (2007) Escherichia coli from Urine of Female Patients with Urinary Tract Infections Is Competent for Intracellular Bacterial Community Formation. Infect Immun 75: 52-60. doi:10.1128/IAI.01123-06. PubMed: 17074856.
28. Dalal E (1994) Moderate stress protects female mice against bacterial-infection of the bladder by eliciting uroepithelial shedding. Infect Immun 62: 5505-5510. PubMed: 7960132.
29. Smith YC (2008) Hemolysin of uropathogenic Escherichia coli evokes extensive shedding of the uroepithelium and hemorrhage in bladder tissue within the first 24 hours after intraurethral inoculation of mice. Infect Immun 76: 2978-2990. doi:10.1128/IAI.00075-08. PubMed: 18443089.
30. Thumbikat P (2009) Bacteria-Induced Uroplakin Signaling Mediates Bladder Response to Infection. PLoS Pathog 5: e1000415. PubMed: 19412341.
31. Hannan TJ, Mysorekar IU, Hung CS, Isaacson-Schmid ML, Hultgren SJ (2010) Early severe inflammatory responses to uropathogenic *E. coli* predispose to chronic and recurrent urinary tract infection. PLoS Pathog 6: e1001042. doi:10.1371/journal.ppat.1001042. PubMed: 20811584.
32. Mysorekar IU, Hultgren SJ (2006) Mechanisms of uropathogenic Escherichia coli persistence and eradication from the urinary tract. Proc Natl Acad Sci U S A 103: 14170-14175. doi:10.1073/pnas.0602136103. PubMed: 16968784.
33. Russo TA (1995) Chromosomal restriction fragment length polymorphism analysis of Escherichia coli strains causing recurrent urinary tract infections in young women. J Infect Dis 172: 440-445. doi: 10.1093/infdis/172.2.440. PubMed: 7622887.
34. Cass AS (1985) Antibacterial perineal washing for prevention of recurrent urinary tract infections. Urology 25: 492-494. doi: 10.1016/0090-4295(85)90458-3. PubMed: 3992773.
35. Brauner A (1992) Urinary *Escherichia coli* causing recurrent infections--a prospective follow-up of biochemical phenotypes. Clin Nephrol 38: 318-323. PubMed: 1468162.
36. Szabados F (2008) *Staphylococcus saprophyticus* ATCC 15305 is internalized into human urinary bladder carcinoma cell line 5637. FEMS Microbiol Lett 285: 163–169. doi:10.1111/j.1574-6968.2008.01218.x. PubMed: 18573154.
37. Rosen DA (2008) Utilization of an intracellular bacterial community pathway in *Klebsiella pneumoniae* urinary tract infection and the effects of fimK on type 1 pilus expression. Infect Immun 76: 3337-3345. doi: 10.1128/IAI.00090-08. PubMed: 18411285.
38. Mandell GL (1973) Interaction of intraleukocytic bacteria and antibiotics. J Clin Invest 52: 1673-1679. doi:10.1172/JCI107348. PubMed: 4718959.
39. Edwards AM, Massey RC (2011) Invasion of Human Cells by a Bacterial Pathogen. J Vis Exp: e2693. PubMed: 21445052.
40. Mohamed JA, Huang DB (2007) Biofilm formation by *Enterococci*. J Med Microbiol 56: 1581-1588. doi:10.1099/jmm.0.47331-0. PubMed: 18033823.
41. Chai WL, Hamimah H, Cheng SC, Sallam AA, Abdullah M (2007) Susceptibility of *Enterococcus faecalis* biofilm to antibiotics and calcium hydroxide. J Oral Sci 49: 161-166.
42. Guiton PS, Hannan TJ, Ford B, Caparon MG, Hultgren SJ (2013) *Enterococcus faecalis* overcomes foreign body-mediated inflammation to establish urinary tract infections. Infect Immun 81: 329-339. doi: 10.1128/IAI.00856-12. PubMed: 23132492.
43. Poulsen L, Bisgaard M, Son N, Trung N, An H et al. (2012) *Enterococcus* and *Streptococcus* spp. associated with chronic and self-medicated urinary tract infections in Vietnam. BMC Infectious Diseases 12: 320. doi:10.1186/1471-2334-12-320.
44. Felmingham D, Wilson AP, Quintana AI, Grüneberg RN (1992) Enterococcus species in urinary tract infection. Clin Infect Dis 15: 295-301. doi:10.1093/clinids/15.2.295. PubMed: 1387807.
45. Hanin A, Sava I, Bao Y, Huebner J, Hartke A et al. (2010) Screening of *In Vivo* activated genes in *Enterococcus faecalis* during insect and mouse infections and growth in urine. PLOS ONE 5: e11879. doi: 10.1371/journal.pone.0011879. PubMed: 20686694.
46. Nichol KA, Sill M, Laing NM, Johnson JL, Hoban DJ et al. (2006) Molecular epidemiology of urinary tract isolates of vancomycin-resistant *Enterococcus faecium* from North America. Int J Antimicrob Agents 27: 392-396. doi:10.1016/j.ijantimicag.2005.12.006. PubMed: 16621463.
47. Swaminathan S, Alangaden GJ (2010) Treatment of resistant *Enterococcal* urinary tract infections. Curr Infect Dis Rep 12: 455-464. doi:10.1007/s11908-010-0138-8. PubMed: 21308555.
48. Dukes C (1928) Some Observations on Pyuria. Proc R Soc Med 21: 1179-1183. PubMed: 19986501.
49. Gill K, Kupelian AS, Swarmy S, Malone-Lee J (2011) The Problem of Pyuria 1-9 wbc ul-1; Are We Missing Significant Disease. Int Urogynecol J 22: 1769-2008. doi:10.1007/s00192-011-1521-1.
50. Wu XR, Lin JH, Walz T, Häner M, Yu J et al. (1994) Mammalian uroplakins. A group of highly conserved urothelial differentiation-related membrane proteins. J Biol Chem 269: 13716-13724. PubMed: 8175808.
51. Wu XR, Manabe M, Yu J, Sun TT (1990) Large scale purification and immunolocalization of bovine uroplakins I, II, and III. Molecular markers of urothelial differentiation. J Biol Chem 265: 19170-19179.
52. Sizemore RK, Caldwell JJ, Kendrick AS (1990) Alternate gram staining technique using a fluorescent lectin. Appl Environ Microbiol 56: 2245-2247. PubMed: 1697149.
53. Romero R, Schaudinn C, Kusanovic JP, Gorur A, Gotsch F et al. (2008) Detection of a microbial biofilm in intraamniotic infection. Am J Obstet Gynecol 198: 135. PubMed: 18166328.
54. Stender H (2003) PNA FISH: an intelligent stain for rapid diagnosis of infectious diseases. Expert Rev Mol Diagn 3: 649-655. doi: 10.1586/14737159.3.5.649. PubMed: 14510184.
55. Rosen DA, Pinkner JS, Walker JN, Elam JS, Jones JM et al. (2008) Molecular variations in *Klebsiella pneumoniae* and *Escherichia coli* FimH affect function and pathogenesis in the urinary tract. Infect Immun 76: 3346-3356. doi:10.1128/IAI.00340-08. PubMed: 18474655.
56. Snyder JA, Lloyd AL, Lockatell CV, Johnson DE, Mobley HLT (2006) Role of phase variation of type 1 fimbriae in a uropathogenic *Escherichia coli* cystitis isolate during urinary tract infection. Infect Immun 74: 1387-1393. doi:10.1128/IAI.74.2.1387-1393.2006. PubMed: 16428790.
57. Wright KJ (2006) Sticky fibers and uropathogenesis: bacterial adhesins in the urinary tract. Future Microbiol 1: 75-87. doi: 10.2217/17460913.1.1.75. PubMed: 17661687.
58. Wright KJ (2007) Development of intracellular bacterial communities of uropathogenic Escherichia coli depends on type 1 pili. Cell Microbiol 9: 2230-2241. doi:10.1111/j.1462-5822.2007.00952.x. PubMed: 17490405.
59. Schembri MA, Klemm P (2001) Biofilm formation in a hydrodynamic environment by novel FimH variants and ramifications for virulence. Infect Immun 69: 1322-1328. doi:10.1128/IAI.69.3.1322-1328.2001. PubMed: 11179294.
60. Sava IG, Heikens E, Huebner J (2010) Pathogenesis and immunity in *enterococcal* infections. Clin Microbiol Infect 16: 533-540. doi:10.1111/j.1469-0691.2010.03213.x. PubMed: 20569264.
61. Sartingen S, Rozdzinski E, Muscholl-Silberhorn A, Marre R (2000) Aggregation substance increases adherence and internalization, but not translocation, of *Enterococcus faecalis* through different intestinal epithelial cells in vitro. Infect Immun 68: 6044-6047. doi:10.1128/IAI.68.10.6044-6047.2000. PubMed: 10992519.
62. Bubeník J, Baresová M, Viklický V, Jakoubková J, Sainerová H et al. (1973) Established cell line of urinary bladder carcinoma (T24) containing tumour-specific antigen. Int J Cancer 11: 765-773. doi: 10.1002/ijc.2910110327. PubMed: 4133950.
63. Eto DS (2006) Actin-gated intracellular growth and resurgence of uropathogenic *Escherichia coli*. Cell Microbiol 8: 704–717. doi: 10.1111/j.1462-5822.2006.00691.x. PubMed: 16548895.

Appendix 2

SCIENTIFIC REPORTS

OPEN

A urine-dependent human urothelial organoid offers a potential alternative to rodent models of infection

Received: 14 July 2017
Accepted: 4 January 2018
Published online: 19 January 2018

Harry Horsley, Dhanuson Dharmasena, James Malone-Lee & Jennifer L. Rohn

Murine models describe a defined host/pathogen interaction for urinary tract infection, but human cell studies are scant. Although recent human urothelial organoid models are promising, none demonstrate long-term tolerance to urine, the natural substrate of the tissue and of the uropathogens that live there. We developed a novel human organoid from progenitor cells which demonstrates key structural hallmarks and biomarkers of the urothelium. After three weeks of transwell culture with 100% urine at the apical interface, the organoid stratified into multiple layers. The apical surface differentiated into enlarged and flattened umbrella-like cells bearing characteristic tight junctions, structures resembling asymmetric unit membrane plaques, and a glycosaminoglycan layer. The apical cells also expressed cytokeratin-20, a spatial feature of the mammalian urothelium. Urine itself was necessary for full development, and undifferentiated cells were urine-tolerant despite the lack of membrane plaques and a glycosaminoglycan layer. Infection with *Enterococcus faecalis* revealed the expected invasive outcome, including urothelial sloughing and the formation of intracellular colonies similar to those previously observed in patient cells. This new biomimetic model could help illuminate invasive behaviours of uropathogens, and serve as a reproducible test bed for disease formation, treatment and resolution in patients.

UTIs are amongst the most common infectious diseases worldwide, but despite being associated with substantial economic and human cost[1,2], they are grossly understudied relative to other human diseases. UTI pathogens are also of particular concern in the global antibiotic resistance crisis, so their burden will only increase in the future[3]. Recurrence of infection even after antibiotic treatment is a particularly troublesome aspect of UTI, usually involving the same strain implicated in the first infection[1,4]. For example, among healthy young women who suffer from their first UTI, the risk of recurrence within 6 months is 24%[2]; in another study, 2% of women studied had six or more episodes in a two-year period[5]. These findings suggest that current treatment regimens are not ideal.

UTI is also problematic in more vulnerable subgroups: the risk of UTI dramatically increases in people with multiple sclerosis (MS)[6,7], spinal injury[8], renal transplant patients[9] and anyone requiring urinary catheterization or other indwelling devices[10]. Finally, amongst our growing elderly population, UTIs are one of the most commonly diagnosed infections[11]. More frequent UTI in these cohorts is not merely bothersome; UTI is known to exacerbate MS[12], lead to confusion and falls in the elderly[13], and increase the risk of organ rejection in renal transplant patients[14]. Furthermore, catheter-associated UTI carries an increased risk of urosepsis[15], and bacteriuria in pregnant women is associated with preterm birth and other maternal morbidities[16].

To understand why urinary infections are often recalcitrant to treatment, the pathogens must be studied in their unique environment. The urinary bladder is lined by a specialised transitional urothelium comprising 3–7 layers of cells: basal cells (above the basement membrane), intermediate cells (above basal cells) and morphologically distinct, highly specialised, often binucleated umbrella cells at the apical surface, which face outward into the bladder lumen[17]. These enlarged, flattened urothelial umbrella cells (or 'facet cells') partition urine and are thought to act as a powerful barrier to protect underlying tissue from harmful waste compounds[18]. They elaborate

Chronic UTI Group, Centre for Nephrology, University College London, London, UK. Correspondence and requests for materials should be addressed to H.H. (email: h.horsley@ucl.ac.uk) or J.L.R. (email: j.rohn@ucl.ac.uk)

a highly durable apical asymmetric unit membrane (AUM) consisting of thousands of regularly arrayed particles approximately 16.5 nm across made up of four mannosylated transmembrane glycoproteins called uroplakins (UP)[18–20].

In addition to the uroplakin family, the urothelium also elaborates a mucopolysaccharide-rich layer of glycosaminoglycans (GAG) which is believed to protect the bladder from infection and urine-borne irritants[21], of which chondroitin sulphate, heparan sulphate, hyaluronic acid, dermatan sulphate and keratin sulphate are the most studied[22]. Chondroitin sulphate, in particular, is believed to play a key role in urothelial barrier function and exhibits luminal and basal expression in both human and porcine bladders[23]. In contrast, only heparan sulphate was detected in the luminal portion of calf bladders, elucidating possible differences between species[24].

A significant proportion of research on the urothelium has been conducted using mouse models[20,25]. These findings have been widely translated into human oncology to locate the primary origin of metastatic tumours[26] and to understand the biology of UTI[25]. While invaluable in many cases and necessary for regulatory approval of drugs, some animal models of human disease, the majority of which are murine, have received widespread criticism in recent years[27–31]. The limitations of murine models are particularly evident when modelling human infection and attempting to treat this induced pathology with novel antimicrobials[27]. In such studies, mice are frequently infected with far higher quantities of log-phase bacteria than would be evident in a slow-growing chronic human infection, and the pharmacokinetic profiles of a given drug are challenging to translate to humans[27,32].

In the case of urinary infection studies, it is known that the human and mouse bladder urothelium differ in a number of structural ways. The markers expressed are similar, but in contrast to the murine model, human bladder urothelial marker expression exhibits a relationship with the level of cellular differentiation[20,33]. For example, the healthy human bladder has been shown to express cytokeratin 20 at the luminal surface whereas cytokeratin 8 is expressed throughout the cells of the urothelium[17,34]. The incorrect spatial expression of cytokeratin 20 by terminally differentiated umbrella cells has been linked to painful bladder syndrome and neurogenic bladder and is thought to predispose people with MS to chronic UTI[6,17,34]. Studies also suggest that murine and human bladders can differ in their innate immune response to uropathogens (for example in their expression and use of Toll-like receptors[35]). Moreover, rodent bladders differ from those of humans functionally. While larger mammals (>3Kg) share a scalable urinary capacity and consistent voiding duration, rodents urinate almost constantly, bringing into question whether their bladders are a true storage organ[36]. The multiple disparities between the rodent and human bladders raise the possibility that relying so heavily on the former could be problematic for understanding UTI in the latter.

Given these species differences, there is a need for alternative human-based models to augment the impressive body of elegant *in vivo* mouse experiments into UTI biology. Human bladder cancer cell lines grow readily and are tractable, but they are genetically abnormal and, therefore, bear little resemblance to primary urothelial cells in terms of structure and function. In particular, although some retain the ability to form a stratified organoid, they do not form an organised and differentiated 3D architecture[37,38], which is crucial not least for understanding host/pathogen interaction, as uropathogens are proposed to invade the urothelium via binding to factors only present in terminally differentiated umbrella cells[25].

On the other hand, a number of promising 3D urothelial models have been described in the literature[21,39]. Briefly, existing bladder models are produced using one of three broad culture techniques: (1) organ culture of intact biopsies or explant culture; (2) culture of urothelial cells naturally shed into the urine or harvested from biopsies; and (3) organotypic culture whereby normal urothelial cells are stimulated to form 3D organoids on filter inserts[21]. Although arguably the most relevant model system, organ culture of intact human tissue is time consuming, yields a finite amount of experimental material and requires fresh human tissue[21,40]. More practical is the cultivation of human urothelial cells isolated from host urine or biopsies which, when grown using a specialist protocol, have been shown to maintain the ability to stratify, differentiate and develop a robust barrier function *in vitro*[21,39,41–44].

Although these models constitute impressive alternatives to animal models, to our knowledge, they last only a few hours up to a day in urine *in vitro*[21,45], the natural apical substrate of this tissue. Therefore, the effect of urine exposure on urothelial differentiation and GAG expression remains unclear. Moreover, none of the human-derived urothelial biomimetics have been reported to correctly express cytokeratin 20 at the apical surface[34]. To address these limitations, we worked to develop a urine-tolerant organotypic human urothelium that could be used as a platform studying for host/uropathogen interactions, treatment, and resolution in humans.

Results

HBLAK and HBEP can form three-dimensional urothelial organoids. HBEP cells were derived from normal human bladder biopsies by CellNTec and provided commercially in cryovials. We also grew HBLAK cells, which are spontaneously immortalised but not transformed version of HBEP available from the same company. These latter cells retain the ability to differentiate but have increased longevity without senescing. On thawing, both cell types were seeded on plastic in fully defined, serum-free, BPE containing CNT-Prime media, which favours the proliferative phenotype. Both HBEP and HBLAK shared a 'spindle-like' morphology, a hallmark of multipotent epithelial progenitors. When 70% confluent, the cells were transferred to Millicell transwells (Millipore) with CNT-Prime media in the apical and basal chambers and grown to confluency. At this point, the media was shifted to high-calcium, differentiation media (CNT-Prime-3D) in both chambers. After overnight incubation, we replaced filter-sterilized human urine in the apical chamber and left the cultures to develop for 14 (HBLAK) to 25 (HBEP) days depending on the experiment, with periodic media and urine changes. At endpoint, the organoid-coated filters were retrieved, fixed, and stained for various biomarkers and inspected microscopically.

3D confocal analyses showed that both cultures were viable despite the prolonged presence of urine. The HBEP tissue contained multiple layers (approximately 3) with tightly-packed spheroid basal cells, intermediate

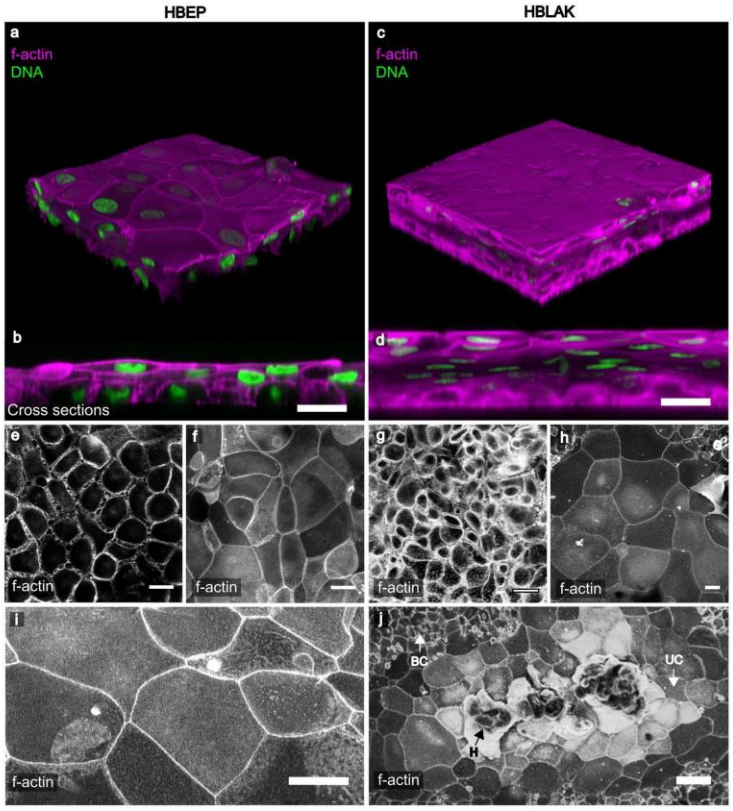

Figure 1. HBLAK cells retain the ability to differentiate into 3D urothelial organoids. Colour images are composites showing the phalloidin-stained F-actin in magenta and DAPI-stained DNA in green. Lower images show phalloidin-stained F-actin in monochrome. (**a**) 3D confocal model constructed from a 200 slice Z-stack of HBEP organoid. Umbrella-like cells are large and flat. (**b**) Orthogonal view of the Z-stack shows the tissue to be ~3 layers in depth and the basal cells to be spheroid in morphology. (**c**) 3D confocal model constructed from a ~300 slice Z-stack of HBLAK organoid. The HBLAK tissue is significantly better developed than the HBEP tissue in terms of thickness and number of cell layers. (**d**) Orthogonal reslice of the HBLAK tissue shows ~5–7 cell layers with flattened apical cells and more spheroid cells beneath. (**e**) Single optical slice at lowest region of the HBEP organoid showing small tightly packed basal cells. (**f**) Single optical slice at apical region of HBEP organoid showing well-differentiated, characteristically large umbrella-like cells. (**g**,**h**) Single optical slices of basal and umbrella-like cells respectively in HBLAK bladder bio-mimetic. Scale bars represent 20 µm. (**i**) A further single optical slice showing large umbrella-like cells at the surface of the HBEP organoid. Scale bar represents 20 µm. (**j**) Maximum projection confocal image of a region of HBLAK organoid formation. Large, flat umbrella-like cells (UC) lined the apical surface of the organoid surrounded by monolayers of small undifferentiated basal-like cells (BC). Areas of hyperplasia (**h**) were noted at the 'peak' of a small proportion of investigated regions of differentiation. Scale bar represents 40 µm.

cells and enlarged and flattened umbrella-like cells at the apical surface (Fig. 1a,b). The HBLAK tissue was morphologically similar, but in contrast, likely due to increased rate of growth, these produced approximately 5–7 cell layers with multiple layers of intermediate cells (Fig. 1c,d). Optical slices at the basal region of the HBEP and HBLAK organoids respectively showed the typically small, tightly-packed and spheroid morphology of urothelial basal cells (Fig. 1e,g). Basal cells in the HBLAK organoid (~ø10 µm) appeared to be slightly smaller than those in the HBEP culture (~ø20 µm) (Fig. 1e,g). Similarly, single optical slices at the apical regions of the HBEP

and HBLAK organoids showed the formation of a large, flat and often hexagonal cellular morphology typical of well-differentiated umbrella cells (Fig. 1f and i for HBEP, Fig. 1h and j for HBLAK). As shown in Fig. 1j, lower-magnification views of HBLAK show a more heterogeneous differentiation pattern, with cells elaborating distinct multi-layered zones of organoid formation with large umbrella-like cells at their surface, flanked by regions of very much smaller undifferentiated basal cell-like monolayers and occasional areas of hypertrophy.

In summary, both models formed large zones of three-dimensional epithelia in a manner reminiscent of a urothelium, with umbrella-like cells at their apical surface. Moreover, both models were exposed to sterile human urine for several weeks (14–25 days) without exhibiting any signs of toxicity.

HBLAK and HBEP organoids exhibit key biomarkers of the human urothelium. We characterised the HBEP and HBLAK human urothelial organoids further by targeting urinary tract-specific antigen expression using indirect IF in conjunction with high-resolution laser scanning confocal microscopy. The resulting organoids had the correct spatial expression of several key biomarkers. Studies exploring cytokeratin (CK) expression in normal human bladders have shown a relationship between the level of cytodifferentiation and sub-type CK expression[17]. Both HBEP- and HBLAK organoids exhibited correct spatial expression of CK8 and CK20; specifically, CK8 was expressed throughout the strata of the *in vitro* tissues whereas CK20 was expressed preferentially by the umbrella-like cells at the apical surface (Fig. 2a,b,c,d). In contrast to the rodent bladder, muscarinic receptors are expressed throughout the human urothelium[46,47]. This finding was echoed in our model with evidence of muscarinic receptors M2 and M3 expressed in all cell layers of both organoids (Fig. 2e and g). Uroplakin-III (UP3), an indispensible part of the asymmetric unit membrane[48], was present in the apical cells of the HBEP (Fig. 2f,i) model, although the orthogonal view (bottom, Fig. 2f) shows that this protein was not heavily enriched on the surface. In contrast, in the HBLAK (Fig. 2h) organoids, UP3 was strongly surface-expressed (see orthogonal view, bottom Fig. 2j). In both models, from the apical view, the UP3 staining appeared in a speckled pattern similar to that seen in urothelial cells shed in the urine of a chronic UTI patient (Fig. 2j,l). Multinucleation of the umbrella-like cells was a relatively rare occurrence (e.g. examples can be seen in Fig. 2gi and k).

HBLAK organoids possess correct topographical and ultrastructural features. Given these promising results, we went forward with the HBLAK model, as it was more tractable, thicker, and presented better surface-staining of UP3. We used scanning electron microscopy (SEM) and transmission electron microscopy (TEM) to analyse its ultrastructure, organisation and overall topography. Low-power SEM echoed what was seen in Fig. 1j, namely that the HBLAK cells elaborated distinct multi-layered zones of organoid formation with umbrella-like cells at their surface (approximately two-thirds of the tissue, 64.8% +/− 10.4) along with zones of undifferentiated basal cell-like monolayers (Fig. 3a) and areas of disorganised hyperplasia (Fig. 3b). The surface of each differentiated zone exhibited very large (up to ~80 µm), often hexagonal umbrella-like cells (Fig. 3c,d,e). A comparison with the undifferentiated basal cells (Fig. 3e vs. f) showed that the umbrella-like cells were up to approximately 50 times larger in terms of surface area than their undifferentiated counterparts. SEM micrographs also showed evidence of potential tight junction formation (Fig. 3c)[49] and structures resembling, in size and spacing, characteristic microplicae or 'hinges' at the apical surface of each umbrella-like cell (Fig. 3g)[49,50]. Specifically, the protrusions were approximately 200 nm long, 100 nm in width and spaced approximately 500 nm apart, which is consistent with the reported size of microplicae[50,51]; this length is far smaller than the usual length of epithelial microvilli, which is usually approximately 1 µm[52]. Orthogonal sections of fully differentiated organoid zones were analysed using TEM. As with the laser scanning confocal imaging, TEM elucidated distinct layers of basal, intermediate and umbrella cells (Fig. 3h). Structures consistent in size and spacing with rigid plaques could be seen residing between the 'hinges' at the apical surface of the umbrella cells (Fig. 3i,j)[49,50]. Structures were also seen that may possibly correspond to the specialised fusiform vesicles (Fig. 3j) necessary for trafficking uroplakins[53] – although the use of specific markers would be necessary to confirm these. In contrast, TEM analysis of the small, undifferentiated cells making up the monolayers flanking the organoid zones did not exhibit the putative hinges, plaques or the structures than might be fusiform vesicles (Fig. 3k,l). Taken together, these observations suggest that the fully differentiated regions of the organoids possess some key features expected of a human urothelium.

Urine strongly influences HBLAK differentiation, organoid development and GAG formation. As shown above, the HBLAK organoid expresses key urothelial markers and is morphologically reminiscent of a urothelium. Of key importance, however, is the tolerance exhibited by these cultures to urine. In this group of experiments we investigated whether urine is merely tolerated or indeed necessary for differentiation in 2D, organoid formation and the elaboration of a GAG layer. To achieve this, we exposed the cells, in 2D and 3D, to various dilutions of sterile human urine before examining microscopically.

To decouple the influence of urine from any effects that might be exerted by developing intermediate cells below, we grew HBLAK cells as 2D monolayers on chamber slides and exposed them to medium containing urine. As shown in Fig. 4, HBLAK cells exhibited a marked dose response to urine after 72 hours. Cells grown in high calcium medium alone took on a small, tightly packed basal cell-like appearance with visually well-formed intercellular junctions as assessed by actin staining (Fig. 4a) and the elaboration of actin-containing microvilli (Fig. 4a inset, red arrow). With the addition of 25% human urine, however, a small proportion of the cells began to exhibit an enlarged morphology, but intercellular junctions were partially disrupted (Fig. 4b). After 72 hours in 50% sterile human urine, extensive colonies of HBLAK cells took on a large, flat umbrella cell-like morphology (Fig. 4c) devoid of microvilli (Fig. 4c inset, red arrow). However, intercellular junctions seemed almost entirely compromised, possibly because increased urine came at the expense of calcium concentration.

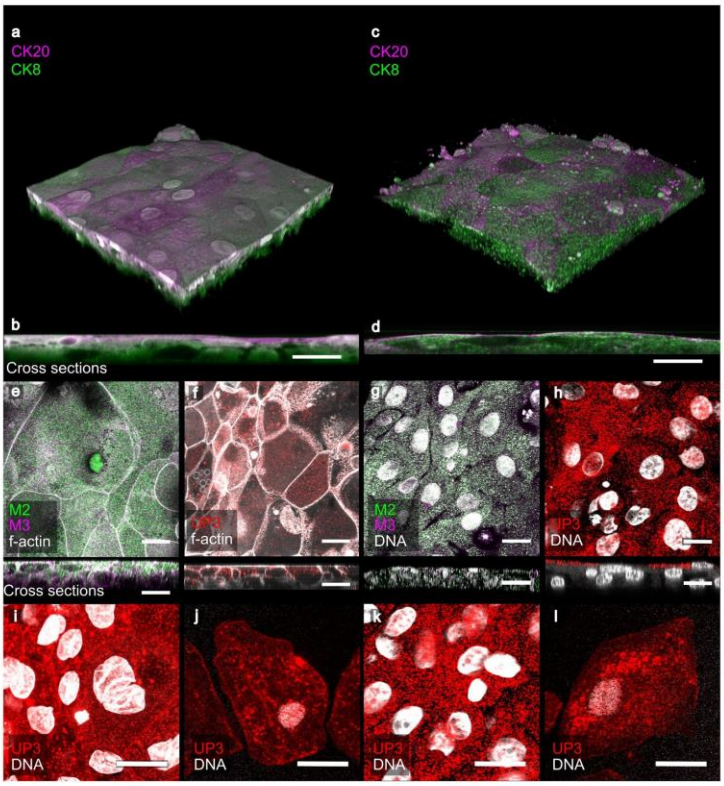

Figure 2. Characterisation of HBEP (left) and HBLAK (right) urothelial organoids using IF (**a**) 3D confocal model and (**b**) orthogonal reslice from a 100 slice Z-stack of HBEP organoid. The HBEP organoid exhibited the correct spatial expression of Cytokeratin-20 (CK20, umbrella cells, magenta) and Cytokeratin-8 (CK8, throughout urothelium, green). (**c**) 3D confocal model and (**d**) orthogonal reslice from a 120 slice Z-stack of HBLAK organoid. As with the primary HBEP mimetic, the HBLAK organoid also expressed CK20 (magenta) at the apical surface and CK8 (green) throughout the tissue. (**e**–**h**) Single optical slices at apical region of HBEP (**e**,**f**) and HBLAK (**g**,**h**) organoids with corresponding orthogonal cross sections shown directly beneath. (**e**,**g**) Expression of muscarinic receptor 2 (M2, green) and muscarinic receptor 3 (M3, magenta). Both receptors were found throughout the tissue in both models. Phalloidin-stained F-actin is presented in grey. (**f**,**h**) Expression of Uroplakin-III (UP3, red) preferentially at apical region of both models. Phalloidin-stained F-actin is presented in grey. (**i**) High-power single optical slice of UP3 (red) expression in HBEP model. (**j**) Pattern of UP3 (red) expression found in an exfoliated urothelial cell harvested from a chronic UTI patient. (**k**) High-power single optical slice of UP3 (red) expression in HBLAK model. (**l**) Further example of the pattern of UP3 (red) expression found in patient-isolated urothelial cells. DAPI-stained DNA is presented in grey. Scale bars represent 20 μm.

Strikingly, we found human urine to be necessary for organoid formation and the elaboration of a GAG layer in HBLAK cells. Cells cultured for 14 days on filter inserts with high calcium medium in the basal and apical compartments were comprised of only one layer, showing no stratified organoid formation, little heparan sulphate, and no detectable expression of chondroitin sulphate (Fig. 4d). Moreover, these cells appeared to exhibit a degree of anaplasia, with a more 'spindle-like' multipotent progenitor cell-like morphology (data not shown). In contrast, HBLAK cells cultured in 50% or 100% human urine at the apical surface produced zones of organoid formation between 3 and 6 cell layers thick (Fig. 4e,f) as previously seen in the experiments presented in Fig. 1, and both stimulated the expression of a heparan and chondroitin sulphate-rich GAG layer at the urine-umbrella

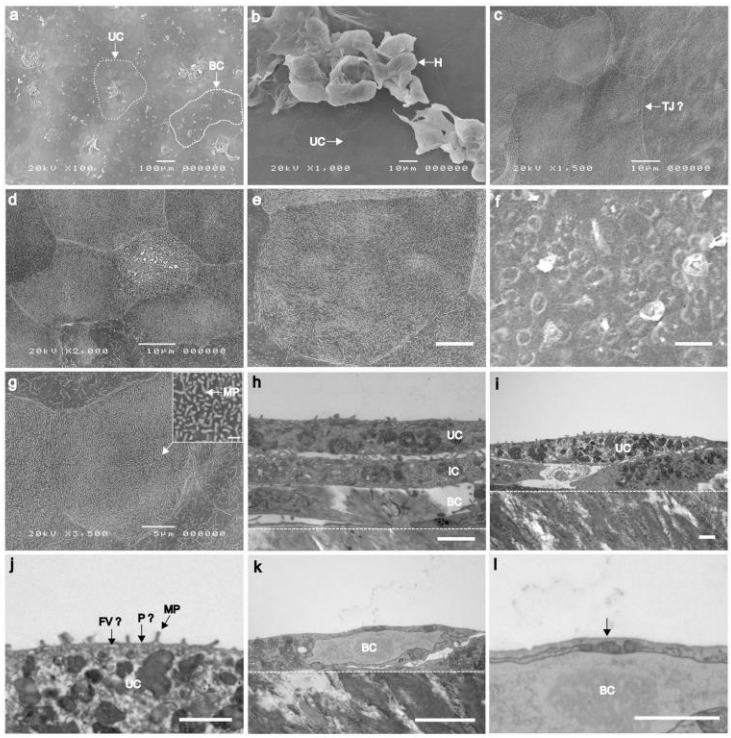

Figure 3. Analysis of HBLAK organoid topography and ultrastructure using scanning electron microscopy (SEM) and transmission electron microscopy (TEM) (**a**) SEM micrograph showing 'islands' of organoid formation. Umbrella-like cells (UC) can be seen at the apical surface of each 'island' interspersed by areas of undifferentiated monolayers of basal-like cells (BC). (**b**) SEM at the apical surface of organoid. Large (~50–60 µm), flat umbrella-like cells (UC) are present at the upper-most surface of each 'island'. Areas of hyperplasia (H), however, were frequently observed. (**c**) SEM of umbrella-like cells showing structures resembling tight junctions (TJ?). (**d**,**e**) SEM of further regions of large, characteristically tessellated umbrella-like cells. Scale bars represents 10 µm. (**f**) SEM of region of small undifferentiated basal-like cells. Scale bar represents 10 µm. (**g**) SEM of a single umbrella cell. Microplicae (MP) or 'hinges' can be seen covering the surface of the umbrella-like cells. Inset scale bar represents 500 nM. (**h**) TEM of 3–4 layered organoid. Basal cells (BC) can be seen above the polycarbonate culture filter (white broken line). Large, distended intermediate cells (IC) and umbrella-like cells (UC) are superior to the basal cells. Scale bar represents 2 µm. (**i**) TEM of 2–3 layered organoid. White broken line represents the upper surface of the polycarbonate culture filter. Scale bar represents 2 µm. (**j**) Enlarged version of TEM image i. Plaque-like structures (P?) are situated between each hinge (microplicae, MP). White structures were evident that might be fusiform vesicles (FV?), responsible for trafficking uroplakin to the umbrella cell plaques. Scale bar represents 1 µm. (**k**) TEM of a monolayer of undifferentiated basal cells (BC, as highlighted in image a) found between the organoid 'islands'. These non-differentiated cells measure ~8 µm across, making them approximately 10–50 times smaller than the umbrella-like cells in the same system. White broken line represents the upper surface of the polycarbonate culture filter. Scale bar represents 2 µm. (**l**) TEM of the apical surface of the basal cell (BC) shown in image i. Structures resembling microplicae, plaques and fusiform vesicles were not seen (white arrow). Scale bar represents 1 µm.

cell interface (Fig. 4e,f). Taken together with the data in Fig. 3, these experiments suggest that urine is an indispensable effector of urothelial differentiation in this model. Nevertheless, despite a lack of GAG layer and of the structures that appear to be asymmetric unit membrane plaques, undifferentiated cells remain viable for long periods in urine, which suggests that these "barriers" are not required for urine tolerance.

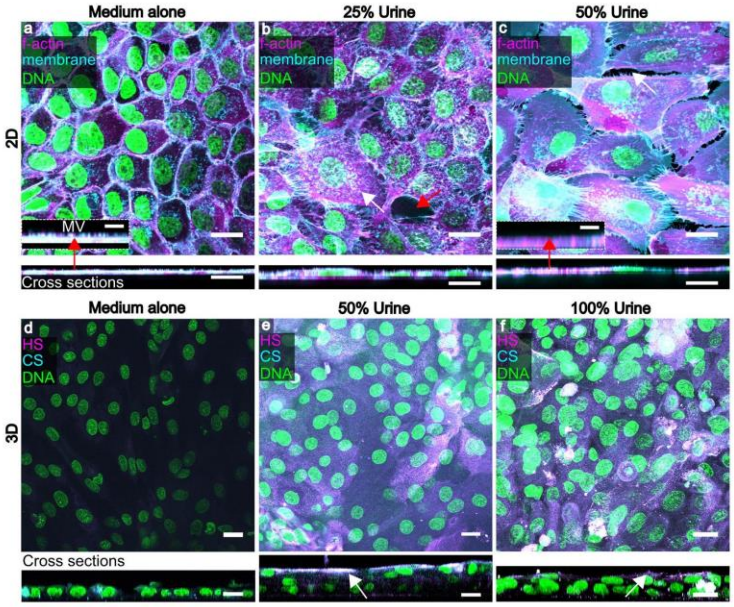

Figure 4. Human urine affects HBLAK differentiation, 3D organoid formation and GAG expression.Upper images are maximum projections and corresponding orthogonal cross sections (below) from 12 slice Z-stacks of HBLAK cells cultured in 2D on glass. Cells were grown to confluency and incubated for 72hrs in varying proportions of human urine in culture medium. WGA-stained plasma membrane is presented in cyan, phalloidin-treated F-actin in magenta and DAPI-labelled DNA in green. (**a**) Monolayer grown in 3D barrier medium alone. Basal cell morphology was maintained and intercellular junctions appeared to be intact. Inset displays high magnification cross section showing actin-rich microvilli (MV) at apical surface. Inset scale bars represents 5 µm. (**b**) HBLAK monolayer cultured in 25% human urine. A subset of cells began to differentiate (white arrow) exhibiting a large, flat umbrella cell-like morhology. Cell junction integrity was disrupted (red arrow). (**c**) HBLAK monolayer cultured in 50% human urine. Large colonies of cells exhibited an umbrella cell-like morphology. Cell junctions, however, were almost entirely compromised (white arrow). Inset shows the lack of microvilli on the surface of the umbrella-like cells. Inset scale bars represents 5 µm. Lower images are maximum projections (and cross sections below) from 20-slice Z-stacks of HBLAK cells grown on 3D culture filter inserts. Cultures were exposed to 3D barrier medium in the basal compartment and varying proportions of human urine at their apical surface for 14 days. The glycosaminoglycan (GAG) constituents heparan sulphate (HS) and chondroitin sulphate (CS) were labelled and are shown here in magenta and cyan respectively. DAPI-stained DNA is shown in green. (**d**) Cells cultured in 3D barrier medium only in the basal and apical compartments. No stratified organoid formation was observed. Little GAG expression was seen. (**e**) Cells cultured with 50% urine at the apical surface. Urothelium-like organoids were formed. Heperan sulphate and chondroitin sulphate were strongly expressed by umbrella-like cells (white arrow). White represents colocalization. (**f**) Cells cultured with 100% urine at the apical surface. Again, well organised bladder organoids were formed and a GAG (heparan sulphate and chondroitin sulphate) mucin layer was elaborated at the cell-urine interface (white arrow). Scale bars represent 20 µm.

The HBLAK organoid is a potential model for studying *Enterococcus* infection. Our laboratory studies the uropathogen *Enterococcus faecalis*. This bacterium is commonly implicated in chronic UTI in the elderly and is frequently associated with multi-drug resistance, hospital-acquired infection, and catheter-associated biofilm formation; we previously demonstrated that it exhibits intracellular invasion in patient cells[54–62]. To determine whether the organoid is a good model for studying host-pathogen interactions with this bacteria, we infected the HBLAK organoid with patient-isolated *E. faecalis*[55]. When we inspected the cultures two hours after infection, we found that *E. faecalis* exhibited robust tropism in this model, with the resulting adherent colonies relatively loosely packed (Fig. 5a). As with human patients suffering from acute and chronic UTI, the apical cell layer was shed in response to bacterial insult[55], leaving an uneven surface of basal and intermediate cells (Fig. 5a,d; also compare the uneven surface of orthogonal views in Fig. 5d to the smooth

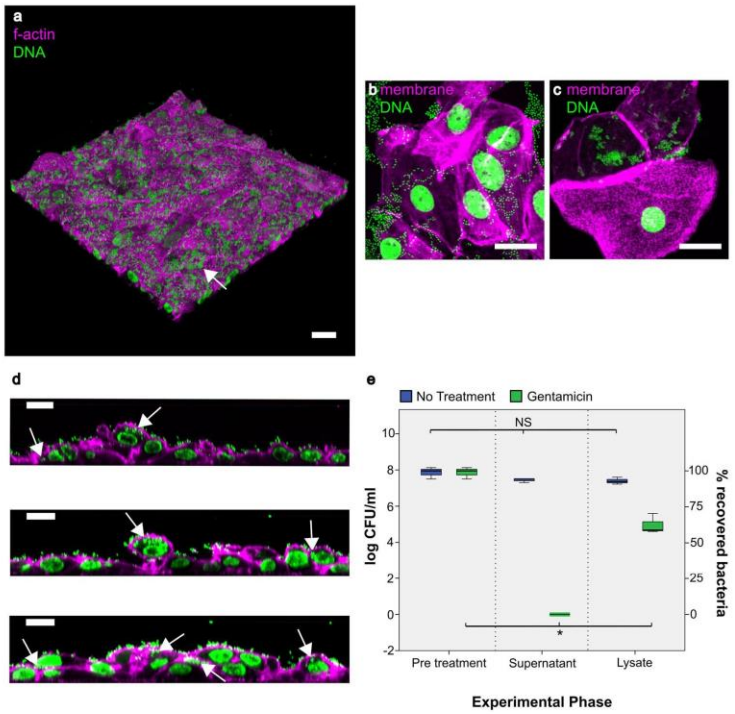

Figure 5. Analysis of HBLAK-derived urothelial organoids infected with uropathogenic *E. faecalis*. Composites showing (**a**) 3D confocal model constructed from a 100 slice Z-stack of HBLAK organoid post infection with *E. faecalis* (MOI of 25). phalloidin-stained F-actin in magenta and DAPI-stained DNA (host and pathogen) in green. The characteristically smooth and flat umbrella-like cell layer was lost in response to infection. Loose colonies of *E. faecalis* could be seen adhering to the now unprotected basal and intermediate cells (white arrow). (**b**) Surface cells shed from organoid in response to infection with *E. faecalis*. WGA-labelled membrane shown in magenta and DAPI-stained DNA (host and pathogen) in green. (**c**) Patient-isolated urothelial cells shed into the urine in response to infection. (**d**) Orthogonal cross sections prepared from image a. White arrows show evidence of intracellular *E. faecalis* within the basal and intermediate cells of the HBLAK organoid. 7.3% of cells exhibited intracellular colonisation with a mean of 37.8 (+/−SD of 11.5) bacteria per cell. Phalloidin-stained F-actin in magenta and DAPI-stained DNA (host and pathogen) in green. Scale bars represent 20 µm. (**d**) Box and whisker plot showing the results of gentamicin protection assays undertaken on HBLAK organoids infected with uropathogenic *E. faecalis*. Results are represented as log10 median CFU/ml with a % bacterial recovery derived axis. Treatment with 2000 µg/ml of gentamicin resulted in zero detected growth within the organoid supernatant. Detergent treatment liberated intracellular bacteria resulting in the detection of 4.8×10^3 cfu/ml in the lysate (approx. 55% bacterial recovery). N = 3 per treatment. NS = No statistically significant difference ($P > 0.05$), *$P \leq 0.05$.

surface evident in orthogonal views of the intact, uninfected HBLAK organoid in Figs 1d and 2d). Inspection of supernatants post-infection revealed extensive shed umbrella-like cells (Fig. 5b) reminiscent of those seen in the urine of infected patients (Fig. 5c and[55]). Significantly, in the tissue that remained, we saw frequent examples of large intracellular bacterial colonies (Fig. 5d, arrows) within the superficial layer of cells, showing a similar loosely-packed morphology to those we previously observed in shed urinary umbrella cells from patients[55]. Image analysis showed that 7.3% of cells harboured intracellular colonies with a mean of 37.8 (+/−SD of 11.5) bacteria per cell. A gentamicin protection assay performed on organoids infected with *E. faecalis* for two hours (Fig. 5e) supported this observation, with viable intracellular bacteria liberated after extracellular sterilization and host cell lysis. Specifically, treatment with 2000 µg/ml of gentamicin resulted in zero detected growth within the organoid supernatant. Detergent treatment liberated intracellular bacteria resulting in the detection of a median

of 4.8×10^3 cfu/ml in the lysate (approx. 55% bacterial recovery). A non-parametric Friedman test of differences among repeated measures was conducted on the median cfu/ml data from the untreated (control, N = 3) and gentamicin treated (N = 3) organoids. A statistically significant difference was found among the gentamicin treated organoids ($\chi^2 = 6$, $p = 0.04$) whereas no difference was found among the untreated control data ($\chi^2 = 3.8$, $p = 0.15$). Taken together, these findings suggest that the model recapitulates some key aspects the host/pathogen interaction of *E. faecalis* with its human host.

In summary, this model, to our knowledge, represents the first long-term urine-tolerant human bladder organoid produced *in vitro*. This tissue is reminiscent of normal human bladder urothelium and expresses a number of key markers in the correct spatial compartments in response to exposure to urine. As with patients, this organoid rapidly sheds the apical cell layer in response to bacterial insult. Moreover, *E. faecalis* displayed invasive phenotypes, supporting our previous findings in shed patient cells[55].

Discussion

The development and use of *in vitro* human tissue mimetics is thought to be accelerating the drug discovery process[63] and improving our understanding of human tissue morphogenesis. Due to improved physiological relevance, such models could even reduce the use of animal models in the coming years[64]. Here, we present a urine-tolerant, three-dimensional urothelial organoid derived from human progenitors that is easy to grow from commercially-sourced, quality-controlled materials, that displays key hallmarks of the human urothelium, and which may serve as an alternative to the murine model. If desired, it should also be possible to create similar urine-tolerant organoids from fresh human biopsies using the protocols and defined medium we describe. An even more physiological response could well be achieved by embedding the organoid into a perfusion-based bioreactor allowing the flow of apical urine, which would introduce relevant shear forces and metabolite flux[45]. Further improvements could be achieved by seeding the organoid onto different scaffolds; by co-culturing cells that could secrete an appropriate extracellular matrix; and/or by introducing a stretch parameter[65].

As this organoid model was generated in a similar manner to others that have been reported[21], it is not clear why it has superior urine tolerance. Additional work in our laboratory has not revealed any differences in outcome depending on the source of the human urine. The primary cells, and their HBLAK derivatives, were obtained from standard healthy adult human biopsy of the trigome region, and we do not anticipate this being materially different from other biopsies; indeed, we achieved good results with similar cells sourced from a different company. Therefore, the most likely factor is the specialized medium, which is free of serum and other growth factor supplements that could impair differentiation. We are currently using an empirical approach to determine which aspects of the growth media and urine are important for differentiation.

Morphologically, the HBEP and HBLAK cells produced tissue with encouraging similarities to human urothelium[17,18,21,25]. HBEP cells produced tissue ~3 cell layers thick whereas HBEP cell-derived tissue elaborated ~5–7 layers. In contrast to mice, higher mammals such as humans have multiple intermediate cell layers, a feature which may favor the use of HBLAK cells[20]. However, rate of cell division could have played a role in this outcome, as could cell senescence in the HBEP population[66]. Both culture types developed an apical layer of enlarged, flattened cells that appeared umbrella-cell-like[20] in morphology. Based on size and visible distension of cells in the tissue, the differentiated layer seemed more akin to a stretched (urine-filled) state rather than a relaxed (empty bladder) state. Multiple nuclei were not very common in these cells, as would be expected from the mouse urothelium. We could find no consensus in the literature about the expected percentage of multinucleation in the human urothelium, with studies being scant, and it is also not clear whether the multinucleated state plays any functional role. Further work is needed to understand how tissue thickness and multinucleation is regulated in both cell types.

Phenotypic analysis of both the HBEP and HBLAK urothelial organoid tissue elucidated the presence of some important urothelial markers. Uroplakins are a group of highly conserved glycoproteins which are unique to mammalian urothelium[48]. Uroplakin-III (UP3) was expressed on the apical surface throughout the differentiated tissue and its expression was morphologically similar to that of patient-shed urothelial cells – with the caveat that these patient cells were infected, and expression might alter after exfoliation. Laguna *et al.* (2006)[17] found that the normal human urothelium expresses a range of cytokeratins in relation to the level of cytodifferentiation. Our 3D culture mimicked these findings with cytokeratin-8 (CK8) found throughout the tissue and cytokeratin-20 (CK20) being a preferential phenotype of well-developed umbrella cells[17]. To our knowledge, this is the first human bladder organoid demonstrating the correct spatial expression of CK20[34].

Patients with overactive bladder symptoms are frequently treated with antimuscarinics which target muscarinic receptors in the detrusor and urothelium[46]. Crucially, rodent bladder urothelial cells do not express muscarinic receptors[47]. In the case of the HBEP and HBLAK tissue grown in this study, muscarinic receptors M2 and M3 were detected throughout the urothelial cell layers, further supporting its physiological relevance and potential use in the development of novel therapeutic agents for the bladder symptoms of MS and other neurogenic disorders.

More detailed analysis revealed several interesting aspects to our HBLAK organoid model. First, EM showed that the tissue was not homogenously differentiated; instead, the surface consisted of three discrete zones: 'valleys' of undifferentiated monolayer; 'plateaus' of fully differentiated 3D tissue; and 'mountains' of hyperplasia. Second, inspection of GAG layer markers revealed that the presence of urine correlates with its elaboration, in parallel with differentiation and organoid formation. Third, focusing on the differentiated plateaus, which comprised about two-thirds of the total area, our EM imaging shows expected key features, including morphologically distinct layers, and the enlarged flat nature of the distended umbrella-like cells. We also noted structures consistent in shape, size and spacing with the characteristic hinges and plaques associated with the AUM, and white lacunae that might possibly represent the fusiform vesicles responsible for trafficking during bladder filling and emptying phases. These structures were entirely absent from the zone of undifferentiated cells, showing a possible

correlation with differentiation status. However, higher resolution EM imaging and immunostaining is needed to confirm their identity.

Intriguingly, when we tested the barrier function of the organoid by several methods, including transepithelial resistance and fluorescent dextran permeability (data not shown), we found a lack of what is traditionally thought of as urothelial "barrier function". We presume that this result was caused by the sporadic presence of undifferentiated cells across the tissue, which in essence short-circuit the apicobasal electrical potential difference. This result, taken together with the fact that the non-differentiated zone devoid of AUM-like structures and GAG can grow for several weeks in the presence of urine, strongly suggests that AUM and GAG are not required for urine tolerance, and that something intrinsic in the cells themselves confer resistance to its toxic effects. It also suggests that apical urine is necessary for full differentiation. Whilst it may be the case that urine is not sufficient for differentiation, given the presence of the undifferentiated 'valleys', it may also be the case that a subset of HBLAK cells are subtly different. Further exploration into the nature of urine tolerance and the effect of urine and other media components on differentiation and hyperplasia are warranted. Genomic analysis of cells from various regions, compared with starting cells, would also be interesting. In the meantime, researchers performing image-based studies should be able to focus on areas of the organoid corresponding to their desired level of differentiation.

Our model shows great promise for studying the host/pathogen interactions of UTI in a human-cell system. The majority of host/pathogen interaction studies in UTI focus on the most common uropathogen *E. coli*, but very little is known about other uropathogens such as *Enterococcus faecalis*, which is more common in certain cohorts, such as the elderly, the hospitalized and those using urinary catheters. We previously reported the discovery of intracellular colonies of *E. faecalis* harbored within the urothelial cells of chronic UTI patients[55]. This previous report also slowed sloughing of umbrella cells from the epithelial lining into the urine, which is known in both mice and humans to be a common response to infection[67–71]. These findings were echoed in our urothelial organoid, where *E. faecalis* formed significant intracellular colonies within the intermediate and basal cells of the urothelial mimetic after its umbrella-cell layer had been jettisoned. These results further support the notion that *E. faecalis* exhibits an intracellular phenotype.

In conclusion, current advances in 3D tissue culture enabled us to grow physiologically relevant, organotypic human models of the bladder. Human bladder biomimetics could be used as a reproducible test bed for chronic infective disease formation, treatment, and resolution in humans.

Materials and Methods

Human Primary progenitor cell expansion and handling in 2D. Commercially available human bladder epithelial progenitor cells (HBEP, Cell N Tec)[72] and their spontaneously immortalised, non-transformed counterparts (HBLAK, Cell N Tec) were supplied in frozen aliquots containing ~5×10^5 cells at passage 2 and ~0.5×10^5 at passage 25 respectively. Cells were isolated from bladder trigone biopsies from male patients undergoing surgery for benign prostatic hyperplasia. HBEP cells are guaranteed to grow for a further 15 population doublings before senescing whereas HBLAK cells, although spontaneously immortalised, should not be differentiated into 3D cultures once they have exceeded a passage number of 40–50. Both cell types were cultured identically, with the exception of slight differences in incubation time between passages, due to the slightly increased rate of cell division exhibited by HBLAK cells.

Thawed cells were seeded (~300 cell clumps/cm^2) into pre-warmed and equilibrated low-calcium, high-bovine pituitary extract, primary epithelial medium (CnT-Prime, Cell N Tec) in 9 cm polystyrene dishes and incubated at 37 °C in a humidified incubator under 5% CO_2. Culture medium was replaced after overnight incubation to remove residual dimethyl sulfoxide (DMSO). Antibiotics were not added to culture medium at any point due to adverse effects on cytodifferentiation, metabolism and morphology[73]. Furthermore, trypsin is known to damage primary cells, so Accutase solution (Innovative Cell Technologies) was used to detach cells at all stages of experimentation[74]. Cells were allowed to expand to ~70% confluency before freezing batches of cells at a density of ~1×10^6 cells/ml in defined freezing medium (CnT-CRYO-50, Cell N Tec) in preparation for later experiments. Cells were not allowed to become fully confluent during cell expansion in an effort to maintain a proliferative phenotype.

Differentiation of 3D human urothelium *in vitro*. In preparation for organotypic culture, previously frozen progenitor cells were thawed and expanded on 9 cm culture dishes as above. Once 70–80% confluent, the cells were washed briefly with calcium- and magnesium-free phosphate buffered saline (PBS, Sigma-Aldrich) and incubated at 37 °C in ~3 ml of pre-warmed Accutase solution for 2–5 min. The dishes were lightly tapped and detached cells re-suspended in 7 ml of warm CnT-Prime. After centrifugation at 200 × g for 5 min, the supernatant was removed and the pellet re-suspended in fresh CnT-Prime. This cell suspension was counted whilst allowing the cells to equilibrate for 3 min at room temperature. 2×10^5 cells in 400 µl of CnT-Prime (internal medium) were added to 6 12 mm 0.4 µm pore polycarbonate filter (PCF) inserts (Millipore) standing in 6 cm culture dishes containing ~3 ml of fresh pre-warmed CnT-Prime medium (external medium, level with insert filters). A further 8 ml of CnT-Prime medium was added to the 6 cm dish (external to the filter inserts) until internal and external fluid levels were the same. The 3D culture inserts were incubated for 3–5 days until 100% confluent. Confluency was determined through the fluorescent staining of 1 insert and visualisation under epi-fluorescence microscopy (see section below). Once deemed confluent, internal and external medium was removed and replaced with low-BPE, calcium-rich (1.2 mM) differentiation barrier medium (CnT-Prime-3D, Cell N Tec) to promote differentiation. Subsequent to overnight incubation, the internal medium (apical surface of cell culture) was removed and replaced with filter-sterilised human urine pooled from healthy volunteers of both genders to aid terminal differentiation into umbrella cells. The external CnT-Prime-3D medium and the internal human urine were replaced every 3 days and the culture incubated for 14–24 days at 37 °C in 5% CO_2.

To explore the effect of urine on differentiation in 2D, the HBLAK cells were seeded on 8-well permanox Lab-Tek slides (Sigma-Aldrich) and grown to confluency. The cells were then exposed to CnT-Prime-3D medium alone, 25%, or 50% sterile human urine diluted in CnT-Prime-3D for 72 hours at 37 °C in 5% CO_2. To analyse the effect of urine on HBLAK organoid formation, cells were grown to confluency on filter inserts as above. The basal compartment was treated with CnT-Prime-3D throughout, however, the apical compartment was filled with either CnT-Prime-3D alone, 50% sterile human urine diluted in CnT-Prime-3D or 100% urine. The specified medium or urine was changed every 3 days and the culture incubated for 14 days at 37 °C in 5% CO_2.

Characterisation of the 3D urothelium. Prior to fluorescent staining and immunofluorescence (IF), filter inserts were carefully transferred to 8-well plates (Nunc) and submerged in 4% methanol-free formaldehyde (Thermo Scientific, Fisher Scientific) in PBS overnight at 4 °C. After fixation, the filter inserts were kept at 4 °C in 1% formaldehyde in sealed containers in preparation for processing.

To determine confluency and analyse morphology, the pre-fixed tissue was permeabilised in 0.2% Triton-X100 (Sigma-Aldrich) in PBS for 15 minutes at RT followed by a single wash with PBS. The cells were stained with TRITC or Alexa Fluor-633-conjugated phalloidin (0.6 µg/ml) (Sigma-Aldrich), to label filamentous actin, and the DNA stain 4′′,6-diamidino-2-phenylindole, (DAPI, 1 µg/µl; Sigma-Aldrich) in PBS for 1 hour at RT. The dual-labelling solution was gently aspirated and the cells washed 5 times in PBS.

For indirect IF, the tissue was permeabilised as above, washed with PBS then blocked with 10% normal goat serum (NGS, Thermo Fisher) in PBS for 1 hour. Tissue was incubated overnight at 4 °C with primary antibodies in PBS containing 1% NGS as follows: 1:10 dilution of mouse anti-uroplakin-III (UP3) monoclonal antibody (clone AU1, 651108, Progen Bioteknik); 1:50 dilution of mouse anti-Cytokeratin 8 (CK8) monoclonal antibody (clone H1, MA1-06317, Thermo Fisher); 1:100 dilution of rabbit anti-Cytokeratin 20 (CK20) polyclonal antibody (PA5-22125, Merck Millipore); 1:200 dilution of rat anti-muscarinic acetylcholine receptor m2 (M2) monoclonal antibody (clone M2-2-B3, Merck Millipore); 1:200 dilution of rabbit anti-muscarinic acetylcholine receptor m3 (M3) polyclonal antibody (ab126168, Abcam); 1:100 dilution of mouse anti-chondroitin sulphate monoclonal antibody (clone CS-56, ab11570, Abcam) or 1:100 dilution of rat anti-heparan sulphate proteoglycan (large) monoclonal antibody (clone A7L6, ab2501, Abcam). Post incubation with primary antibodies, the tissue was washed 5 times with PBS containing 1% NGS then incubated at RT for 1 hour with a 1:250 dilution of the following secondary antibodies (depending on the species of primary antibody used): goat anti-mouse, goat anti-rabbit or goat anti-rat conjugated to either Alexa Fluor-555, Alexa Fluor-488 or Alexa Fluor-633 (Invitrogen). Labelled cells were washed 5 times with PBS to remove unbound secondary antibody before staining with phalloidin and DAPI as above. In some experiments, prior to permeabilization, cell plasma membranes were labelled with 1 µg/ml wheat germ agglutinin (WGA) conjugated to Alexa Fluor-488/633 (Invitrogen) in Hank's balanced salt solution (HBSS, Invitrogen) for 20 min at RT. Controls were performed by using primary and secondary antibodies in isolation.

In preparation for imaging, filters were carefully removed from inserts using a scalpel, mounted with FluorSave reagent (Calbiochem), and a coverslip fixed in place with clear nail varnish. Lab-Tek slide wells and gaskets were carefully removed prior to the addition of FluorSave and a coverslip as above.

Electron microscopy. Electron microscopy was conducted by the Division of Medicine, University College London electron microscopy unit at the Royal Free Campus, Hampstead, London.

For transmission electron microscopy (TEM), samples were fixed in Karnovsky's fixative (2.5% glutaraldehyde/2% paraformaldehyde) and then washed in 1 M PBS 3 × 10 min, followed by a post-fixation in 1% Osmium tetroxide for 1 hour at room temperature. Tissue was rinsed with distilled water 3 × 10 min. Samples were dehydrated in an ethanol series (30, 50, 70, 90 and 100%) then treated with resin-ethanol (1:1) overnight. Subsequently, samples were embedded in 100% LEMIX resin and incubated at 65 °C for 24 hours. Ultra-thin sections of the resin block were cut and post stained with 2% Uranyl acetate and Lead citrate.

For scanning electron microscopy (SEM), the samples were fixed and dehydrated as above. Samples were then incubated in Tetramethylsilane for 10 min and air dried before mounting on stubs and sputter-coated with gold.

Experimental infection of the human urothelial organoid and the gentamicin protection assay. A single strain of *Enterococcus faecalis (E. faecalis)* originally derived from a patient with chronic UTI[55] was grown aerobically in a shaking incubator at 37 °C for 24 hours. Once a batch of 6 HBLAK 3D urothelial cultures had reached 14 days of growth, 1.6×10^7 colony-forming units of each bacteria (MOI of 25) were added to the filter-sterile human urine at the apical liquid-liquid interface of each culture. The experimentally infected cultures were incubated for 2 hours at 37 °C under 5% CO_2. The 3D culture filter inserts were washed with PBS before fixation and staining as above. For the gentamicin protection assay, after the infection was completed, the cultures were washed 3 times in PBS before the addition of 3D barrier medium containing 2000 µg/ml of gentamicin (Sigma-Aldrich) to the apical and basal compartments of the culture filter. The organoids with antibiotics were incubated for a further 2 hours at 37 °C under 5% CO_2 to kill any extracellular bacteria. Post incubation the supernatant was serially diluted in PBS (undiluted, 1:100, 1:1000, 1:10000) and 25 µl of each dilution spread on a quartile of a Columbia blood agar plate (CBA, Oxoid) before being incubated for 24 hours aerobically at 37 °C to enumerate live bacteria. The organoids were washed a further 3 times in PBS before being lysed with 1% Triton-X100 in PBS for 10 minutes at RT. The lysate was added to CBA plates and incubated as above to detect intracellular bacteria. All experiments were completed in triplicate.

Analysis of shed epithelial cells. Patient samples were collected with informed consent and analyzed in accordance with a protocol approved by the East Central London Regional Ethics Committee (REC1) (Ref: 11/H0721/7).

Experimentally infected organoid supernatants, or patient urine specimens, were collected, cytocentrifuged on to glass slides and fixed and stained prior to imaging[55]. Briefly, 80 µl of supernatant or patient urine was cytocentrifuged using a Shandon Cytospin 2 cytocentrifuge at 800 rpm (≈75 g rcf) for 5 minutes. The cellular deposit was circumscribed with a ImmEdge pen (Vector Laboratories) before fixing, staining and mounting as above.

Imaging and Analysis. We performed epi-fluorescence microscopy on an Olympus CX-41 upright microscope, and confocal laser scanning microscopy on Leica SP5 and SP2 microscopes. Images were processed and analysed using Infinity Capture and Analyze V6.2.0, ImageJ 1.50 h[75] and the Leica Application Suite, Advanced Fluorescence 3.1.0 build 8587 Software.

TEM was conducted using a Jeol 1200-Ex digital image capture system with a side mount 2 Kv AMT camera. SEM was performed using a Jeol JSM-5300 fitted with a Semafore digital image capture system.

The proportion of the HBLAK organoids exhibiting evidence of differentiation was calculated by analyzing low-power SEM micrographs (N = 3) using ImageJ automatic thresholding and measure tools[75]. The number of bacteria per cell was calculated using nearest neighbour 3D connectivity analysis with the ImageJ Object counter3D plugin[75,76]. The DAPI channel of 3D laser scanning confocal constructs were analysed using Differential Voxel Filters allowing the enumeration of mammalian nuclei and bacteria.

Statistical analysis. Data were analysed using IBM SPSS Statistics version 24. Non-parametric Friedman tests of differences among repeated measures were performed due to non-normal distributions. 3 experimental replicates were performed for statistical testing.

Data availability. All data generated or analysed during this study are included in this published article.

References

1. Foxman, B. Epidemiology of urinary tract infections: incidence, morbidity, and economic costs. *Disease-a-month: DM* **49**, 53–70, https://doi.org/10.1067/mda.2003.7 (2003).
2. Foxman, B. The epidemiology of urinary tract infection. *Nature reviews. Urology* **7**, 653–660, https://doi.org/10.1038/nrurol.2010.190 (2010).
3. WHO. Antimicrobial resistance: *global report on surveillance* 2014. (2014).
4. Russo, T. A., Stapleton, A., Wenderoth, S., Hooton, T. M. & Stamm, W. E. Chromosomal restriction fragment length polymorphism analysis of Escherichia coli strains causing recurrent urinary tract infections in young women. *The Journal of infectious diseases* **172**, 440–445 (1995).
5. Laupland, K. B., Ross, T., Pitout, J. D., Church, D. L. & Gregson, D. B. Community-onset urinary tract infections: a population-based assessment. *Infection* **35**, 150–153, https://doi.org/10.1007/s15010-007-6180-2 (2007).
6. Mahadeva, A., Tanasescu, R. & Gran, B. Urinary tract infections in multiple sclerosis: under-diagnosed and under-treated? A clinical audit at a large University Hospital. *American journal of clinical and experimental immunology* **3**, 57–67 (2014).
7. Buljevac, D. Prospective study on the relationship between infections and multiple sclerosis exacerbations. *Brain: a journal of neurology* **125**, 952 (2002).
8. Pannek, J. Treatment of urinary tract infection in persons with spinal cord injury: guidelines, evidence, and clinical practice: A questionnaire-based survey and review of the literature. *The journal of spinal cord medicine* **34**, 11–15, https://doi.org/10.1179/107902610X12886261091839 (2011).
9. Giessing, M. Urinary tract infection in renal transplantation. *Arab Journal of Urology* **10**, 162–168, https://doi.org/10.1016/j.aju.2012.01.005 (2012).
10. Hooton, T. M. *et al*. Diagnosis, Prevention, and Treatment of Catheter-Associated Urinary Tract Infection in Adults: 2009 International Clinical Practice Guidelines from the Infectious Diseases Society of America. *Clinical Infectious Diseases* **50**, 625–663, https://doi.org/10.1086/650482 (2010).
11. Cotter, M., Donlon, S., Roche, F., Byrne, H. & Fitzpatrick, F. Healthcare-associated infection in Irish long-term care facilities: results from the First National Prevalence Study. *Journal of Hospital Infection* **80**, 212–216, https://doi.org/10.1016/j.jhin.2011.12.010 (2012).
12. Correale, J., Fiol, M. & Gilmore, W. The risk of relapses in multiple sclerosis during systemic infections. *Neurology* **67**, 652–659, https://doi.org/10.1212/01.wnl.0000233834.09743.3b (2006).
13. Soliman, Y., Meyer, R. & Baum, N. Falls in the Elderly Secondary to Urinary Symptoms. *Reviews in Urology* **18**, 28–32 (2016).
14. Lorenz, E. C. & Cosio, F. G. The impact of urinary tract infections in renal transplant recipients. *Kidney international* **78**, 719–721, https://doi.org/10.1038/ki.2010.219 (2010).
15. Peach, B. C., Garvan, G. J., Garvan, C. S. & Cimiotti, J. P. Risk Factors for Urosepsis in Older Adults: A Systematic Review. *Gerontology and geriatric medicine* **2**, 2333721416638980, https://doi.org/10.1177/2333721416638980 (2016).
16. Schieve, L. A., Handler, A., Hershow, R., Persky, V. & Davis, F. Urinary tract infection during pregnancy: its association with maternal morbidity and perinatal outcome. *American Journal of Public Health* **84**, 405–410 (1994).
17. Rosette, J. D. L. *et al*. Keratin Expression Profiling of Transitional Epithelium in the Painful Bladder Syndrome/Interstitial Cystitis. *American Journal of Clinical Pathology* **125**, 105–110, https://doi.org/10.1309/w342bwmdmddbctvh (2006).
18. Khandelwal, P., Abraham, S. N. & Apodaca, G. Cell biology and physiology of the uroepithelium. *Am J Physiol-Renal* **297**, F1477–F1501, https://doi.org/10.1152/ajprenal.00327.2009 (2009).
19. Chen, Y. R. *et al*. Rab27b is associated with fusiform vesicles and may be involved in targeting uroplakins to urothelial apical membranes. *Proceedings of the National Academy of Sciences of the United States of America* **100**, 14012–14017, https://doi.org/10.1073/pnas.2436350100 (2003).
20. Wu, X. R., Kong, X. P., Pellicer, A., Kreibich, G. & Sun, T. T. Uroplakins in urothelial biology, function, and disease. *Kidney international* **75**, 1153–1165, https://doi.org/10.1038/ki.2009.73 (2009).
21. Baker, S. C., Shabir, S. & Southgate, J. Biomimetic urothelial tissue models for the *in vitro* evaluation of barrier physiology and bladder drug efficacy. *Molecular pharmaceutics* **11**, 1964–1970, https://doi.org/10.1021/mp500065m (2014).
22. Cervigni, M. Interstitial cystitis/bladder pain syndrome and glycosaminoglycans replacement therapy. *Translational andrology and urology* **4**, 638–642, https://doi.org/10.3978/j.issn.2223-4683.2015.11.04 (2015).

23. Janssen, D. A. W. *et al*. The Distribution and Function of Chondroitin Sulfate and Other Sulfated Glycosaminoglycans in the Human Bladder and Their Contribution to the Protective Bladder Barrier. *The Journal of urology* **189**, 336–342, https://doi.org/10.1016/j.juro.2012.09.022 (2013).
24. Rübben, H., Friedrichs, R., Stuhlsatz, H. W., Cosma, S. & Lutzeyer, W. Quantitative analysis of glycosaminoglycans in urothelium and bladder wall of calf. *Urology* **22**, 655–657, https://doi.org/10.1016/0090-4295(83)90321-7 (1983).
25. Hunstad, D. A. & Justice, S. S. Intracellular lifestyles and immune evasion strategies of uropathogenic Escherichia coli. *Annual review of microbiology* **64**, 203–221, https://doi.org/10.1146/annurev.micro.112408.134258 (2010).
26. Tian, W. *et al*. Utility of uroplakin II expression as a marker of urothelial carcinoma. *Human pathology* **46**, 58–64, https://doi.org/10.1016/j.humpath.2014.09.007 (2015).
27. Craig, W. Relevance of animal models for clinical treatment. *Eur. J. Clin. Microbiol. Infect. Dis.* **12**, S55–S57, https://doi.org/10.1007/BF02389879 (1993).
28. van der Worp, H. B. *et al*. Can Animal Models of Disease Reliably Inform Human Studies? *PLoS Med* **7**, e1000245, https://doi.org/10.1371/journal.pmed.1000245 (2010).
29. Perel, P. *et al*. Comparison of treatment effects between animal experiments and clinical trials: systematic review. *Bmj* **334**, 197, https://doi.org/10.1136/bmj.39048.407928.BE (2007).
30. Bhogal, N. & Combes, R. The relevance of genetically altered mouse models of human disease. *Alternatives to laboratory animals: ATLA* **34**, 429–454 (2006).
31. Lin, J. H. Applications and limitations of genetically modified mouse models in drug discovery and development. *Curr Drug Metab* **9**, 419–438 (2008).
32. Mordenti, J. Forecasting cephalosporin and monobactam antibiotic half-lives in humans from data collected in laboratory animals. *Antimicrobial agents and chemotherapy* **27**, 887–891 (1985).
33. Wu, X. R., Manabe, M., Yu, J. & Sun, T. T. Large scale purification and immunolocalization of bovine uroplakins I, II, and III. Molecular markers of urothelial differentiation. *The Journal of biological chemistry* **265**, 19170–19179 (1990).
34. Vaidyanathan, S. *et al*. A study of cytokeratin 20 immunostaining in the urothelium of neuropathic bladder of patients with spinal cord injury. *BMC urology* **2**, 7 (2002).
35. Smith, N. J. *et al*. Toll-Like Receptor Responses of Normal Human Urothelial Cells to Bacterial Flagellin and Lipopolysaccharide. *The Journal of urology* **186**, 1084–1092, https://doi.org/10.1016/j.juro.2011.04.112 (2011).
36. Yang, P. J., Pham, J., Choo, J. & Hu, D. L. Duration of urination does not change with body size. *Proceedings of the National Academy of Sciences* **111**, 11932–11937, https://doi.org/10.1073/pnas.1402289111 (2014).
37. Bubenik, J. *et al*. Established cell line of urinary bladder carcinoma (T24) containing tumour-specific antigen. *Int J Cancer* **11**, 765–773 (1973).
38. Georgopoulos, N. T. *et al*. Immortalisation of normal human urothelial cells compromises differentiation capacity. *Eur Urol* **60**, 141–149, https://doi.org/10.1016/j.eururo.2011.02.022 (2011).
39. Bouhout, S., Goulet, F. & Bolduc, S. A Novel and Faster Method to Obtain a Differentiated 3-Dimensional Tissue Engineered Bladder. *The Journal of Urology* **194**, 834–841, https://doi.org/10.1016/j.juro.2015.03.001 (2015).
40. Knowles, M. A., Finesilver, A., Harvey, A. E., Berry, R. J. & Hicks, R. M. Long-term organ culture of normal human bladder. *Cancer research* **43**, 374–385 (1983).
41. Feil, G. *et al*. Immunoreactivity of p63 in Monolayered and *In Vitro* Stratified Human Urothelial Cell Cultures Compared with Native Urothelial Tissue. *European Urology* **53**, 1066–1073, https://doi.org/10.1016/j.eururo.2007.10.026 (2008).
42. Nagele, U. *et al*. *In vitro* investigations of tissue-engineered multilayered urothelium established from bladder washings. *Eur Urol* **54**, 1414–1422, https://doi.org/10.1016/j.eururo.2008.01.072 (2008).
43. Sugasi, S. *et al*. *In vitro* engineering of human stratified urothelium: analysis of its morphology and function. *The Journal of urology* **164**, 951–957 (2000).
44. Cross, W. R., Eardley, I., Leese, H. J. & Southgate, J. A biomimetic tissue from cultured normal human urothelial cells: analysis of physiological function. *American Journal of Physiology - Renal Physiology* **289**, F459–F468, https://doi.org/10.1152/ajprenal.00040.2005 (2005).
45. Andersen, T. E. *et al*. Escherichia coli uropathogenesis *in vitro*: invasion, cellular escape, and secondary infection analyzed in a human bladder cell infection model. *Infect Immun* **80**, 1858–1867, https://doi.org/10.1128/IAI.06075-11 (2012).
46. Andersson, K. E. Current and future drugs for treatment of MS-associated bladder dysfunction. *Annals of Physical and Rehabilitation Medicine* **57**, 321–328, https://doi.org/10.1016/j.rehab.2014.05.009 (2014).
47. Saito, M., Nakamura, I. & Miyagawa, I. [Autoradiographic localization of muscarinic receptors in diabetic rat bladder]. *Nihon Hinyokika Gakkai zasshi. The japanese journal of urology* **88**, 858–867 (1997).
48. Wu, X. R. *et al*. Mammalian uroplakins. A group of highly conserved urothelial differentiation-related membrane proteins. *The Journal of biological chemistry* **269**, 13716–13724 (1994).
49. Lavelle, J. P., Apodaca, G., Meyers, S. A., Ruiz, W. G. & Zeidel, M. L. Disruption of guinea pig urinary bladder permeability barrier in noninfectious cystitis. *American Journal of Physiology - Renal Physiology* **274**, F205–F214 (1998).
50. Liebhold, M., Wendt, M., Kaup, F. J. & Drommer, W. [Light- and electron-microscopic studies of the structure of normal bladder epithelium in female swine]. *Anatomia, histologia, embryologia* **24**, 47–52 (1995).
51. Andrews, P. M. Microplicae: characteristic ridge-like folds of the plasmalemma. *The Journal of Cell Biology* **68**, 420 (1976).
52. Wayt, J. & Bretscher, A. Cordon Bleu serves as a platform at the basal region of microvilli, where it regulates microvillar length through its WH2 domains. *Mol Biol Cell* **25**, 2817–2827, https://doi.org/10.1091/mbc.E14-06-1131 (2014).
53. Derganc, J., Božič, B. & Romih, R. Shapes of Discoid Intracellular Compartments with Small Relative Volumes. *PloS one* **6**, e26824, https://doi.org/10.1371/journal.pone.0026824 (2011).
54. Khasriya, R. *et al*. The spectrum of bacterial colonisation associated with urothelial cells from patients with chronic lower urinary tract symptoms. *J Clin Microbiol*, https://doi.org/10.1128/JCM.03314-12 (2013).
55. Horsley, H. *et al*. Enterococcus faecalis subverts and invades the host urothelium in patients with chronic urinary tract infection. *PloS one* **8**, e83637, https://doi.org/10.1371/journal.pone.0083637 (2013).
56. Guiton, P. S., Hannan, T. J., Ford, B., Caparon, M. G. & Hultgren, S. J. Enterococcus faecalis overcomes foreign body-mediated inflammation to establish urinary tract infections. *Infection and immunity* **81**, 329–339, https://doi.org/10.1128/IAI.00856-12 (2013).
57. Poulsen, L. L. *et al*. Enterococcus and Streptococcus spp. associated with chronic and self-medicated urinary tract infections in Vietnam. *BMC Infect Dis* **12**, 320, https://doi.org/10.1186/1471-2334-12-320 (2012).
58. Mohamed, J. A. & Huang, D. B. Biofilm formation by enterococci. *Journal of medical microbiology* **56**, 1581–1588, https://doi.org/10.1099/jmm.0.47331-0 (2007).
59. Felmingham, D., Wilson, A. P., Quintana, A. I. & Gruneberg, R. N. Enterococcus species in urinary tract infection. *Clinical infectious diseases: an official publication of the Infectious Diseases Society of America* **15**, 295–301 (1992).
60. Hanin, A. *et al*. Screening of *in vivo* activated genes in Enterococcus faecalis during insect and mouse infections and growth in urine. *PloS one* **5**, e11879, https://doi.org/10.1371/journal.pone.0011879 (2010).
61. Nichol, K. A. *et al*. Molecular epidemiology of urinary tract isolates of vancomycin-resistant Enterococcus faecium from North America. *Int J Antimicrob Agents* **27**, 392–396, https://doi.org/10.1016/j.ijantimicag.2005.12.006 (2006).

62. Swaminathan, S. & Alangaden, G. J. Treatment of resistant enterococcal urinary tract infections. *Current infectious disease reports* **12**, 455–464, https://doi.org/10.1007/s11908-010-0138-8 (2010).
63. Bhadriraju, K. & Chen, C. S. Engineering cellular microenvironments to improve cell-based drug testing. *Drug discovery today* **7**, 612–620 (2002).
64. Knight, E. & Przyborski, S. Advances in 3D cell culture technologies enabling tissue-like structures to be created *in vitro*. *Journal of anatomy*, https://doi.org/10.1111/joa.12257 (2014).
65. Jerman, U. D., Kreft, M. E. & Veranic, P. Epithelial-Mesenchymal Interactions in Urinary Bladder and Small Intestine and How to Apply Them in Tissue Engineering. *Tissue Eng Part B Rev* **21**, 521–530, https://doi.org/10.1089/ten.TEB.2014.0678 (2015).
66. Maqsood, M. I., Matin, M. M., Bahrami, A. R. & Ghasroldasht, M. M. Immortality of cell lines: challenges and advantages of establishment. *Cell biology international* **37**, 1038–1045, https://doi.org/10.1002/cbin.10137 (2013).
67. Dalal, E. Moderate stress protects female mice against bacterial-infection of the bladder by eliciting uroepithelial shedding. *Infection and immunity* **62**, 5505–5510 (1994).
68. Smith, Y. C., Rasmussen, S. B., Grande, K. K., Conran, R. M. & O'Brien, A. D. Hemolysin of uropathogenic Escherichia coli evokes extensive shedding of the uroepithelium and hemorrhage in bladder tissue within the first 24 hours after intraurethral inoculation of mice. *Infection and immunity* **76**, 2978–2990, https://doi.org/10.1128/Iai.00075-08 (2008).
69. Thumbikat, P. *et al.* Bacteria-induced uroplakin signaling mediates bladder response to infection. *PLoS pathogens* **5**, e1000415, https://doi.org/10.1371/journal.ppat.1000415 (2009).
70. Hannan, T. J., Mysorekar, I. U., Hung, C. S., Isaacson-Schmid, M. L. & Hultgren, S. J. Early severe inflammatory responses to uropathogenic *E. coli* predispose to chronic and recurrent urinary tract infection. *PLoS pathogens* **6**, e1001042, https://doi.org/10.1371/journal.ppat.1001042 (2010).
71. Rosen, D. A., Hooton, T. M., Stamm, W. E., Humphrey, P. A. & Hultgren, S. J. Detection of intracellular bacterial communities in human urinary tract infection. *PLoS Med* **4**, e329, https://doi.org/10.1371/journal.pmed.0040329 (2007).
72. Hertting, O. *et al.* Vitamin D induction of the human antimicrobial Peptide cathelicidin in the urinary bladder. *PloS one* **5**, e15580, https://doi.org/10.1371/journal.pone.0015580 (2010).
73. Kuhlmann, I. The prophylactic use of antibiotics in cell culture. *Cytotechnology* **19**, 95–105, https://doi.org/10.1007/BF00749764 (1995).
74. Bajpai, R., Lesperance, J., Kim, M. & Terskikh, A. V. Efficient propagation of single cells Accutase-dissociated human embryonic stem cells. *Molecular reproduction and development* **75**, 818–827, https://doi.org/10.1002/mrd.20809 (2008).
75. Schneider, C. A., Rasband, W. S. & Eliceiri, K. W. NIH Image to ImageJ: 25 years of image analysis. *Nat Meth* **9**, 671–675 (2012).
76. Bolte, S. & CordeliÈRes, F. P. A guided tour into subcellular colocalization analysis in light microscopy. *Journal of Microscopy* **224**, 213–232, https://doi.org/10.1111/j.1365-2818.2006.01706.x (2006).

Acknowledgements

We thank the MS Society for their generous support of this work (grant ref. 986), Peter Girling and other members of our lab for helpful discussion, and Anthony Kupelian, Jakob Møller-Jensen and Paola Bonfanti for critical comments on the manuscript. We are also grateful to the Royal Free Elecron Microscopy Unit and to Linda Collins for expert technical assistance.

Author Contributions

H.H. and J.R. conceived the experiments, H.H. and D.D. conducted the experiments, H.H., J.M.L. and J.R. analysed the results, and H.H. and J.R. wrote the manuscript. All authors reviewed the manuscript.

Additional Information

Competing Interests: J.R. has received funding from AtoCap Ltd, a spin-off company from academic researchers at University College London interested in finding novel drug delivery systems for UTI. H.H., D.D. and J.M.L. declare no competing financial interests.

Publisher's note: Springer Nature remains neutral with regard to jurisdictional claims in published maps and institutional affiliations.

Appendix 3

National Research Ethics Service
NRES Committee London - Bentham
Research Ethics Committee Offices
Room 4W/12, 4th Floor
Charing Cross Hospital
Fulham Palace Road
London
W6 8RF

Telephone: 020 331 10100

02 August 2011

Professor James Malone-Lee
Professor of Medicine
University College London
Research Dept of Clinical Physiology
Whittington Campus, Clerkenwell Building
Highgate Hill, London
N19 5LW

Dear Professor Malone-Lee

Study title:	**A randomised, single blind comparative study of urine sampling methods.**
REC reference:	**11/LO/1096**
Protocol number:	**11/0157**

The Research Ethics Committee reviewed the above application at the meeting held on 07 July 2011. Thank you for attending to discuss the study.

Ethical Discussion

The Committee welcomed you and Sanchutha Sathiananthamoorthy to the meeting and thanked you for attending to discuss the application.

The Committee raised the following questions:

A. It is unclear why there is said to be no planned public dissemination of the results of the study. You said that this was an error and that there will definitely be reporting and publication of the study outcome.

B. The risk of infection, and if possible quantification of this risk, had not been explained in the Participant Information Sheet. You explained that the risk is less than one per cent and agreed that the Participant Information Sheet should say that "the precise risk of infection cannot be estimated since it is so low and so unlikely". If infection is indeed found, then it will be treated in standard fashion.

C. Will a standard urinary pregnancy test be performed on all potential participants? You explained that pregnancy tests will be mandatory and that pregnant women would be excluded.

D. Who will be catheterising the participants and taking the samples? You clarified that this will be one of two available female nurses in the clinic, and agreed that participants need to be informed of this

E. The possible reasons why non-English speakers will be excluded from the study were explored. You explained that there could be considerable difficulty in explaining the process to non-English speaking potential participants. In this instance the fact that such participants were not included would not influence the cross cultural applicability of the outcome as the key variable is handling of the urine sample itself.

F. The problems of fluid intake in the clinic and production of a second urine sample might be burdensome to participants. You explained that a refractometer is used to test urine concentration. Participants are not asked to drink an excess of liquids between tests as experience has shown that they are able to provide another sample within the hour.

G. The reasons why seven different participant groups are required were not clear. You explained that the different groups would exhibit different groups of symptoms and that these would be used for the secondary statistical analysis.

You and Sanchutha Sathiananthamoorthy left the meeting

Ethical Decision

The members of the Committee present gave a favourable ethical opinion of the above research on the basis described in the application form, protocol and supporting documentation, subject to the conditions specified below.

Ethical review of research sites

NHS Sites

The favourable opinion applies to all NHS sites taking part in the study, subject to management permission being obtained from the NHS/HSC R&D office prior to the start of the study (see "Conditions of the favourable opinion" below).

Non NHS sites

The Committee has not yet been notified of the outcome of any site-specific assessment (SSA) for the non-NHS research site(s) taking part in this study. The favourable opinion does not therefore apply to any non-NHS site at present. I will write to you again as soon as one Research Ethics Committee has notified the outcome of a SSA. In the meantime no study procedures should be initiated at non-NHS sites.

Conditions of the favourable opinion

The favourable opinion is subject to the following conditions being met prior to the start of the study.

Management permission or approval must be obtained from each host organisation prior to the start of the study at the site concerned.

Management permission ("R&D approval") should be sought from all NHS organisations involved in the study in accordance with NHS research governance arrangements.

Guidance on applying for NHS permission for research is available in the Integrated Research Application System or at http://www.rdforum.nhs.uk.

Where a NHS organisation's role in the study is limited to identifying and referring potential participants to research sites ("participant identification centre"), guidance should be sought from the R&D office on the information it requires to give permission for this activity.

For non-NHS sites, site management permission should be obtained in accordance with the procedures of the relevant host organisation.

Sponsors are not required to notify the Committee of approvals from host organisations

Other conditions specified by the REC

1. Participant Information Sheet:

i. Clarify that pregnant women are excluded from the study rather than using the current statement of "not advisable".

ii. Amended to state that the risk of infection is "so low that it cannot be estimated".

iii. Amended to state explicitly that if infection is found, the participant will be treated.

2. Consent Form

i. Amended to make provision for "gifting" of samples for possible ethically approved future research.

It is responsibility of the sponsor to ensure that all the conditions are complied with before the start of the study or its initiation at a particular site (as applicable).

You should notify the REC in writing once all conditions have been met (except for site approvals from host organisations) and provide copies of any revised documentation with updated version numbers. Confirmation should also be provided to host organisations together with relevant documentation

Approved documents

The documents reviewed and approved at the meeting were:

Document	*Version*	*Date*
Covering Letter		21 June 2011
Evidence of insurance or indemnity		16 May 2011
GP/Consultant Information Sheets	1.0	06 June 2011
Investigator CV		22 February 2011
Participant Consent Form: Controls	1.0	06 June 2011
Participant Consent Form: Patients	1.0	06 June 2011
Participant Information Sheet: Controls	1.0	21 June 2011
Participant Information Sheet: Patients	1.0	21 June 2011
Protocol	1.0	06 June 2011
Questionnaire: Hybrid Fluts-Appendix 1, ICIQ-LUTSqol		
REC application		21 June 2011

Membership of the Committee

The members of the Ethics Committee who were present at the meeting are listed on the attached sheet.

Professor David Katz knows Professor Malone Lee

Statement of compliance

The Committee is constituted in accordance with the Governance Arrangements for Research Ethics Committees (July 2001) and complies fully with the Standard Operating Procedures for Research Ethics Committees in the UK.

After ethical review

Reporting requirements

The attached document "After ethical review – guidance for researchers" gives detailed guidance on reporting requirements for studies with a favourable opinion, including:

- Notifying substantial amendments
- Adding new sites and investigators
- Notification of serious breaches of the protocol
- Progress and safety reports
- Notifying the end of the study

The NRES website also provides guidance on these topics, which is updated in the light of changes in reporting requirements or procedures.

Feedback

You are invited to give your view of the service that you have received from the National Research Ethics Service and the application procedure. If you wish to make your views known please use the feedback form available on the website.

Further information is available at National Research Ethics Service website > After Review

11/LO/1096	**Please quote this number on all correspondence**

With the Committee's best wishes for the success of this project

Yours sincerely

Professor David Katz
Chair

Email: laura.keegan@nhs.net

Enclosures: *List of names and professions of members who were present at the meeting and those who submitted written comments*
"After ethical review – guidance for researchers"

Copy to: *Mr David Wilson*
Ms Senga Steel, The Whittington Hospital NHS Trust

NRES Committee London - Bentham

Attendance at Committee meeting on 07 July 2011

Committee Members:

Name	*Profession*	*Present*	*Notes*
Judge Stuart Appleman	Lawyer/Judge	Yes	
Dr Joan Box	Medical Practitioner	Yes	
Mr Adrian Cook	Statistician	No	
Ms Sally Davis	Former Barrister and Civil Servant	No	
Professor David Katz	Professor of Immunopathology	Yes	
Mr Stephen Leyshon	Patient Safety Lead for Primary Care and Ambulance Services	No	
Dr Vera Mann	Lecturer in Medical Statistics	No	
Dr Jacqueline (Jackie) Maxmin	Retired GP	Yes	
Mrs Michelle McPhail	Lay member	Yes	
Mr Robin Offord	Director of Clinical Pharmacy	Yes	
Dr Nicholas Paton	Senior Clinical Scientist	No	
Mr Jonathan Simons	Investment Manager	Yes	
Dr Anne Marie Swart	Clinical Epidemiologist	Yes	
Rev Rachel Taylor	Reverend	No	
Dr Robert Urquhart	Head of Pharmacy & Divisional Clinical Director	No	
Dr Sarah Jane Wong	Associate GP	Yes	
Ms Vivien Yule	Director, Ruston Poole International	Yes	

Also in attendance:

Name	*Position (or reason for attending)*
Miss Laura Keegan	REC Co-ordinator

Appendix 4

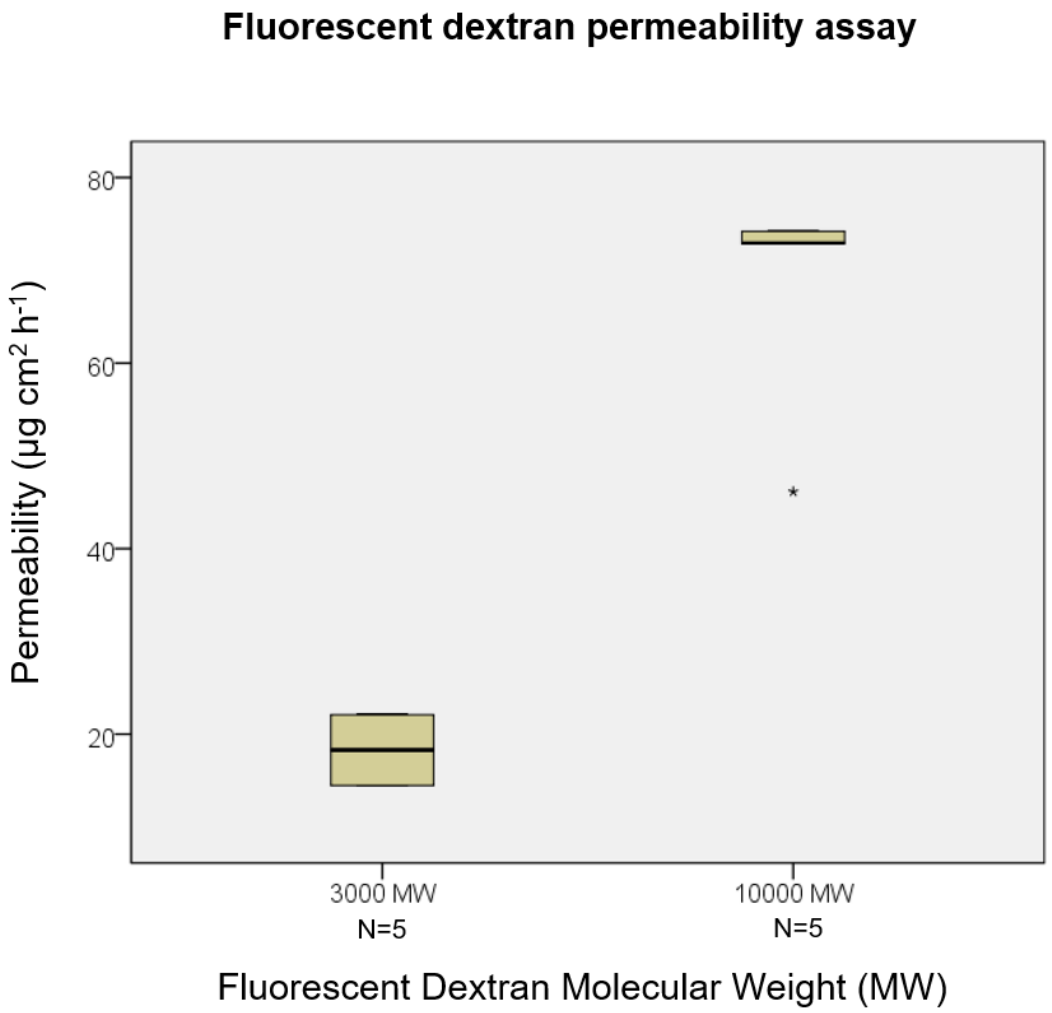

Box and whisker plot showing the median concentration of fluorescent dextran (3000 and 10000 MW respectively) that passed through the urothelial organoid per hour.